EXPLORING AND HARNESSING PEG-IMMUNE SYSTEM INTERACTIONS TO ENGINEER TARGETED STEALTH NANOPARTICLES

Qi Yang

A dissertation submitted to the faculty at the University of North Carolina at Chapel Hill in partial fulfillment of the requirements for the degree of Doctor of Philosophy in the Department of Pharmaceutical Sciences in the School of Pharmacy.

Chapel Hill
2016

Approved by:

Samuel K. Lai

Leaf Huang

Rudolph L. Juliano

Steven I. Park

Andrew Z. Wang

ABSTRACT

Qi Yang: Exploring and harnessing PEG-immune system interactions
to engineer targeted stealth nanoparticles
(Under the direction of Samuel K. Lai)

Effective nanoparticle drug delivery to tumor cells typically relies on prolonged systemic circulation of the nanoparticles to allow for extravasation and accumulation in tumor tissue, as well as targeting ligands on the nanoparticles that can mediate receptor-specific uptake by target tumor cells. Due to the ability of polyethylene glycol (PEG) to effectively reduce nonspecific protein binding and cell clearance, PEGylation has become a commonplace strategy for formulating long-circulating nanoparticle systems. However, the precise characteristics (e.g., PEG molecular weight and density) that influence the interactions between PEG-coated nanoparticles and phagocytic immune cells remain poorly understood for many nanoparticle systems, and findings from human studies suggest that the body is further able to mount PEG-specific humoral responses to PEG-coated agents. Additionally, the presence of targeting ligands on the nanoparticle surface may also compromise the extended circulation profile of PEG-coated nanoparticles. To address these challenges and gaps in our understanding, in this dissertation quantitative approaches and systematic analyses were utilized to 1) evaluate the interactions between phagocytic cells and various PEG coatings on polymeric nanoparticles, 2) determine the prevalence and concentrations of different anti-PEG antibody isotypes amongst the general human population, and 3) apply an alternative approach for PEGylated nanoparticle delivery to tumors. The results indicated that extremely dense PEG coatings ($R_F/D >> 2.8$) are required to

effectively minimize nonspecific clearance by immune cells. Using competitive ELISAs and engineered antibody standards, the anti-PEG IgG1-4 and IgM levels in a large number of healthy human samples were quantified, with the majority of samples possessing detectable anti-PEG IgG and/or IgM. Finally, a multistep targeting (i.e., pretargeting) approach was tested for the delivery of biotin PEG-modified nanoparticles to disparate tumor cells *in vitro* and *in vivo*. The analytical methodologies and overall findings described here can inform future studies of PEGylated nanoparticle-immune system interactions and nanoparticle targeting strategies.

ACKNOWLEDGEMENTS

Completion of this work was made possible through the contributions and support of many people. First, I would like to thank my advisor, Dr. Samuel Lai, who has offered a deftly balanced mixture of freedom and guidance as I pursued my Ph.D. and has helped to nurture and push me as a scientist. Next, I would like to acknowledge Dr. Leaf Huang, who, in addition to serving as the chair of my committee, gave me an opportunity to work in his lab as an undergraduate and served as my first research mentor, for which I am truly grateful. I would also like to thank my other committee members Dr. Steven Park, Dr. Rudolph Juliano, and Dr. Andrew Wang for their time, advice, and feedback. Special thanks go to the UNC small animal imaging, flow cytometry, and animal studies cores, as well as to all of the other labs in MOPH/DPMP for letting me constantly run over to use an instrument or borrow some chemicals.

My time in graduate school has been enriched and enlivened by the company of all of the present and past members of the Lai lab: Christina Parker, Justin McCallen, Holly Schroeder, Justin Huckaby, Dr. Tim Jacobs, Jasmine Edelstein, Morgan McSweeney, Jennifer Schiller, Dr. Dimple Harit, Kenetta Nunn, Arthi Kannan, and Dr. Babu Subramani, among others. I would also like to thank Clark Meshaw and James Lemieux for always being there for me and providing much-needed distraction from research work. In addition, I owe so much to my parents, who have always been full of unconditional love and support. Lastly, I would like to thank my cat Tundra for brightening up my life with her fluffy company.

TABLE OF CONTENTS

LIST OF TABLES

LIST OF FIGURES

LIST OF ABBREVIATONS

Ab	antibody
ABC	accelerated blood clearance
Ag	antigen
ANOVA	analysis of variance
APC	allophycocyanin
ASNase	asparaginase
AUC	area under the curve
BsP	bispecific protein
BSA	bovine serum albumin
CA	clearing agent
CDR	complementarity-determining region
CI	confidence interval
COOH	carboxyl
D	PEG grafting density
DSPE	1,2-distearoyl-*sn*-glycero-3-phosphoethanolamine
EDC	1-ethyl-3-(3-dimethylaminopropyl)carbodiimide
ELISA	enzyme-linked immunosorbent assay
EPR	enhanced permeability and retention
FP	fusion protein
GMC	geometric mean concentration
GRAS	Generally Recognized As Safe

HCV	hepatitis C virus
HRP	horseradish peroxidase
ID/g	injected dose per gram
IFN	interferon
IHC	immunohistochemistry
i.m.	intramuscular
i.v.	intravenous
IVIM	intravital imaging
MAb	monoclonal antibody
MPS	mononuclear phagocyte system
MW	molecular weight
MYO	myoglobin
NH_2	amine
NHL	non-Hodgkin's lymphoma
NP	nanoparticle
PAL	phenylalanine ammonia lyase
PDAM	1-pyrenylyldiazomethane
PEG	polyethylene glycol
PK	pharmacokinetics
PL	phospholipid
PRIT	pretargeted radioimmunotherapy
PS	polystyrene
R_F	Flory radius

RIT	radioimmunotherapy
S-NHS	*N*-hydroxysulfosuccinimide
SA	streptavidin
s.c.	subcutaneous
scFv	single-chain variable fragment
TCO	trans-cyclooctene
TI	T cell-independent
TMB	3,3',5,5'-tetramethylbenzidine
Tz	tetrazine
V_D	volume of distribution

CHAPTER 1: INTRODUCTION

1.1 Nanoparticle and MPS clearance

The application of nanotechnology to delivery of therapeutic and/or diagnostic agents has become an important area of pharmaceutical science, with several nanoparticle formulations already on the market and many more in development [1]. Nanoparticles are commonly defined as being 1-100 nm in diameter, though submicron-sized particles are often also included in this category. Nanoparticles can protect their cargo from the biological microenvironment, alter drug solubility, and provide controlled drug release. Furthermore, owing to their unique physicochemical properties (e.g., size, shape, surface charge), nanoparticle formulations can also significantly improve an encapsulated drug's biodistribution and bioavailability, and consequently its pharmacokinetic and pharmacodynamics profile, compared to free drug [2]. In addition, by reducing the level of free drug in the blood, nanoparticles can reduce toxicity associated with drug accumulation in nontarget tissue and broaden the drug's therapeutic window. It is important to note, however, that the use of nanoparticles can also introduce new problems. For example, liposomal formulations of doxorubicin exhibit reduced cardiotoxicity compared to the free drug but increase the likelihood of side effects such as hand-foot syndrome [3].

A major biological barrier encountered by nanoparticles injected into the systemic circulation is rapid clearance by mononuclear phagocyte system (MPS) cells (e.g., Kupffer cells in the liver and macrophages in the spleen and lymph nodes). The MPS comprises a branch of the innate immune system that, among other functions, is responsible for the elimination of

foreign materials, including bacteria, viruses, and fungi. Similar to these naturally occurring particles, nanoparticles can be rapidly opsonized by adsorption of plasma proteins such as serum albumin, complement factors, apolipoproteins, and immunoglobulins, generating an abundant protein corona that marks the nanoparticles for receptor-mediated phagocytosis by MPS cells [4]. The process of opsonization and sequestration by MPS cells is extremely efficient: unmodified nanoparticles can be fully eliminated from systemic circulation within minutes [5, 6].

1.2 Nanoparticle PEGylation

Surface modification of nanoparticles with polyethylene glycol (PEG) was first introduced in the 1990s to reduce the rapid clearance of nanoparticles by MPS cells [5]. Currently, PEG remains the most popular compound within the genre of so-called "stealth" polymers—polymers that, when grafted on the surface of nanoparticles, can reduce their opsonization and subsequent immune cell-mediated clearance. In the case of PEG, these effects are largely due to its hydrophilicity and high flexibility, which generates a thick, amorphous hydration shell that repels nonspecific protein adsorption and improves colloidal stability [4, 6, 7]. Thus, modification with PEG (i.e., PEGylation) can significantly prolong nanoparticle circulation times in the blood, increasing the half-life of nanoparticles to several hours or even days [8, 9].

Although PEGylation is a frequently exploited nanoparticle modification strategy, the extent to which PEGylation improves nanoparticle circulation times remains highly variable [9]. The diverse classes of nanoparticle systems (e.g., liposomal, micellar, metallic, polymeric, silica, and carbon nanoparticles) have necessitated the development of a variety of PEGylation strategies, including post-insertion of PEG-lipids, surface conjugation to reactive groups,

adsorption of PEG-containing surfactants, and particle formulation using PEG copolymers. Nanoparticle composition and formulation processes not only affect the PEGylation method(s) that can be used but also introduces different limitations on the density of PEG grafting that can be achieved. As a result, PEG coating characteristics (e.g., PEG density, PEG MW, potential PEG shedding) can vary greatly. An additional complicating factor is the lack of methods to accurately measure the extent of PEG grafting on most nanoparticles. Overall, the precise characteristics of PEG coatings that influence opsonization and clearance of PEG-coated nanoparticles by MPS cells remain not well-understood.

1.3 Humoral immune responses

Adaptive immunity is critical for immune defense against reinfection by foreign pathogens. In contrast to innate immune responses that rely on recognition of shared features of pathogens, adaptive immune responses are mediated by immune cells and humoral macromolecules, particularly antibodies, that can bind specific epitopes on individual foreign molecules (i.e., antigens). Antibodies are Y-shaped proteins with complementarity-determining regions (CDRs) at the ends of their two arms that can bind target epitopes (Fig. 1.1). Recombination and hypermutation of antibody gene segments produces a diverse and random pool of antibodies able to recognize a wide array of potential antigens and to adapt in order to bind antigens with high affinity [10]. Antibodies are produced by B lymphocytes and are classified into IgG, IgM, IgA, IgD and IgE isotypes, with IgG further divided into IgG1, IgG2, IgG3, and IgG4 subclasses. Upon binding, antibodies can opsonize, agglutinate, and/or directly neutralize pathogens, thereby preventing pathogens from reaching and infecting more host cells. Additionally, antibodies can activate the complement cascade, as well as facilitate the

elimination of infected cells through antibody-dependent cell-mediated cytotoxicity. Generally, antibodies are produced by B cells after activation by helper T cells, although certain antigens (i.e., T cell-independent antigens) are able to activate B cell antibody production without stimulation from T cells. Upon initial exposure to an antigen, IgM antibodies are produced after a lag phase of 1-2 weeks, typically followed by a peak of IgG antibodies as the differentiated B cells undergo class-switching. Long-lived plasma cells and memory B cells generated after the primary response can result in more rapid secondary antibody responses, which are predominantly IgG. However, the features of induced antibody responses can vary depending on the specific antigen, dose, route of exposure, and individual host genetics and environmental exposure [11]. For example, IgG1 (~60% of all IgG) is typically associated with responses to protein antigens and memory B cell induction, whereas IgG2 (~30% of all IgG) is commonly induced by polysaccharide antigens, often in a T cell-independent manner that may not generate a meaningful memory response [12].

While humoral responses are invaluable for defense against infectious pathogens, these same mechanisms can limit the safety and efficacy of exogenous therapeutic molecules. For example, monoclonal antibodies (MAb) of murine origin were first introduced in the 1980s, but their success was limited by the induction of strong anti-mouse antibodies in the majority of patients. Indeed, >85% of patients treated with muromonab-CD3, the first clinically approved MAb, developed antibodies against the drug [13, 14]. In an effort to reduce immunogenicity, the pharmaceutical industry has transitioned from fully murine to chimeric, humanized, and finally fully human MAb formats (Fig. 1.1), but even fully human antibodies may induce some immune responses [13, 15]. Anti-drug antibodies pose a major challenge to effective therapy not only due to neutralization and/or rapid clearance of antibody-bound drugs, which can reduce or

completely abrogate drug efficacy, but also because they can induce serious, potentially life-threatening, side effects such as anaphylactic and hypersensitivity reactions [16-18].

Antibodies can potentially form against foreign components of nanoparticle carriers, including PEG. Although PEG was long assumed to be immune inert due to its ability to resist protein binding, growing evidence indicates that both animal subjects and human patients treated with PEGylated drugs can develop antibodies to PEG, leading to a marked reduction in the efficacy of PEGylated systems and/or unexpected anti-PEG antibody-associated side effects [19, 20]. Interestingly, PEG-specific antibodies have even been observed among "treatment-naïve" donors [21, 22]. Unfortunately, the overall prevalence, systemic concentration, and potential clinical impact of these anti-PEG antibodies is currently unclear. A thorough characterization of anti-PEG antibodies among the general population will likely have important implications for the future clinical use of the many PEGylated drugs on the market and in development.

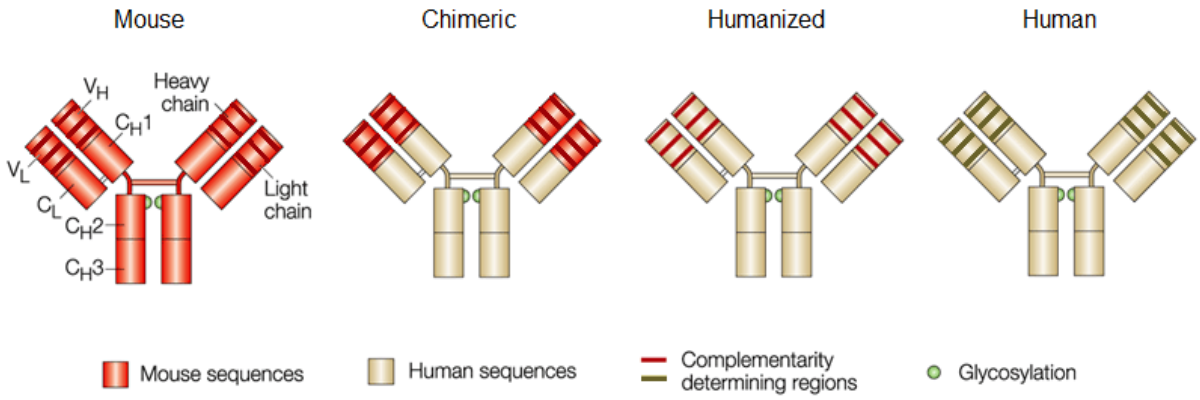

Figure 1.1. Antibody structure. Antibodies are Y-shaped macromolecules composed of two heavy and two light chains. Within these chains, the variable heavy and light domains (V_H and V_L, respectively) contain the complementarity-determining regions (CDRs) responsible for antigen binding, and the effector functions of the antibody are determined by the constant domains (C_L, C_H1, C_H2, and C_H3), in particular the C_H2 and C_H3 domains, which comprise the F_c region that is recognized by complement proteins and various receptors on immune cells. Chimeric antibodies contain nonhuman V_H and V_L sequences, whereas in humanized antibodies, only the CDR sequences are of nonhuman origin. Figure was modified from Ref [23] with permission from Nature Publishing Group.

1.4 Nanoparticle drug delivery to tumors

The application of nanomedicine to oncology has been largely driven by the unique properties of tumor tissues. Once tumors develop beyond a critical size, typically 1-2 mm^2, angiogenesis is required to supply adequate nutrients to support further tumor growth [24]. This neovascularization is induced through the release of vascular endothelial growth factor (VEGF) and other proangiogenic factors by the tumor cells. However, the unbalanced secretion of these factors, results in abnormal and heterogeneous vessels with irregular function and structure, characterized by fenestrations in the endothelium that range from hundreds of nanometers to several micrometers in size [25, 26]. Combined with a lack of adequate draining lymphatic vessel formation for most tumors, the "leaky" vasculature allows the preferential extravasation and accumulation of macromolecules and nanoscale materials in tumor tissues, compared to normal tissue with tight endothelial vessel linings. This phenomenon, termed the enhanced permeability and retention (EPR) effect, is the basis for "passive" targeting of tumors using nanoparticles, as any sufficiently long-circulating nanoparticle smaller than the tumor vessel fenestrations should be able to exploit the EPR effect to accumulate in tumor tissues [27].

Another feature of tumor cells is overexpression of various cell surface receptors. Through the introduction of ligands (e.g., antibodies, small molecules, peptides, aptamers) that specifically bind to these overexpressed receptors, researchers can generate nanoparticles that "actively" bind tumor cells and undergo receptor-mediated endocytosis. However, tumor biodistribution of actively targeted nanoparticles remains largely dependent on the EPR effect. Because the inclusion of a large number of targeting ligands may offset the long circulation characteristics of PEG coatings, the targeting ligand density must be carefully tuned and

optimized for each nanoparticle formulation to balance the stealth properties imparted by PEGylation and the ability to specifically target cancer cells.

1.5 Thesis overview

In this thesis, my goal is to provide a blueprint for the engineering of nanoparticle systems that can better target specific cells and tissues by rigorously characterizing the interactions of PEGylated nanoparticles with cells and antibodies of the immune system. This goal is divided into the following three aims:

Aim 1: Elucidate interactions between PEGylated nanoparticles and innate immune system. I synthesized a series of PEGylated nanoparticles with carefully tuned physicochemical properties comprised of a range of PEG molecular weights and densities. Next, I developed an indirect fluorogenic probe-based assay to quantify the number of PEG groups conjugated onto the nanoparticles. I further assessed the influence of PEG MW and grafting density on nanoparticle uptake by cultured human macrophage-like cells and primary human leukocytes using flow cytometry and monitored the systemic circulation time of various PEGylated nanoparticles in BALB/c mice using intravital imaging and pharmacokinetics analysis.

Aim 2: Investigate human adaptive immune responses against PEG (anti-PEG antibodies). To enable quantitative analysis of pre-existing anti-PEG antibody responses in humans, I engineered a variety of chimeric anti-PEG monoclonal Ab standards. Using these standards in combination with rigorously validated competitive ELISAs, I was able to quantify the levels of anti-PEG IgM and different subclasses of anti-PEG IgG (IgG1-4) in both contemporary and historical human samples. The relationship between anti-PEG antibody levels and various demographic factors such as age, gender, and race was explored.

Aim 3: Evaluate the use of a pretargeting strategy for nanoparticle delivery to heterogeneous tumors. I synthesized densely PEGylated model polymeric nanoparticles with a range of surface biotin groups and, using flow cytometry, determined the optimal biotin ligand density required to maximize specific uptake by B-cell and T-cell tumor cells pretargeted with streptavidin-based bispecific fusion proteins recognizing CD20 (B cell-specific) or TAG72 (T cell-specific). I also evaluated the utility of this pretargeted nanoparticle strategy in single or dual tumor-bearing nude mice by first dosing with the bispecific fusion protein(s), followed by the biotinylated PEGylated nanoparticles and measuring nanoparticle biodistribution using whole-organ imaging.

CHAPTER 2: BACKGROUND ON HUMORAL ANTI-PEG IMMUNITY*

2.1 Introduction

Extended circulation of proteins and nanoparticle therapeutics is often necessary to achieve adequate drug concentrations in target tissues [9, 28, 29]. Unfortunately, many peptide and protein drugs are rapidly degraded and/or cleared from the systemic circulation due to their small size [30], and nanoparticulate drug carriers are readily eliminated by the cells of the mononuclear phagocyte system (MPS) [9, 31]. To overcome these challenges, proteins and nanoparticles are frequently conjugated to various hydrophilic polymers, which can significantly reduce degradation and opsonization, consequently extending the circulation half-lives of the modified therapeutics [28, 32]. These polymers are frequently referred to as "stealth" polymers, reflective of their ability to render proteins and particles inert to the biological environment.

Polyethylene glycol (PEG) has been, and continues to be, the most widely used stealth polymer in drug delivery, with over a dozen PEGylated pharmaceuticals currently on the market and many more in clinical testing [9, 29]. PEG has a long history of safe use in humans, and the polymer is classified under the Generally Recognized As Safe (GRAS) category by the FDA. Despite the frequent use of PEG to extend circulation kinetics, a number of investigators have observed the rapid clearance of some PEGylated systems upon repeated administration [19, 33]. This "accelerated blood clearance" phenomenon was ultimately attributed to the formation of PEG-specific antibodies [34]. Indeed, animals that receive repeated doses of PEGylated systems often generate a potent IgM antibody response to PEG, which causes the complete elimination of

*This chapter is based on an article that previously appeared in WIREs Nanomedicine and Nanobiotechnology. The original citation is as follows: Yang Q, Lai SK. *WIREs Nanomed Nanobiotechnol*. **2015**, *7*(5), 655-77.

subsequent doses of PEGylated agents from the circulation within minutes to a few hours [19]. The induction of anti-PEG antibodies (anti-PEG Abs) in humans was also observed in recent clinical trials of PEGylated proteins and has been correlated with poor drug efficacy [35, 36]. Interestingly, there is emerging evidence that anti-PEG Abs can be found in the general population in individuals who likely have never received PEGylated therapeutics injected systemically [21, 37]. As many more PEGylated protein and nanoparticle therapeutics are expected to enter the market over the next several years, an improved understanding of the prevalence, induction, and effects of anti-PEG immunity is undoubtedly critical for the continued clinical use of PEGylated systems.

2.1.1 Advantages and physicochemical properties of effective stealth PEGylation

The stealth properties of PEG are rooted in several distinctive molecular and physical characteristics. First, PEG is exceedingly hydrophilic, with each ethylene glycol subunit (-CH_3-CH_3-O-) surrounded by a minimum of 2-3 water molecules [38, 39]. Thus, PEG coatings generate a hydration shell with a large excluded volume that sterically prevents biomacromolecules from penetrating into the polymer layer and binding to the underlying core via hydrophobic or electrostatic interactions [7, 40, 41]. Second, PEG is highly flexible and exhibits high chain mobility, which results in an exceedingly large number of polymer chain conformations. As a result, any substantial reduction in the conformational freedom of PEG, including the displacement of PEG chains by intruding biomacromolecules, is thermodynamically unfavorable [42-44]. Together, these features greatly suppress interactions between PEGylated systems and the biological environment.

For proteins, PEG conjugation decreases enzymatic degradation, opsonization, and immunogenicity of the protein core [30]; PEGylation can also improve stability and solubility [29]. Additionally, the resulting increase in the hydrodynamic diameter can reduce renal elimination and improve the biodistribution and pharmacokinetics of PEGylated proteins [30]. For nanocarriers, PEGylation reduces opsonization and MPS cell clearance, resulting in significantly prolonged circulation kinetics [31, 32]. For oncological applications, this effect often leads to greater tumor distribution via the enhanced permeability and retention (EPR) effect, while decreasing accumulation in non-targeted organs [9]. PEGylation can also improve nanocarrier stability and minimize the premature release of cargo therapeutics. Finally, PEG coatings have been shown to decrease nanocarrier association with structural components of mucus and extracellular matrix, thereby improving distribution and delivery to regions such as mucosal surfaces and brain tissues [45, 46].

Naturally, the effectiveness of PEG as a nanoparticle coating polymer is critically dependent on the density and resulting conformations assumed by conjugated PEG chains. The thickness of the PEG coating is dictated by its Flory radius (R_F; a function of the molecular weight) and the distance between two neighboring PEG chains (D; a function of the PEG coating density) [47]. When neighboring PEG chains are sparsely packed and do not overlap, PEG occupies a diffuse volume generally termed a "mushroom" conformation ($R_F/D \leq 1$). As more PEG polymers are introduced, the excluded volume and repulsion by neighboring PEG chains cause the polymer to transition from a diffuse conformation to a more extended "brush" conformation ($R_F/D > 1$) [4, 9], eventually reaching a "dense brush" regime, where the height of the PEG layer exceeds the R_F by at least two-fold (at $R_F/D > 2.8$) (Fig. 2.1a) [43, 48, 49]. The mushroom/brush transition has long been considered to be the critical threshold at which PEG

begins to exhibit stealth polymer functions. However, we and others have recently found that both rigid polymeric and metallic nanoparticles require PEG grafting densities far exceeding the minimum for brush conformation to demonstrate effective stealth nanoparticle behavior [49, 50]. Indeed, maximal reduction of uptake by mouse and human phagocytes *in vitro* required at least a dense brush PEG coating (Fig. 2.1b), and PEG grafting densities extending well into the dense brush conformation were necessary for the evasion of serum protein adsorption (Fig. 2.1c), as well as to achieve sustained circulation *in vivo*.

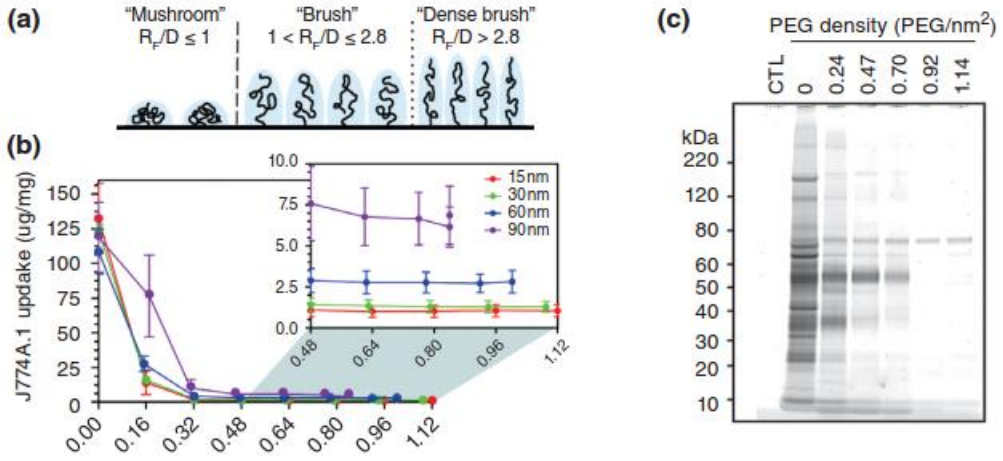

Figure 2.1. Impact of PEG density and conformation. a) The conformation adopted by PEG chains at various grafting densities. At low grafting densities (R_F /D ≤ 1), the PEG chains adopt a diffuse "mushroom" conformation. At higher densities, the PEG chains are increasingly able to repel opsonization and cell uptake as they transition into a more extended "brush" conformation (R_F /D > 1) and eventually reach a "dense brush" regime (R_F/D > 2.8). **b)** Uptake of PEG_{5k}-grafted gold NPs by mouse J774A.1 macrophage-like cells. A PEG_{5k} density of 0.16 PEG/nm^2 corresponds to brush conformation; all other PEG densities correspond to dense brush conformation. **c)** Qualitative analysis of the serum proteins adsorbed onto 30 nm gold NPs modified with varying amounts of PEG_{5k}. A PEG_{5k} density of 0.24 PEG/nm^2 corresponds to brush conformation; all other PEG densities correspond to dense brush conformation. Panels B and C were reprinted with permission from Ref [50] (copyright 2012 ACS), and panel A was adapted with permission from Ref [49] (copyright 2014 ACS).

2.2 PEG-specific immunity in animal models

2.2.1 The first report of anti-PEG Abs in vivo

Because proteins are generally excluded from densely PEG-coated surfaces, it is

convenient and intuitive to assume that PEG should be immunologically inert and escape binding by antibodies. However, in 1983, less than a decade after the introduction of protein PEGylation, Richter and Akerblom reported the generation of PEG-specific antibodies following intramuscular (i.m.) or subcutaneous (s.c.) injections of various PEG-modified proteins in Complete Freund's Adjuvant [51]. In contrast, they found that free PEG (MW 10-5.9 x 10^3 kDa) administered under similar conditions exhibited little to no immunogenicity. This landmark study demonstrated for the first time that antibodies can be formed against PEG polymers. Later studies confirmed that not only can anti-PEG Abs be elicited by immunization with PEGylated proteins [52, 53], but also that the induction of PEG-specific immunity can occur in the absence of adjuvants [54, 55].

2.2.2 Accelerated blood clearance of PEGylated systems is attributed to anti-PEG Abs

While single doses of PEGylated therapeutics often demonstrate extended system circulation times *in vivo*, some PEGylated systems exhibit rapid elimination upon repeated administration. For example, Moghimi and Gray reported in 1997 that when long-circulating polystyrene particles coated with poloxamine 908 (a PEG-containing surfactant) were administered 3-4 days after an initial dose, the particles were swiftly cleared from systemic circulation by MPS cells in rats [56]. Similarly, Dams *et al*. and several other groups observed that repeated weekly dosing of empty PEG liposomes also significantly reduced the circulating half-lives of the subsequent doses (Fig. 2.2a), with a corresponding increase in liver accumulation and hepatic clearance (Fig. 2.2b), as well as moderate increases in splenic accumulation (Table 2.1) [33, 57-60]. This unexpected effect was termed the "accelerated blood clearance" (ABC) phenomenon, and the biological factors underlying the phenomenon remained

unclear for a number of years after its discovery. Because the infusion of "naïve" mice with plasma from animals pre-dosed with poloxamine-coated polystyrene beads failed to generate an ABC effect, Moghimi and Gray suggested that the observed phenomenon was not due to plasma factors but rather potentially resulted from an change in phagocyte receptor expression and/or activity elicited by the initial particle dose [56]. In contrast, Dams *et al*. reported that the transfusion of blood or serum from rats pre-treated with PEGylated liposomes generated an ABC effect and observed that this effect was dependent on the presence of a heat-labile, 150-kDa serum factor. Because ABC was observed for serum depleted of IgG or IgM, they proposed that the observed effect was likely due to complement protein(s) [33]. However, because the extent of IgM depletion appeared incomplete, the involvement of residual IgM could not be discounted. Although Laverman *et al*. did not identify the specific immune factors responsible, they observed that the ABC phenomenon occurs in two phases: the induction phase, when the immune system is primed by the initial injection, and the effectuation phase, when the pharmacokinetics and biodistribution of the PEGylated therapeutics are affected by the resulting immune response [60].

Since then, mounting and irrefutable evidence has established that anti-PEG Abs can be elicited by PEGylated systems and is likely responsible for the observed ABC that can greatly alter the pharmacokinetics and efficacy of PEGylated therapeutics *in vivo*. Ishida *et al*. first observed that the serum of pre-treated rats, as compared to naïve animals, demonstrated greater antibody adsorption onto PEGylated liposomes, suggesting that antibodies were the dominant serum factor responsible for the ABC effect [61, 62]. Soon afterwards, the same group reported that intravenous injection of PEGylated liposomes strongly induced the production of PEG-specific antibodies (Fig. 2.2c) [63], and the presence of these antibodies was correlated with hepatic clearance [34]. Cheng *et al*. demonstrated that the injection of monoclonal anti-PEG IgM

into naïve mice resulted in the rapid clearance of PEGylated therapeutic proteins (e.g., 38-fold reduction in systemic concentration compared to uninjected control) [55, 64]. Numerous other groups have subsequently corroborated the relationship between anti-PEG Abs and the ABC phenomenon [65-70]. The observed anti-PEG Ab response is predominantly IgM [34, 69, 71, 72], although the development of anti-PEG IgG has also been reported (Fig. 2.2c and d, Table 2.1) [53, 65, 73].

Anti-PEG Ab-mediated complement activation may also be involved in the MPS clearance of repeatedly dosed PEGylated therapeutics. Antibodies, particularly IgM, can efficiently activate the complement system, and opsonization by complement proteins such as C3b facilitates particle phagocytosis and clearance. Serum from rats generating an ABC response demonstrated complement activation upon incubation with PEGylated liposomes [74], and heat-treatment (complement inactivation) of this serum abrogated the first-pass hepatic clearance of PEGylated liposomes [75]. A proteomics analysis indicated that, after the induction of anti-PEG Abs, PEGylated liposomes are predominantly bound by plasma IgM and complement proteins (i.e., C1, C3) in mice [76]. Additionally, complement proteins can disrupt liposomal membranes; indeed, the leakage of cargo epirubicin from PEG-liposomes was associated with complement activation [77] Altogether, these results suggest that complement can play an important role in the ABC of PEGylated liposomes, although the role of complement in the ABC of various non-liposomal PEGylated systems (e.g., polymeric nanoparticles, proteins) remains to be further investigated.

The development of anti-PEG Abs and its resulting effects on clearance has been reported not only in a variety of animal models, ranging from rodents, rabbits, and canines to non-human primates [33, 52, 70, 78], but also for different classes of PEGylated systems,

including polymeric nanoparticles, micelles, adenovirus, and proteins (Table 2.1) [54, 68, 79]. Across fifteen studies, the presence of anti-PEG Abs reduced the circulation half-lives of PEGylated agents by 2- to 10-fold on average and increased the hepatic and splenic accumulation by roughly 2- to 5-fold and 1- to 2-fold, respectively. These results clearly underscore the potency and impact of anti-PEG immunity, which represents a particularly important concern in light of increasing number of PEGylated therapeutic proteins and nanomedicines that are FDA-approved or currently in clinical development. Indeed, recent FDA guidelines recommend screening for anti-PEG Abs when evaluating the potential immunogenicity of therapeutic proteins [80].

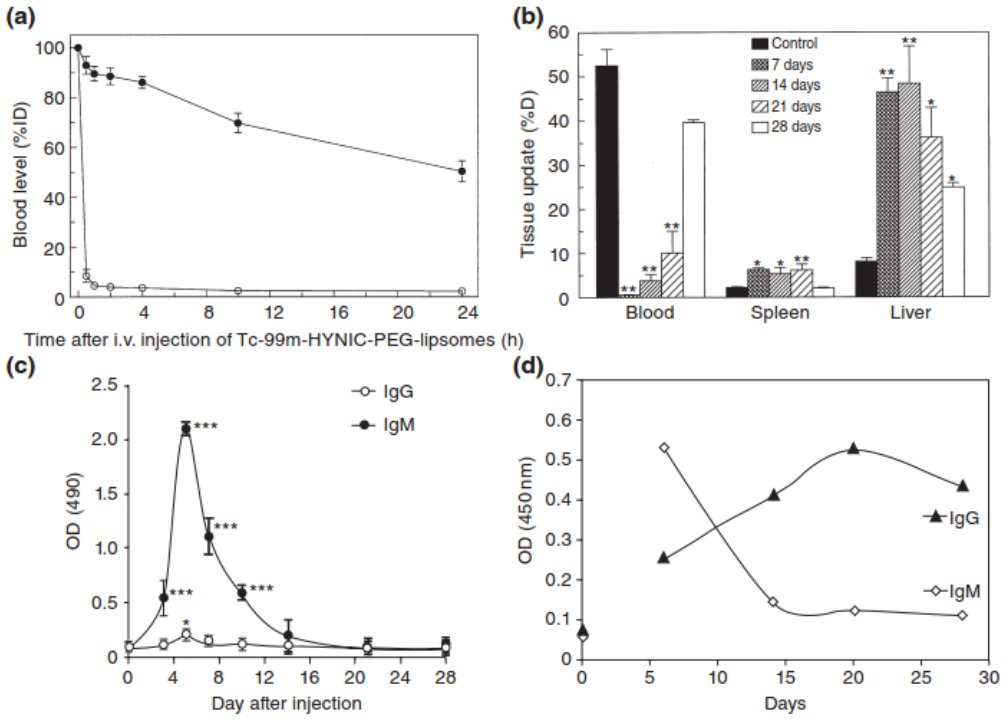

Figure 2.2. Accelerated blood clearance and anti-PEG antibodies in animal models. **a)** Amount of ^{99m}Tc-labeled PEGylated liposomes remaining in circulation after i.v. administration in rats quantified by scintigraphic image analysis. (●) indicates the first dose, and (○) indicates the second dose given 7 days later. **b)** Tissue biodistribution of ^{99m}Tc-labeled PEGylated liposomes in rats for the initial injection (control) and for second doses given after 7, 14, 21, or 28 days. *$p < 0.05$, **$p < 0.01$. **c)** PEG-specific antibodies responses after an initial injection of PEGylated liposomes (0.001 μmol/kg) in rats, as

determined using ELISA. *$p < 0.05$, ***$p < 0.005$. **d)** PEG-specific antibodies responses after an initial injection of PEGylated liposomes (100 μg/animal) in mice, as determined using ELISA. Panels A and B were reprinted from Ref [33]; panel C was reprinted from Ref [63] with permission from Elsevier; and panel D was reprinted from Ref [65] with permission from Elsevier.

2.2.3 Immunological mechanism(s) of anti-PEG Ab induction

Given PEG's well-documented anti-fouling properties, the induction of PEG-specific antibodies no doubt appears paradoxical, and the precise mechanism(s) underlying the formation of anti-PEG Abs has received much attention. To date, research efforts have primarily focused on elucidating the cellular processes involved in the generation of PEG-specific immunity in rodent models after repeated intravenous (i.v.) dosing of PEGylated liposomes.

In both rats and mice, splenectomy prior to or immediately following the injection of an initial dose of PEGylated liposomes dramatically reduced the extent of anti-PEG IgM responses, whereas splenectomy performed 4 or more days after the initial injection did not eliminate the ABC of PEGylated systems, suggesting that splenic cells serve as the primary site of anti-PEG Ab induction [54, 61, 72, 81]. In addition, the ABC phenomenon appears to involve B cells functioning through T-cell independent (TI) mechanisms, as T cell-deficient nude mice, but not SCID mice (B and T cell-deficient), generated an ABC response to both empty and nucleic acid-containing PEGylated liposomes [72, 81, 82]. In general, marginal zone B cells are involved in immune responses to TI antigens [83]. Consistent with a TI response to PEG, splenic marginal zone B cell depletion in rats eliminated the formation of PEG-specific IgM antibodies, and PEGylated liposomes are initially localized in the marginal zone upon repeat injection [84].

Due to PEG's structural similarity to other highly repetitive polymeric antigens such as microbial polysaccharides, the research groups of Kiwada and Ishida have explored the possibility of a type 2 T-cell independent (TI-2) mechanism (Fig. 2.3) [19, 83]. In this proposed mechanism, the initial dose of a PEGylated therapeutic first enters the spleen, where it comes in

contact with marginal zone B cells and crosslinks surface antibodies present on these cells, triggering the production of PEG-specific IgM antibodies. Then, the induced anti-PEG IgM binds to subsequent doses of PEGylated agents in the circulation and activates complement binding, ultimately resulting in hepatic clearance through Kupffer cell uptake [19].

While the majority of published findings on the induction of anti-PEG are consistent with this TI-2 mechanism, there are a small number of studies that present contrasting results. TI responses typically do not induce significant memory or antibody class switching unless there is strong co-stimulation by non-cognate immune cells and/or secreted factors such as cytokines (e.g., IL-1, IL-6, TNFα) [85-87]. While IgM is indeed the dominant anti-PEG Ab isotype observed, a few studies have reported anti-PEG IgG responses [53, 65, 73]. For example, Judge *et al*. observed a strong initial IgM response that was replaced by an elevated IgG response (peaks at day 7 and 20, respectively) after a single dose of PEGylated liposomes (Fig. 2.2d) [65]. Whether PEG-specific IgG was formed due to exceptional B cell stimulation that generated class switching or to the induction of anti-PEG Abs through non-TI-2 mechanisms remains unclear. The ABC phenomenon was also elicited after the s.c. injection of PEGylated solid nanoparticles, leading Zhao *et al*. to suggest that regional lymph nodes can also directly produce anti-PEG immune responses [88]. However, because a minor amount of the s.c. administered nanoparticles were distributed to the spleen, the involvement of splenic lymphocytes cannot be excluded. Additionally, macrophage depletion prior to an initial dose of PEGylated liposomes completely abrogated the ABC of subsequent doses of PEGylated liposomes in rats, suggesting the potential dependence of anti-PEG Ab induction on non-B cell populations as well [60].

Reflective of the immunological pathway(s) responsible for the formation of anti-PEG immunity, there are also substantial variations reported for the formation of long-term memory

responses. In many studies, the ABC effect is generated 3-7 days after the initial dose (Fig. 2.2a and b) and diminishes over the period of a couple weeks [67, 72]. Nevertheless, Semple *et al*. did report an anti-PEG IgM response that persisted for at least 50 days in dogs (1, 2, 3, or 7 d dosing intervals), highlighting the potential for long-term ABC responses *in vivo* and the need to further evaluate not only acute but also long-term anti-PEG Ab responses [81].

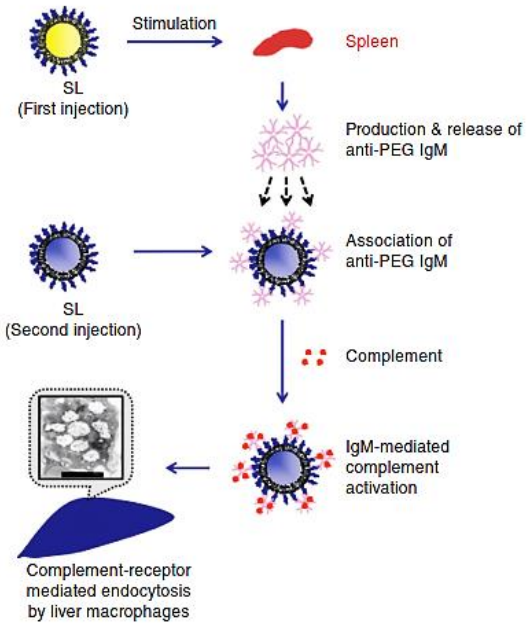

Figure 2.3. Proposed type-2 T-cell independent (TI-2) response mechanism for the formation of anti-PEG Abs and the ABC effect. Splenic B cells are stimulated by an initial dose of PEGylated therapeutic and produce anti-PEG IgM. These antibodies then associate with subsequent doses of PEGylated systems and activate complement proteins, which then opsonize PEGylated system and lead to its eventual clearance through hepatic MPS cells. Reprinted from Ref [19] by permission from Macmillan Publishers Ltd.

2.2.4 Properties of the anti-PEG Ab epitope

How anti-PEG Abs specifically bind to PEG polymers remains a mystery, as is the antigenic determinant that leads to anti-PEG Ab responses. As noted above, TI-2 antigens are typically composed of identical, repeating epitopes that crosslink B cell receptors to generate significant and prolonged activation of B cells without co-stimulation by T cells [19, 83]. The

typical PEG chain lengths for modified nanoparticles and proteins are approximately 1-5 kDa and 5-40 kDa, respectively, which covers a range from several tens to hundreds of ethylene glycol subunits and could readily and extensively crosslink any receptors capable of binding PEG. Richter and Akerblom reported hapten inhibition of anti-PEG Ab precipitation with PEG of 300 MW, suggesting that the antigenic epitope of PEG may consist of a 6-7 subunit region [51]. This value has been commonly cited as the size of the anti-PEG Ab binding epitope. Nevertheless, a recent study observed that tri(ethylene glycol) (MW 150-160) was bound by anti-PEG Abs in direct and competitive ELISAs (see section 2.5 for methods of anti-PEG Ab detection) [89]. We have likewise found that both anti-PEG IgM and IgG can bind to polymers composed of repeating methacrylate PEG_{300} subunits (Fig. 2.4). Together, these findings suggest that the anti-PEG Ab binding epitope could be smaller than the proposed 6-7 subunit length.

Since free PEG is known to be non-immunogenic, the antigenic determinant for anti-PEG Abs has been suggested to occur at the linkage between PEG and other materials. Based on the observations that anti-PEG Abs induced by hydrophobic PEGylated micelles were able to bind to PEGylated liposomes, and vice versa, whereas hydrophilic PEGylated micelles avoided the induction of and opsonization by anti-PEG Abs, Shiraishi *et al*. proposed that the anti-PEG Ab epitope is the interphase between a hydrophobic core and conjugated PEG groups [69]. Nevertheless, because free PEG can inhibit anti-PEG Ab binding in competitive ELISAs and hemagglutination assays [51, 52], at least some of the observed anti-PEG Ab responses must be specific to PEG itself. Due to the disparity in the immune responses to free PEG versus PEGylated therapeutics, as well as the frequent immunogenicity of therapeutic agents that require PEGylation, PEG has been proposed to function as a hapten (i.e., a molecule that elicits immune responses only when conjugated to a carrier agent) [35, 37].

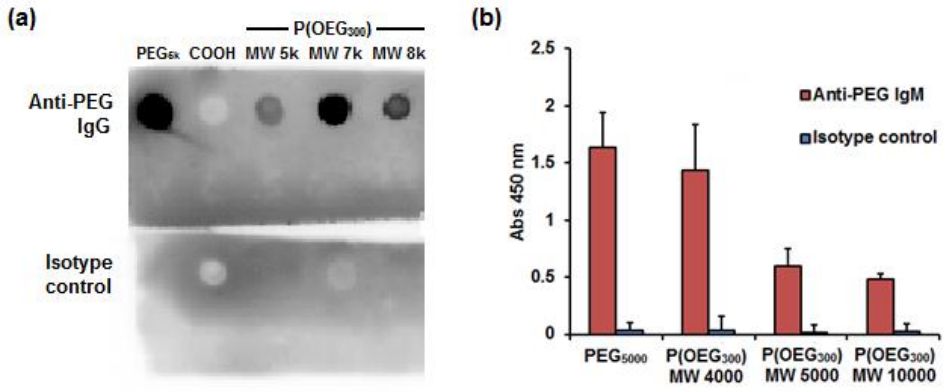

Figure 2.4. Preliminary studies of mouse anti-PEG IgG and IgM binding to poly(methacrylate PEG$_{300}$) [P(OEG$_{300}$)]. **a)** Dot blot of mouse anti-PEG IgG binding to unmodified polystyrene beads (COOH) or polystyrene beads coated with PEG$_{5k}$ or P(OEG$_{300}$). **b)** Binding of mouse anti-PEG IgM antibodies to magnetic polystyrene beads coated with PEG$_{5k}$ or P(OEG$_{300}$) was determined using ELISA.

2.2.5 Factors influencing the formation of anti-PEG immunity and ABC in animals

The ABC phenomenon and immune responses to PEG are affected by a number of factors such as the dosing regimen [67], animal model [78], drug/cargo incorporation [90], nanocarrier/protein identity and composition [51, 59], and PEG structure [54, 91]. For example, the dosing interval that generates a maximal ABC response is dependent on the timing for anti-PEG Ab formation, which typically peaks at 3-7 days post-injection (Fig. 2.2a and b). Additional doses administered after less than 48 h or more than 4 weeks typically exhibit extended circulation times comparable to the initial dose [92, 93]. High doses of PEGylated therapeutics can also influence anti-PEG Ab formation, likely due to the induction of immune tolerance or B cell anergy [34, 62]. Encapsulated drug cargo can also play a key role in PEG-specific immune responses to PEGylated nanocarriers. For example, the incorporation of immunostimulatory substances such as CpG DNA enhances anti-PEG Ab responses [94], while the loading of cytotoxic chemotherapeutics can directly suppress anti-PEG Ab induction [60, 95, 96], likely through the direct killing or impaired proliferation of B cells. Additionally, the presence of endotoxins, which can elicit strong inflammatory responses, may have potentially affected the

immunogenicity of the administered PEGylated agents; however, only a small number of studies reported testing for endotoxin contaminants [56, 65, 81]. The composition and physicochemical properties (e.g., size [68, 97], lipid membrane rigidity [78], curvature, PEG density and terminal groups [52, 54, 66]) of PEGylated systems can also affect anti-PEG Ab induction and ABC responses. For an excellent review of these various factors, please refer to Ref [19].

2.3 Anti-PEG immunity in humans

PEGylation has been critical to the success of numerous therapeutic agents currently on the market, including uricase, interferon-α, and liposomal doxorubicin, as well as many protein and nanomedicines currently drugs in clinical trials [30, 98, 99]. However, a growing body of evidence clearly suggests that the induction of anti-PEG Abs is possible in humans. In contrast to most animal studies, the anti-PEG Ab response in humans is more skewed towards IgG isotype antibodies (Table 2.2). Interestingly, we and others have found that a significant fraction of the normal population actually possesses pre-existing anti-PEG (i.e., the presence of PEG-specific antibodies in the absence of treatment with PEGylated therapeutics), which may become even more prevalent in the years ahead [100]. Both pre-existing and induced anti-PEG Abs present significant challenges to the clinical efficacy of PEGylated therapeutics [37, 100].

2.3.1 Pre-existing anti-PEG Abs in the general population

In 1984, Richter and Akerblom first observed that 0.2% and 3.3% of normal subjects and untreated allergy patients, respectively, exhibited relatively high titers of mostly anti-PEG IgM (Table 2.2) [101]. Almost 20 years later, Armstrong *et al*. reported a much higher incidence rate of 27-28% among normal healthy subjects [100]. Interestingly, they observed predominantly

PEG-specific IgG, with 19%, 5%, and 3% of the total individuals possessing IgG only, IgM only, and both IgM and IgG antibodies, respectively. The reasons for the discrepancy in the observed anti-PEG Ab incidence rates are unclear. Both studies utilized passive hemagglutination of PEG-modified RBCs to detect PEG-specific antibodies, so the differences are unlikely to be caused by the method of detection. In light of the decades-long gap between the reports, these variations could reflect a substantial increase in the prevalence of pre-existing anti-PEG Abs in the general population, but this hypothesis has not been carefully assessed.

How pre-existing anti-PEG are generated in individuals who have never received any formal treatment with PEGylated therapeutics remains largely unknown. As a GRAS product, PEG is widely used in cosmetics, processed foods, pharmaceuticals, agriculture, and industrial manufacturing. PEG-containing surfactants, as well as PEG itself, are found in the vast majority of household and hygiene products (e.g., soap, shampoo, toothpaste, lotion, detergent). It is natural to assume that frequent exposure to PEG could lead to the inevitable formation of anti-PEG Abs, but this constant exposure does not offer insight into the actual mechanism(s) underlying anti-PEG immunity. While we have no direct supportive evidence to date, we wish to offer the following speculation: the human body is frequently subjected to insults (e.g., abrasions, lacerations, skin tears) that may result in local inflammatory responses and recruitment of immune cells. Due to the ubiquitous presence of PEG in products used in daily life, as well as in many disinfecting agents (e.g., soaps and detergents used to clean wounds), PEG is likely present at or introduced to sites of inflammation. The presence of PEG in close proximity to highly active immune cells, particularly in an immunostimulatory environment containing microbes and/or bactericidal chemicals, may be sufficient to drive the induction of

anti-PEG Abs. Subsequent persistent exposure to PEG-containing products may further induce a robust memory immune response to the polymer.

Beyond the initial reports by Richter and Akerblom and by Armstrong *et al*., the prevalence of pre-existing anti-PEG Abs has been further reported in both healthy donors and untreated controls of clinical trials (Table 2.2). Tillmann *et al*. observed an incidence rate of 7%-8% in healthy individuals and in hepatitis and lupus patients, whereas 44% of hepatitis C patients were found to be positive for anti-PEG Abs prior to treatment with PEGylated interferon [102]. Treatment-naïve gout and hemophilia patients and patients with phenylketonuria demonstrated pre-existing anti-PEG Ab incidence rates of 19%, 6%, and 16%, respectively [103-105]. In addition, 38% of pediatric leukemia patients receiving unmodified asparaginase were also found to possess anti-PEG Abs [106]. Importantly, the relatively high incidence rate in this study was observed for patients with a mean age of 8.8 years, suggesting that anti-PEG Abs can be developed relatively early in life.

2.3.2 Induction and effects of anti-PEG Abs in individuals treated with PEGylated therapeutics

Studies of PEGylated therapeutics in humans began nearly three decades ago, but early results indicated that anti-PEG Ab responses were non-existent or clinically insignificant in humans. In a clinical trial of PEG-modified allergens, 50% of allergy patients had high anti-PEG Ab titers after one year of hyposensitization treatment, compared to 3.3% of untreated patients [101]. However, the occurrence of anti-PEG Abs did not appear to prime further immune responses, as the anti-PEG Ab incidence rate decreased to 28.5% in patients receiving two years of treatment. The potential effect of anti-PEG Abs on the efficacy of hyposensitization treatment or adverse effects was not examined. Ten of seventeen patients (59%) treated with PEG-

modified bovine adenosine deaminase (PEG-ADA, Adagen) generated IgG anti-PEG-ADA antibodies, but competitive ELISAs using ADA and different PEGylated proteins indicated that these antibodies were formed against ADA rather than the PEG moiety [107]. In a study of hepatitis C (HCV) patients, the presence of pre-existing anti-PEG Abs in 44% of the patients did not appear to affect the efficacy of antiviral PEG-interferon therapy [102]. The potential reasons for the apparent lack of anti-PEG Ab effects, including immune impairment and hepatic damage caused by HCV, were not explored.

Unlike most studies that report anti-PEG Ab responses in only a subset of patients, 100% of phenylketonuria patients developed PEG-specific Abs within 6 weeks of a s.c. injection of PEGylated phenylalanine ammonia lyase (PEG-PAL) [103]. Although the authors found that neither pre-existing nor induced anti-PEG Abs appeared to influence the efficacy of a single dose of PEG-PAL, peak therapeutic efficacy was observed on day 6, whereas testing for anti-PEG Abs was performed on days 0, 14, 28, and 42. Thus, the potential effects of the observed anti-PEG responses on the activity of multiply-dosed PEG-PAL is unclear. Importantly, two patients in the study later experienced severe adverse reactions to i.m. injections of medroxyprogesterone acetate, which contains both free PEG and polysorbate as excipients. While there is insufficient data to prove causation or statistical significance, this observation indicates that future studies should also investigate whether anti-PEG responses may impact not only the repeated administration of PEGylated therapeutics but also the use of pharmaceutical formulations comprising free PEG or PEG-containing chemicals excipients.

The correlation between the presence of anti-PEG Abs and reduced therapeutic efficacy of PEGylated drugs has been observed for only two PEG-modified proteins to date: PEG-asparaginase (PEG-ASNase) and PEG-urate oxidase (PEG-uricase, pegloticase) (Table 2.2). In

pediatric acute lymphoblastic leukemia patients treated with PEG-ASNase, anti-PEG IgM antibodies were observed in 46% of the patients, and the presence of anti-PEG Abs was strongly correlated with the rapid clearance of PEG-ASNase and loss of protein activity (Fig. 2.5a) [106]. In contrast, anti-PEG Abs present in patients treated with unmodified ASNase exhibited no effect on therapeutic protein clearance or activity (Fig. 2.5b). Because serum samples were only collected after treatment, it is not clear whether the observed anti-PEG Abs were induced or pre-existing. However, given that 38% of patients treated with control ASNase also exhibited anti-PEG Abs, the authors suggested that the antibodies observed in the PEG-ASNase group were likely pre-existing.

In the earliest clinical trial of PEG-uricase, 38% of refractory gout patients developed anti-PEG Abs, which was correlated with poor efficacy, after a single s.c. injection of the PEGylated drug [98]. This PEG-specific antibody response demonstrated apparent class switching, with IgM and IgG predominating at days 3-7 and 7-14, respectively, after injection. One patient was later re-challenged with PEG-uricase and demonstrated an anamnestic antibody response to the PEGylated protein [98]. In a separate study, anti-PEG Ab responses were generated in 35% of gout patients after a single i.v. infusion of PEG-uricase, and anti-PEG Ab formation also associated with rapid protein clearance [108]. Additionally, one patient with a pre-existing anti-PEG Ab response exhibited a correspondingly reduced half-life for PEG-uricase.

Repeated dosing of PEG-uricase generated two distinct patient populations: responders (sustained low plasma uric acid levels) and non-responders (early decrease in plasma uric acid levels followed by a rebound to baseline levels) (Fig. 2.5c) [22, 109]. The production of high titer anti-PEG-uricase antibodies, most of which appeared to be specific to PEG (Fig. 2.5d), was

correlated with the loss of PEG-uricase activity [22]. Similar results were obtained in a study by Hershfield *et al.*, with 37% of treatment-naïve patients establishing an anti-PEG Ab response and non-responsive to PEG-uricase treatment by the end of the clinical trial; half of these anti-PEG Ab responses were pre-existing [104]. Three patients that received PEG-uricase during previous studies (1-3 years prior) were also non-responsive to the new round of treatment, exhibiting loss of PEG-uricase efficacy earlier than the affected treatment-naïve patients (2-7 days vs. ~2 weeks). Interestingly, of the demographic characteristics (e.g., age, gender, BMI, renal function) examined during the repeated dosing studies, only age (>60-70 years) and organ recipient status, both of which involve some level of immunoinsufficiency, were found to be associated with reduced anti-PEG Ab formation [22, 104]. In addition to rapid PEG-uricase clearance, anti-PEG Ab-positive individuals also demonstrated an increased rate of infusion reactions [98, 104, 109], but the precise involvement of anti-PEG Abs in adverse reactions to PEG-uricase and other PEGylated therapeutics remains unclear [35].

In recent clinical trials of pegnivacogin, a PEGylated RNA aptamer, the presence of pre-existing anti-PEG Ab has alarmingly been associated with first-dose allergic reactions to the PEGylated drug. A phase IIb study of pegnivacogin was terminated after 3 patients (out of 640) developed serious allergic reactions, one of which was deemed life-threatening, within less than thirty minutes of a first dose of the drug [17]. Competitive ELISA analysis of the patient samples indicated that all three patients possessed high levels of pre-existing antibodies against PEG (>97th percentile for all analyzed samples), but no antibodies against the aptamer itself. In a subsequent phase III trial, pre-existing anti-PEG Ab were also linked with severe allergic reactions to pegnivacogin [110]. Eighty-three percent of patients with severe allergic reactions to treatment possessed anti-PEG Ab at baseline, compared to 15% of patients who did not

experience any adverse reactions. For patients with anti-PEG IgG levels one- or three-fold above the assay cutoff point, the likelihood of experiencing a severe allergic reaction was 5% and 16%, respectively. The authors suggested that the presence of both high anti-PEG Ab levels and large dose of PEGylated drug (~0.8 PEG mg/kg, i.v. bolus) was a key factor in the observed anaphylactic responses, although other unidentified contributing factors are also likely involved [17, 110].

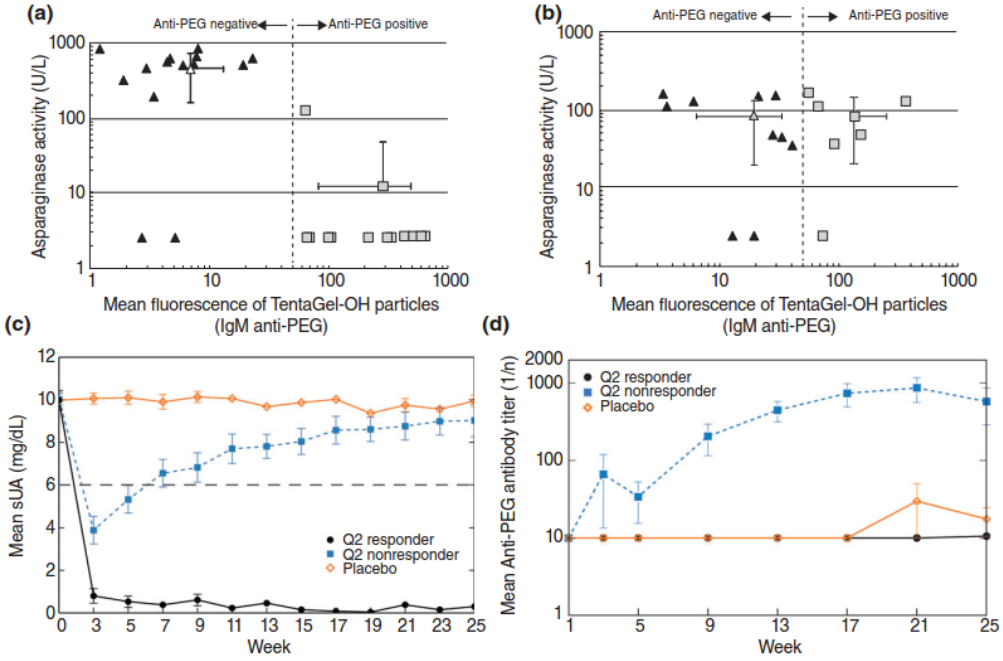

Figure 2.5. Anti-PEG antibodies in human patients. Anti-PEG IgM vs. asparaginase (ASNase) activity for patients treated with **a)** PEG-ASNase and **b)** ASNase. Flow cytometry was used to detect anti-PEG Abs bound to PEG hydrogel (TentaGel-OH) particles. **c)** Mean serum uric acid (sUA) levels in patients receiving biweekly i.v. infusions of PEG-uricase. Normal sUA levels are typically defined as ≤6 mg/dL (indicated by gray dashed line). **d)** Mean anti-PEG Ab titers in patients receiving biweekly i.v. infusions of PEG-uricase. Panels A and B were reprinted from Ref [106], and panels C and D were modified from Ref [22].

2.3.3 Clinical implications of and strategies to overcome anti-PEG Abs

The first-dose allergic reactions to pegnivacogin and the reduced efficacy of PEG-ASNase and PEG-uricase in the presence of anti-PEG Abs highlights the potential impact of

PEG-specific immune responses on the growing clinical use of PEGylated therapeutics and underscores the need to incorporate testing for anti-PEG Abs in clinical trials of PEG-containing drugs. Standard laboratory tests (see section 2.5) that can quantitatively and accurately measure anti-PEG Ab levels and determine a patient's anti-PEG Ab status are crucial to this effort, as suggested by others [21, 35, 111]. Importantly, clinical trial designs must screen for pre-existing anti-PEG immunity, as well as monitor treatment history, since previous exposure to PEGylated therapeutics could prime future responses to subsequent therapy with PEGylated drugs. Furthermore, the true extent of anti-PEG Abs in the human population and the factors that lead to anti-PEG Ab immunity must be further investigated.

In addition to an improved understanding of the prevalence and development of anti-PEG immunity in humans, strategies to avert or overcome anti-PEG Ab responses must be developed. Unfortunately, the effect of important dosing regimen factors identified in animal studies remains to be fully evaluated in human subjects. In the clinical trials of PEG-uricase, neither the dose (0.5-24 mg/patient), dosing interval (2-4 weeks), nor route of administration (s.c. or i.v.) appeared to affect anti-PEG Ab induction or its effects [22, 98, 104], but these results must be corroborated for other PEGylated drugs. The use of cleavable or sheddable PEG has been demonstrated to decrease or eliminate anti-PEG Ab and ABC responses *in vivo* [65, 81, 112], but the rapid loss of the stealth PEG coating also significantly reduces the circulation half-life and may render the modified therapeutics ineffective. As was observed for a small number of organ transplant recipients, co-treatment with immunosuppressive agents may be able to effectively reduce anti-PEG Ab induction [104], but these drugs also can generate undesirable side effects and health risks that may contraindicate their use in patients with existing illnesses [113]. Once the precise mechanisms of human anti-PEG Ab induction are better understood, the use of drugs

that specifically target immunological pathways related anti-PEG immunity may allow the specific suppression of anti-PEG Ab generation while avoiding unwanted side effects.

The use of alternative stealth polymers such as chitosan, poly(carboxybetaine), poly(2-oxazaline), XTEN peptide, and poly(glycerol) has also received growing attention [114-117]. These polymers are less ubiquitous in everyday household items and thus may not encounter the problem of pre-existing antibodies. Nevertheless, antibodies against various natural and synthetic repeating polymers have been reported [118, 119], suggesting that stealth polymers other than PEG may also prove immunogenic upon repeated administration in humans. In individuals with induced or pre-existing anti-PEG Abs, the elimination of circulating anti-PEG Abs could be achieved through selective plasmapheresis, although the use of such a complicated procedure clearly poses additional cost burdens and may not be warranted if alternative strategies to remove anti-PEG Abs are available. Additionally, it may be possible to overwhelm PEG-specific immune responses by simply administering a much greater dose of the PEGylated therapeutic [60, 81, 120]. Nevertheless, dosage increases will obviously be limited by the maximum tolerated dose and potential toxicity to various clearance organs. A conceptually similar but more desirable approach would be to first saturate pre-existing anti-PEG Abs with free, low molecular weight PEG. Indeed, Moghimi reported that the administration of free PEG and PEG-containing molecules 1-3 h prior to a second dose of poloxamine-modified polystyrene beads reduced the ABC of these particles in rats [121]. Further animal and human studies are needed to confirm the safety and efficacy of such a strategy.

2.4 Ongoing questions regarding anti-PEG antibodies

There are many questions related the phenomenon of anti-PEG Abs, particularly as it applies

to human patients, that are of great interest to the scientific and clinical communities. While a full discussion of these questions is beyond the scope of this review, we wish to highlight a few of them below:

- *How are anti-PEG Abs able to specifically bind PEG polymers?* Due to PEG's flexible, neutral, and hydrophilic character, the precise antibody-polymer interactions that allow anti-PEG Abs to specifically bind to such an amorphous target in the absence of hydrophobic and electrostatic interactions are of interest.
- *What is the immunological pathway of anti-PEG Ab formation in humans?* The features of human anti-PEG Ab responses (i.e., pre-existing anti-PEG Abs, high prevalence of IgG, and memory responses to PEGylated products) suggests that the mechanisms underlying PEG-specific immunity may differ greatly between humans and animal models currently used to study anti-PEG immunity. Due to the difficulty of performing mechanistic studies in humans, the use of animal models that more accurately recapitulate human anti-PEG Ab responses are necessary to improve our understanding of anti-PEG immunity, including that elicited by long-term exposure to PEG and PEG-containing products.
- *What factors predispose individuals towards anti-PEG Ab formation and are certain portions of the human population more, or less, inclined towards anti-PEG immunity?* The majority (≥50%) of patients treated with PEGylated therapeutics do not appear to develop anti-PEG Abs, and the reasons underlying the incongruity of anti-PEG immune responses remain largely unknown. Increased age and immunosuppressive treatments were found to be associated with reduced anti-PEG Ab induction in response to PEG-uricase [22, 104]. Further analysis of patients receiving PEGylated therapeutics may

identify other factors that affect PEG-specific immunity, as well as reveal additional strategies to manage anti-PEG Ab responses.

- *What is the current and likely future prevalence of pre-existing anti-PEG Abs?* The reported prevalence of anti-PEG Abs varies significantly, with values ranging from as low as 5% to over 40%. Thus, a precise estimate of the level of anti-PEG Abs in both the general and special populations is sorely needed. Additionally, given the disparity in the incidence rate between early and more recent studies, the potential for further increases in the prevalence of pre-existing anti-PEG Abs must be explored.
- *How can anti-PEG immunity be efficiently and effectively managed in a clinical setting?* Strategies to overcome pre-existing and/or induced anti-PEG Abs, including the administration of an excess dose of PEGylated therapeutic or prior injection of free PEG polymer, should be further investigated.

2.5 Detection of anti-PEG Abs by validated ELISA methods

Anti-PEG Abs have been detected in animal models and humans using a variety of methods, including passive hemagglutination, immunodiffusion, flow cytometry, Western blotting, and enzyme-linked immunosorbent assays (ELISAs) [51, 65, 73, 106]. Of these methods, ELISAs can simultaneously provide high sensitivity, rapid screening of multiple samples, and antibody isotype/subclass detection. As a result, most recent studies have used ELISAs almost exclusively to analyze anti-PEG Ab responses. However, for many reports of anti-PEG Abs, particularly those using animal models, antibody specificity to the PEG moiety was not always thoroughly confirmed. Indeed, most in vivo studies of treated animals only performed direct ELISAs using plates coated with the same PEGylated material (e.g., PEG-lipid)

that was injected; thus the possibility that induced antibodies were actually bound to the carrier rather than PEG itself cannot be fully discounted. As noted by others, there is a critical need for more rigorous, validated anti-PEG Ab detection methods [35, 100]. In our opinion, both direct and competitive ELISAs should be used in combination to confirm the PEG-specificity of anti-PEG Abs with the application of proper controls and conditions (see Fig. 2.6), as was carried out in some recent human trials [22, 98, 104]. Standard curves can be generated using commercially available anti-PEG Abs (e.g., mouse, rat, rabbit, chicken, goat, and monkey host Abs) to quantify induced or pre-existing anti-PEG Abs. Additionally, the validation of ELISA protocols (e.g., determination of precision, sensitivity, reagent interference) must be performed and reported [22, 104]. Importantly, the use of Tween and other PEG-containing detergents must be avoided, as they can significantly reduce the sensitivity of anti-PEG Ab detection assays [52]. The development of standardized laboratory tests that can quantitatively and accurately measure anti-PEG Ab levels is crucial to furthering our understanding of anti-PEG immunity.

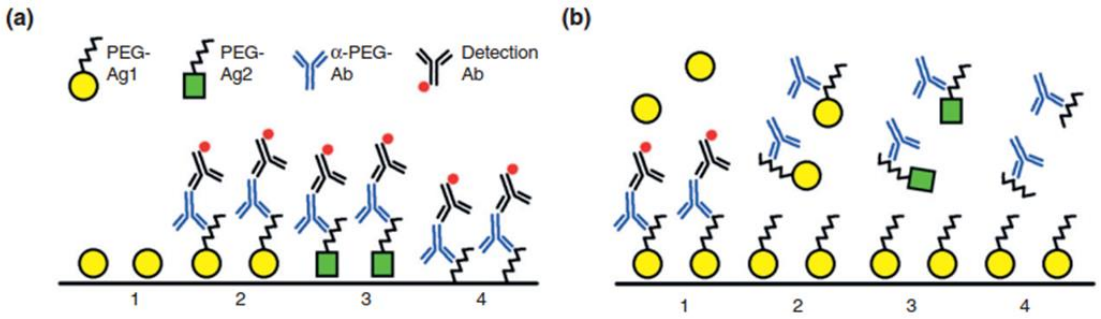

Figure 2.6. ELISA methods for detection of anti-PEG antibodies. a) Direct and **b)** competitive enzyme-linked immunosorbent assays (ELISAs) should be used in combination to determine the PEG-specificity of Ab responses induced after treatment with a PEGylated agent (PEG-Ag1), as well as pre-existing anti-PEG Abs. In direct ELISAs, PEG specificity can be confirmed by the cross-reactivity of anti-PEG Abs to plates coated with pure PEG polymers (see a4) or other PEGylated materials (see a3). In competitive ELISAs, PEG specificity can be confirmed via the inhibition of anti-PEG Ab binding by increasing concentrations of free PEG (see b4) or other PEGylated materials (see b3). Additionally, anti-PEG Abs should not directly bind to non-PEGylated treatment agents (see a1) nor be competitively inhibited in their presence (see b1).

2.6 Conclusions

Because of its ability to significantly prolong the circulation of nanoparticles and proteins, as well as its presumed lack of immunogenicity, PEG has been widely used to modify various therapeutic agents. However, a growing body of evidence indicates that potent and specific antibody responses can be generated against the PEG polymer, and anti-PEG Ab induction can lead to substantial reductions in the circulation half-life and therapeutic efficacy of PEGylated drugs in both animal models and humans. In light of the relatively high prevalence of pre-existing and induced anti-PEG Ab responses observed in clinical studies, PEG-specific immunity will likely pose a major challenge to the increasing number of PEGylated therapeutics used in the clinic. An improved understanding of the precise means by which anti-PEG Abs develop and are able to bind to the polymer are needed, as are strategies to overcome the challenge of PEG-specific immunity.

Table 2.1. Examples of anti-PEG Ab and/or accelerated blood clearance responses to PEGylated systems.

Type of PEGylated system	Animal model	Dose*,†	Dosing interval*	Parameters of initial or control dose	Parameters of subsequent dose(s)	Fold change in parameters‡	Anti-PEG Ab response#	Ref
PEGylated liposome	Balb/c mice	0.01-1 µmol PL/kg	5-7 d	N.D.	N.D.	-	IgM + (no to weak) IgG	[72]
PEGylated liposome	Std:ddY mice	25 µmol PL/kg	10 d	$t_{1/2,\beta}$ **12.9** h Cl **0.07** mL/h $AUC_{0\text{-}24h}$ **486**%dose·h/mL	$t_{1/2,\beta}$ **6.3** h Cl **0.2** mL/h $AUC_{0\text{-}24h}$ **221**%dose·h/mL	**0.5** ($t_{1/2,\beta}$) **2.9** (Cl) **0.5** ($AUC_{0\text{-}24h}$)	N.D.	[57]
PEGylated liposome	KM mice	0.1 µmol PL/kg (initial); 5 µmol PL/kg (subsequent)	6 d	**44%**$ID_{blood,4h}$ **13%**$ID_{liver,4h}$ **12%**$ID_{spleen,4h}$	**14%**$ID_{blood,4h}$ **28%**$ID_{liver,4h}$ **18%**$ID_{spleen,4h}$	**0.3** ($\%ID_{blood,4h}$) **2.2** ($\%ID_{liver,4h}$) **1.5** ($\%ID_{spleen,4h}$) **0.2** ($t_{1/2}$), **0.2** (AUC)º	IgM§	[78]
PEGylated liposome	Wistar rats	0.001 µmol PL/kg	-	N.D	-	-	IgM + (weak) IgG	[63]
PEGylated liposome	Wistar rats	5 µmol PL/kg	7 d	$t_{1/2,\alpha}$ **2.4** h **52.5%**$ID_{blood,4h}$ **8.1%**$ID_{liver,4h}$ **2.2%**$ID_{spleen,4h}$	$t_{1/2,\alpha}$ **0.1** h **0.6**%$ID_{blood,4h}$ **46.4%**$ID_{liver,4h}$ **6.3**%$ID_{spleen,4h}$	**0.04** ($t_{1/2,\alpha}$) **0.01** ($\%ID_{blood,4h}$) **5.7** ($\%ID_{liver,4h}$) **2.9** ($\%ID_{spleen,4h}$)	N.D.	[33]
PEGylated liposome	Wistar rats	0.001 µmol PL/kg (initial); 5 µmol PL/kg (subsequent)	4-6 d	$t_{1/2}$ **14.8** h Cl_h **<1** mL/min **8%**$ID_{liver,24h}$ **8%**$ID_{spleen,24h}$	$t_{1/2}$ **0.3-1.8** h Cl_h **25-55** mL/min **67-72%**$ID_{liver,24h}$ **8-12%**$ID_{spleen,24h}$	**0.02-0.12** ($t_{1/2}$) **>25-55** (Cl_h) **8.4-9.0** ($\%ID_{liver,24h}$) **1.0-1.5** ($\%ID_{spleen,24h}$)	IgM	[71]
PEGylated liposome	Wistar rats	0.001 µmol PL/kg (initial); 5 µmol PL/kg (subsequent)	5 d	**51%**$ID_{blood,24h}$ **6%**$ID_{liver,24h}$	**<2%**$ID_{blood,24h}$ **68%**$ID_{liver,24h}$	**<0.02** ($\%ID_{blood,24h}$) **11** ($\%ID_{liver,24h}$)	IgM + (weak) IgG	[61]
PEGylated liposome	Wistar rats	5 µmol PL/kg	7 d	**76.4%**$ID_{blood,4h}$ **15%**$ID_{liver,4h}$	**0.6%**$ID_{blood,4h}$ **68%**$ID_{liver,4h}$	**0.01** ($\%ID_{blood,4h}$) **4.5** ($\%ID_{liver,4h}$)	N.D.	[60]
PEGylated liposome	Sprague-Dawley rats	7 µmol PL/kg	7 d	$t_{1/2}$ **16.7** h Cl **1.7** mL/h AUC **856** µg·h/mL	$t_{1/2}$ **0.2** h Cl **74.3** mL/h AUC **17** µg·h/mL	**0.01** ($t_{1/2}$) **43.7** (Cl) **0.02** (AUC)	IgM§	[68]
PEGylated liposome	Dunkin-Hartley guinea pigs	0.1 µmol PL/kg (initial); 5 µmol PL/kg (subsequent)	6 d	**34%**$ID_{blood,4h}$ **12%**$ID_{liver,4h}$ **<2%**$ID_{spleen,4h}$	**12%**$ID_{blood,4h}$ **37%**$ID_{liver,4h}$ **<2%**$ID_{spleen,4h}$	**0.4** ($\%ID_{blood,4h}$) **3.1** ($\%ID_{liver,4h}$) **~1** ($\%ID_{spleen,4h}$) **0.6** ($t_{1/2}$), **0.6** (AUC)º	IgM§	[78]
PEGylated liposome	Rhesus monkey	5 µmol PL/kg	7 d	$t_{1/2}$ **87.5** h **17.6%**$ID_{liver,4h}$	$t_{1/2}$ **14.2** h **41.2%**$ID_{liver,4h}$	**0.2** ($t_{1/2}$) **2.3** ($\%ID_{liver,4h}$)	N.D.	[33]

Type of PEGylated system	Animal model	Dose*,†	Dosing interval*	Parameters of initial or control dose	Parameters of subsequent dose(s)	Fold change in parameters‡	Anti-PEG Ab response#	Ref
PEGylated liposome	Rabbits	9 mg PL/animal	7 d	N.D.	N.D	-	IgG¶,Δ	[73]
PEGylated liposome	Japanese white rabbits	0.1 μmol PL/kg (initial); 5 μmol PL/kg (subsequent)	6 d	**47%**$ID_{blood,4h}$ **15%**ID_{liver} **4%**ID_{spleen}	**13%**$ID_{blood,4h}$ **35%**ID_{liver} **6%**ID_{spleen}	**0.3** (%$ID_{blood,4h}$) **2.3** (%$ID_{liver,4h}$) **1.5** (%$ID_{spleen,4h}$) **0.5** ($t_{1/2}$), **0.4** (AUC)ᵠ	IgM§	[78]
PEGylated pDNA liposome	ICR mice	100 μg pDNA/animal	7 d	**80%**$ID_{blood,1h}$ **8%**$ID_{liver,1h}$ **2%**$ID_{spleen,1h}$	**23%**$ID_{blood,1h}$ **41%**$ID_{liver,1h}$ **4%**$ID_{spleen,1h}$	**0.3** (%$ID_{blood,1h}$) **5.1** (%$ID_{liver,1h}$) **2.0** (%$ID_{spleen,1h}$)	IgG + IgMΔ	[65]
PEGylated ODN vesicles	ICR mice	50 mg PL/kg, 10 mg ODN/kg	7 d	**70%**$ID_{blood,1h}$	**6%**$ID_{blood,1h}$	**0.1** (%$ID_{blood,1h}$)	IgM§	[81]
PEGylated Gd liposome	C57BL/6 and Balb/c mice	5 μmol PL/kg	7 d	**11%**$ID_{blood,6h}$ **9%**$ID_{liver,6h}$ **10%**$ID_{spleen,6h}$	**<0.5%**$ID_{blood,6h}$ **31%**$ID_{liver,6h}$ **1%**$ID_{spleen,6h}$	**<0.05**(%$ID_{blood,6h}$) **3.4** (%$ID_{liver,6h}$) **0.1** (%$ID_{spleen,6h}$)	IgMΔ	[69]
PEGylated Hb vesicles	ddY mice	0.1 mg Hb/kg	7 d	$t_{1/2}$ **2.7** h Cl **3.7** mL/h AUC **27.1**%dose·h/mL	$t_{1/2}$ **1.3** h Cl **22.3** mL/h AUC **4.5**%dose·h/mL	**0.5** ($t_{1/2}$) **6.0** (Cl) **0.2** (AUC)	IgM	[122]
PEGylated EPI liposome	Wistar rats	1 μmol PL/kg, 0.08 EPI/kg (initial); 5 μmol PL/kg, 0.4 mg EPI/kg (subsequent)	7 d	**52%**$ID_{blood,4h}$ **16%**$ID_{liver,4h}$ **8%**$ID_{spleen,4h}$	**8%**$ID_{blood,4h}$ **36%**$ID_{liver,4h}$ **15%**$ID_{spleen,4h}$	**0.2** (%$ID_{blood,4h}$) **2.3** (%$ID_{liver,4h}$) **1.9** (%$ID_{spleen,4h}$)	IgM§	[77]
PEGylated DXR liposome	Beagle dogs	0.67 μmol PL/kg and 2 mg DXR/m^2	3 wk	$t_{1/2}$ **24.1** h Cl **1.5** mL/h/kg $AUC_{0-\infty}$ **76.0** μg·h/mL	$t_{1/2}$ **1.5** h Cl **127.8** mL/h/kg $AUC_{0-\infty}$ **0.6** μg·h/mL	**0.06** ($t_{1/2}$) **85.2** (Cl) **0.01** ($AUC_{0-\infty}$)	IgM§	[120]
PEGylated TOPO liposome	Beagle dogs	0.5 mg TOPO/kg	7 d	C_{max} **7.9** mg/L Cl **0.4** mL/min/kg AUC_{0-t} **1.4** mg·min/mL	C_{max} **1.7** mg/L Cl **6.7** mL/min/kg AUC_{0-t} **0.1** mg·min/mL	**0.2** (C_{max}) **16.8** (Cl) **0.07** (AUC_{0-t})	IgM§	[66]
PEGylated solid lipid nanoparticle	Wistar rats	5 μmol PL/kg (initial s.c., subsequent i.v.)	7 d	AUC_{0-4h} **27.3** mg·h/L **8** μg/g (liver, 4 h) **9** μg/g (spleen, 4 h)	AUC_{0-4h} **6.6** mg·h/L **25** μg/g (liver, 4 h) **26** μg/g (spleen, 4 h)	**0.2** (AUC_{0-4h}) **3.1** (liver, 4 h) **2.9** (spleen, 4 h)	IgM§	[88]
PEGylated solid lipid nanoparticle	Kunming mice	10 μmol PL/kg	7 d	**71.3**%$ID_{blood,0.5h}$ **5.4**%$ID_{liver,0.5h}$ **4**%$ID_{spleen,0.5h}$	**42.6**%$ID_{blood,0.5h}$ **23.3**%$ID_{liver,0.5h}$ **9**%$ID_{spleen,0.5h}$	**0.6** (%$ID_{blood,0.5h}$) **4.3** (%$ID_{liver,0.5h}$) **2.3** (%$ID_{spleen,0.5h}$)	N.D.	[70]
PEGylated solid lipid nanoparticle	Beagle dogs	2 μmol PL/kg	7 d	$t_{1/2,\beta}$ **3.4** h Cl **0.2** mL/min/kg AUC_{0-24h} **90.6** mg·h/L	$t_{1/2,\beta}$ **1.6** h Cl **0.4** mL/min/kg AUC_{0-24h} **34.0** mg·h/L	**0.5** ($t_{1/2,\beta}$) **2.0** (Cl) **0.4** (AUC_{0-24h})	IgM§	[70]

Type of PEGylated system	Animal model	Dose*,†	Dosing interval*	Parameters of initial or control dose	Parameters of subsequent dose(s)	Fold change in parameters‡	Anti-PEG Ab response#	Ref
PEGylated emulsion	Wistar rats	5 µmol PL/kg	7 d	$AUC_{0\text{-}0.5h}$ **30.8** mg·h/L **50%**$ID_{blood,1h}$ **11** µg/g (liver, 12 h) **14** µg/g (spleen, 12 h)	$AUC_{0\text{-}0.5h}$ **10.8** mg·h/L **7%**$ID_{blood,1h}$ **22** µg/g (liver, 12 h) **23** µg/g (spleen, 12 h)	**0.4** ($AUC_{0\text{-}0.5h}$) **0.1** (%$ID_{blood,1h}$) **2.0** (liver, 12 h) **1.6** (spleen, 12 h)	$IgM^{§}$	[91]
PEGylated micelle	Sprague-Dawley rats	7 µmol PL/kg	7 d	$t_{1/2}$ **8.8** h Cl **3.3** mL/h AUC **442** µg·h/mL	$t_{1/2}$ **9.6** h Cl **3.5** mL/h AUC **408** µg·h/mL	**1.1** ($t_{1/2}$)◊ **0.9** (Cl)◊ **1.1** (AUC)◊	$IgM^{§}$	[68]
PEG-PBLA micelles	C57BL/6 and Balb/c mice	3 mg/kg	7 d	**65%**$ID_{blood,6h}$	**50%**$ID_{blood,6h}$	**0.8** (%$ID_{blood,6h}$)◊	$IgM^{Δ}$	[69]
PEG-PLGA ETO nanoparticles	Wistar rats	0.01-1 mg polymer/kg (initial); 20 mg polymer/kg, 8 mg/kg ETO (subsequent)	7 d	$t_{1/2}$ **3.5** h Cl **0.6** mL/min AUC **3.7** mg·min/mL	$t_{1/2}$ **1.0-1.2 h** Cl **3.2-3.3** mL/min AUC **0.6** mg·min/mL	**0.3** ($t_{1/2}$) **5.3-5.5** (Cl) **0.2** (AUC)	$IgM^{§}$	[67]
PEG-PLA PGE_1 nanoparticles	Wistar rats	133 µg PGE_1/kg	7 d	$AUC_{0\text{-}24h}$ **6.4** µg·min/mL **50%**$ID_{blood,3h}$	$AUC_{0\text{-}24h}$ **1.1** µg·min/mL **3%**$ID_{blood,3h}$	**0.2** ($AUC_{0\text{-}24h}$) **0.06** (%$ID_{blood,3h}$)	$IgM^{§,Δ}$	[79]
Poloxamine-coated polystyrene nanoparticles	Wistar rats	3.5 mg polystyrene/kg, 5-7 mg poloxamine/kg	4 d	**66.3%**$ID_{blood,3h}$ **9.4%**$ID_{liver,3h}$ **1.1%**$ID_{spleen,3h}$	**11.5%**$ID_{blood,3h}$ **50.1%**$ID_{liver,3h}$ **6.1%**$ID_{spleen,3h}$	**0.2** (%$ID_{blood,3h}$) **5.3** (%$ID_{liver,3h}$) **5.5** (%$ID_{spleen,3h}$)	N.D.	[56]
PEG-adenovirus	Wistar rats	10^{11} particles/animal	-	N.D.	-	-	$IgM^{§,Δ}$	[54]
PEG-BSA	Wistar rats	1 µg/animal	-	N.D.	-	-	$IgM^{§,Δ}$	[54]
PEG-uricase	Sprague-Dawley rats	1 mg/kg	7 d	**20-26** h ($t_{1/2,β}$)	N.D.	-	$IgM^{Δ}$	[123]
PEG-uricase, PEG-IFNα, PEG-HSA	New Zealand white rabbits	N.D.	7 d	N.D.	N.D.	-	$Ig^{ϕ,Δ}$	[52]
PEG-OVA, PEG-SOD, PEG-Rag	New Zealand white rabbits	100 µg/animal (i.m.) with Freund's adjuvant	4 wk	N.D.	N.D.	-	$Ig^{ϕ,£,Δ}$	[51]

* Treatment conditions that generated a maximal ABC and/or anti-PEG Ab response; † i.v. administration, unless otherwise indicated; ‡ fold change calculated as (subsequent dose)/(initial dose); # anti-PEG Ab detection was performed using ELISA, unless otherwise indicated; ° data not available for individual injections; § anti-PEG IgG was not evaluated; ¶ anti-PEG IgG detection was performed using Western blotting and IgM was not evaluated; Δ antibody specificity to PEG confirmed through cross-reactivity and/or competition with other PEGylated agents or free PEG; ◊ no ABC effect was observed; £ anti-PEG Abs were detected using passive hemagglutination and radial immunodiffusion; ϕ antibody isotype was not evaluated or could not be determined.

N.D., not determined or not stated; PL, phospholipid; pDNA, plasmid DNA; ODN, oligonucleotide; Hb, hemoglobin; EPI, epirubicin; DXR, doxorubicin; TOPO, topotecan; ETO, etoposide, PGE_1, prostaglandin E_1; BSA, bovine serum albumin; IFN, interferon; HSA, human serum albumin; OVA, ovalbumin; SOD, superoxide dismutase; Rag, ragweed pollen extract.

Table 2.2. Human studies and clinical trials demonstrating anti-PEG Ab responses.

PEGylated therapeutic	Dosing regimen	Anti-PEG Ab isotype*	Pre-existing anti-PEG Ab incidence rate	Induced/post-treatment anti-PEG Ab incidence rate	Effects of anti-PEG Abs	Method of anti-PEG Ab detection	Ref
PEGylated bee venom or ragweed extract	47-4,630 μg (median cumulative dose), 6-40 total weekly or biweekly injections	IgM[†]	Healthy donors: **0.2%** (1/453) high titer (≥1:32), **4.9%** (22/453) any titer Untreated allergy patients: **3.3%** (3/92) high titer (≥1:32), **20.6%** (19/92) any titer	1 treatment course: **50%** (29/58) high titer (≥1:32), **78%** (45/58) any titer 2 treatment courses: **29%** (8/28) high titer (≥1:32), **86%** (24/28) any titer	N.D.	Agglutination	[101]
PEG-IFN-2α (Pegasys®) or PEG-IFN-2β (PegIntron®)	N.D.	N.D.	Healthy controls: **7%** (2/29) NASH patients: **7%** (2/30) SLE patients: **8%** (3/40) HCV patients: **44%** (30/68)	No observed increase in anti-PEG	No observed effects on HCV antiviral treatment	ELISA	[102]
PEG-asparaginase (Oncaspar®)	1,000 U/m^2 i.v. infusion	IgG + IgM (69%) IgM (31%)	Unmodified asparaginase group: **38%** (6/16) PEG-asparaginase group: **46%** (13/28)[#]		Strongly correlated with rapid PEG-ASNase clearance and loss of activity	Agglutination, flow cytometry[Δ]	[106]
PEG-PAL	0.01-0.10 mg/kg single s.c. dose	IgG + IgM (72%) IgG (18%)	Treatment-naïve patients: **16%** (4/25)	**100%** (21/21)	No observed effect on drug efficacy; associated with adverse reactions to subsequent administration of other PEGylated therapeutics	N.D.	[103]
PEG-uricase (Krystexxa® / Puricase)	4-24 mg single s.c. dose	IgG + IgM	Treatment-naïve patients: **0%** (0/13)	**38%** (5/13)	Associated with rapid PEG-uricase clearance and loss of activity, as well as late injection site reactions	ELISA[Δ]	[98]
PEG-uricase (Krystexxa® / Puricase)	0.5-12 mg single i.v. infusion	IgG[§]	Treatment-naïve patients: **4%** (1/24)	**35%** (8/23)	Associated with rapid PEG-uricase clearance and loss of activity	ELISA[Δ]	[108]
PEG-uricase (Krystexxa® / Puricase)	8 mg biweekly or monthly i.v. infusions over 6 months	IgG + IgM[¶]	N.D.	**33%** (69/212)	Correlated with rapid PEG-uricase clearance and loss of activity, as well as increased risk of infusion reactions[¶]	ELISA[Δ]	[22]

PEGylated therapeutic	Dosing regimen	Anti-PEG Ab isotype*	Pre-existing anti-PEG Ab incidence rate	Induced/post-treatment anti-PEG Ab incidence rate	Effects of anti-PEG Abs	Method of anti-PEG Ab detection	Ref
PEG-uricase (Krystexxa® / Puricase)	8 mg i.v. infusion at 3-week intervals, 5 doses	IgG + IgM$^{\Phi}$	Treatment-naïve patients: **19%** (5/27) Previously treated patients: **100%** (3/3)	**23%** (5/22)	Associated with rapid PEG-uricase clearance and loss of efficacy, as well as a 2-fold increase in the risk of infusion reactions	ELISA$^{\Delta}$	[104]
Peginterferon beta-1a	125 µg s.c. at 2- or 4-week intervals for 1 or 2 years	IgG and/or IgM$^{£}$	Treatment-naïve patients: **6%** (82/1468)	1 year: **7%** (97/1397) 2 years: **7%** (95/1363)	No observed effect on drug efficacy or incidence of adverse effects	ELISA$^{\Delta}$	[124]
Pegnivacogin	1 mg/kg i.v. bolus	IgG§	Treatment-naïve patients: estimated **36%**	N.D.	Associated with serious allergic reactions in 3 out of 640 patients	ELISA$^{\Delta}$	[17]
Pegnivacogin	1 mg/kg i.v. bolus	IgG§	Treatment-naïve patients: **15%** (13/87) control-treated or non-allergic patients, **71%** (17/24) allergic patients, **83%** (15/18) severely allergic patients, **94%** (15/16) patients suffering allergic reactions within 1 h	N.D.	Association between anti-PEG IgG levels and the severity of allergic reactions to pegnivacogin	ELISA$^{\Delta}$	[110]
-	-	IgG (69%) IgM (18%) IgG + IgM (12%)	Healthy donors: **27-28%** (94/350-97/350)	-	-	Agglutination, flow cytometry$^{\Delta}$	[100]
-	-	IgG (43%) IgM (42%) IgG + IgM (15%)	Healthy donors: **23%** (307/1310) Hemophilia patients: **6%** (7/110)§	-	-	ELISA$^{\Delta}$	[124]

* Indicated as percentage of total anti-PEG-positive individuals; †as determined by mercaptoethanol denaturation; ‡ serum samples were typically collected after the initial dose; $^{\#}$ pre-existing and induced anti-PEG Abs could not be differentiated because anti-PEG Ab levels were determined in post-analysis; $^{\Delta}$ antibody specificity to PEG confirmed through cross-reactivity and/or competition with other PEGylated agents or free PEG; § anti-PEG IgM was not evaluated or reported; ¶results for anti-PEG-uricase antibodies, no comparable results available for anti-PEG; $^{\Phi}$ anti-PEG IgM results available for only 2 patients; $^{£}$ breakdown between anti-PEG IgG and IgM was not specified.

N.D., not determined or not reported; IFN, interferon; NASH, non-alcoholic steatohepatitis; SLE, systemic lupus erythematous; HCV, hepatitis C virus; PAL, phenylalanine ammonia lyase.

CHAPTER 3: BACKGROUND ON HETEROGENEOUS TUMOR TREATMENT AND BISPECIFIC PROTEIN-MEDIATED PRETARGETED DRUG DELIVERY[2]

3.1 Introduction

Targeted drug delivery for cancer offers the potential to significantly improve the therapeutic index of anticancer agents by increasing drug concentration at tumor sites while reducing side effects and toxicity in non-targeted tissues. A long-standing approach in the field has been to exploit the leaky tumor vasculature in tumor tissues by encapsulating therapeutic cargo into nanoparticles that remain sufficiently stable when introduced to the systemic circulation in order to reach and extravasate into cancer tissues. To further facilitate selective delivery into cancer cells, many researchers have functionalized nanoparticles with ligands that bind specific receptors on cancer cells, a strategy commonly referred to as "active" targeting [125]. Unfortunately, the accumulation of both ligand-free and ligand-conjugated systems in tumors is generally modest at best, limiting the efficacy of various therapies against cancer [126, 127].

Due to advances in the genetic and phenotypic analysis of tumors, tumor heterogeneity has recently emerged as yet another biological barrier that could limit efficient distribution, retention, and uptake of ligand-conjugated nanoparticles at tumor sites [126, 128, 129]. Tumor heterogeneity also encompasses the highly variable expression of target receptors, both intertumorally between patients or different tumors and intratumorally within a given tumor, and has been reported for a wide range of human tumors [130, 131]. Due to the absence or

[2]This chapter is based on an article that previously appeared in the Journal of Controlled Release. The original citation is as follows: Yang Q, Parker CL, McCallen JD, Lai SK. *J Control Release*. **2015**, *220*(Pt B):715-26.

suboptimal expression of their target receptor on many tumor cell subpopulations, actively targeted drug carriers, which typically consist of single-ligand nanoparticles, are unable to effectively bind and internalize into the full spectrum of tumor cells present in any particular tumor. As noted by Bae *et al*., "aiming at cancer cells with a single surface marker results in aiming at a single population among mixed populations which are constantly changing and moving" [126]. Inadequate drug delivery to all cancer cell subpopulations typically results in only partial suppression of the cancer and eventually leads to tumor regrowth and/or the emergence of therapy-refractory tumor cell populations [132-134]. Thus, targeting strategies that can directly address the challenges associated with tumor heterogeneity and enable effective delivery of nanoparticles are sorely needed.

One promising targeting strategy is to decouple molecular homing and delivery of therapeutics into two separate steps. This approach involves first introducing bispecific proteins (BsPs) that can specificially bind (i.e., "pretarget") cancer cells, followed by the administration of a drug-carrying effector such as a nanoparticle that can be captured by the BsPs accumulated on the surface of tumor cells (Fig. 3.1). By introducing multiple distinct BsPs, a single effector nanoparticle could in theory bind with molecular specificity to the full diversity of cancer cells present in any particular tumor. In this review, we will discuss the concept of, important considerations for, and key challenges associated with exploiting the pretargeted strategy to enhance the delivery of therapeutics to heterogeneous tumors.

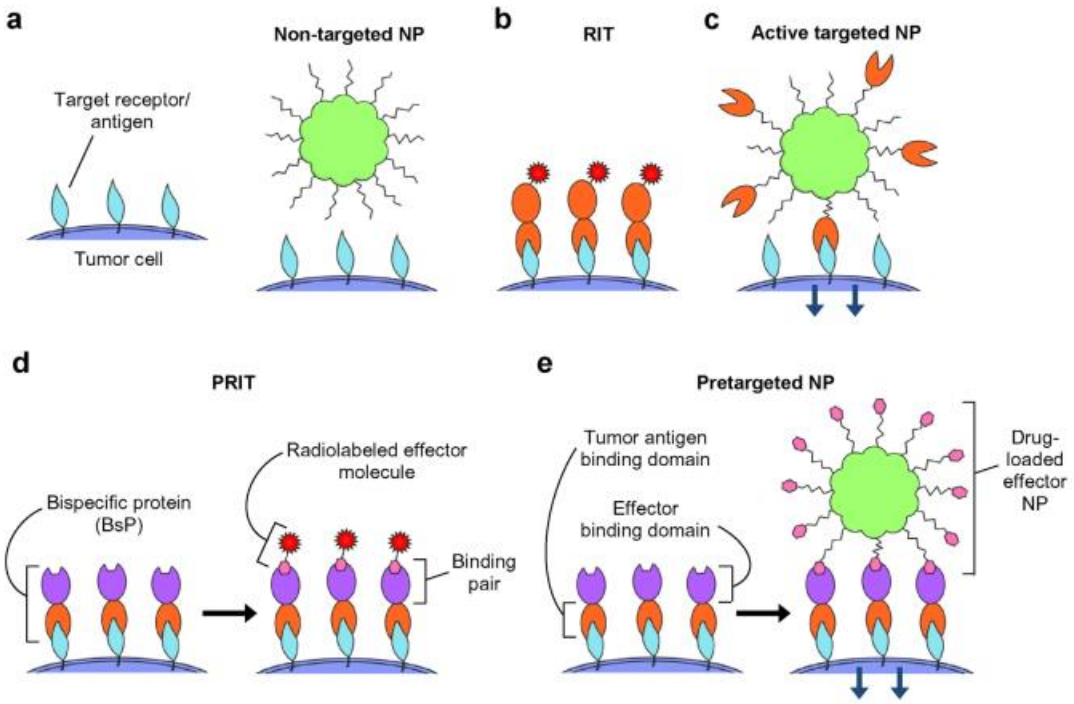

Figure 3.1. Strategies for the delivery of nanoparticle drug carriers and/or radioisotopes to tumor cells. These strategies include **a**) non-targeted, **b** & **c**) directly targeted (1-step), and **d** & **e**) pretargeted (multistep) approaches. **a**) Passively targeted nanoparticles coated solely with stealth polymers typically do not exhibit specific interactions with tumor cells. **b**) Radioimmunotherapy (RIT) uses radiolabeled tumor receptor-specific antibodies to deliver therapeutic doses of radiation to target cells. **c**) Modification with receptor-specific ligands allows the active targeting of nanoparticles (NPs) to tumor cells, which commonly induces receptor-dependent internalization. **d**) Pretargeted radioimmunotherapy (PRIT) splits tumor targeting and radioisotope delivery into sequential steps: 1) binding of bispecific proteins (BsPs) to target receptors and 2) binding of radiolabeled effector molecules to the BsPs. **e**) For pretargeted drug delivery systems, 1) bispecific proteins (BsPs) bind target receptors, and 2) a drug-loaded effector nanoparticle binds to the BsPs, which should ideally result in internalization.

3.2 Conventional cancer targeting strategies: passive targeting

In 1986, Matsumura and Maeda discovered that macromolecules can preferentially accumulate in tumors due to anatomical and pathophysiological differences between solid tumors and healthy tissue [27, 135, 136]. Specifically, tumors initiate extensive angiogenesis to maintain their rapid growth, but the newly formed blood vessels display abnormal architecture including fenestrated endothelial lining of vessel walls [135-137]. The more permeable tumor vasculature then allows macromolecules and nanoparticles to extravasate from the bloodstream

and accumulate in the tumor [136, 137]. Presumably poor lymphatic drainage further permits enhanced retention of drug delivery systems within tumors [135, 137]. The combination of leaky tumor vasculature and impaired lymphatic drainage constitute the phenomenon termed the enhanced permeability and retention (EPR) effect.

Harnessing the EPR phenomenon simply requires nanoparticles to (i) fall within an appropriate size range and (ii) evade rapid elimination by the mononuclear phagocytic system (MPS). While smaller nanoparticles can naturally extravasate more efficiently than larger nanoparticles, most studies suggest the tumor vasculature in mouse xenografts can permit extravasation of nanoparticles ranging from 10 to 200 nm in diameter [136, 138-140], with some studies reporting EPR of particles up to 500 nm in diameter [137, 141]. In addition to size, prolonged circulation kinetics also directly improve the extent of nanoparticle extravasation through leaky tumor blood vessels by maximizing the number of times a nanoparticle will pass through the tumor vasculature [135, 141]. Polyethylene glycol (PEG) was among the first "stealth" polymers used to extend liposome and other nanoparticle circulation times by minimizing opsonin adsorption and nanoparticle elimination by MPS cells, and PEGylation is the most widely adopted strategy to enhance nanoparticle tumor uptake via EPR [135-137, 141]. Other coating polymers used to improve particle circulation profiles, and thereby exploit the EPR effect, include flexible, hydrophilic polysaccharides such as dextran, hyaluronic acid, and chitosan [142, 143]; synthetic polymers such as polyvinyl alcohol [144] and polyvinylpyrrolidone [145]; zwitterionic polymers [146, 147]; and polyoxazolines [148]. Indeed, dextran-, hyaluronic acid-, chitosan-, and N-(2-hydroxylpropyl) methylacrylamide (HPMA)-coated particles all exhibited improved EPR-mediated tumor accumulation due to prolonged circulation [28, 149-151]. Because nanoparticles of the appropriate size and with MPS-resistant

surface chemistry can naturally achieve a low to moderate level of tumor targeting without using specific ligands, these non-molecularly targeted systems are frequently classified as *passively targeted*.

It is important to note that the EPR effect is highly variable and may not be readily exploitable for all tumors [152]. For example, hepatocellular and renal cell carcinomas are characterized by high vascular density and exhibit increased EPR effects compared to low vascular density pancreatic and prostate cancers that demonstrate diminished EPR effects [152, 153]. Additionally, EPR of drug carriers is not observed homogenously throughout individual tumors, as the central foci of tumors tend to be characterized by necrotic [152, 154], hypoxic [152, 155], and hypovascular areas [135] that do not display the EPR effect [27, 156, 157]. EPR heterogeneity may also vary between primary tumor and metastases [125]. Therefore, harnessing EPR to enhance therapeutic responses in the clinic requires an improved understanding of how tumor heterogeneity impacts the EPR effect both within and between tumors [125, 136, 152, 158, 159].

3.3 Conventional cancer targeting strategies: active targeting

To further improve nanoparticle-based delivery to cancer cells, numerous investigators have developed nanoparticles decorated with ligands specific to receptors overexpressed on cancer cells, an approach generally termed *active targeting* [125]. Ligands on actively targeted systems are typically grafted to the distal end of polymer chains that are used to coat the particles and provide prolong circulation kinetics [141]. These systems are presumed to effectively extravasate from the tumor vasculature based on the underlying stealth polymer coating, while the presence of ligands can facilitate nanoparticle binding to and subsequent internalization into

specific tumor cells expressing the corresponding receptor [141, 160]. Actively targeted systems were thought to directly address the shortcoming of inefficient cellular uptake of passively targeted systems [137, 141]. Numerous targeting ligands have been utilized to actively target nanoparticles to cancer cells, including antibodies and antibody fragments [161, 162], aptamers [163], peptides [164], proteins, sugars [165], and low molecular weight ligands such as folate [166]. For excellent reviews of the features and design of actively targeted systems, please refer to Refs [125, 141, 160, 167]

Unfortunately, active targeting systems face several challenges that may limit their efficacy in practice. The target cell surface receptors must be highly overexpressed or selectively expressed solely on malignant cells, as opposed to healthy cells, to maximize tumor-specific delivery [167-169]. Additionally, the choice and density of ligand are critical to optimizing the effect of the targeting moiety. Greater ligand density was previously assumed to enhance nanoparticle targeting to tumors *in vivo* due to generally observed improvements in cancer cell uptake *in vitro* [168]. Nevertheless, an increasingly number of studies have shown that maximal accumulation of nanoparticles in tumors *in vivo* is typically achieved with an intermediate ligand density [168, 170-173]. For example, increasing the surface aptamer density on polymeric nanoparticles actually resulted in reduced tumor accumulation and increased particle distribution in the liver [170]. The poor *in vivo* performance of particles with high ligand densities was attributed to ligand shielding or adulteration of the underlying stealth polymer coat, leading to rapid MPS clearance and a reduction in the fraction of particles that can reach and extravasate into tumors [168, 169].

3.4 Tumor heterogeneity and implications for targeted drug delivery systems

Variations in accumulated genetic mutations, which can be further exacerbated by alterations in the local tumor microenvironment, frequently lead to genomically distinct subclonal populations within the same tumor or between tumor lesions. This in turn creates a phenomenon termed tumor heterogeneity, which describes the functional and phenotypic profile differences between cancer cells such as cellular morphology, gene expression, metabolism, motility, proliferation, level of drug resistance, and metastatic potential. Additionally, the highly variable presence of stromal cell populations such as fibroblasts, immune cells, and endothelial cells within tumors is critical in shaping the tumor microenvironment [174, 175]. Interactions between the non-tumor cell populations and tumor cells contribute to different tumor phenotypes, impact tumor response to various therapies, and influence disease progression [176, 177].

Tumor heterogeneity (Fig. 3.1) encompasses both (i) intertumoral heterogeneity, which describes differences between tumors in an individual patient as well as clinical response differences between patients with the same tumor subtype, and (ii) intratumoral heterogeneity, which refers to the genetic, epigenetic, and phenotypic features that vary within malignant cell populations of the same tumor mass [178]. Intratumoral heterogeneity is further classified into spatial heterogeneity, which refers to differences between distinct anatomical regions or individual cells within a tumor, and temporal heterogeneity, which refers to changes in a tumor's molecular profile and receptor expression over time. An example of intratumoral spatial heterogeneity is the highly discordant HER2 expression observed in different areas within a single biopsy from HER2-positive metastatic breast cancer patients (Fig. 3.3a) [179]. Temporal

heterogeneity can be observed for relapsed lesions that exhibit a disparate molecular profile, compared to their original tumor.

In addition to morphological and spatiotemporal variations within the same tumor or between primary tumors, tumor heterogeneity can also directly result from metastasis. Metastatic heterogeneity (Fig. 3.2) has been observed to include (i) discordant biomarker or receptor expression between metastases arising from distinct subclonal populations in the primary tumor ("intermetastatic" heterogeneity) and (ii) heterogeneity within individual metastases ("intrametastatic" heterogeneity), which may have a substantial impact on therapeutic outcome [131, 174, 178, 180, 181]. For example, Gerlinger *et al*. reported a case of intrametastatic heterogeneity in which significant changes in the mutational profiles of spatially separated biopsy samples from primary renal-cell carcinomas and metastases were identified using next-generation sequencing [182]. Additionally, Albino *et al*. observed intermetastatic heterogeneity in a melanoma patient whose multiple metastases displayed contrasting morphologies and surface antigen expression [181]. Other studies have also investigated variable estrogen, progesterone, and HER2 receptor expression between primary breast tumors and metastases, with discordance rates that varied greatly from 18% to 54% [174, 183, 184]. Additional types of heterogeneity include non-genetic phenotypic and functional heterogeneity [184] and tumor microenvironment heterogeneity [174, 175]. Because tumor cells interact with their environment, tumor microenvironment heterogeneity exerts a crucial influence on disease progression. For example, the heterogeneous distribution of stromal cells, extracellular matrix organization, and especially hypoxic regions within the tumor microenvironment may promote metastasis and development of drug resistance [174].

Tumor heterogeneity has been reported in a wide range of human tumors such as breast [174, 179], non-small cell lung [185, 186], ovarian [174, 187-189], prostate [174, 190], and lymphoma [191] and poses a significant challenge for diagnosis, prognosis, and efficacy of molecularly-targeted therapies (Fig. 3.3b) [189, 192]. The presence of heterogeneous cancer cell populations within tumors will likely limit the efficacy of any therapeutics targeted against any single tumor-associated receptor, leading to poor/varied outcomes, including cancer recurrence and therapeutic resistance [130, 178]. For example, the heterogeneous expression of programmed death 1 (PD-1) was reported in two distinct T-cell subpopulations and differentially impacted survival in patients with follicular lymphoma [191]. Similarly, heterogeneous HER2 expression in breast cancer has prompted treatment stratification in the clinic based on receptor expression [174]. Indeed, intratumoral HER2 heterogeneity, both genetic and spatial, affected the trastuzumab treatment responses and survival of patients with HER2-positive metastatic breast cancer [179]. Only a small fraction of trastuzumab-treated patients achieved complete disease eradication, and the majority of patients developed relapsed tumors that were resistant to trastuzumab therapy due to the proliferation of HER2-negative breast cancer cells.

In addition to therapy with monoclonal antibodies such as trastuzumab, variable target receptor expression in heterogeneous tumors also presents a critical bottleneck for actively targeted drug delivery systems. The common active targeting approach, in which drug-loaded particles are surface modified with a single ligand group, cannot target and facilitate intracellular delivery to the full diversity of malignant cells. One potential strategy is the administration of a cocktail of single-ligand particles. Unfortunately, this would pose considerable challenges and substantial cost burden in the context of particle formulation and complexity in clinical evaluation [169], which has generally limited particles to one or two distinct targeting ligand

groups. More importantly, a single universal targeted nanoparticle cocktail for all patients is unlikely to succeed due to interpatient heterogeneity; inadequate levels or the complete lack of corresponding target cells for a significant fraction of the ligand-modified particles could lead to increased hepatic and splenic biodistribution and, correspondingly, reduced tumor accumulation. Alternatively, multiple different targeting ligands could be theoretically conjugated onto the surface of a single nanoparticle. However, as discussed above, increased density of ligands beyond a particular threshold will likely trigger rapid MPS clearance of the particles.

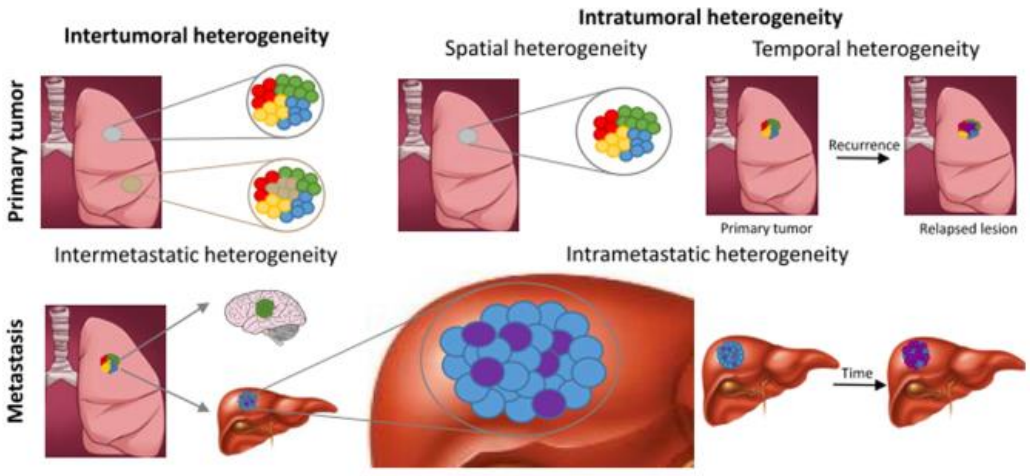

Figure 3.2. Different types of tumor heterogeneity. Spatial heterogeneity refers to differences between distinct anatomical regions or individual cells within a tumor, while temporal heterogeneity illustrates changes in a tumor's molecular profile over time. Intermetastatic heterogeneity arises from distinct subclonal populations in the primary tumor, and intrametastatic heterogeneity reflects the discordant molecular profiles of cells within individual metastases.

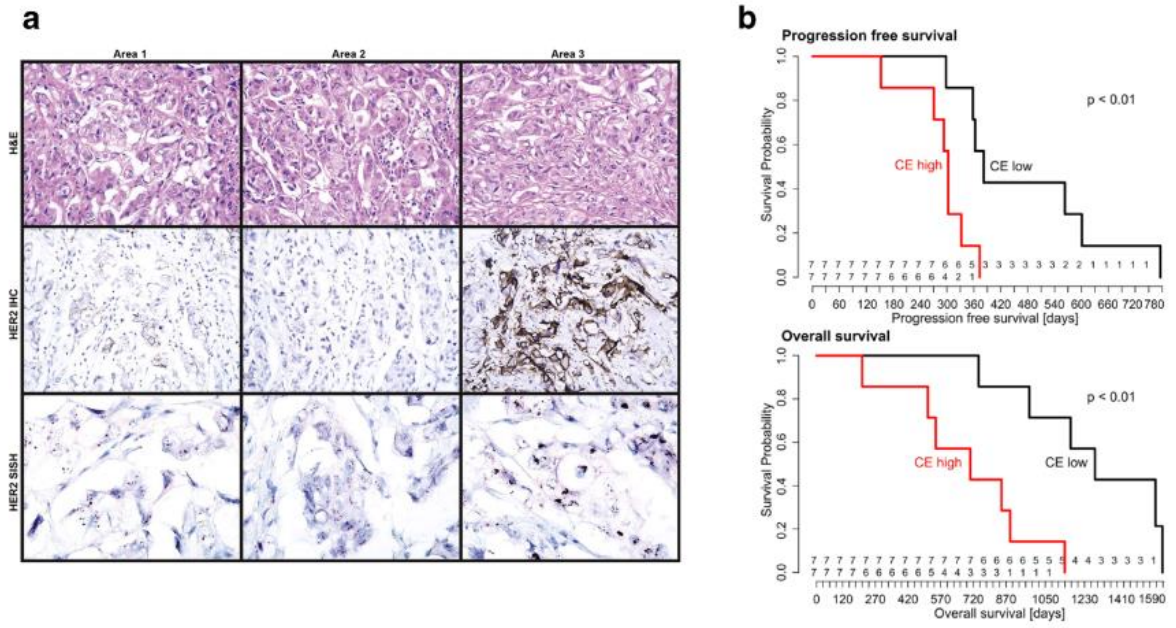

Figure 3.3. Clinical tumor heterogeneity. **a**) Spatial heterogeneity in HER2 expression between three different areas of an invasive ductal carcinoma biopsy sample. HER2 amplification was confirmed using immunohistochemistry (IHC) and silver in situ hybridization (SISH). H&E, ×200; IHC, ×200; SISH, ×400. Reprinted with permission from Lee *et al.* [179]. **b**) Progression free survival (top) and overall survival (bottom) of high-grade serous ovarian cancer patients treated with platinum-based chemotherapy and surgery, stratified by degree of clonal expansion (CE). CE reflects the accumulation of mutations that promote cell expansion into varying subclonal populations from the original cell. Higher CE is correlated with divergent subclonal populations and thus greater tumor heterogeneity. Reprinted with permission from Schwarz *et al*. [189].

3.5 Pretargeted radioimmunotherapy (PRIT)

The discovery that human tumor-associated antigens could be used as targets for antibodies to differentiate tumors from normal tissue helped spawn the field of monoclonal antibody (MAb)-based immunotherapy of cancer. The multiple applications of cancer immunotherapy include radioimmunotherapy (RIT) (Fig. 3.1b), which uses radioisotope-conjugated Mabs to treat radiosensitive tumors such as non-Hodgkin's lymphoma (NHL) [193]. Unfortunately, the therapeutic efficacy of RIT is limited by the long circulatory half-life of many MAbs, as well as high non-specific deposition of the MAbs in normal organs, resulting in low tumor-specific delivery of radiation and significant toxicity [194].

To overcome the shortcomings of radioimmunotherapy (RIT), many researchers have adopted a multistep approach (Fig. 3.1d) to more specifically deliver radionuclides to tumor cells by first injecting BsPs that contain a tumor cell binding domain and an effector binding domain. Subsequently, radiolabeled effector molecules are introduced and interact with BsPs bound on the surface of tumor cells. Such an approach has been termed pretargeted radioimmunotherapy (PRIT) [195, 196]. Because the BsPs are non-radioactive and the radiolabeled effector molecules typically consist of modified small molecule metal chelators that can be rapidly cleared, PRIT can significantly improve the therapeutic index of radioisotope treatment compared to RIT [194, 197, 198], as well as increase the maximum tolerated dose for radionuclides [196]. Pagel *et al*. demonstrated that anti-CD45 PRIT improved the specificity of radiation delivery to leukemia in a rodent model, delivering twice as much radiation to bone marrow and five times more activity to the spleen than conventional RIT [199, 200]. *In vivo* PRIT was able to mediate broad tumor growth suppression and prolonged survival with the use of BsPs against receptors expressed at different levels on lymphoma cells, with CD20 and HLA-DR proving to be superior targets compared to CD22 [201, 202]. CD38-specific PRIT achieved tumor-to-blood ratios as high as 638:1 after 24 hours for a multiple myeloma model, compared to a ratio of ~1:1 with conventional RIT [203]. Subbiah *et al*. reported that treating athymic mice bearing Ramos human Burkitt's lymphoma xenografts with a pretargeted system consisting of anti-CD20 scFv-conjugated streptavidin (SA) and ^{90}Y-DOTA-biotin cured 100% of mice with allowable toxicity, whereas conventional RIT with ^{90}Y-1F5 at the same dose produced no cures, generated profound pancytopenia, and was lethal to all mice [204]. Zhang *et al*. demonstrated that both ^{90}Y-DOTA-biotin and ^{213}Bi-DOTA-biotin could both be used in combination with anti-CD25 scFv-

conjugated SA for PRIT of a murine T-cell lymphoma xenograft model, with the beta-emitter ^{90}Y curing 10 of 10 mice and alpha-emitter ^{213}Bi curing 7 of 10 mice [205].

These encouraging results with PRIT studies in animal models led to clinical studies of PRIT, which have yielded promising results with reasonable tumor response rates and limited toxicity [206]. Forero *et al*. evaluated the pharmacokinetics and immunogenicity of an anti-CD20 scFv-SA conjugate in 15 patients with NHL [207]. Although the complete remission rate was low (2 of 15), the majority (12/15) patients exhibited no signs of hematologic toxicity, suggesting that the dose of radionuclide could be further increased. Another phase I/II PRIT clinical trial was performed using a chimeric anti-CD20 IgG-SA in combination with ^{90}Y-DOTA-biotin. Six of seven NHL patients demonstrated significant tumor regression, with an estimated tumor-to-whole body dose ratio of 38:1. While six of the ten patients developed humoral responses to streptavidin, the transient nature of the responses appeared to result in no significant long-term effects [208, 209]. Kraeber-Bodere *et al*. evaluated the therapeutic efficacy of PRIT using a bispecific monoclonal antibody that binds to carcinoembryonic antigen (CEA) and to a ^{131}I-labeled effector molecule for PRIT of medullary thyroid cancer. Of the 17 patients treated, 4 reported pain relief, 5 demonstrated minor tumor responses, and 4 achieved biological responses (decrease in thyrocalcitonin); however, 9 patients also generated human anti-mouse antibodies [210-212].

While PRIT has led the way in preclinical and clinical studies of pretargeting, it is important to note that the applications for pretargeted strategies extend far beyond radiotherapy. For example, solid cancers, which will account for more than 90% of all newly diagnosed cancer cases and deaths in the United States in 2015 [213], are significantly more resistant to radioimmunotherapy compared to hematological malignancies such as NHL. To date, little is

known about whether the pretargeting approach can enhance the delivery of other therapeutic agents such as nanoparticle drug carriers that can encapsulate and slowly release chemodrugs to solid tumors.

3.6 Pretargeted drug delivery to heterogeneous tumors

The growing interest in precision/personalized medicine, coupled with the incomplete treatment of heterogeneous cancers using common passively or single-ligand targeted therapies that can give rise to recurrent, more aggressive, and/or drug-resistant tumors [131, 178] highlights the need for alternative nanoparticle targeting strategies to improve treatment responses. The modular nature of pretargeted systems is particularly useful in addressing the challenge of and many barriers to effective drug delivery to heterogeneous tumors [174] because it enables pretargeted systems to be targeted to new or different tumor antigens by simply modifying the tumor binding domain of BsPs, as opposed to direct, ligand-based targeting systems that would require the formulation of a new nanoparticle system. This flexibility is expected to markedly reduce the production costs and complexity, as well as the potential regulatory burden, for pretargeted nanoparticles. Another equally appealing feature of pretargeting is the ability to pretarget multiple receptors simultaneously. The administration of a cocktail of pretargeting BsPs that can all bind to the same drug carrier could in theory enable the delivery of a drug carrier to the full spectrum of a patient's cancer cells (Fig. 3.4). Drug cocktails containing mixtures of different MAbs have already been applied to cancer therapy, with one combination of pertuzumab, trastuzumab, and docetaxel significantly improving the overall survival of patients with HER2-positive breast cancer [214]. Antibody mixtures have also been used for *in vitro* and *in vivo* imaging and diagnosis of tumors [215, 216]. Additionally,

pretargeting with individual or mixed BsPs was able to differentially label a range of human tumor cell lines *in vitro* (Fig. 3.5a) [217, 218]. To our knowledge, no studies have been published on the simultaneous use of multiple pretargeting BsPs to enhance nanoparticle delivery to date, although Khaw *et al*. did report the receptor-dependent efficacy of doxorubicin nanoparticles pretargeted with anti-HER2 affibody-based BsPs in a dual tumor model [219]. In that study, tumor growth inhibition was achieved for HER2-positive BT-474 breast cancer tumors, while the HER2-negative BT-20 breast cancer tumors were simultaneously unresponsive to the treatment, further emphasizing the opportunity for improved cancer treatment through appropriate targeting of all tumor cell populations.

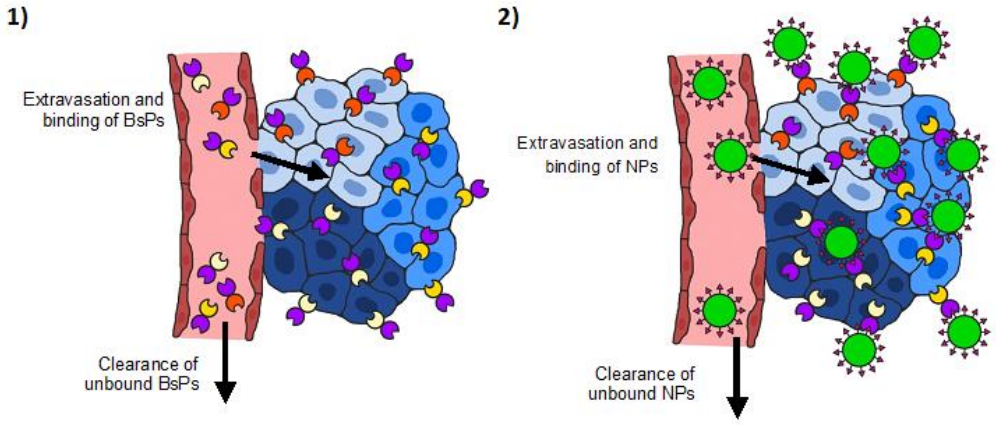

Figure 3.4. Pretargeted delivery of nanoparticles (NPs) to heterogeneous tumors. 1) A cocktail of bispecific proteins (BsPs) is administered and allowed to fully clear from systemic circulation prior to 2) dosing with nanoparticles that can be captured by BsPs on the tumor cell surface. To enable effective targeting of multiple tumor cell subpopulations using a single nanoparticle, the tumor antigen-binding domain (Figure 3.1e) of the BsPs can be modified to reflect the full diversity of tumor cells, while the effector (NP)-binding domain remains the same for all BsPs.

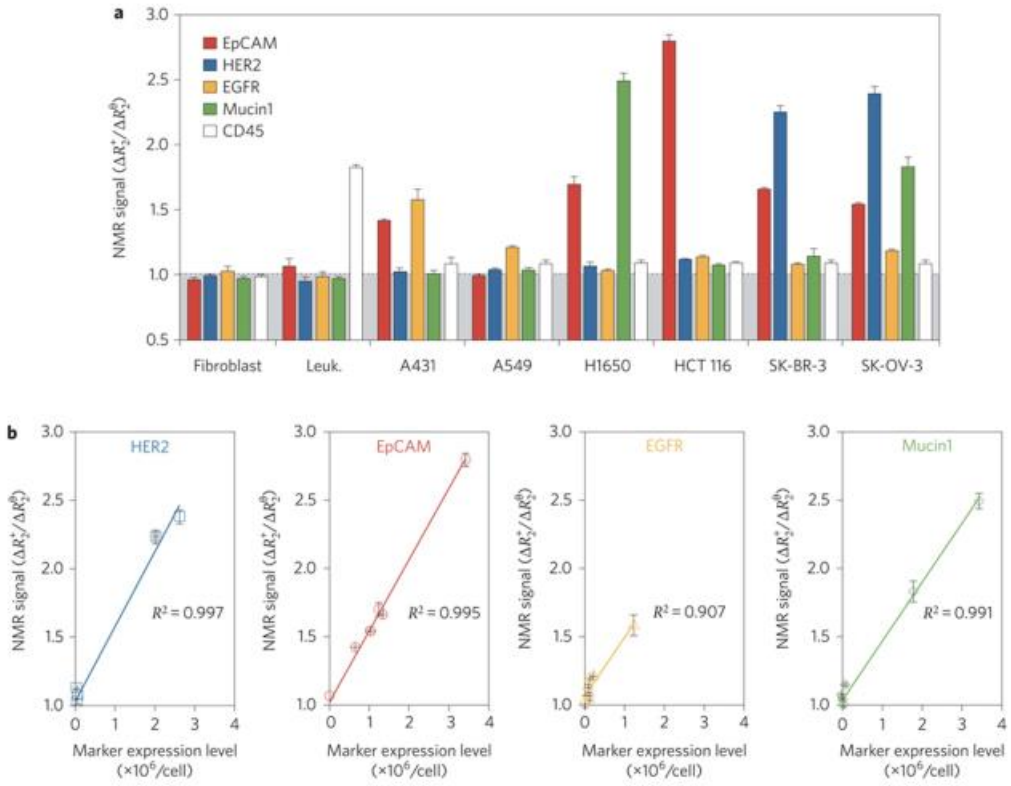

Figure 3.5. Diagnostic magnetic resonance profiling of human tumor cell lines, fibroblasts, and leukocytes using a pretargeted approach *in vitro*. The cells were labeled using various *trans*-cyclooctene (TCO)-conjugated antibodies followed by tetrazine-modified magneto-fluorescent nanoparticles (Tz-MFNPs) prior to the measurement of the transverse relaxation rate (R_2). Figure reprinted with permission from Haun *et al.* [217].

3.7 Biological and pharmaceutical aspects and considerations of pretargeted drug delivery

As multicomponent systems, the potential arsenal of pretargeted therapies is sizeable and highly diverse. Thus, many features (e.g., choice of target receptor/antigen, binding pair technology, and drug carrier) must be taken into account when developing a pretargeted drug delivery system to maximize transport of drug cargo to target cells and overall therapeutic efficacy. Because only a few publications have evaluated the use of pretargeting for nanoparticle delivery, the majority of the current knowledge about optimal pretargeted conditions have been gleaned from *in vivo* PRIT studies, but, due to the overlap of components for multistep targeting

approaches (Fig. 3.1d & e), many of the lessons learned from PRIT likely apply to pretargeted nanocarriers.

3.7.1 Binding pairs

A key consideration of any pretargeted delivery approach is the binding interaction between the pretargeting BsP and nanoparticle effector, as the affinity of the binding pair directly influences the capture and retention of the drug carrier at the tumor site. In addition, the immunogenicity of the BsP and its interactions with endogenous ligands can also alter the efficacy of pretargeted therapies [193].

The first binding pairs used in pretargeted systems were based on antibody-hapten interactions. In 1985, Reardan *et al*. reported the development of antibodies against indium chelates of EDTA, and suggested the possibility of bispecific antibodies that can simultaneously recognize target antigens and metal chelates [194, 220]. Soon afterwards, Goodwin *et al*. developed an early pretargeted imaging approach using a murine tumor model through the injection of anti-chelate antibodies, followed by the administration of a radiolabel [221]. Since then, a number of antibodies against various haptens have been utilized for binding to effector molecules, including anti-DTPA complex [222, 223], anti-peptide [224-226], anti-methotrexate [227], and anti-cotinine antibodies [228]. In addition to bispecific antibodies [223, 224, 229], a range of antibody fragments and derivatives have been developed as pretargeting BsPs [193, 228, 230]. Most antibodies, including those used to capture radioisotope-carrying effector molecules in PRIT, exhibit nanomolar to high picomolar affinity (K_D ~10^{-7}-10^{-10} M) for the antigen target on the surface of cancer cells [220, 227, 231]. Because PRIT typically uses single radionuclide-loaded agents, the improvement of antibody-hapten binding through multivalency

can significantly enhance the specificity of radioisotope localization and retention in tumor sites [224, 230, 231]. For example, the application of pretargeted bivalent haptens, termed the affinity enhancement system (AES), was able to improve the tumor biodistribution of bivalent ^{111}In-diDTPA by more than 7-fold compared to monovalent ^{111}In-DTPA (tumor biodistribution: 52.9% vs. 7.6% ID/g at 1 h and 92.5% vs. 0.9% ID/g at 72 h, respectively) [232].

As a binding pair with one of the strongest noncovalent binding affinities (K_D ~10^{-14}-10^{-15} M), the streptavidin (SA)-biotin system was quickly adopted by the pretargeting field [233, 234]. Additionally, SA is a tetravalent protein and could enable the capture of multiple biotinylated drug molecules. SA and biotin can be attached to tumor-specific pretargeting proteins and/or effector molecules through a variety of methods, including direct conjugation [204, 235, 236], genetic engineering of fusion proteins [237-239], and enzymatic conjugation [240]. While SA-based PRIT systems have demonstrated increased tumor specificity and higher therapeutic indices relative to directly targeted systems [204, 239] and have even been evaluated in clinical trials [207, 236, 241], the immunogenic nature of SA, a bacterial protein, represents a major challenge to widespread clinical use of SA-biotin binding pairs [207, 209]. The immunogenicity of SA can be reduced through site-specific mutations [242, 243], although it remains unclear whether these SA mutants will be sufficiently hypoimmunogenic to allow for repeated dosing in humans. The problem of interference from endogenous biotin [244], which necessitates the use of biotin-free feed for *in vivo* studies, could also be potentially addressed by SA mutants that selectively bind bis-biotin instead of biotin [245, 246]. Other proteins that naturally bind to specific substrates (e.g., enzymes) can also be modified to bind to exogenous molecules for use in pretargeting, although only a few such systems have been reported in the literature [247, 248].

The majority of published pretargeted and multistep targeting systems utilize antibody-hapten or protein-ligand interactions, but research in areas such as complementary synthetic nucleic acids and peptides and bioorthogonal chemistry continues to generate novel classes of binding pairs. Morpholinos (MORFs) are the most popular class of synthetic nucleic acid analogs for pretargeting using complementary nucleic acids and have been evaluated preclinically in combination with tumor-specific pretargeting antibodies and a variety of radionuclides [249-253]. In addition to relatively low immunogenicity, optimized complementary morpholinos exhibit high specificity and binding affinity [254], and the use of bivalent MORFs may further enhance affinity [255]. Bioorthogonal chemistry comprises reactions that can rapidly occur in a living system with high selectivity and without any off-target reactions or toxicity. These properties enable pretargeting using small molecule binding pairs with low immunogenicity, although the relative merits of different bioorthogonal chemistries vary based on reaction kinetics, complexity of synthesis, and stability of the resulting conjugate (see refs [193, 256, 257]). Rossin *et al*. demonstrated the feasibility of using "click" chemistry for pretargeting of radioisotopes *in vivo* by treating tumor-bearing mice with an anti-TAG72 antibody (CC49) modified with *trans*-cyclooctene (TCO), which then reacted with ^{111}In-tetrazine (^{111}In-Tz) administered 24 h later [258]. The CC49-TCO predosed mice exhibited a tumor uptake of 4.2% ID/g and tumor-to-muscle (T/M) ratio of 13.1, compared to tumor uptake and T/M ratios of 0.3% ID/g and 0.5 and 1% ID/g and 2.1 for unmodified CC49 and control Ab-TCO groups, respectively. Further preclinical studies have confirmed the utility of TCO-tetrazine and other bioorthogonal chemistries for tumor imaging and treatment [193, 259-261].

While all of the aforementioned classes of binding pairs have also been used in the pretargeting of nanoparticles and other potential drug carriers [217, 262-264], the ability of

pretargeted systems to actually deliver therapeutics to tumor cells has only been evaluated in a few studies [219, 265-267]. Pretargeted poly-lysine polymers [268], liposomes [269], and carbon nanotubes [270] have been used to deliver higher doses of encapsulated or conjugated radionuclides to both solid tumor and hematologic cancer cells, suggesting that the application of nanocarriers could further improve the efficacy of PRIT. In the context of cancer chemotherapy, pretargeted biotinylated polymeric nanoparticles loaded with pactilaxel (PTX) increased the *in vitro* cell killing of glioma and breast cancer cells, relative to free drug or Taxol and nontargeted nanoparticles [265, 266]. The injection of an anti-HER2 affibody-anti-DTPA Fab complex (BAAC) 8 h prior to the administration of ^{99m}Tc-DTPA-succinylated polylysine enabled the specific labeling of tumors (5.3% ID/g vs. 0.5% ID/g for anti-DTPA Fab-pretargeted particles) [219]. BAAC pretargeting of doxorubicin- and DTPA-conjugated polyglutamic acid produced tumor growth inhibition results that were similar to those of free doxorubicin, but pretargeting through the combination of BAAC and polymer-drug conjugate minimized weight loss in mice relative to the free drug treatment [219], underscoring the ability of pretargeting to improve the therapeutic index of chemotherapeutics *in vivo*.

Although BsP considerations such as immunogenicity and competition with endogenous ligands apply to both PRIT and pretargeted nanoparticles, other features and characteristics of binding pairs required for pretargeted drug delivery systems may differ from those for pretargeting based on small molecule effectors. Nanoparticles are inherently highly multivalent due to their large surface area, which allows the grafting of tens to possibly thousands of a given binding partner moiety. Thus, BsPs with lower affinity to a hapten may still be able to capture hapten-coated nanoparticles with high avidity compared to individual radiolabeled haptens. However, as is the case with actively targeted systems, the incorporation of peptides, nucleic

acids, proteins and other macromolecular components onto drug carrier particles could negatively impact their circulation kinetics and efficiency of extravasation into tumors. For highly asymmetric binding pairs that consist of a large protein and a smaller moiety (e.g., SA-biotin, antibody-hapten), the smaller, the more immunologically inert moiety should be assigned to the effector nanoparticle, rather than the BsP, to minimize MPS clearance. Steric considerations may further support the modification of drug carriers with smaller BsP-binding components. For instance, Haun *et al*. reported that, in addition to relatively to providing a 10- to 15-fold increase in cell binding relative to directly targeted iron oxide nanoparticles, a pretargeted antibody-TCO/Tz-NP system demonstrated significantly higher fluorescent labeling of various tumor cell lines, compared to an antibody-biotin/avidin-NP system [217]. The authors attributed this difference to the large footprint of avidin (~67 kDa) on the particles, which likely resulted in the reduced accessibility and valency of biotin-binding sites. The use of a PEG spacer for TCO-antibody modificiation also improved the pretargeting of quantum dots by reducing masking of reactive groups [271].

3.7.2 Target antigen(s)

A diverse array of receptors and other antigens overexpressed on tumor cells have been exploited for active targeting of nanoparticles and for RIT [125, 272]. In contrast, the number of target cancer antigens/receptors suitable for pretargeted approaches is certainly more limited. The multistep nature of pretargeting requires that the tumor cell-binding BsP must remain on the tumor cell surface to capture subsequently injected effector drug carriers. Indeed, the majority of PRIT studies to date utilize BsPs that target epitopes generally considered to be non-internalizing, including CD20, CD45, TAG72, and CEA [197, 207, 237, 255, 264, 267, 270].

However, Liu *et al*. observed the fairly rapid internalization of radiolabeled anti-TAG72 and anti-CEA antibodies, with about 60% of the antibodies internalized by LS174T colon carcinoma cells after 5 h [250]. Similarly, although HER2 is thought to be an internalizing epitope, pretargeting using bispecific antibodies against HER2 mediated enhanced tumor accumulation *in vivo* [219, 228, 273]. Whether these apparently counterintuitive results are due to differences in antibody internalization kinetics between *in vitro* and *in vivo* conditions (e.g., differences in receptor density, receptor turnover rates, and/or endocytosis and cell signalling pathways), dosing of the pretargeting molecules at sufficiently high levels that compensate for loss due to antigen/BsP internalization, or other factors remains unknown.

While the pretargeting molecule should initially remain non-internalized, many therapeutics require intracellular delivery to be effective and/or exhibit maximal potency; thus, the ideal pretargeted nanoparticle must be internalized only after binding of the drug carrier (Fig. 3.1). Although internalization mediated by a non-internalizing pretargeting molecule may appear paradoxical, cellular entry could be achieved by relying on the eventual endocytosis of bound receptors or, more preferably, through multivalent nanoparticle binding effects such as crosslinking of receptors. Mulvey *et al*. observed that anti-A33-MORF conjugates remained stably on the surface of LS174T cells for up to 24 h, and that the addition of complementary MORF-modified carbon nanotubes resulted intracellular punctate staining indicative of internalization (Fig. 3.6) [270]. In contrast, free complementary MORFs failed to induce internalization (Fig. 3.6). Gunn *et al*. similarly reported that iron oxide nanoparticles pretargeted to CD20-expressing cells were found in endosomes, as visualized by transmission electron microscopy [262]. These results suggest that BsPs that bind non-internalizing epitopes can still facilitate pretargeted intracellular delivery of nanocarriers.

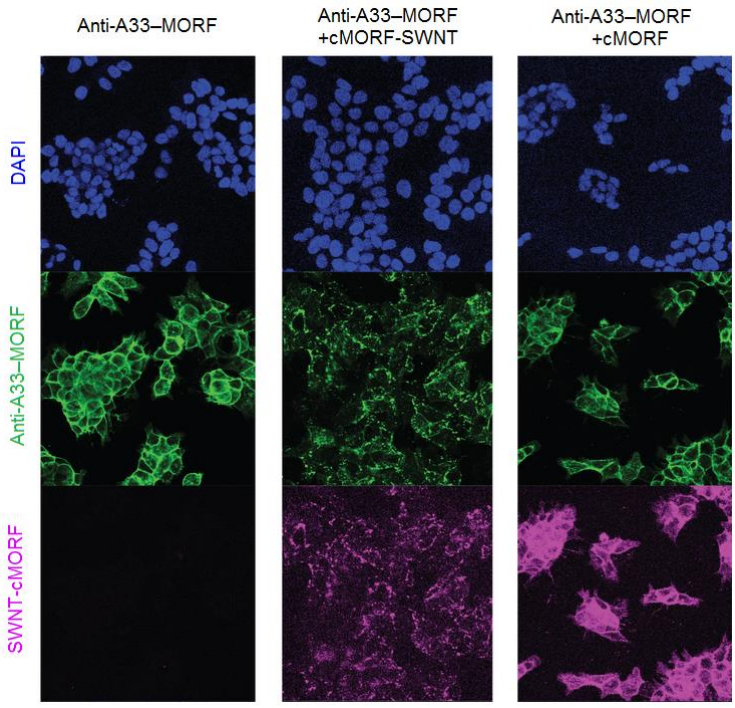

Figure 3.6. Internalization of pretargeted single-walled carbon nanotubes (SWNTs). LS174T (A33-positive) colon carcinoma cells were preincubated anti-A33 antibodies conjugated to morpholino oligonucleotide (anti-A33-MORFs) for 4 h prior to washing and further incubation with complementary MORF (cMORF)-SWNT-AlexaFluor 647 or free cMORF-AlexaFluor 647. Figure reprinted with permission from Mulvey *et al.* [270].

3.7.3 Pharmacokinetics and biodistribution

The theoretical improvements in the therapeutic index of drug delivery systems that can be achieved using pretargeting are based on the decoupling of the tumor targeting vs. drug-carrying functions. This in turn implies that the efficacy of a given pretargeted system is dependent on the pharmacokinetics and biodistribution of each component. One of the most important requirements is that the pretargeting BsPs are maximally cleared from systemic circulation prior to the administration of the drug carrier, particularly for pretargeted systems based on high affinity binding pairs such as SA-biotin. Indeed, SA-coated liposomes were detectable in circulation for at least 24 h after i.v. administration in mice, whereas SA-coated liposomes premixed with biotinylated anti-Thy1.2 antibodies prior to dosing were rapidly cleared

within 4 h [267], illustrating the potential problem of circulating BsP binding to effector nanoparticles before the particles can extravasate into the tumor. Correspondingly, Karacay *et al*. found that, while an anti-CEA IgG x anti-DTPA Fab' conjugate demonstrated superior tumor labeling relative to $F(ab')_2$ x Fab' and Fab' x Fab' constructs, the $F(ab')_2$ x Fab' conjugate provided better pretargeting of a divalent DTPA peptide due to the high residual blood concentration of IgG x Fab' even 6 days after administration [222]. In order to simultaneously optimize tumor distribution and retention along with systemic clearance, a variety of techniques have been used to modify the size, valency, and composition of pretargeting BsPs, including the "dock-and-lock" method [274, 275] and fusion protein engineering [207, 237, 247].

An alternative approach to ensure elimination of residual pretargeting molecules from the systemic circulation is the use of clearing agents (CAs) prior to the dosing of nanoparticles or therapeutic effector molecules. These multivalent agents are generally designed to bind tightly to the pretargeting molecules and are sufficiently large enough to be rapidly cleared from the systemic circulation without extravasating into tumors. Previously reported CAs include secondary antibodies [276] and avidin [277], as well as biotinylated and galactosylated human serum albumin [278] and dendrimers [200, 237]. The use of a CA can effectively purge circulating BsP molecules (reducing blood concentrations by up to 10-fold) without affecting the tumor accumulation of pretargeting molecules [237, 277, 279]. The potential drawback of CA use is the addition of yet another dose and wait step to the course of therapy. For example, the use of CAs with the sequential combination of biotinylated antibodies, SA, and finally biotinylated radionuclide resulted in a *5-step* PRIT strategy (biotinylated MAb/avidin CA/streptavidin/ biotinylated CA/biotinylated radiolabeled chelate) [280, 281]. Although the radioimmunotherapy was well-tolerated and effective in glioma patients, with a median survival

of 33.5 months (compared to 8 months for untreated control patients) in a nonrandomized phase I/II study, the need for several parenteral injections to deliver a single dose of radiation or drug not only introduces a high degree of complexity but also increases the cost of therapy. A simpler 2-step approach is likely far more preferable, particularly when using antibody-hapten binding pairs. These pretargeted systems appear to better tolerate the presence of minute amounts of uncleared pretargeting BsP, possibly due to the lower affinity and the dissociation of BsP-effector complexes formed in the blood [282].

The pharmacokinetics of the pretargeted drug carrier must also be taken into consideration. Because the commonly utilized pretargeting molecules are generally much smaller than nanoparticle drug carriers, the overall tumor distribution and accumulation of pretargeted systems is therefore limited by the circulation and extravasation kinetics of the drug carrier. To minimize premature elimination from the circulation and maximize tumor accumulation, drug carriers should be effectively coated with stealth polymers, whereas the use of bulky, charged, and/or hydrophobic moieties to facilitate particle binding to the pretargeting molecule should be avoided if possible. As noted in the previous section, this latter requirement may affect the choice of binding pair technology for pretargeted nanoparticle systems, as well as the assignment of binding pair components to the BsP and effector particle. For example, if using a SA-biotin binding system, the nanoparticle should be biotinylated, with the SA component in the pretargeting molecule, rather than vice versa.

3.8 Challenges and unknowns

The combination of a bispecific pretargeting cocktail with nanoparticle drug carriers is a promising but vastly underexplored approach to targeting nanoparticles to heterogeneous tumors.

Thus, many aspects of this proposed strategy must be rigorously evaluated to confirm its suitability for clinical applications.

One of the major challenges is that a greater dose of pretargeting BsP could potentially reduce nanoparticle binding and accumulation to tumor cells. Because tumor receptor expression varies both spatially and temporally, and receptor testing is typically performed on primary tumor biopsies obtained close to the time of diagnosis, "personalized" pretargeting cocktails based on those patient biopsy results is unlikely to capture the full heterogeneity of cancer cells in a patient over time, particularly for relapsed and/or highly metastatic tumors [130]. Thus, truly personalized pretargeted therapy would greatly benefit from improvements in noninvasive molecular profiling of cancers [178, 283]. As an alternative to the fine-tuning of individual pretargeting cocktails, the properties of BsPs could be optimized to allow rapid elimination of non-binding BsPs from the circulation. The mechanism, rate, and extent of pretargeting BsP clearance with and without the use of clearing agents must be carefully investigated, particularly since Pagel and colleagues observed that the administration of high doses of MAb-SA conjugates specific to receptors poorly expressed on certain lymphoma tumors overloaded the capacity of mice to hepatically clear MAb-SA/CA complexes, resulting in low tumor-to-normal organ biodistribution ratios and toxicity [201, 284]. The increased doses of total protein required for a cocktail pretargeting approach may also affect the immunogenicity of the pretargeting BsPs used.

Additionally, the limited number of appropriate target receptor/antibody combinations that have been evaluated for pretargeting to date may hinder the development of useful pretargeting cocktails. The main driving forces behind the discovery of novel tumor-specific receptors and their corresponding ligands/antibodies are diagnostic biomarkers, imaging

applications and targeted drug and MAb therapy. Unfortunately, few of these studies focus on *non-internalizing* antibodies, a critical requirement of pretargeting. However, the use of (pre)clincially validated ligands and therapeutic MAbs could lead to fortuitous combinations for pretargeting. For example, anti-CD20 MAbs can induce apoptosis clinically [285], and anti-CD20 Fab' fragments linked to MORFs have been found to also induce apoptosis of B-cell lymphomas *in vitro* and inhibit development of diffuse tumors *in vivo* upon crosslinking by cMORF-modified polymers [263]. The use of antibodies with inherent therapeutic efficacy for pretargeting of drug carriers could allow for synergistic treatment effects. Improvements in the generation of diverse bispecific proteins and antibodies will also certainly expand the diversity of available pretargeting molecules [274, 275, 286].

Other concerns regarding the application of pretargeted drug delivery systems include the clinical feasibility of multistep parenteral injections and the poor tumor accumulation of many drug carriers in patient tumors. Similar to passively and actively targeted nanoparticles, the tumor accumulation of pretargeted drug carriers would still rely on the EPR effect [267], which has been found to be highly variable [158].

3.9 Conclusion

Despite marked advances in biotechnology, nanotechnology and drug delivery, effective therapy for cancer remains exceedingly challenging, with few treatment options that can provide durable suppression or elimination of the tumor without resulting in eventual recurrence and/or the development of drug-resistant tumors. Emerging insights into tumor physiology have underscored tumor heterogeneity as one of the key bottlenecks to targeted therapy. The concept of pretargeting using a cocktail of bispecific pretargeting proteins combines the strengths of

precision medicine and personalized medicine by offering the potential to deliver nanoparticle therapeutics to diverse cell populations while avoiding the pharmacokinetic pitfalls typically associated with actively targeted nanoparticles. Although the radioimmunotherapy field has offered substantial evidence supporting the pretargeting strategy, its application for enhancing targeted delivery of nanoparticle therapeutics remains underexplored to date. We believe further rigorous evaluation of pretargeted NP systems is both warranted and needed to confirm whether pretargeting can indeed prove superior to current passive and active targeting approaches.

CHAPTER 4: EFFECT OF PEG DENSITY AND CONFORMATION ON IMMUNE CELL UPTAKE[3]

4.1 Introduction

Due to the flexible, neutral, and hydrophilic nature of poly(ethylene glycol) (PEG), PEG grafting can create a thick and dynamic hydration shell that renders the adsorption of biomacromolecules to PEG-coated surfaces thermodynamically highly unfavorable [7, 42, 287]. As a result, PEGylation reduces the aggregation of liposomes and other particles, as well as the adsorption of various serum proteins to the underlying particle core [40, 41, 50, 288]. These effects in turn decrease opsonization and clearance by the mononuclear phagocyte system (MPS) [31] and prolong the circulation kinetics of PEG-modified nanoparticles [32, 289, 290]. The resulting improved pharmacokinetics have been critical to the clinical success of many PEGylated therapeutics for systemic applications, including proteins [29, 291] and liposomes [99, 292]. PEG coating has similarly been used to reduce particle interactions with constituents of other biological environments, including mucus secretions [45, 293] and extracellular matrices [46, 294].

Naturally, the effectiveness of the "stealth" behavior of PEG-modified nanoparticles is critically dependent on the density and conformation of the surface PEG chains. The adopted PEG conformation is dictated by the grafting distance (D: the distance between two closest neighboring PEG anchors, which is inversely correlated to the grafting density) and the Flory radius (R_F) of the PEG coils, which is directly dependent on the PEG molecular weight. At low

[3]This chapter is based on an article that previously appeared in Molecular Pharmaceutics. The original citation is as follows: Yang Q, Jones SW, Parker CL, Zamboni WC, Bear JE, Lai SK. *Mol Pharm*. **2014**, *11*(4):1250-8.

grafting densities ($R_F/D \leq 1$), PEG chains adopt a diffuse "mushroom" conformation. At increasing grafting densities ($R_F/D>1$), the PEG chains transition into a more extended "brush" conformation [47], eventually reaching a "dense brush" regime when the PEG layer thickness exceeds the R_F by at least two-fold ($R_F/D>2.8$, see Materials & Methods section for calculation) [43, 48].

The ability to resist protein adsorption and evade clearance by immune cells is generally thought to require, at minimum, sufficient PEG coverage to coat the underlying particle core, which occurs at grafting densities at the mushroom/brush transition when PEG chains begin to overlap [4, 9, 295]. However, whether grafting at the mushroom/brush transition is sufficient to render polymeric nanoparticles effectively stealth in complex biological environments, including the systemic circulation that is rich in proteins and cells, remains not well understood. There are large variations in the circulation kinetics reported for different PEGylated nanoparticles in the literature, with some exhibiting systemic half-lives in excess of many hours but others persisting for only minutes [9, 48, 50, 296]. These differences are likely attributed in part to variations in the density of surface PEG grafting among different particle systems and formulations. For polymeric particles, differences between the chemical structures and concentrations of various polymers, as well as the properties of the organic solvents and/or surfactants utilized can all influence the efficiency with which PEG chains phase separate to or adsorb onto the nanoparticle surface [9]. In the case of liposomes, the extent of surface PEG grafting is also limited by colloidal instability due to the excess incorporation of PEG-conjugated lipids [296].

In addition to limitations in effective PEGylation, there are also significant technical hurdles associated with quantifying *surface* PEG grafting, especially on biodegradable polymeric particles [9]. Formulating particles using PEG conjugated with fluorophores or other labels at its

terminus can enable the quantitative assessment of PEG associated with particles, but these approaches fail to discriminate between *surface* vs. *embedded* PEG. Other PEG analysis methods are generally limited to specific classes of nanoparticles and often require complex methodologies and instrumentation [43, 297-299]. The presence of a PEG coating on nanoparticles is thus most frequently inferred by changes in the particle ζ-potential, which provides at best a cursory analysis confirming the presence of an indeterminate amount of PEG. Among the few papers that have specifically quantified PEG coating density, the majority report grafting densities ranging from <0.1 to at most ~1.2 PEG/nm^2 [9, 46, 48, 300].

To circumvent these challenges and gain improved mechanistic insight into the structure-function relationship between PEG coatings and their interactions in biological environments, we covalently conjugated amine-functionalized PEG to prefabricated, monodisperse polystyrene (PS) beads with well-defined densities of surface carboxylic acid groups via standard carboiimide chemistry. This method enabled us to precisely tune the extent of *surface* PEG grafting (the solid PS core would prevent PEG penetration into the particle) simply by varying the input NH_2:COOH ratio. Interestingly, this approach also enables PEG grafting on particles at sufficient densities to achieve not only brush but even dense brush conformations. Using these well-characterized nanoparticles, we systematically explored the effect of the PEG coating density and PEG MW on the reduction in particle uptake by immune cells and clearance *in vitro* and *in vivo*.

4.2 Materials and methods

4.2.1 PS-PEG synthesis and characterization

Carboxylate-modified green fluorescent polystyrene (PS) beads with mean diameters of

93 and 100 nm were purchased from Bang's Laboratories (Fishers, IN, USA) and Invitrogen (Carlsbad, CA, USA), respectively. The surface COOH densities of the particles (2.1 and 5.1 COOH/nm^2 for 93 and 100 nm beads, respectively) were calculated from the mEq/g values provided by the manufacturers. Methoxy PEG amine (NH_2-PEG) 2 and 5 kDa in MW were obtained from Rapp Polymere (Tuebingen, Germany); 10 kDa and 20 kDa from JenKem (Allen, TX, USA); and 207, 383, and 559 Da from ThermoScientific (Waltham, MA, USA). NH_2-PEG was conjugated to the PS particles, as previously described [301, 302]. Briefly, the beads were washed thrice with MilliQ H_2O and resuspended in 50 mM borate buffer (pH 7.8). Methoxy PEG amine was added to the PS beads at varying PEG:COOH ratios, and 1-ethyl-3-(3-dimethylaminopropyl)carbodiimide (EDC, Invitrogen) and N-hydroxysulfosuccinimide (S-NHS, ThermoScientific) were added at five-fold molar excess of PEG. The EDC/S-NHS reaction was allowed to proceed overnight at RT. The reaction mixture was quenched with excess glycine, and the PEG-modified particles were washed with MilliQ H_2O and resuspended in water to stock concentrations (~10-20 mg/mL). The hydrodynamic size and ζ-potential of the synthesized particles were determined by dynamic light scattering and laser Doppler anemometry, respectively, using a Zetasizer Nano (Malvern, UK).

4.2.2 Direct fluorescent quantification of the PEG coating density

Fluorescent PEG was used to directly quantify the PEG grafting density. Rhodamine B and Cy5 PEG amine (5 kDa) were purchased from NanoCS (New York, NY, USA). Maleimide ATTO 590 and ATTO 610 were obtained from Sigma-Aldrich (St. Louis, MO, USA). The fluorophores were conjugated in excess onto thiol PEG amine (5 kDa, JenKem) via overnight incubation at RT in PBS/methanol (80%/20%) or PBS. Unreacted dye was removed using an

Amicon Ultra-0.5 mL filter device MWCO 3 kDa (Millipore, MA, USA). The different fluorescent PEG amines (5 kDa) were mixed with methoxy PEG amine at a 1:4, 1:20, or 1:40 ratio, followed by conjugation to PS beads at various total PEG:COOH ratios. The fluorescence of the PS-PEG Rhodamine B, Cy5, ATTO 590, and ATTO 610 particles were measured at 570/595, 645/675, 590/625, and 610/640 nm, respectively, using a SpectraMax 2 microplate reader (Molecular Devices, CA, USA). Sample fluorescence was compared to a standard curve generated using free PEG-fluorophores to quantify the number of conjugated fluorescent PEG groups and the effective total PEG grafting.

4.2.3 PEG coating density quantification by PDAM assay

The residual carboxylic groups present on the PS-PEG particles were quantified using 1-pyrenylyldiazomethane (PDAM; Invitrogen), a fluorogenic compound that rapidly reacts with free carboxylate groups [303]. The PS-PEG beads (1 μL) were diluted in 20 μL of Pluronic F127 solution (15 mg/mL) in a half-area black 96 well plate. Ten microliters of a saturated PDAM solution (~0.3 mg/mL in methanol) were added to each well, and the PDAM and particle fluorescence intensities were measured at 340/395 and 480/520 nm, respectively, using a SpectraMax 2 microplate reader. The sample PDAM fluorescence was compared to a standard curve of unmodified PS beads to determine the residual carboxylic group density (% COOH). The density of conjugated PEG groups (P) was calculated using the following equation: $P = C \times (100 - \%COOH)$, where C is the density of COOH groups present on the unmodified PS bead. Duplicate samples were tested per run, and the grafting estimates reflect an average of at least three independent experiments. To confirm the PDAM assay results, non-fluorescent PS beads (110 nm diameter; Bang's Laboratories) modified with PEG ATTO 590 at varying

PEG:COOH ratios were analyzed using the PDAM assay, and the indirectly estimated PEG density was compared to the PEG density directly quantified using ATTO 590 fluorescence.

4.2.4 PEG conformational regime calculations

The Flory radius R_F and grafting distance D were determined using the following equations: $R_F = \alpha N^{3/5}$, $A = \frac{1}{P}$, and $D = 2\sqrt{\frac{A}{\pi}}$; where α is the monomer length of PEG (0.35 nm), N the number of PEG repeats, and A the area occupied per PEG chain. The mushroom and brush conformations were defined by $R_F/D \leq 1$ and $R_F/D>1$, respectively [47]. The dense brush conformation occurs when the thickness of the PEG layer ($L = \frac{N\alpha^{5/3}}{D^{2/3}}$) exceeds the R_F by at least two-fold (i.e., when $R_F/D>2.8$) [43, 48].

4.2.5 THP-1 culture and uptake assay

Human monocytic THP-1 cells were obtained from the University of North Carolina at Chapel Hill's tissue culture facility and were maintained at 5×10^5 cells/mL in RPMI 1640 medium containing 10% fetal bovine serum and 1X penicillin-streptomycin, with incubation at 37°C and 5% CO_2. For the uptake studies, THP-1 cells seeded into 24 well plates at 1.70×10^5 cells/mL were differentiated in culture medium containing 200 nM phorbol 12-myristate 13-acetate (PMA; Sigma-Aldrich) [304]. The PMA-containing medium was removed 3 d later and replaced with fresh culture medium, followed by incubation with carboxylate PS or PS-PEG particles at a $1{:}10^4$ cell-to-particle ratio for 4 h, 12 h, or 24 h; the fluorescent nanoparticle concentrations were determined by comparison to stock nanoparticles of known concentration. Flow cytometry was performed using a FACSCanto instrument (BD, Franklin Lakes, NJ, USA),

and propidium iodide (Invitrogen) staining was used for live/dead cell determination. At least 10,000 events were recorded per sample, and the data were analyzed using BD FACSDiva software. The data represents *n*=3 independent experiments performed in triplicate.

4.2.6 Primary human leukocyte culture and uptake assay

Individual human buffy coat units were purchased from Innovative Research (Novi, MI, USA). The peripheral blood mononuclear and polymorphonuclear cells were collected by Ficoll-Paque Premium separation and were resuspended at 3×10^6 cells/mL in RPMI 1640 medium containing 25 mM HEPES, 1X penicillin-streptomycin, 1X sodium pyruvate, 0.1% β-mercaptoethanol, and 10% human serum. For uptake studies, leukocytes were seeded in 96 well plates and incubated with carboxylate PS or PS-PEG particles at a $1:10^4$ cell-to-particle ratio for 4 or 24 h, with incubation at 37°C and 5% CO_2 and shaking at 200 rpm. After detachment with trypsin and washing with cold PBS, the cells were incubated with Fc block for 5 min on ice (eBioscience, San Diego, CA, USA). For the detection of cell surface markers, monoclonal mouse anti-human antibodies $IgG1_\kappa$ CD56 APC-eFluor® 780, CD16 APC, or CD14 APC-eFluor® 780 (eBioscience); IgM_κ CD66b PerCP-Cy5.5 (BD); or $IgG1_\kappa$ CD3 APC (Invitrogen) or CD19 PE were incubated with the cells for 20 min in the dark on ice. SYTOX® Blue dead cell stain (Invitrogen) was added prior to cell analysis for live/dead cell determination. Flow cytometry was performed using a Dako CyAn instrument (Beckman-Coulter, Brea, CA, USA). At least 50,000 events were recorded per sample, and the data were analyzed using Kaluza software (Beckman-Coulter). The data represents *n*=3 independent experiments performed in triplicate.

4.2.7 Intravital imaging of particle circulation

Female BALB/c mice (20-24 g body weight) were obtained from Charles River Laboratories (Wilmington, MA, USA), and all animal experiments carried out in accordance with an animal use protocol (#12-137) approved by the University of North Carolina Animal Care and Use Committee. Intravital imaging was performed according to a previously published protocol [48, 305]. Briefly, the mice were anesthetized with isoflurane, and a tail vein catheter was inserted. After the hair was removed from the left ear, the mice were placed onto a heated stage (37°C) in a prone position with the left ear immobilized by taping onto an aluminum block. The vasculature was located manually on an IV 100 Olympus laser scanning microscope by the detection of green autofluorescence from red blood cells under white light excitation. A suspension of green fluorescent PS or PS-PEG$_{5\ kDa}$ particles (300 µg/20 g mouse, *n*=3-4 per group) in a total of 100 µL PBS was slowly injected via the catheter, followed by a 50 µL flush of PBS and imaging with a 488 nm laser for 2 h at 5 s intervals. To analyze the particle blood circulation, the image files from each scan were exported to ImageJ, and the images were stacked in groups of 4. For each sample scan, the region of interest containing the vasculature was analyzed for the fluorescent signal. If needed, a correction for variation in laser intensity or drift was performed by background correcting each image to the signal from a vasculature-free region of the scan. The data were exported to GraphPad Prism for area under the curve (AUC) analysis.

4.2.8 PS-PEG biodistribution

After 2 h, the mice were sacrificed, and tissues (heart, liver, kidneys, spleen, lungs) were collected. Blood was also collected by cardiac puncture and added in 100 µL aliquots to a black

96 well plate. The tissues from treated and untreated animals were imaged using an IVIS Kinetic fluorescence imaging system with excitation at 465 nm. The fluorescent signal present in the tissues was calculated as a percentage of the total recovered fluorescence for the collected tissue samples. The fluorescence of particles in the blood was measured using a SpectraMax 2 microplate reader and compared to a standard curve generated using green fluorescent PS beads added to untreated blood. The collected liver and spleen tissues were homogenized using an Omni Bead Ruptor 24 (Omni, Kennesaw, GA, USA) at a speed of 5.65 m/s for two cycles of 45 sec, followed by centrifugation at 15,000 rpm for 5 min at room temperature. The fluorescence of particles in the tissues was measured using a SpectraMax 2 microplate reader and compared to a standard curve generated using green fluorescent PS beads added to untreated homogenized tissues.

4.2.9 Extended circulation and biodistribution of densely PEGylated particles

Additional mice (*n*=4 per group) were injected with densely PEGylated particles (5 kDa PEG, 3.61 PEG/nm^2; 300 µg/20 g mouse) in a total of 100 µL PBS via the tail vein, and the mice were sacrificed at various time points (0, 12, 24, and 48 h). Tissues (heart, liver, kidneys, spleen, lungs) and blood were collected, and the tissue distribution and particle concentration in the blood were determined (see above). PK analysis of the blood concentration data was conducted with PKSolver; one- and two-compartment models were fit to the data to determine the best fit [48, 306].

4.2.10 Statistical analysis

Group comparisons were performed using one-way ANOVA, followed by Tukey's post

hoc test, on SAS 9.3 software. A p-value<0.05 was considered to indicate statistical significance. All data are presented as mean ± S.D.

4.3 Results

4.3.1 Synthesis and characterization of PS-PEG nanoparticles

ζ-potential measurements are commonly used to confirm and infer the density of PEG coating on charged nanoparticles. Thus, we decided to begin by evaluating whether the ζ-potential can serve as an adequate measure of the extent of PEG grafting on various PS-PEG nanoparticles covering a broad range of input PEG:COOH ratios and PEG lengths (Table 4.1). Although we found that the particles generally exhibited increasingly neutral ζ-potentials with increasing input PEG:COOH ratios (Fig. 4.1a), we observed a virtually neutral ζ-potential for particles formulated with relatively low PEG:COOH ratios. This result underscored the inability of ζ-potential measurements to accurately quantify even moderately dense PEG coatings. The particle hydrodynamic diameter also scaled with increasing PEG density, but similar to the ζ-potentials measurements, the difference in hydrodynamic diameters were only slightly correlated to the total final PEG coating, as determined by the fluorimetric assay described later (Fig. 4.1b).

To more sensitively quantify PEG grafting, we directly conjugated fluorescently labeled PEG polymers to PS nanoparticles. Across four different fluorophores at various labeling ratios, we consistently observed that we were able to finely tune the PEG grafting density simply by varying the input PEG:COOH ratio and that we could reliably obtain exceedingly dense PEG grafting at excess input PEG ratios (Fig. 4.1c). Because terminal fluorophores may influence particle interactions with immune cells, we further explored whether we could estimate the PEG grafting density by quantifying the residual COOH groups on PS-PEG nanoparticles using

fluorogenic 1-pyrenylyldiazomethane (PDAM, MW 242.3). These indirect quantification values were highly correlated to PEG densities quantified using fluorophore-conjugated PEG (Fig. 4.1d), underscoring the rigor and accuracy of this indirect measurement approach. More importantly, this method allowed us to accurately measure the grafting density of PS-PEG beads modified solely with methoxy-PEG-amine, thus eliminating the potentially confounding influence of conjugated fluorophores on particle uptake. The PEG grafting densities on all particles used in subsequent *in vitro* and *in vivo* experiments were determined using this indirect PDAM assay.

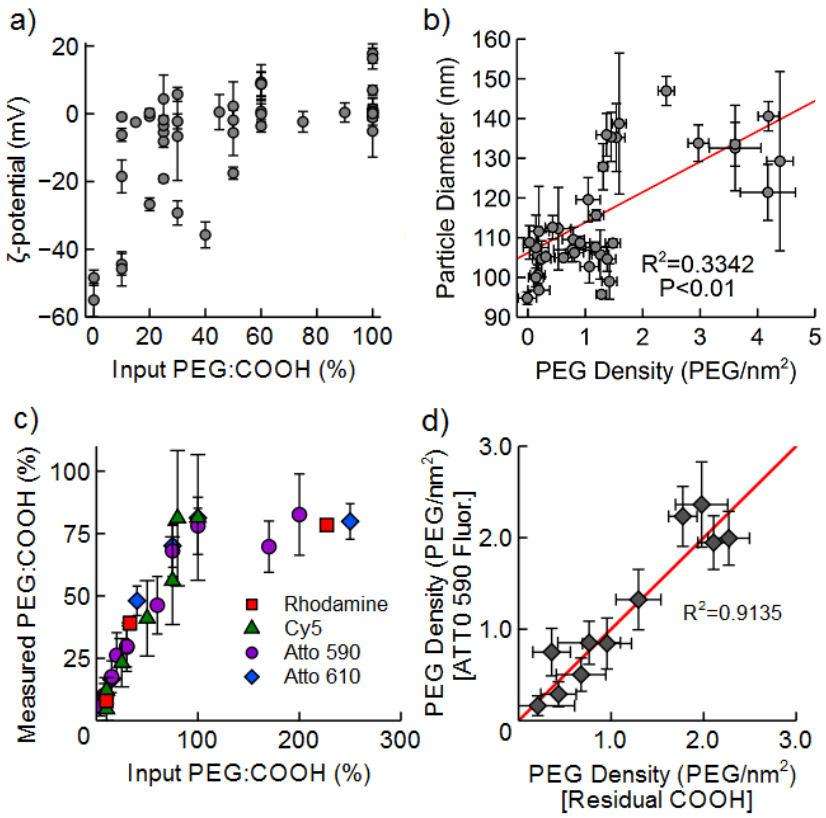

Figure 4.1. Direct and indirect characterization of PS-PEG density. a) Surface charge and **b)** hydrodynamic diameter of 100 nm polystyrene (PS) beads conjugated with amine PEG (207-20,000 Da) at various PEG:COOH ratios. Linear regression was performed using SAS 9.3 software. **c)** The extent of PEG grafting on 100 nm PS particles at various input PEG:COOH ratios was directly quantified using fluorescent NH_2-$PEG_{5\ kDa}$ (Rhodamine B, Cy5, ATTO 590 and ATTO 610). **d)** The PEG densities on PS-$PEG_{5\ kDa}$ ATTO 590 particles were indirectly measured by quantifying residual COOH groups using 1-

pyrenylyldiazomethane (PDAM). The linear fit (y=1.01x-0.04; linear regression was performed by minimization of sum of squares) suggests strong agreement between the two methods. The data represents $n \geq 2$ independent experiments performed in at least triplicate.

4.3.2 Influence of PEG coating characteristics on particle uptake by cultured macrophage cells

Improved evasion of phagocytic uptake and clearance by MPS cells is a principal outcome of PEGylation. To investigate the minimum PEG grafting density necessary to suppress uptake of polymeric nanoparticles by macrophages and other immune cells, we first prepared PS-PEG nanoparticles conjugated with different amounts of 5 kDa PEG and quantified their uptake by differentiated human THP-1 cells (a macrophage-like cell line) via flow cytometry. We found that coating PS-PEG with ≥0.8 PEG/nm^2, which translates to PEG grafted at $R_F/D \geq 4.7$, effectively suppressed particle uptake by THP-1 cells (defined by ≥20-fold reduction in uptake relative to uncoated PS particle control) for at least 24 h (Fig. 4.2). In contrast, particles that were less densely PEGylated but still possessed a brush PEG coat (~0.2 PEG/nm^2; $R_F/D=2.6$) did not evade THP-1 uptake as readily, and these particles exhibited continued uptake over time, as reflected by greater cellular mean fluorescence at 12 and 24 h than at 4 h (Fig. 4.2b). We next evaluated the influence of PEG MW (range: 207 Da–20 kDa) at grafting densities exceeding 1.2 PEG/nm^2 ($R_F/D>3.6$, except 559 Da PEG with $R_F/D=1.7$). Contrary to previous findings that suggest very short PEGs cannot adequately reduce particle uptake [307-309], we found that even PEGs with as few as 12 ethylene oxide subunits (559 Da) were able to effectively reduce uptake when grafted at densities exceeding 1.2 PEG/nm^2.

To correlate the observed cell uptake to the theoretical PEG conformational regime, we mapped particle uptake by human THP-1 macrophages to a phase diagram reflecting a wide range of PEG MWs and grafting densities (Fig. 4.3). We found that effective suppression of macrophage uptake required dense brush PEG at surface densities substantially exceeding the

mushroom-brush transition (R_F/D =1; dashed line), which is often cited as the threshold for achieving effective stealth behavior [9, 295]. Nearly all formulations that exhibited a ≥20-fold reduction in THP-1 uptake relative to the unmodified particle control possessed PEG coatings with R_F/D values in excess of 2.8 (dotted line, Fig. 4.3), indicative of PEG grafting in the dense brush regime. For longer PEG chains (≥10 kDa), although the inherently greater R_F suggests that even a minimal PEG coating (~0.1 PEG/nm^2) should theoretically generate PEG grafting in the dense brush regime, we found that a significantly higher PEG density ($R_F/D>8$) was required to maximally reduce macrophage uptake/cell association.

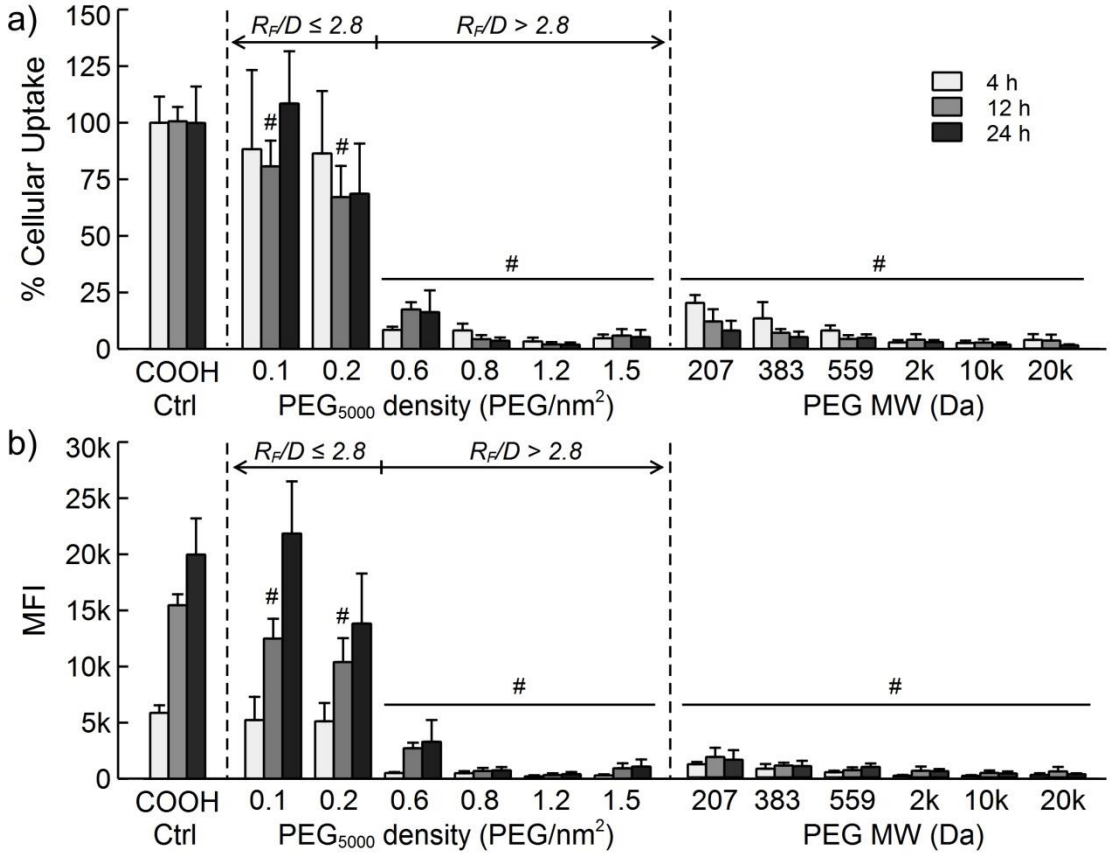

Figure 4.2. Differentiated THP-1 cell uptake of PS-PEG beads. The a) uptake, relative to unmodified PS beads, and b) mean cellular fluorescence intensity of differentiated human THP-1 cells incubated with PEG-coated particles with various grafting densities (0.1-1.5 PEG/nm^2; 5 kDa) and PEG MWs (207 Da -

20 kDa; coating density >1.3 PEG/nm^2) was quantified using flow cytometry. All data represents at least *n*=3 independent experiments performed in triplicate. # indicates P<0.01 vs. control PS beads.

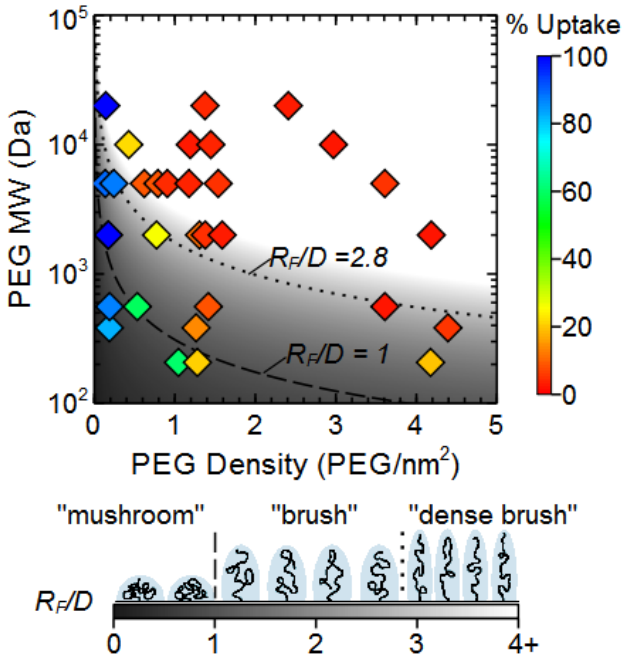

Figure 4.3. Phase diagram of particle uptake by differentiated THP-1 cells. Uptake at 4 h is shown as a function of PEG length (MW) and coating density (PEG groups/nm^2). The gray shading represents the various R_F/D values; the transitions between the mushroom-brush and brush-dense brush conformations are indicated by the dashed (R_F/D=1.0) and dotted (R_F/D=2.8) lines, respectively. All data represents at least *n*=3 independent experiments performed in triplicate.

4.3.3 Influence of PEG coating characteristics on particle uptake by primary human peripheral leukocytes

The blood contains an abundance of circulating white blood cells such as monocytes and neutrophils that represent the earliest phagocytic cells that systemically dosed nanoparticles would encounter upon intravenous administration. Therefore, we sought to test whether the PEG coating characteristics that effectively suppressed uptake by cultured human THP-1 macrophages can similarly evade uptake by primary human leukocytes. We isolated peripheral blood mononuclear cells and polymorphonuclear leukocytes from the blood of healthy human donors,

incubated them with PS-PEG and control beads, and quantified particle uptake by various cells populations (e.g., monocytes, neutrophils) using flow cytometry. Although PEGylated particles with $R_F/D>2.8$ exhibited markedly reduced uptake by both granulocytes and monocytes (Fig. 4.4), the extent of reduced uptake relative to uncoated PS particles was not quite as effective compared to with THP-1 cells. Primary human lymphocytes did not exhibit substantial uptake of either the control or PEGylated particles (Fig. 4.4c).

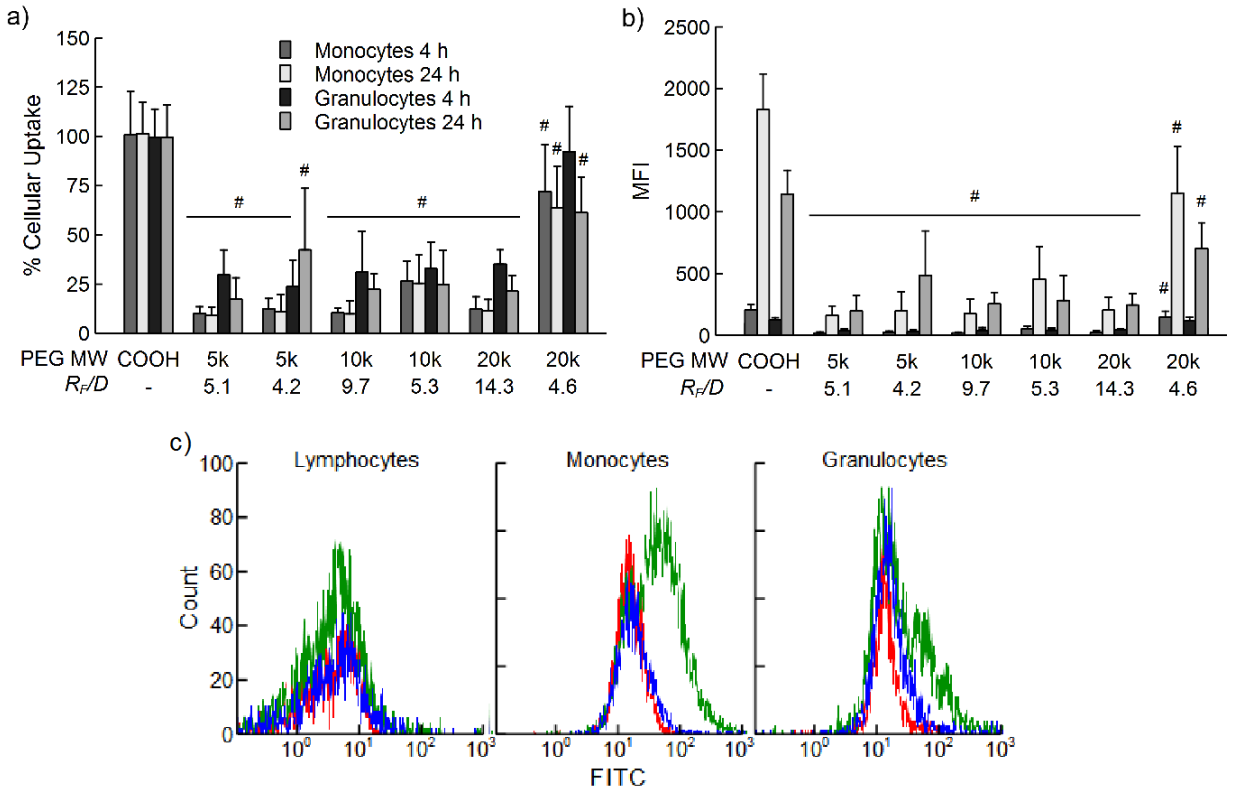

Figure 4.4. Primary human peripheral blood leukocyte uptake of PS-PEG beads. The **a)** uptake, relative to unmodified PS beads (COOH), and **b)** mean cellular fluorescence intensity of primary human immune cells incubated with various PEG-coated particles was quantified by flow cytometry. All data represents at least n=3 independent experiments performed in triplicate. # indicates P<0.01 vs. control PS beads. **c)** Representative flow cytometry histograms for the untreated (red), unmodified PS (green), and PS-PEG (blue; 5 kDa, 0.91 PEG/nm2) groups with various primary human leukocyte populations.

4.3.4 Influence of PEG coating characteristics on particle circulation kinetics in vivo

Intravital imaging (IVIM) is an excellent tool for quantifying the circulation times of particles over relatively short durations (≤ 2 h) in real-time. Because we anticipated that inadequately PEGylated particles would be quickly eliminated from the circulation, we decided to use IVIM to evaluate the circulation kinetics of particles with different PEG grafting densities following tail vein injection. In particular, we chose to perform our studies in BALB/c mice, which exhibit enhanced Th2 immune activity that leads to markedly faster particle clearance than those commonly observed with Th1-prone C57BL6 mice [310]. Prolonged circulation of polymeric nanoparticles appeared to require PEG grafting substantially beyond the minimum for a dense brush regime (Fig. 4.5a-b). Very densely coated particles, with ≥1.5 PEG/nm^2 ($R_F/D \geq 6.6$), were able to effectively evade clearance and persist in systemic circulation (<20% cleared after 2 h). In contrast, particles with slightly less dense PEG coatings, even those within the brush or dense brush regimes (R_F/D=2.0 and 4.2, respectively), were largely eliminated within 2 h, resulting in rapid accumulation in the liver (Fig. 4.5c), presumably due to clearance by MPS cells.

We next monitored the circulation kinetics and tissue biodistribution of the very densely coated PS-PEG nanoparticles (≥1.5 PEG/nm^2, $R_F/D \geq 6.6$) across longer time scales (0, 12, 24, and 48 h). The trend of reduced PEG blood clearance of these particles at 2 h directly translated to prolonged circulation times in excess of 24 h (Fig. 4.6a). The best-fit one-compartment model yielded a half-life of 14 h for the very densely PEGylated particles (Table 4.2), a 450-fold increase relative to the unmodified PS beads. Upon their eventual elimination, they were found primarily accumulated in the liver (Fig. 4.6b). Interestingly, we observed very little particle

accumulation in the spleen (<10% of the total recoverable dose, and ~8- to 10-fold less than the particle dose in the liver).

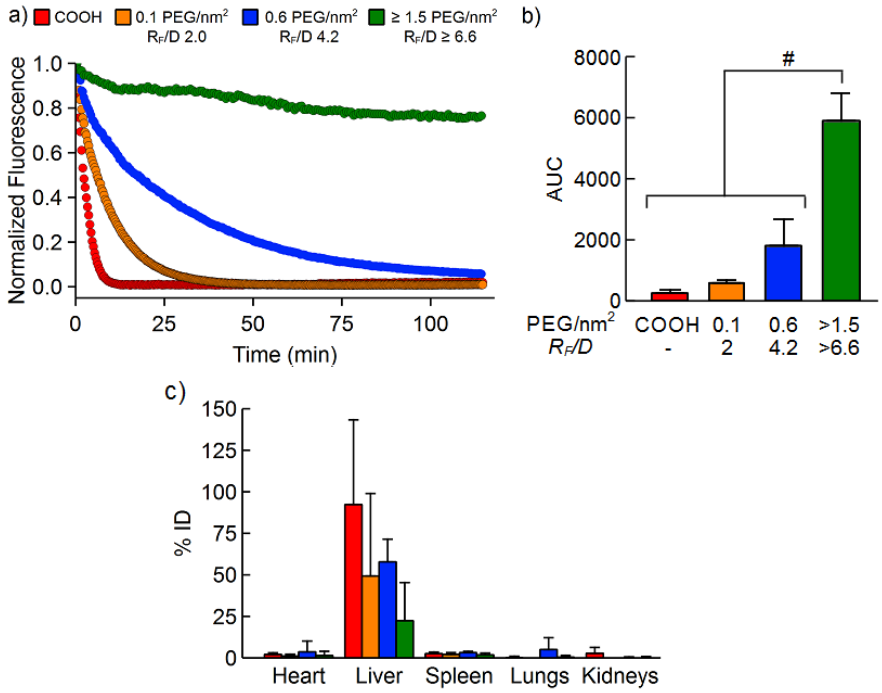

Figure 4.5. Circulation and biodistribution of PS-PEG beads. a) Blood circulation profiles of PS and various PS-PEG_{5kDa} beads observed using intravital microscopy. The data represent the fraction of the maximum fluorescence for particles in each animal and were collected from n=3-4 BALB/c mice. **b)** Area under the curve (AUC, fluorescence*sec) plot for the blood profiles of PS and various PS-$PEG_{5\ kDa}$ beads observed using intravital imaging. # indicates P< 0.01. **c)** The biodistribution of the different formulations 2 h after i.v. injection in each animal was quantified from the 2D fluorescent image signal intensities and confirmed through fluorimetric analysis of the homogenized whole tissue samples.

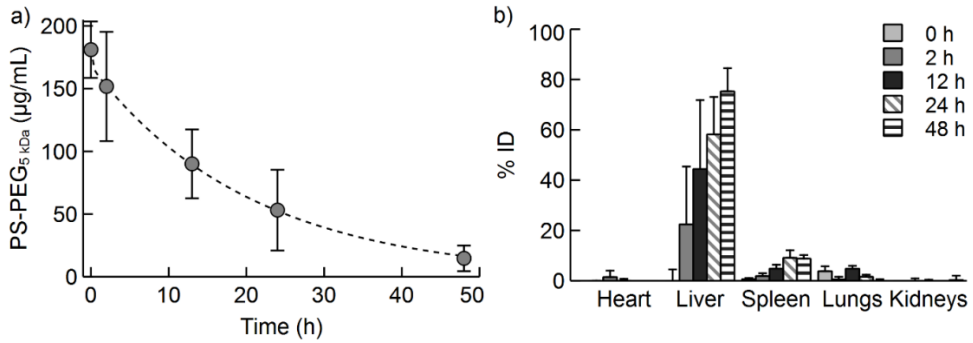

Figure 4.6. Circulation and biodistribution of densely modified PS-PEG beads. a) The blood circulation profile of very densely PEGylated particles with $R_F/D \geq 6.6$ over an extended time period

(n=4); dashed line represents the fit for a one-compartment model. **b)** The biodistribution of PS-PEG beads with very dense surface coating after i.v. injection in each animal was quantified from the 2D fluorescent image signal intensities and confirmed through fluorimetric analysis of the homogenized whole tissue samples.

4.4 Discussion

Evasion of uptake and clearance by MPS cells, and consequently prolonged circulation and/or improved targeting to specific tissues, remains a critical challenge for systemically administered nanomedicines. Numerous physicochemical properties have been exploited to engineer nanoparticles that can persist in the circulation, including controlling particle size [311, 312], surface chemistries [28, 313], shape [314], and rigidity/deformability [305]. Among these approaches, the most frequently adopted strategy is PEGylation, motivated in part by its clinical success in extending the circulation times and improving the efficacies of many protein and liposomal therapeutics. Despite the long history of PEG modifications in drug delivery, the precise extent of *surface* PEG grafting on polymeric nanoparticles necessary to effectively evade uptake by various immune cells remains poorly defined. The convenient assumption is that PEG coatings that adequately coat the underlying particle core, attained when individual PEG chains begin to overlap at the mushroom-brush transition, should effectively resist binding by surrounding biomacromolecules and cells [4, 9, 295].

Surprisingly, we observed that rigid polymeric nanoparticles must be coated with PEG at a very dense brush regime ($R_F/D \geq 2.8$; equivalent to >1 PEG/nm^2 for ~2 kDa PEG) to effectively evade uptake by macrophages and peripheral leukocytes *in vitro*, as well as achieve sustained circulation *in vivo*. Our findings differ substantially from a number of recent reports that suggest PEG grafting near the mushroom-brush interface appeared to be exceptionally inert in biological environments. Perry *et al*. found that grafting ~0.1 PEG_{5k}/nm^2 (R_F/D ~1.5) onto PEG hydrogel nanoparticles, whereby the PEG grafting was quantified using fluorescein-labeled PEG, afforded

markedly longer circulation times [48]. The discrepancy is likely attributed in part to the presence of PEG in the particle core, as well as the soft mechanical nature of hydrogel nanoparticles [305]. Nance *et al*. likewise reported that latex beads grafted with ~0.1 PEG_{5k}/nm^2, estimated using ^1H NMR with bis(trimethylsilyl) benzene as an internal standard, exhibited improved diffusion in the extracellular space of brain tissues [46]. However, compared to the leukocyte-rich environment of the blood or the macrophage-rich environment in MPS organs such as the liver and spleen, brain tissues possessed far fewer macrophages and immune cells for particles to encounter, particularly during the relatively short time scales in the study. In good agreement with our findings, Walkey *et al*. observed that PEG_{5k}, when coated at a minimum density of ~0.5 PEG/nm^2 (R_F/D ~3.5) effectively suppressed the uptake of 90 nm gold nanoparticles by cultured mouse macrophages *in vitro* [50]. It should be noted that the R_F/D threshold is influenced by the PEG MW; although the $R_F/D \geq 2.8$ threshold appears to be a reasonable fit for PEG MWs commonly used in nanoparticle drug delivery (1-5 kDa), we found that a higher R_F/D was necessary for longer PEG chains (≥10 kDa). It remains to be determined whether this discrepancy is a result of differences in the effective R_F when polymers are grafted at very high densities, as the tendency for distinct polymer chains to entangle and inter-penetrate with each other is dependent on MW.

In light of the long-held notion that PEG grafting at the mushroom-brush transition or brush regime should confer sufficient stealth properties, the need for PEG grafting at densities substantially exceeding its Flory radius (beyond even a moderately dense brush regime) to evade uptake by immune cells may seem perplexing. However, PEG is hydrophilic, flexible, and capable of assuming an almost infinite number of spatial configurations over very short time intervals [315]. Thus, even when PEG is grafted at densities where neighboring chains begin to

overlap, there is likely periodic and relatively frequent appearance of gaps exposing the inner particle core when two neighboring PEG chains assume an extended conformation simultaneously. In line with this hypothesis, Walkey *et al*. found that high PEG grafting densities in the dense brush regime were necessary to minimize adsorption of serum proteins on PEG-coated gold nanoparticles; the thickness and composition of the adsorbed "protein corona" has been demonstrated to have a profound impact on the biological fate of PEGylated particles both *in vitro* and *in vivo* [50, 316, 317]. Indeed, the extremely high concentrations of proteins and other biomacromolecules in the blood create an environment whereby each nanoparticle constantly collides with a very large number of individual molecules capable of interacting with the underlying core. Thus, even very short-lived appearance of gaps in the PEG coating may be efficiently exploited by proteins and other biomacromolecules in the immediate vicinity, eventually leading to opsonization and clearance by the immune system. Therefore, to effectively eliminate gap formation in the PEG coating, the particle surface would likely need to be coated by an abundance of protruding PEG chains, at a PEG grafting density corresponding to a very dense brush regime.

Unfortunately, for biodegradable polymeric particles formed by conventional solvent diffusion or single emulsion methods using PEG-containing block copolymers, PEG coatings in the dense brush regime may not be readily achievable. The vast majority of such PEG-coated nanoparticles in literature exhibit moderately negative or positive ζ-potentials indicative of inadequate PEG coverage, which reflects inefficient phase separation of PEG from the emulsion core to the organic/aqueous solvent interface, perhaps due to steric impediment by other PEG chains [9]. The inadequate PEG coatings observed with many nanoparticle systems implies that there is likely room for further improvements in PEGylation methodologies. One such approach

is “grafting from” methods such as those involving living radical polymerization (e.g., atom transfer radical polymerization [ATRP]) can enable higher density polymer grafting than “grafting to” strategies, particularly on 2D surfaces [318, 319]. Here, we demonstrate that “grafting to” strategies based on covalent conjugation, which likely facilitates greater PEG grafting density compared to post-insertion, adsorption, or phase separation strategies [50, 320], can also facilitate sufficient grafting density to readily resist uptake by immune cells.

Beyond improving PEGylation, there is also a sore need for improved methods to characterize PEG coatings, as the current lack of sensitive methods to quantify *surface* PEG chains presents a critical hurdle to validating any improvements in PEGylation. As shown in Fig. 4.1, commonly used ζ-potential measurements are, at best, an insensitive inference of PEG grafting density and a poor predictor of the effective stealth properties of the resulting nanoparticles. Other PEG quantification methods such as NMR, XPS, and measurement of residual, unbound PEG often fail to differentiate between *total* and *surface* PEG or require complex methodologies and instrumentation that are not readily available [43, 50, 297, 300]. The most desirable solution would be a label-free, quantitative assay for surface PEG grafting that can be readily adopted across a diverse array of nanoparticle platforms.

The primary mechanism of nanoparticle elimination from the systemic circulation has long been attributed to efficient phagocytic clearance by resident macrophages in the liver and spleen, in part because both organs represent primary sites of particle accumulation *in vivo*. Consequently, a common approach to evaluate the stealth properties of PEGylated particles is to measure uptake by different cultured macrophage cell lines such as mouse RAW264.7 macrophages. Nevertheless, emerging evidence suggests that a considerable portion of PEG-coated nanoparticles may instead be eliminated from the systemic circulation via uptake by

circulating monocytes and granulocytes. For example, Jones *et al*. found that in mice prone to Th2 immune responses (e.g., BALB/c mice), circulating monocytes and granulocytes accounted for a significant portion of PEG hydrogel nanoparticle clearance [310]. Patient monocyte function was also able to serve as a predictor of rapid elimination of Doxil in some refractory ovarian cancer patients [321]. In agreement with these findings, we observed that even very densely PEGylated latex beads did not evade uptake by primary human monocytes and granulocytes as readily compared to differentiated THP-1 cells (Fig. 4.3 and 4.4). Our results suggest that *in vitro* uptake studies using primary monocytes and granulocytes may provide a more rigorous screen of the stealth properties of PEG-coated particles than conventional studies using tissue culture-adapted macrophages.

4.5 Conclusions

Grafting PEG onto particles is a common approach to extend circulation times essential for many nanomedicine applications. Here, we systematically varied PEG MW and grafting densities to identify PEG coating characteristics that effectively evade uptake of polymeric nanoparticles by immune cells *in vitro* and *in vivo*. We found that particle interactions with MPS cells is critically dependent on the conformation of individual PEG chains and that a very dense brush conformation is essential to extending particle circulation times. Our results underscore the broad need to rigorously assess the density of PEG coatings in nanoparticle systems, as well as the need for improved PEGylation strategies.

Table 4.1. PS-PEG density, hydrodynamic diameter, ζ-potential, and theoretical R_F/D and PEG conformation values.

Core PS Size (d. nm)	PEG MW (Da)	PEG Density (PEG/nm^2)	Particle Size (d. nm)	ζ-potential (mV)	R_F/D	PEG Conformation
93	-	0.0 ± 0.2	95 ± 2	-48 ± 2	-	-
100	-	0.0 ± 0.1	109 ± 4	-55 ± 5	-	-
93	207	1.1 ± 0.2	120 ± 6	-7 ± 13	0.8	mushroom
93	207	1.3 ± 0.1	96 ± 1	9 ± 5	0.9	mushroom
100	207	4.1 ± 0.5	121 ± 7	18 ± 3	1.6	brush
93	383	0.2 ± 0.2	112 ± 11	-27 ± 2	0.5	mushroom
93	383	1.3 ± 0.2	106 ± 6	9 ± 4	1.3	brush
100	383	4.4 ± 0.2	129 ± 23	16 ± 3	2.4	brush
93	559	0.2 ± 0.2	97 ± 1	-36 ± 4	0.6	mushroom
93	559	0.5 ± 0.2	112 ± 10	-6 ± 5	1.0	brush
93	559	1.4 ± 0.1	99 ± 5	9 ± 3	1.7	brush
100	559	3.6 ± 0.5	133 ± 11	7 ± 1	2.7	brush
93	2 kDa	0.2 ± 0.1	101 ± 3	-38 ± 8	1.3	brush
93	2 kDa	0.8 ± 0.3	107 ± 3	-2 ± 2	2.7	brush
93	2 kDa	1.3 ± 0.1	128 ± 6	-5 ± 8	3.5	dense brush
93	2 kDa	1.4 ± 0.2	105 ± 3	-2 ± 4	3.6	dense brush
93	2 kDa	1.6 ± 0.1	139 ± 18	1 ± 3	3.9	dense brush
100	2 kDa	4.2 ± 0.2	141 ± 4	1 ± 1	6.3	dense brush
93	5 kDa	0.1 ± 0.2	108 ± 8	-46 ± 5	2.0	brush
93	5 kDa	0.2 ± 0.2	105 ± 5	-45 ± 3	2.6	brush
93	5 kDa	0.6 ± 0.2	105 ± 1	4 ± 7	4.2	dense brush
93	5 kDa	0.8 ± 0.2	110 ± 3	-2 ± 3	4.7	dense brush
93	5 kDa	0.9 ± 0.2	109 ± 2	-4 ± 2	5.1	dense brush
93	5 kDa	1.2 ± 0.2	108 ± 1	1 ± 3	5.8	dense brush
93	5 kDa	1.5 ± 0.2	135 ± 9	0 ± 2	6.6	dense brush
100	5 kDa	3.6 ± 0.1	134 ± 6	-1 ± 1	10.1	dense brush
93	10 kDa	0.4 ± 0.1	113 ± 3	-2 ± 1	5.3	dense brush
93	10 kDa	1.2 ± 0.1	116 ± 1	-0 ± 3	8.8	dense brush
93	10 kDa	1.5 ± 0.1	135 ± 6	0 ± 4	9.7	dense brush
100	10 kDa	3.0 ± 0.2	134 ± 5	-0 ± 1	13.9	dense brush
93	20 kDa	0.1 ± 0.1	100 ± 2	-46 ± 2	4.6	dense brush
93	20 kDa	1.4 ± 0.2	136 ± 5	-0 ± 1	14.3	dense brush
100	20 kDa	2.4 ± 0.1	147 ± 4	1 ± 2	18.9	dense brush

Table 4.2. PK model and parameters for various PS-$PEG_{5\ kDa}$ particles (*n*=3-4).

PEG Density (PEG/nm^2)	R_F/D	Best-fit Model	R^2	$t_{1/2}$ (h)	CL (mL/h)*	AUC_{0-t} (mg/mL*h)*	V_D (mL)*
COOH	-	One-compartment	0.991	0.03	-	-	-
0.1	2.0	One-compartment	0.995	0.11	-	-	-
0.6	4.2	One-compartment	0.991	0.41	-	-	-
3.6	10.1	One-compartment	0.999	13.51	0.088	3.13	1.71

[*] Due to the relatively rapid clearance of the carboxylate PS and 0.1 and 0.6 PEG/nm^2 PS-$PEG_{5\ kDa}$ particles within 2 h, the normalized intravital imaging data were used to generate PK models, and the volume of distribution (V_D) and other related parameters cannot be determined accurately using this data.

CHAPTER 5: ANALYSIS OF PRE-EXISTING ANTI-PEG ANTIBODIES IN THE GENERAL POPULATION[4]

5.1 Introduction

Immunogenicity encompasses the entirety of innate, humoral, and cellular immune responses against therapeutic molecules and is frequently associated with the induction of antibodies that directly bind to therapeutic molecules (i.e., anti-drug antibodies) after the initial or repeated administration of the drug. Both innate and adaptive immune responses can result in decreased efficacy or treatment failure due to either direct neutralization of the therapeutic molecules [322] or inadequate drug dosing at target cells/tissues because of altered pharmacokinetics and biodistribution [323]. Worse, hypersensitivity reactions may lead to adverse or even fatal reactions to a therapy [324, 325]. While major strides have been made to reduce immunogenicity, such as development of humanized or fully human monoclonal antibodies, immunogenicity continues to be a major concern for safety and efficacy of many novel drug products [326].

An emerging class of anti-drug antibodies are those that specifically recognize and bind poly(ethylene glycol) (PEG), a synthetic polymer routinely used both as an excipient in pharmaceutical formulations and also as a polymer conjugate to improve the stability and circulation kinetics of protein drugs and nanocarriers [9, 29]. PEG is a hydrophilic and highly flexible polymer comprised of repeating subunits of ethylene glycol ($[-CH_2-CH_2-O-]_n$). Because densely PEG-grafted surfaces are exceptionally resistant to protein adsorption [7, 9, 295], PEG

[4] This chapter is based on an article submitted to *Analytical Chemistry*.

has long been assumed to possess little to no immunogenicity, and PEGylation has even been used to mitigate the immunogenicity of therapeutic proteins [327]. Although the potential immunogenicity of PEG was underappreciated at the time, Richter & Akerblom in 1983 reported the possibility that PEGylated proteins, unlike free PEG that generated minimal responses, can actually induce PEG-specific antibodies [51]. Later on, various research groups observed that repeat doses of otherwise long-circulating nanocarriers modified with PEG or PEG-containing molecules were rapidly cleared by mononuclear phagocyte system (MPS) cells in rodent and other animal models [33, 56]. These early *in vivo* observations were eventually categorized into a phenomenon termed the accelerated blood clearance (ABC) effect, whereby the first dose of a PEG-containing agent induces anti-PEG antibodies (anti-PEG Ab) that then opsonize and facilitate rapid elimination of subsequent doses of PEGylated therapeutics [19]. In nearly all animal studies, anti-PEG Ab responses were largely mediated by IgM class antibodies and were transient in nature [20, 71].

Growing evidence suggests that human patients can also generate immune responses to PEG-modified therapeutics, with significant effects on clinical outcomes. The presence of anti-PEG Ab has been associated with rapid clearance of various PEGylated proteins in clinical trials [104, 106], as well as anaphylactic or hypersensitivity reactions after the administration of PEG-containing formulations [103, 110]. In contrast to most anti-drug antibodies, an important feature of human anti-PEG Ab responses is that these Ab can be found even in "treatment-naïve" individuals (i.e., as "pre-existing" anti-PEG Ab) [20], presumably due to prior exposure to PEG. Indeed, PEG and PEG-derivatives are common ingredients in personal care, beauty, and household cleaning products (e.g., soap, sunblock, cosmetics, detergent), as well as processed foods. Given the popular use of PEG in biologics and nanomedicines as well, the presence of

pre-existing anti-PEG Ab poses significant concerns for the efficacy and safety of a wide range of therapeutics.

Despite these serious implications, the true prevalence and levels of pre-existing anti-PEG Ab responses remains not well understood. The reported prevalence of pre-existing anti-PEG Ab varies widely across different studies, ranging from <1%-44% [17, 20, 105]. In addition to natural variations among subjects, the differences are likely due in part to the use of assay techniques such as hemagglutination tests or endpoint dilution ELISAs with different sensitivities and specificities of detection. Here, we sought to rigorously characterize pre-existing anti-PEG Ab in the general population by measuring the prevalence, concentration and isotype of anti-PEG Ab in contemporary and historical plasma and serum samples from healthy adults. To enable reproducible quantitation of anti-PEG Ab that could serve as a reference for future investigations, we generated chimeric monoclonal anti-PEG IgG and IgM with known binding affinities to PEG, and used them as standards in quantitative competitive ELISA assays.

5.2 Materials and methods

5.2.1 Human plasma and serum samples

Whole blood (K2-EDTA anticoagulant) from 68 individual healthy subjects was purchased from Bioreclamation (Hicksville, NY, USA), and the samples were centrifuged at 1500 g for 15 min at room temperature. Aliquots of the top plasma layer were collected and stored at -80°C until use. An additional 309 frozen plasma samples from healthy subjects were purchased from ProMedDx (Norton, MA, USA); samples were thawed, aliquoted, and stored at -20°C until use. Serum collected during the periods 1970-1979, 1980-1989, and 1990-1999 (30, 30, and 19 samples, respectively) from patients with no history of malignancies were purchased

from Mayo Clinic Bioservices (Rochester, MN, USA) and were thawed, aliquoted, and stored at -20°C until use. Patient demographics are listed in Table 5.1.

5.2.2 Chimeric anti-PEG antibody standards

Sequences for chimeric anti-PEG Ab were generated by combining the V_H/V_L regions of commercially available murine anti-PEG Ab (6.3 IgG_1 and AGP.3 IgM; IBMS Academia Sinica) [328] with the C_H1/C_L and Fc regions of human IgG1-4 or IgM Ab. Plasmids encoding chimeric heavy, light-chains, along with J-chain (IgM only) were co-transfected into Expi293 cells (ThermoFisher) and grown for 72 h. The chimeric 6.3 (c6.3) IgG antibodies were purified from expression supernatant by single-step protein A/G purification (ThermoFisher) and assessed for purity by SDS-PAGE electrophoresis. Chimeric AGP.3 (cAGP.3) IgM antibodies were used directly from expression supernatant.

The concentration of the c6.3 IgG1-4 and cAGP.3 IgM standards were determined using ELISA. Briefly, high-binding half-area 96-well Costar plates (Corning) were coated with 500 ng/mL of anti-human Fab (#I5260, Sigma-Aldrich) or anti-human IgM (#609-1107, Rockland Immunochemicals) capture antibody in 50 nM bicarbonate buffer (pH 9.6) overnight at 4°C. The chimeric antibodies were diluted in 1% milk in PBS-0.05% Tween and detected using anti-human IgM HRP (#609-1307, 1:75000 dilution Rockland Immunochemicals), anti-human IgG HRP (#709-1317, 1:15000 dilution, Rockland Immunochemicals), and/or corresponding IgG subclass secondary antibodies (see Methods & Materials *Anti-PEG Ab ELISA* section). Pooled human IgG1 (Sigma-Aldrich), IgG2 (Abcam), IgG3 (Sigma-Aldrich), IgG4 (Sigma-Aldrich), and IgM (ImmunoReagents, Raleigh, NC, USA) were used as quantitation standards.

The K_D of the generated chimeric Ab were determined using an Octet QK instrument (ForteBio, Menlo Park, CA, USA). Streptavidin biosensors were loaded with biotin-PEG_{10k} and, following a baseline step in DPBS with 0.01% bovine serum albumin (BSA), the sensors were then exposed to c6.3 IgG1-4 or cAGP.3 at 0–100 nM in DPBS-0.01% BSA. Dissociation was monitored in DPBS-BSA. Raw data was processed using ForteBio's Data Analysis Software 6.4.

5.2.3 Anti-PEG Ab ELISA

For detection of PEG-specific antibodies, 1,2-distearoyl-sn-glycero-3-phosphoethanolamine-methoxy PEG_{5k} (DSPE-PEG; Nanocs, New York, NY, USA) was coated onto medium-binding half-area 96-well Costar plates (Corning) at 50 µg/mL in DPBS overnight at 4°C. After blocking the plates with 5% non-fat milk in DPBS, the plasma or serum samples, which were diluted 5- to 200-fold in 1% non-fat milk in DPBS, were added in the presence or absence of free diol-PEG_{8k} (4 mg/mL) and incubated for 1 h, followed by washes with DPBS. Antibodies bound to the DSPE-PEG coat were detected using the following detection antibodies and 1-step Ultra TMB (ThermoFisher): anti-human IgG_1 HRP (A10648, 1:1000 dilution, ThermoFisher); mouse anti-human IgG_2 (05-3500, 1:1000 dilution, ThermoFisher) along with anti-mouse IgG HRP secondary (sc-2005, 1:4000 dilution, Santa Cruz Biotechnology); anti-human IgG_3 HRP (#053620, 1:1000 dilution, Invitrogen); anti-human IgG_4 HRP (A10654, 1:750 dilution, ThermoFisher); or anti-human IgM HRP (#609-1307, 1:15000 dilution, Rockland Immunochemicals). After stopping the HRP reaction with 2 N sulfuric acid, the absorbance at 450 nm was measured using a Spectramax M2 plate reader (Molecular Devices). All wash and incubation steps were performed using DPBS without any surfactant, as commonly used surfactants such as Tween contain PEG chains, which could artificially alter the ELISA results

[52]. All assays included the respective c6.3 IgG1-IgG4 or cAGP.3 IgM standard curves (range 0-275 ng/mL), and the level of anti-PEG Ab present in the samples was determined using a 5-PL regression curve of the absorbance, which was corrected for the non-specific background of sample wells treated with free diol-PEG_{8k}. Total anti-PEG IgG was calculated as the sum of the anti-PEG IgG1-IgG4 levels.

Detection cut-offs were established based on the corrected absorbance of the lowest standard curve point for each c6.3 IgG1-4 and cAGP.3 IgM standard curve according to the method described by Frey *et al.* [329]. Assay precision was established by calculating the average coefficient of variation (CV%) for all detectable standard curve points, and the accuracy was calculated as 100% x observed concentration/expected concentration for all detectable standard curve points (Table 5.2). To further confirm the specificity of the ELISA results, free methoxy-PEG_{40k}-myoglobin (PEG-MYO, Alfa Aesar) was used instead of free diol-PEG_{8k}, and the calculated anti-PEG IgG1 concentrations obtained using the two different competitive molecules was compared for a range of samples.

5.2.4 Human antibody isotyping quantification

The levels of total IgG1, IgG2, IgG3, IgG4, and IgM in the human plasma and serum samples were quantified using a Bio-Plex Pro human isotyping 6-plex panel kit (BioRad) on a Luminex MAGPIX instrument (EMD Millipore) in duplicate according to the manufacturer's instructions. Samples were diluted 1:40000 in the provided isotyping diluent. The total IgG1, IgG2, IgG3, IgG4, and IgM concentrations were calculated using MILLIPLEX Analyst 5.1 software, and the total IgG was calculated as the sum of the total IgG1-IgG4 levels.

5.2.5 Statistical analyses

Transformations for the anti-PEG IgM and IgG, as well as IgG1 and IgG2, variables were investigated using the Box-Cox procedure within generalized linear models. The covariates of interest were as follows: gender, age, age categorized, race, and historical time period (i.e, 1970-1979, 1980-1989, 1990-1999, and contemporary). The PEG IgM and IgG variables were also dichotomized to 'above' and 'below' their respective predetermined detection thresholds. Fisher's exact tests were used to evaluate general association for data categorized into contingency tables with nominal categories. Multivariable general linear models were also explored. Since this was an exploratory study, nominal (or unadjusted) p-values have been reported. P-values >0.05 were considered significant. Statistical analyses were performed using SAS version 9.4 (SAS Institute), and all graphs were generated using Graphpad Prism version 6.0.

5.3 Results

5.3.1 Validation and specificity of ELISA assays for measuring anti-PEG Ab levels

Previous studies of anti-PEG Ab responses generally measured relative amounts of PEG-binding Ab through either hemagglutination assays with PEG-coated red blood cells or endpoint dilution ELISAs that determine Ab status based on absorbance readings above an often arbitrary threshold [22, 100, 104-106, 109]. Unfortunately, both methods only estimate the relative amounts of Ab present, making comparisons between studies difficult. Quantitative ELISA offers the potential to provide precise measurements of absolute antibody concentrations but requires well-characterized Ab standards with a human Ab backbone in order to convert measured absorbance to absolute amounts of Ab. One potential challenge to such an approach is

that endogenous serum Ab responses in individuals are undoubtedly polyclonal in nature. Generally, monoclonal Ab may not be appropriate as antibody standards for characterizing a polyclonal response, since polyclonal Ab can bind different portions of a pathogen or even different regions of a particular antigen and thus can accumulate to a greater extent on the pathogen surface compared to a monoclonal Ab. However, since the PEG backbone consists of identical ethylene glycol repeats, the chimeric monoclonal Ab standards we developed should bind the same epitope as a polyclonal anti-PEG Ab response. This led us to engineer chimeric monoclonal anti-PEG IgM and IgG1-4 based on merging human IgG1-4 and IgM backbones with PEG-binding V_H and V_L domains previously isolated from mouse IgM and IgG [328]. As expected, the 4 subclasses of chimeric anti-PEG IgG all possessed relatively similar binding affinities, with K_D values spanning the range of 4.8×10^{-9} to 5.8×10^{-9} M (Table 5.3). The K_D for chimeric anti-PEG IgM was 6.8×10^{-11}.

A frequent criticism of prior anti-PEG ELISA measurements was the lack of confirmation of specificity to PEG. To ensure that we were indeed detecting PEG-specific Ab, we performed competitive binding with free diol-PEG_{8k}, and only reported signal that was saturated by the free PEG. Using this competitive ELISA setup with chimeric Ab standards, our assay afforded sensitive detection of anti-PEG Ab, with final detection cut-off limits of 14.2, 15.1, 3.9, 4.4, and 6.4 ng/mL for anti-PEG IgG1, IgG2, IgG3, IgG4, and IgM, respectively (Table 5.2). To further confirm specificity to PEG, we also tested an additional ELISA format using a methoxy-PEG_{40k}-myoglobin conjugate as the competing molecule instead of diol-PEG_{8k} and found comparable anti-PEG Ab levels for a range of samples (Fig. 5.1).

In animals, anti-PEG Ab have been found against both the PEG backbone (CH_2-CH_2-O repeating units) and PEG terminal groups such as methoxy and hydroxy moieties [52, 89]. Here,

we chose to focus on backbone-specific anti-PEG Ab by using a methoxy-PEG_{5k}-lipid as the capture antigen and free diol-PEG_{8k} as the competing molecule in our competitive ELISA assay, for a number of reasons. First, the PEG backbone is by definition common to all PEGylated therapeutics, whereas terminal groups on different PEGylated systems can technically vary, even though all current PEGylated products currently on the market utilize methoxy-terminal PEG. In addition, Hershfield *et al*. found that binding of induced and pre-existing anti-PEG Ab was significantly inhibited by free diol-PEG_{10k}, leading the authors to conclude that anti-PEG Ab detected were backbone-specific [104]. Similarly, Ganson *et al*. demonstrated that competition with free diol-PEG_{10k} and methoxy-PEG_{10k} reduced binding of pre-existing anti-PEG Ab to pegloticase to an equal extent [17]. Other existing literature reports of pre-existing and induced anti-PEG Ab against other commercially available PEGylated drugs, including peginterferon beta-1a [124] and pegfilgrastim [330], did not specify the terminal groups of the PEG molecules used to confirm the specificity of anti-PEG Ab. Thus, while we can be certain that the reported Ab responses must encompass Ab that binds the PEG backbone, the same may not be true of PEG terminal groups.

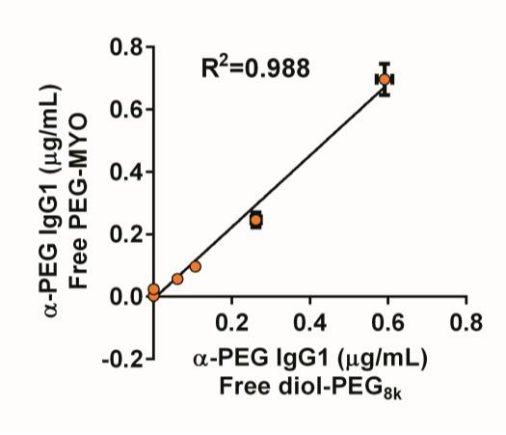

Figure 5.1. Confirmation of anti-PEG ELISA specificity. Comparison between the anti-PEG IgG levels determined through competitive ELISAs using free diol-PEG_{8k} or free methoxy-PEG_{40k}-myoglobin (PEG-MYO).

5.3.2 Anti-PEG Ab levels in the contemporary population

To quantify the levels and prevalence of pre-existing PEG-specific Ab in the general population, we screened a total of 377 commercially sourced plasma samples from healthy human blood donors for anti-PEG IgG and IgM levels using the competitive ELISA assay with diol-PEG_{8k} described above. Interestingly, we found that a high proportion of the plasma samples possessed detectable anti-PEG Ab levels. PEG-specific Ab levels statistically (90% confidence interval) above the detection cut-off limits were detected in ~72% of individuals, with 18%, 25% and 30% of all samples possessing anti-PEG IgG only, anti-PEG IgM only, and both anti-PEG IgG and IgM, respectively (Table 5.4). Our findings differ substantially from previously reported prevalence rates for pre-existing anti-PEG Ab, which ranged from <1% to 44% [20, 101, 102], with more recent studies averaging 20%-30% for healthy donors or treatment-naïve patients [17, 104, 105, 124], and which were generally determined using hemagglutination and endpoint dilution ELISAs. In our study, since most individuals exhibited only low anti-PEG Ab levels, the high prevalence of anti-PEG Ab is likely attributed in part to the high sensitivity of our competitive ELISA method (detection cut-off limits 2-15 ng/mL). Indeed, the majority of these "positive" plasma specimens had only low levels of anti-PEG Ab, with geometric mean anti-PEG IgG and IgM concentrations of 52 ng/mL and 22 ng/mL, respectively (Fig. 5.2a-b). Using higher threshold values, ~37% of samples possessed anti-PEG Ab above 100 ng/mL (28% IgG only, 6% IgM only, 3% both IgG and IgM), and plasma samples with anti-PEG IgG and/or IgM above 500 ng/mL represented only 8% of the total (Table 5.4), which would more closely align with the reported values in the existing literature.

Various IgG subclasses reflect different humoral immune responses and effector functions [12]. Thus, we evaluated the levels of different subclasses of anti-PEG IgG (IgG1-4)

among the contemporary human plasma samples. Interestingly, detected anti-PEG IgG were almost exclusively of the IgG1 and IgG2 subclasses, with IgG2 as the dominant subclass (57% positive individuals, geometric mean 41 ng/mL) vs. IgG1 (26% positive individuals, geometric mean 12 ng/mL) (Table 5.5, Fig. 5.3). All 97 serum samples that were positive for anti-PEG IgG1 also contained anti-PEG IgG2. PEG-specific IgG3 and IgG4 were rarely detected (Table 5.5, Fig. 5.3). In individuals positive for anti-PEG IgG, anti-PEG IgG1, IgG2, IgG3 and IgG4 accounted for ~16%, 83%, 0% and 1% of the total detectable anti-PEG IgG on average. For comparison, the relative abundance of all IgG subclasses in humans is ~60%, 32%, 4% and 4% for IgG1-4, respectively [12].

We next performed linear regression analysis to evaluate the relationship between the prevalence and levels of pre-existing anti-PEG Ab and available demographics factors such as age, gender, and race. Both the concentration and prevalence of anti-PEG IgG, but not anti-PEG IgM, decreased with greater age ($p<0.01$), with a 63% reduction in the prevalence between the oldest vs. youngest age group (Fig. 5.4a-d). However, the extent of correlation between the anti-PEG IgG and age was weak, with $R^2<0.10$ for most analyses (Fig. 5.5). The prevalence and serum levels of anti-PEG IgG were not correlated to gender, whereas females were slightly more likely to possess anti-PEG IgM ($p<0.01$) (Fig. 5.4e-h). No observed relationship was found for race with anti-PEG IgM and IgG (Fig. 5.4i-l). Similar to total anti-PEG IgG, anti-PEG IgG1 and IgG2 concentrations were correlated with age (all $p<0.01$) but not gender or race (Fig. 5.4). To determine whether the observed relationship with age was attributed to reduction in total antibody levels, we quantified the total concentrations of human IgG1-4 and IgM in all samples. The amount of anti-PEG IgG, IgG1 and IgG2 as a fraction of the total IgG, IgG1 and IgG2 levels, respectively, also decreased with age (all $p<0.01$) but not with race or gender (Fig. 5.6),

indicating that the decline in prevalence and levels of anti-PEG Ab is not attributed to a broad decrease in total Ab. Whether the relationship between anti-PEG IgG and age reflects overall changes in the immune system with age (e.g., reduced B cell repertoire or reduced isotype switching from low affinity IgM to higher affinity IgG) [331], decreased affinity of the PEG-specific IgG in older vs. younger individuals, differences in recent or total lifetime exposure to PEG, or other factors remains unclear.

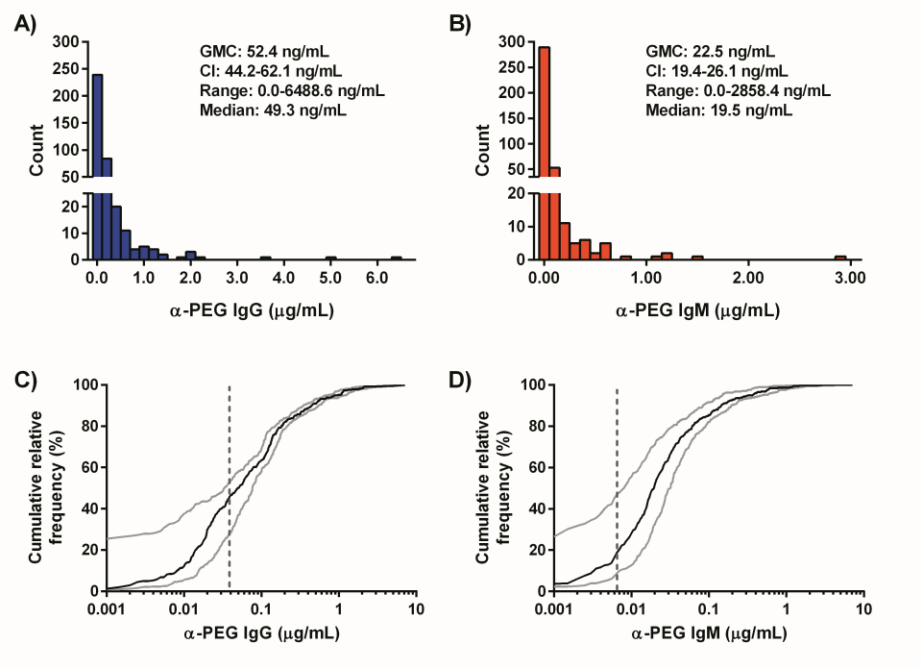

Figure 5.2. Anti-PEG IgG and IgM in the general population. Frequency distribution of **a)** anti-PEG IgG and **b)** anti-PEG IgM levels in contemporary human plasma samples (n=377). GMC: geometric mean concentration, CI: 95% confidence intervals for the GMC. Cumulative frequency distribution of **c)** anti-PEG IgG and **d)** anti-PEG IgM levels in contemporary human plasma samples. Light gray lines represent the 90% CI, and detection cut-off limits are indicated by the vertical gray dashed lines.

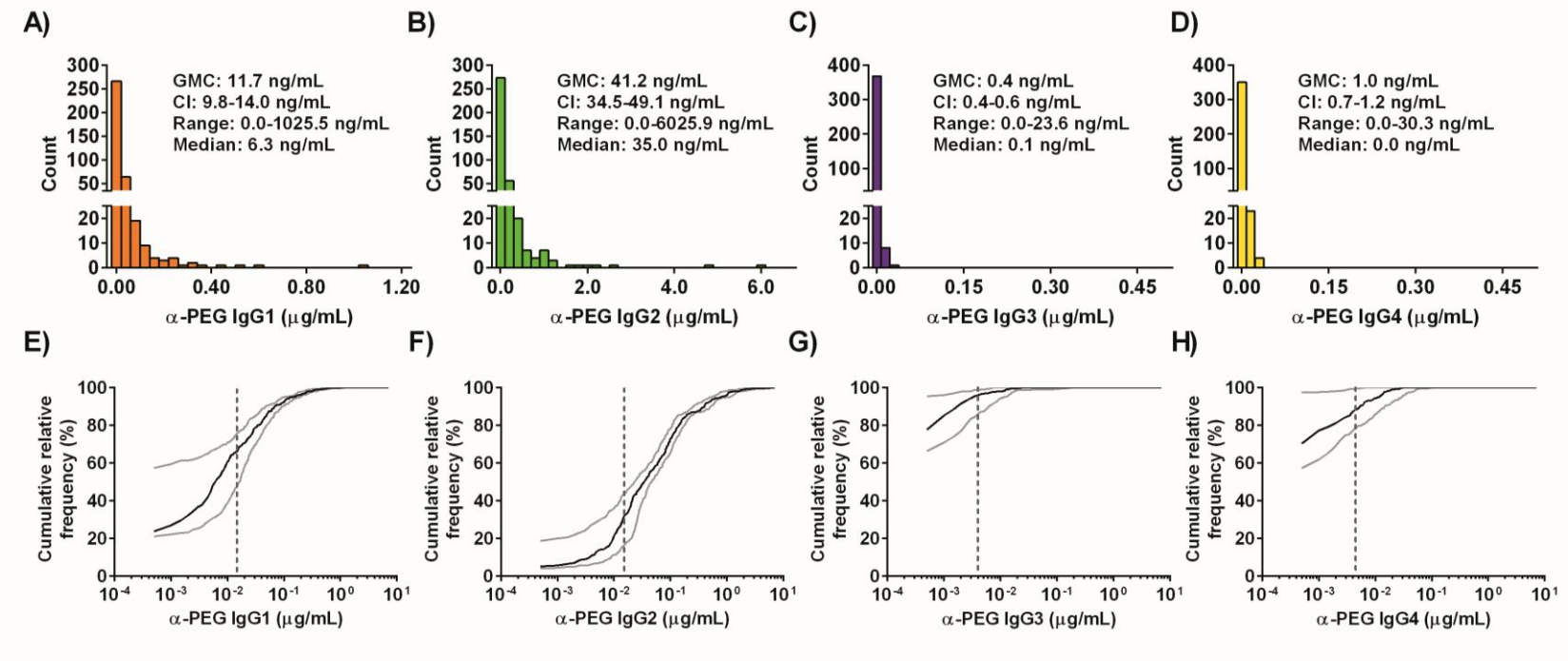

Figure 5.3. Anti-PEG IgG1-4 in the general population. Frequency distribution of **a)** anti-PEG IgG1, **b)** IgG2, **c)** IgG3, and **d)** IgG4 levels in contemporary human plasma samples (n=377). GMC: geometric mean concentration, CI: 95% confidence intervals for the GMC. Cumulative frequency distribution of **e)** anti-PEG IgG1, **f)** IgG2, **g)** IgG3, and **h)** IgG4 levels in contemporary human plasma samples. Light gray lines represent the 90% CI, and detection cut-off limits are indicated by the vertical gray dashed lines.

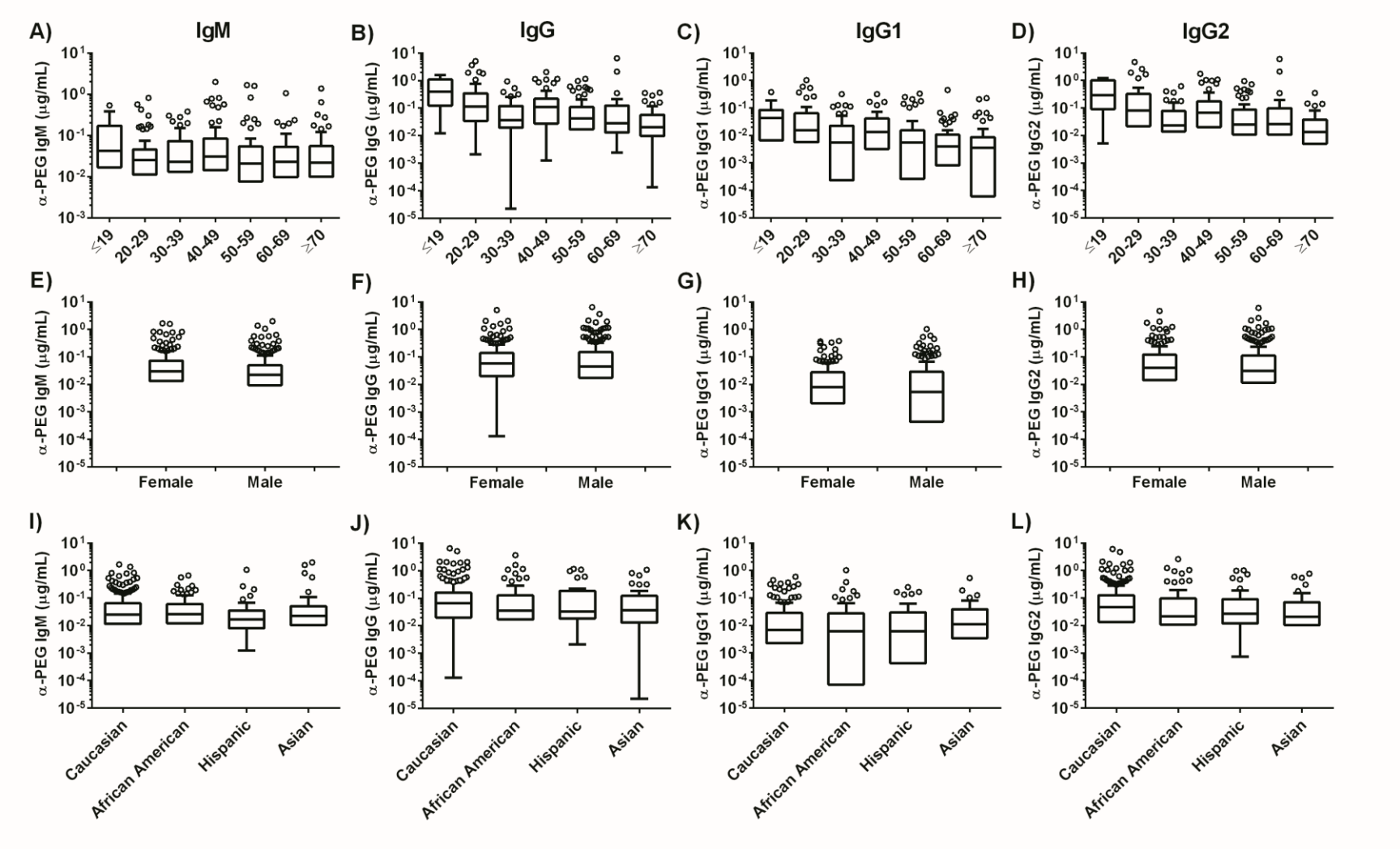

Figure 5.4. Anti-PEG IgM, IgG, IgG1, and IgG2 levels in healthy individuals by a-d) age group, e-h) gender, i-l) and race (n=377). The data are depicted using Tukey's method for box-and-whisker plots, with samples outside of the whiskers shown as open circles.

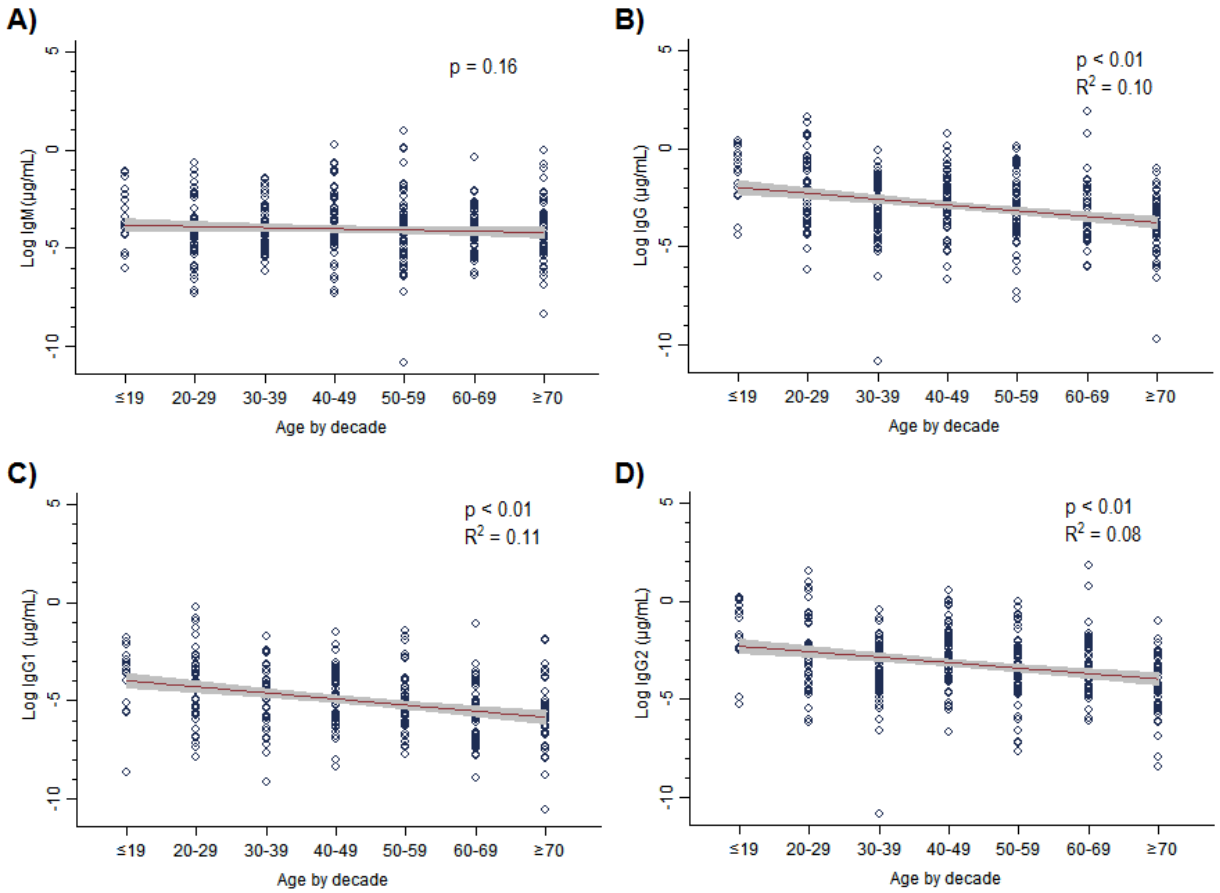

Figure 5.5. Relationship between anti-PEG Ab levels and age. Linear regression of log concentrations of A) anti-PEG IgM, B) anti-PEG IgG, C) anti-PEG IgG1, and D) anti-PEG IgG2 concentrations and age by decade. The fitted regression line is shown in red, with 95% confidence intervals shown in gray.

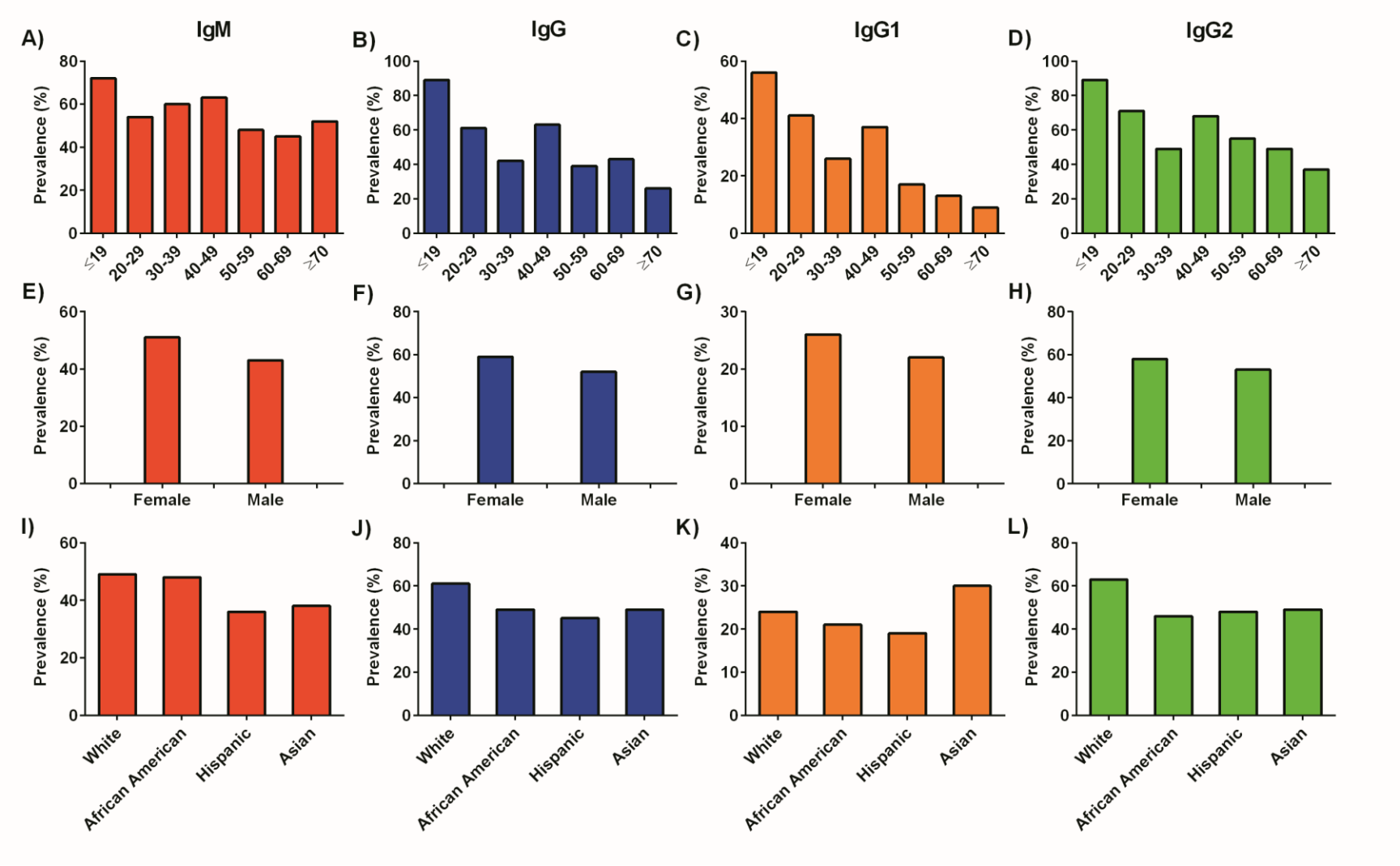

Figure 5.6. Anti-PEG IgM, IgG, IgG1, and IgG2 prevalence in healthy individuals by a-d) age group, e-h) gender, and i-l) race (n=377).

5.3.3 Anti-PEG Ab levels in historical samples

In the earliest report of human anti-PEG antibodies, Richter and Akerblom observed pre-existing anti-PEG Ab in <5% of healthy donors [101]. Since then, the reported values for pre-existing anti-PEG Ab compiled across various clinical studies and reports has spanned a wide range, with more recent studies reflecting higher prevalence rates, typically >20% [20, 100, 105]. To determine whether these disparities reflect a true increase in anti-PEG Ab levels among the population over time or are likely attributed to differences in sensitivity of detection assays, we obtained healthy human serum samples banked from the 1970s, 1980s and 1990s, and quantified the levels of anti-PEG Ab in these samples. We detected anti-PEG IgG alone, anti-PEG IgM alone, and both anti-PEG IgG and IgM in 20%, 19%, and 16% of all historical samples, respectively (Table 5.6, Fig. 5.7). Although the overall prevalence of anti-PEG Ab among the historical samples was slightly lower than among the contemporary samples ($p<0.001$), the observed prevalence rates of anti-PEG Ab were far higher than those previously reported in historical human samples (e.g., 0.2%-4.9% in healthy donors in 1984 [101]). In contrast, the anti-PEG IgG and IgM concentrations did not differ significantly between the historical and contemporary samples. Other major characteristics of the anti-PEG Ab response, such as higher concentrations of IgG relative to IgM and the presence of IgG2 as the dominant anti-PEG IgG subclass, were consistent between historical and contemporary samples as well (Fig. 5.7-5.9). The amount of total antibody present in the historical serum samples was similar to that in the contemporary plasma samples (Fig. 5.10), indicating that the obtained samples remained intact over years of storage and were unlikely to have negatively impacted the measured anti-PEG Ab levels. We observed no clear relationship between any demographic factors and anti-PEG Ab prevalence or concentration for the historical samples, although the small sample size likely limited the power of our analysis.

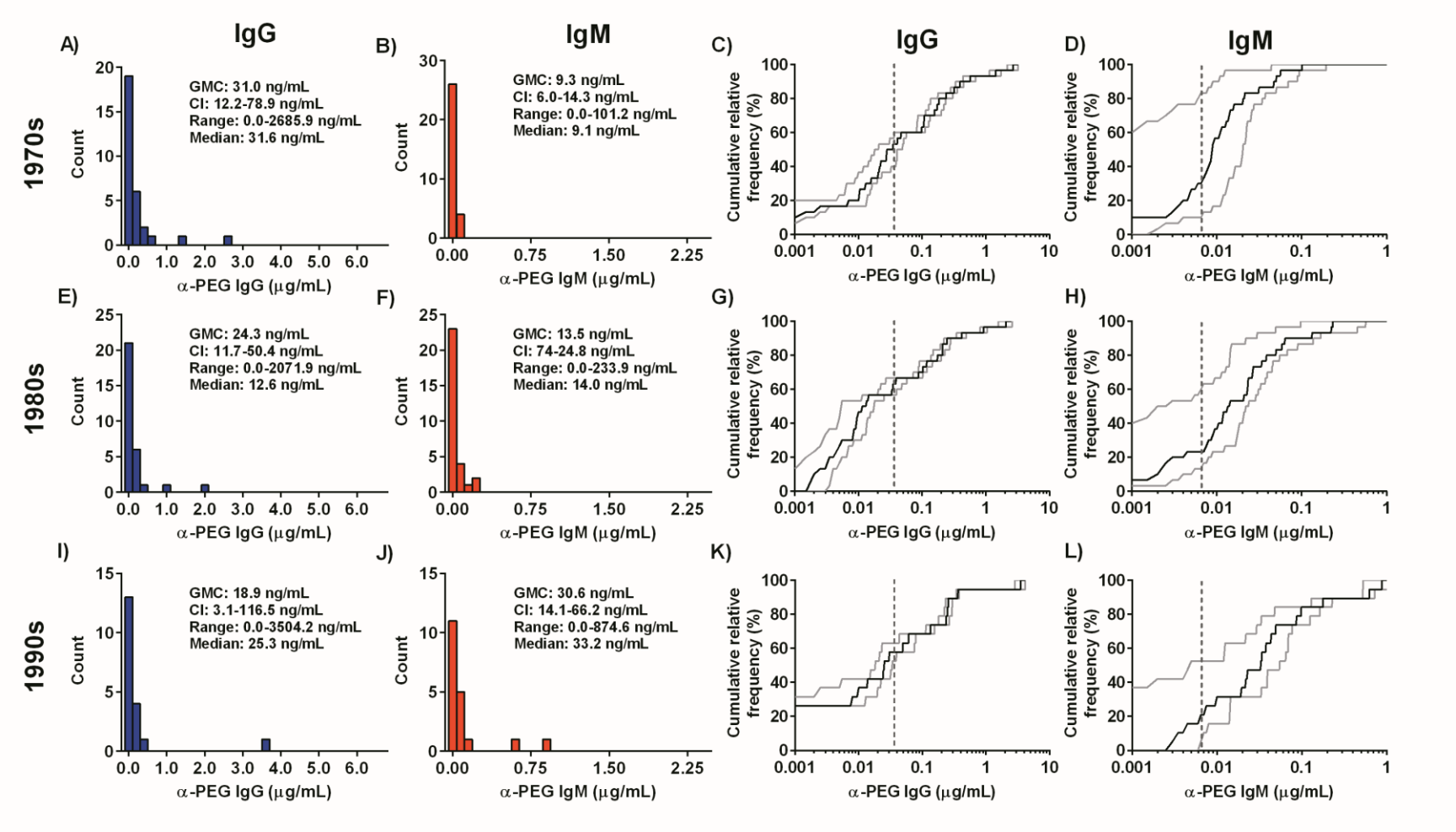

Figure 5.7. Anti-PEG IgG and IgM in historical samples. Frequency distribution of anti-PEG IgG and IgM levels in historical human serum samples collected in the **a-b)** 1970s, **e-f)** 1980s, and **i-j)** 1990s (n=30, 30, and 19, respectively). GMC: geometric mean concentration, CI: 95% confidence intervals for the GMC. Cumulative frequency distribution of anti-PEG IgG and IgM levels in historical human serum samples collected in the **c-d)** 1970s, **g-h)** 1980s, and **k-l)** 1990s. Light gray lines represent the 90% CI, and detection cut-off limits are indicated by the vertical gray dashed lines.

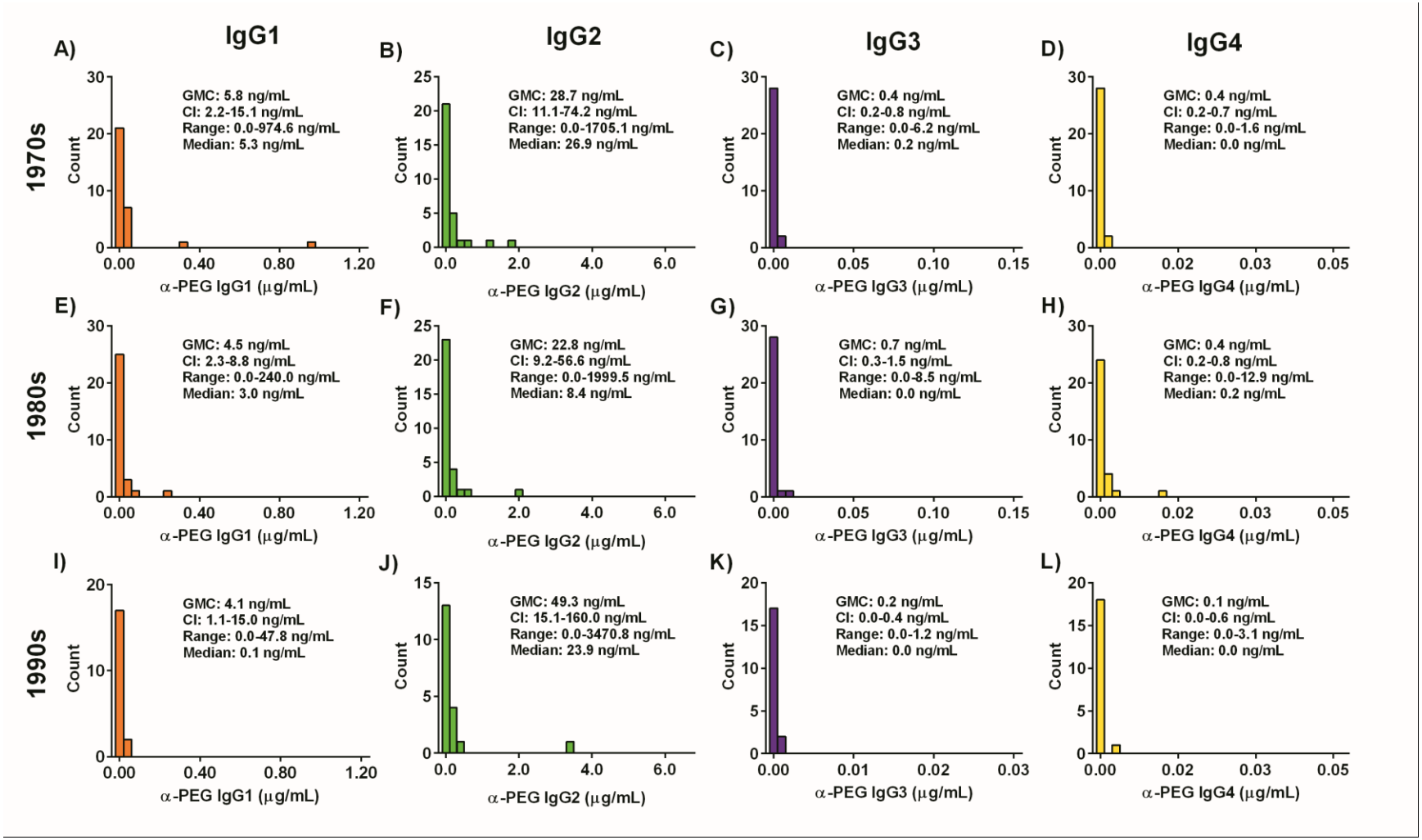

Figure 5.8. Anti-PEG IgG1-4 levels in historical samples. Frequency distribution of anti-PEG IgG1 **(panels a,e,i)**, IgG2 **(panels b,f,j)**, IgG3 **(panels c,g,k)**, and IgG4 **(panels d,h,l)** in human serum samples from the 1970s **(panels a-d)**, 1980s **(panels e-h)**, and 1990s **(panels i-l)** (n=30, 30, 19, respectively). GMC: geometric mean concentration, CI: 95% confidence intervals for the GMC.

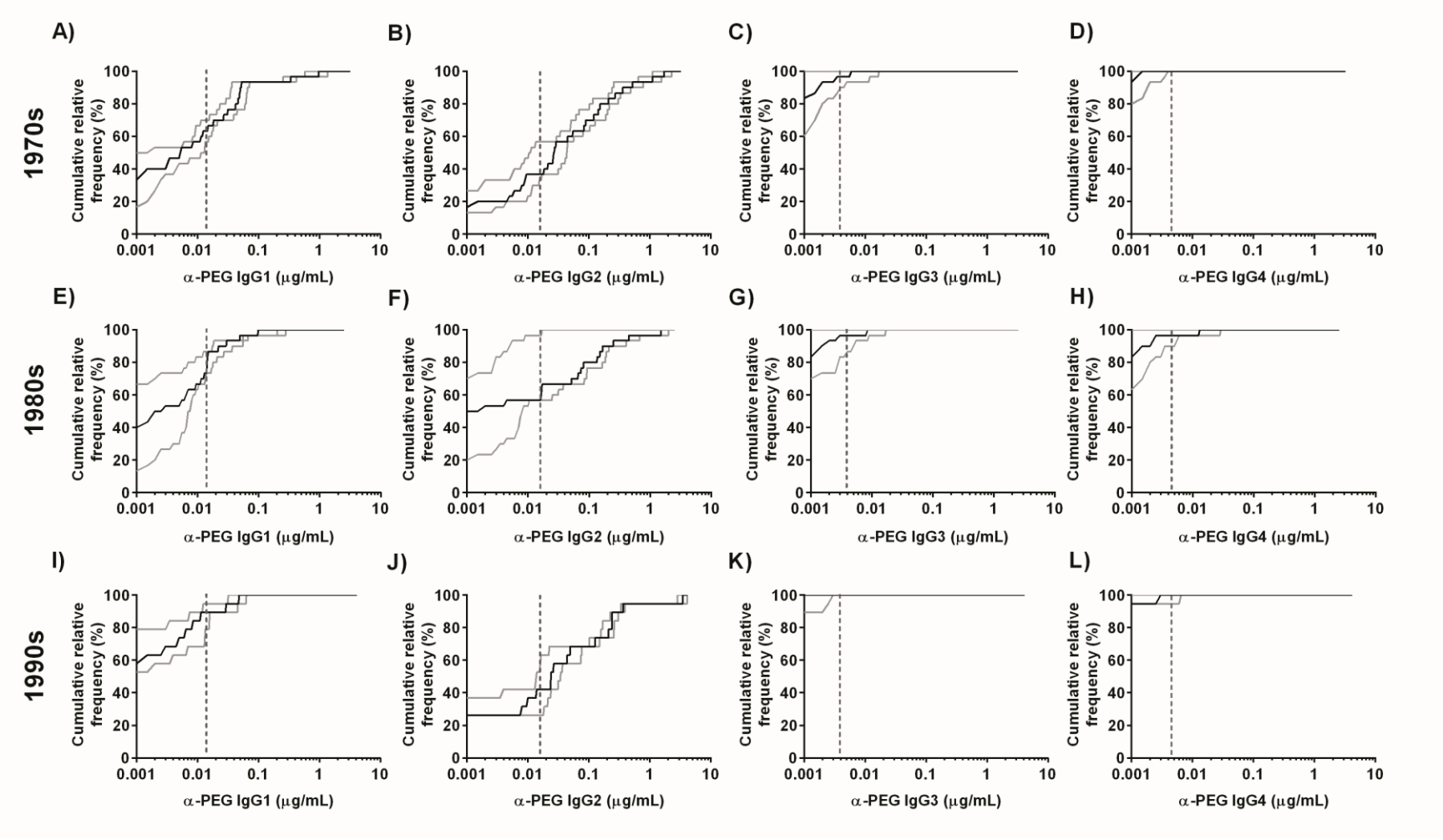

Figure 5.9. Anti-PEG IgG1-4 prevalence in historical samples. Cumulative distribution of anti-PEG IgG1 **(panels a,e,i)**, IgG2 **(panels b,f,j)**, IgG3 **(panels c,g,k)**, and IgG4 **(panels d,h,l)** in human serum samples from the 1970s **(panels a-d)**, 1980s **(panels e-h)**, and 1990s **(panels i-l)** (n=30, 30, 19, respectively). Light gray lines represent the 90% CI, and detection cut-off limits are indicated by the vertical gray dashed lines.

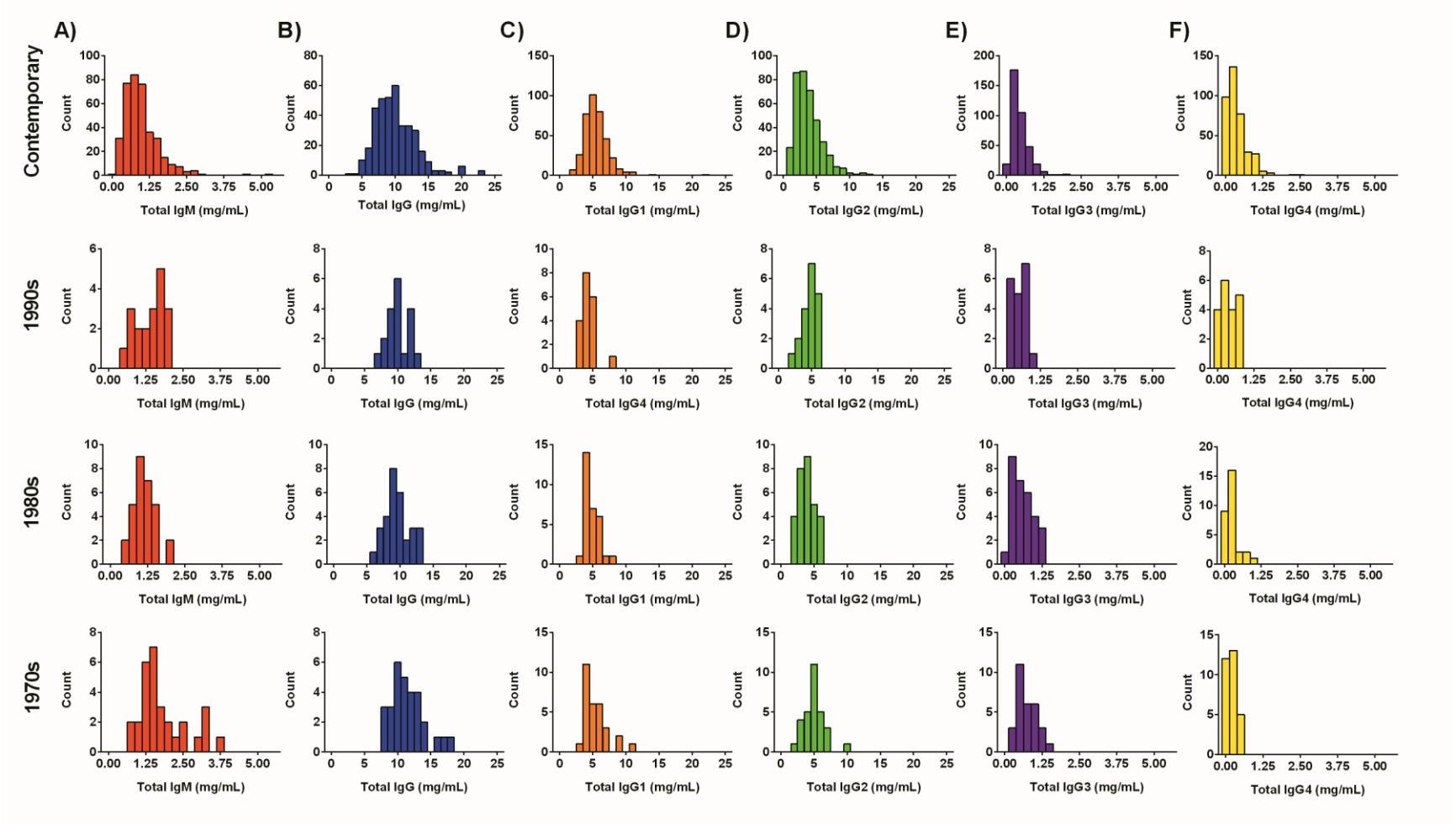

Figure 5.10. Total antibody levels in contemporary and historical samples. Frequency distribution of total **a)** IgM, **b)** IgG, **c)** IgG1, **d)** IgG2, **e)** IgG3, and **f)** IgG4 in contemporary human plasma samples **(row 1)** and serum samples from the 1990s **(row 2)**, 1980s **(row 3)**, and 1970s **(row 4)** (n=377, 19, 30, 30, respectively).

5.4 Discussion

Immune responses to therapeutic agents can reduce or completely eliminate their efficacy, as well as lead to undesirable side effects such as hypersensitivity and anaphylactic reactions that pose significant concerns for patient safety. Although PEG was long thought to be non-immunogenic and had even been used to reduce the immunogenicity of protein antigens, growing evidence suggests that both animals and humans can form antibodies that specifically recognize the PEG component of various PEGylated therapeutics [17, 22, 89]. A particularly concerning phenomenon is the potential presence of anti-PEG Ab in treatment-naïve individuals without previous exposure to specific PEGylated therapeutics (i.e., individuals with pre-existing anti-PEG Ab). Here, we observed a surprisingly high prevalence of pre-existing anti-PEG Ab in the general contemporary population, with ~72% of the samples possessing detectable levels of anti-PEG IgG and/or IgM, including a small fraction of samples (~8%) that exhibited modest to high levels of either anti-PEG Ab (Table 5.4). The widespread prevalence of anti-PEG Ab underscores the importance of assessing potential Ab responses to the growing number of PEGylated protein and drug delivery systems that are in development, in clinical trials, and on the market [332].

Our findings differ substantially from previously reported prevalence rates for anti-PEG Ab that ranged from <1% to 44% [20, 101, 102]. Those estimates are generally based on hemagglutination and end-titer ELISAs that utilize subjective threshold cut-offs with limited sensitivity, and estimates can be difficult to interpret across the various assay formats. Since most individuals exhibited only low anti-PEG Ab levels, the high prevalence of anti-PEG Ab in our study is likely attributed in part to the high sensitivity of our competitive ELISA method (detection cut-off 2-15 ng/mL). Using more stringent thresholds such as 100 ng/mL or 500

ng/mL, only 37% and 8% of the contemporary samples, respectively, would be considered positive for anti-PEG Ab, which would more closely align with the reported values in the existing literature.

It has been recently hypothesized that anti-PEG immunity may be gaining in prevalence, based on a comparison of the results from Richter and Akerblom in 1984 (detectable and high titer anti-PEG Ab in 4.9% and 0.2% of healthy donors, respectively) [101] to later results such that those of Armstrong *et al*. in 2003 (27%-28% of their healthy donors) [100], with the increased use of PEG in household, food, beauty, and health products being a primary driver of the gaining prevalence. However, albeit only from a limited number of specimens, we found that over 50% of the serum samples from 1970s-1990s actually possessed anti-PEG Ab, which suggests that the hypothesis of emerging anti-PEG prevalence may not be true. Instead, immunological responses to PEG are likely longstanding yet underappreciated, and the increasing incidence of adverse events with PEG-modified therapeutics may simply reflect its increasing parenteral use in pharmaceutical and clinical settings.

Given the generally strong safety profile of many PEG-modified therapeutics, and assuming that the prevalence and concentrations of anti-PEG Ab measured here are correct, our findings would seem to support the conclusion that low to perhaps even modest levels of circulating anti-PEG Ab in most individuals would not adversely affect the safety and efficacy of PEG-modified therapeutics. In other words, below certain threshold concentrations, anti-PEG Ab in the blood may not accumulate on a substantial fraction of injected PEG-modified therapeutics at a sufficient level or at a sufficiently rapid rate, and thus would not meaningfully alter their PK/PD or trigger adverse immunological responses. Consistent with this hypothesis, in several recent clinical trials, accelerated clearance or adverse reactions to PEGylated drug have primarily

been reported in subjects with high titers of anti-PEG Ab [17, 22, 103]. Unfortunately, the precise threshold concentrations of anti-PEG Ab that could begin to impact the safety and efficacy of PEG-modified therapeutics remain poorly understood, and would likely vary depending on the specific therapeutic(s) in use. It should be noted that antibody levels as low as 100 ng/mL have been associated with altered pharmacokinetics of monoclonal Ab drugs due to anti-drug Ab, as well as vaccine efficacy [333-335]. Thus, the possibility exists that the PK/PD, as well as safety profile, of certain PEGylated proteins and drug delivery systems may be sensitive to modest levels of circulating anti-PEG Ab. This possibility, coupled with the small but not trivial number of healthy individuals who exhibit high levels of pre-existing anti-PEG Ab, suggests that sensitive detection and precise quantitation of anti-PEG Ab levels in a clinical setting will be essential to ensuring the safe use of PEGylated drugs in all target patient populations going forward.

The mechanism through which antibodies can be generated against a polymer that demonstrates strong anti-fouling properties remains a mystery. In rodent models intravenously dosed with PEGylated liposomes, anti-PEG Ab formation has been proposed to occur through a T-cell independent mechanism involving splenic B cells [19, 61]. This process generates anti-PEG IgM almost exclusively, and does not induce memory; hence, depending on the frequency of administration, the accelerated blood clearance effect, as well as adverse reactions mediated by anti-PEG IgM can be largely minimized in animal studies [57, 67, 336]. In contrast to these *in vivo* results, we found a mixture of anti-PEG IgG and IgM in the human samples, with higher levels of IgG than IgM and far more IgG2 than IgG1. IgG2 antibodies are often associated with T-cell independent antibody induction, which appears to support the mechanism of anti-PEG Ab induction observed in mice. The IgG2 subclass is primarily responsible for antibody responses to

polysaccharide antigens [12]; PEG, as a highly repetitive and hydrophilic polymer, may bear some structural resemblance to such antigens. However, it should be noted that high levels of anti-PEG IgG2 alone do not necessarily signify a solely T-cell independent mechanism of antibody induction. The presence of anti-PEG IgG1, which was found in approximately half of all anti-PEG IgG2-positive individuals and comprised ~16% of the total anti-PEG IgG/individual on average, reflects a likely complex and variable mechanism of anti-PEG Ab formation.

IgG antibodies are a hallmark of immunological memory in humoral immune response. The high presence of detectable anti-PEG IgG, even if the average baseline concentrations is low, implies that immunological memory likely exists in the majority of the population that could in turn result in rapid increase of anti-PEG Ab following dosing of PEGylated drugs. When combined with the increasing use of PEGylation, this reality could present a unique medication management and polypharmacy issue, as patients may have elevated levels of pre-existing anti-PEG Ab in response to an unrelated therapeutic prior to receiving the PEG-modified therapy of interest. Even the inclusion of PEG as an inactive ingredient could pose a challenge for individuals with sufficiently high anti-PEG Ab levels, as evidenced by the serious adverse reactions experienced by two patients in a clinical trial for PEGylated phenylalanine ammonia lyase who received unrelated intramuscular injections of contraceptives containing PEG as an excipient [103]. Interestingly, Lubich *et al*. reported that repeated measurements of anti-PEG levels in some individuals can vary over time in the absence of known treatment with PEGylated drugs [105]. Further understanding of the mechanism, risk factors, critical threshold, and other characteristics of anti-PEG Ab would significantly improve our ability to identify, mitigate, or avoid PEG-related immunogenicity in patients.

5.5 Conclusions

PEG has a variety of useful applications in the pharmaceutical industry, and a number of PEGylated therapeutics have been highly successful. However, growing evidence from recent clinical trials suggests that the presence of high anti-PEG Ab levels, including pre-existing humoral responses, can abrogate the efficacy of PEG-modified drugs or result in serious adverse reactions. Using a rigorously validated quantitative ELISA method, we detected low levels of anti-PEG IgG and IgM in the majority of the population, and high levels (>500 ng/mL) in a small but non-trivial number of individuals. The presence of anti-PEG implies the existence of immunological memory that could result in rapid elevation of anti-PEG Ab levels. In light of the increasing number of PEG-modified or PEG-containing pharmaceutical products on the market, we believe it is prudent to introduce regular monitoring of anti-PEG Ab responses in patients receiving PEGylated therapies, as it could affect clinical trial design, testing, and dosing regimens for PEGylated therapeutics.

Table 5.1. Summary of patient demographics for contemporary and historical samples.

	Contemporary (n=377)	**1970-1979** (n=30)	**1980-1989** (n=30)	**1990-1999** (n=19)
Age, *n* (%)				
≤19	18 (5%)	0 (0%)	1 (3%)	0 (0%)
20-29	56 (15%)	8 (27%)	5 (17%)	0 (0%)
30-39	65 (17%)	7 (23%)	5 (17%)	0 (0%)
40-49	62 (16%)	8 (27%)	5 (17%)	9 (47%)
50-59	69 (18%)	7 (23%)	5 (17%)	5 (26%)
60-69	53 (14%)	0 (0%)	5 (17%)	4 (21%)
≥70	54 (14%)	0 (0%)	4 (13%)	1 (5%)
Gender, *n* (%)				
Male	226 (60%)	15 (50%)	15 (50%)	13 (68%)
Female	151 (40%)	15 (50%)	15 (50%)	6 (32%)
Race, *n* (%)				
Caucasian	200 (53%)	30 (100%)	30 (100%)	19 (100%)
Black/African American	49 (13%)	0 (%)	0 (%)	0 (%)
Hispanic	42 (11%)	0 (%)	0 (%)	0 (%)
Asian	37 (10%)	0 (%)	0 (%)	0 (%)

Table 5.2. ELISA assay details for anti-PEG IgG1, IgG2, IgG3, IgG4, and IgM.

	Anti-PEG IgG1	**Anti-PEG IgG2**	**Anti-PEG IgG3**	**Anti-PEG IgG4**	**Anti-PEG IgM**
Detection threshold	14.2 ng/mL	15.1 ng/mL	3.9 ng/mL	4.4 ng/mL	6.4 ng/mL
Precision (CV%)	24 ± 6%	24 ± 9%	35 ± 10%	26 ± 6%	32 ± 10%
Accuracy (%)	103 ± 8%	102 ± 4%	99 ± 6%	101 ± 3%	102 ± 4%

Table 5.3. Binding kinetics of chimeric anti-PEG IgG and IgM.

	c6.3 anti-PEG IgG1	c6.3 anti-PEG IgG2	c6.3 anti-PEG IgG3	c6.3 anti-PEG IgG4	cAGP.3 anti-PEG IgM
K_D (M)	$5.8 \pm 0.2 \times 10^{-9}$	$5.3 \pm 0.2 \times 10^{-9}$	$4.8 \pm 0.08 \times 10^{-9}$	$5.1 \pm 0.2 \times 10^{-9}$	$6.6 \pm 0.4 \times 10^{-11}$
k_{on} (1/M•s)	$6.7 \pm 0.07 \times 10^{4}$	$8.6 \pm 0.1 \times 10^{4}$	$7.1 \pm 0.04 \times 10^{4}$	$4.9 \pm 0.04 \times 10^{4}$	$1.1 \pm 0.03 \times 10^{7}$
k_{off} (1/s)	$3.9 \pm 0.07 \times 10^{-4}$	$4.6 \pm 0.08 \times 10^{-4}$	$3.4 \pm 0.04 \times 10^{-4}$	$2.5 \pm 0.05 \times 10^{-4}$	$7.1 \pm 0.02 \times 10^{-4}$
R^2	0.993	0.993	0.998	0.997	0.974

Table 5.4. Prevalence of anti-PEG IgG and IgM in contemporary human plasma samples (n=377).

Prevalence of anti-PEG Ab response	Total Ab	IgG	IgM	IgG and IgM
Positive individuals, *n* (%)	273 (72%)	67 (18%)	93 (25%)	113 (30%)
Individuals ≥100 ng/mL, *n* (%)	139 (37%)	107 (28%)	22 (6%)	10 (3%)
Individuals ≥500 ng/mL, *n* (%)	30 (8%)	26 (7%)	4 (1%)	0 (0%)

Table 5.5. Prevalence of anti-PEG IgG1-4 in contemporary human plasma samples (n=377).

Prevalence of anti-PEG Ab response	IgG1	IgG2	IgG3	IgG4
Positive individuals, *n* (%)	97 (26%)	214 (57%)	5 (1%)	3 (1%)
Individuals ≥100 ng/mL, *n* (%)	19 (5%)	83 (22%)	0 (0%)	0 (0%)
Individuals ≥500 ng/mL, *n* (%)	1 (0%)	19 (5%)	0 (0%)	0 (0%)

Table 5.6. Prevalence of anti-PEG IgG and IgM in historical human serum samples collected from the 1970s, 1980s, and 1990s (n=30, 30, 19, respectively).

	Prevalence of anti-PEG Ab response	Total Ab	IgG	IgM	IgG and IgM
1970s	Positive individuals, *n* (%)	14 (47%)	8 (27%)	2 (7%)	4 (13%)
	Individuals ≥100 ng/mL, *n* (%)	9 (30%)	9 (30%)	0 (0%)	0 (0%)
	Individuals ≥500 ng/mL, *n* (%)	2 (7%)	2 (7%)	0 (0%)	0 (0%)
1980s	Positive individuals, *n* (%)	18 (60%)	5 (17%)	8 (27%)	5 (17%)
	Individuals ≥100 ng/mL, *n* (%)	7 (23%)	7 (23%)	0 (0%)	0 (0%)
	Individuals ≥500 ng/mL, *n* (%)	2 (7%)	2 (7%)	0 (0%)	0 (0%)
1990s	Positive individuals, *n* (%)	12 (63%)	3 (16%)	5 (26%)	4 (21%)
	Individuals ≥100 ng/mL, *n* (%)	8 (42%)	5 (26%)	2 (11%)	1 (5%)
	Individuals ≥500 ng/mL, *n* (%)	3 (16%)	1 (5%)	2 (11%)	0 (0%)

CHAPTER 6: PRETARGETING WITH BISPECIFIC FUSION PROTEINS TO FACILITATE DELIVERY OF NANOPARTICLES TO MOLECULARLY DISTINCT TUMORS

6.1. Introduction

Effective delivery of therapeutic drug molecules or imaging contrast agents to cancer cells continues to be one of the biggest challenges in cancer therapy and diagnostics. Strategies used to target nanoparticles to cancer cells generally exploit unique features of tumor physiology such as (1) the poorly formed and leaky blood vessels that facilitate enhanced nanoparticle extravasation from the tumor vasculature relative to normal vasculature (i.e., the Enhaced Permeation and Retention [EPR] effect), and (2) the differential expression of surface receptors relative to normal tissues [135, 141]. Unfortunately, the extent of the EPR effect varies substantially among different tumors and different subjects [152, 156]. “Stealth” nanoparticles that rely solely on “passive targeting” via the EPR effect are also poorly internalized, limiting the efficiency of intracellular delivery [137, 141]. Although, “actively targeted” nanoparticles with tumor-specific ligands can theoretically bind and internalize into specific tumor cells, they are often quickly eliminated from the circulation due to rapid mononuclear phagocyte system (MPS) clearance [125]; this can result in a far lower fraction of the administered dose of ligand-conjugated nanoparticles extravasating at target tissue(s) relative to passively targeted nanoparticles. Indeed, in numerous reports in the literature, actively targeted nanoparticle systems did not appreciably improve nanoparticle delivery to tumors when compared to passively targeted nanoparticles [126, 337, 338].

The aforementioned challenges are further exacerbated by tumor heterogeneity, which encompasses the functional and phenotypic differences between cancer cells such as cellular morphology, gene and protein expression, metabolism, motility, proliferation, level of drug resistance, and metastatic potential. Tumor heterogeneity can be caused by variations in accumulated genetic mutations, along with alterations in the local tumor microenvironment, that frequently lead to genomically distinct subclonal populations within the same tumor or between tumor lesions [131, 178]. In turn, the existence of diverse cancer cell populations poses a major challenge to targeted delivery of diagnostic and/or therapeutic agents. Single ligand-conjugated nanoparticles generally fail to facilitate delivery to the diverse range of cells present in a given tumor lesion or patient [126]. Tumor heterogeneity can also result in variable EPR effects within different regions of the same tumor. As a result, many cancers are only partial suppressed after treatment with nanomedicines, leading to eventual tumor regrowth and/or the development of drug-resistant tumors. A potential solution involves the conjugation of multiple ligands onto a single nanoparticle. Unfortunately, such an approach would not only incur exorbitant developmental costs but also require conjugation of excess targeting ligands that would likely result in rapid phagocytic clearance of the modified particles. Most current nanoparticle-based drug delivery strategies fail to deliver adequate therapeutic payload to the full spectrum of tumor cells present in a given patient.

A recently emerged strategy to facilitate targeted delivery of therapeutics is “pretargeting,” which involves first introducing pretargeting molecules that can specifically bind the tumor cells of interest and then capture the therapeutic and/or diagnostic payload administered in a second injection (Fig. 6.1). Pretargeting in the form of pretargeted radioimmunotherapy (PRIT) has been extensively studied *in vivo* and in human subjects to improve the delivery of radioactive payload

relative to antibody-radiolabel drug conjugates [195] and has generally shown greater tumor specificity and safety compared to conventional radioimmunotherapy [194]. Despite the considerable success of PRIT, pretargeting has rarely been applied to improve drug delivery by polymeric nanoparticles. Consequently, the potential applications, limitations, and challenges of this targeting strategy remain largely unknown [339]. A particular attractive feature of pretargeting is the theoretical ease in increasing the breadth of nanoparticle targeting to heterogeneous and molecularly distinct tumors simply by tuning the combination of pretargeting molecules used. For a given pretargeting molecule, the tumor-binding domain can be modified, while the nanoparticle-binding domain remains unchanged (Fig. 6.1). In this study, we sought to evaluate whether pretargeting with two different pretargeting bispecific fusion proteins (FPs) consisting of single-chain variable fragments (scFvs) linked to streptavidin (SA), which have been successfully used in PRIT [207, 340], can enhance the delivery of the same biotinylated polymeric nanoparticles simultaneously to corresponding T- and B-lymphoma cells *in vitro* and *in vivo*.

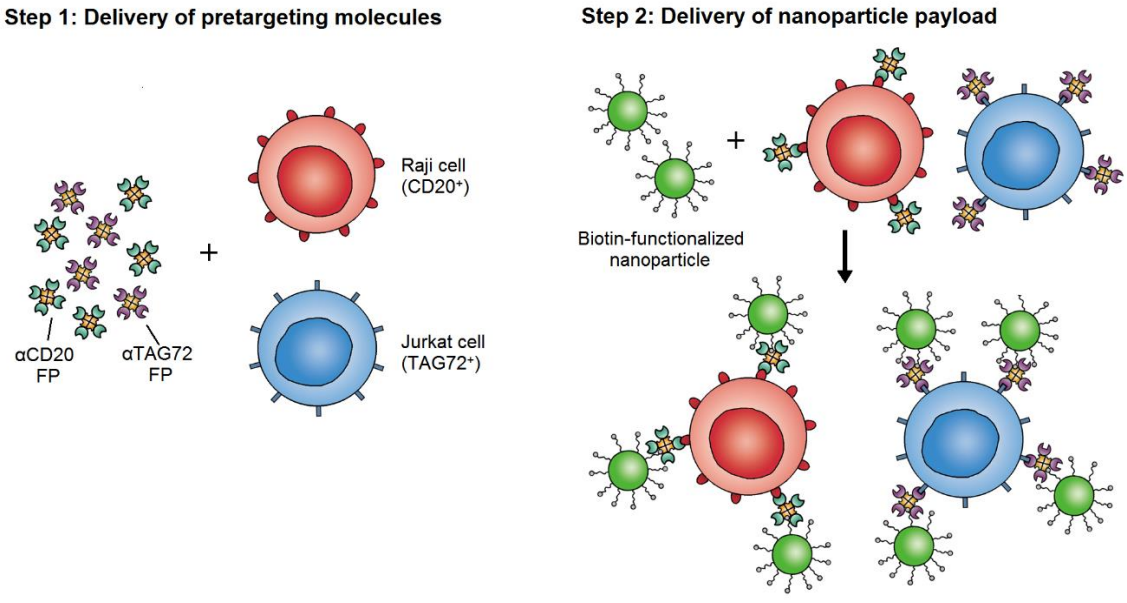

Figure 6.1. Schematic illustration of pretargeted nanoparticle delivery to a heterogeneous population of lymphoma cells. In the first step, a cocktail of pretargeting fusion proteins (FPs), based on

streptavidin linked to single-chain variable fragments, is used to specifically label Raji B-cell lymphoma ($CD20^+$) and Jurkat T-cell lymphoma ($TAG72^+$) cells. In the second step, biotin-functionalized nanoparticles are administered and will be captured by FPs bound to the surface of target cells.

6.2. Materials and methods

6.2.1 Preparation and characterization of PS-PEG-biotin nanoparticles

Carboxylate-modified yellow-green fluorescent polystyrene (PS) beads with mean diameters of ~100 nm were purchased from Invitrogen (Carlsbad, CA, USA). The surface COOH densities of the particles (3.4 COOH groups/nm^2) were calculated from the mEq/g values provided by the manufacturer. Methoxy PEG amine (mPEG-NH_2, 3 and 5 kDa) was purchased from JenKem (Allen, TX, USA), and biotin PEG amine (bPEG-NH_2, 3 kDa) was obtained from Rapp Polymere (Tuebingen, Germany). Amine-modified PEGs were conjugated to the PS particles as previously described [341]. Briefly, the beads were washed thrice with MilliQ H_2O and resuspended in 50 mM borate buffer (pH 7.8). mPEG-NH_2 and bPEG-NH_2 were added to the PS beads at varying methoxy PEG:biotin PEG ratios, and 1-ethyl-3-(3-dimethylaminopropyl)carbodiimide (EDC; Invitrogen) and N-hydroxysulfosuccinimide (S-NHS; Thermo Scientific, MA) were each added at five-fold molar excess of total PEG amine. The EDC/S-NHS reaction was allowed to proceed overnight at RT. The reaction mixture was quenched with excess glycine, and the PEG-modified particles were washed with MilliQ H_2O and resuspended in water to stock concentrations (~20 mg/mL). The hydrodynamic size and ζ-potential of the synthesized particles were determined by dynamic light scattering and laser Doppler anemometry, respectively, using a Zetasizer Nano ZS (Malvern, UK). The final PEG grafting density was indirected quantified using a 1-pyrenylyldiazomethane (PDAM; Invitrogen)-based assay, as previously described [341]. Biotin conjugation was confirmed using a dot blot assay: 1 µg of each PS-PEG or PS-PEG-biotin bead was blotted onto a nitrocellulose membrane, blocked with

5% nonfat milk in PBS-Tween 20 (PBS-T) for 1 h at room temperature, incubated with streptavidin-horseradish peroxidase (SA-HRP, 1:5000 dilution) for 1 h at room temperature, and then detected using an ECL kit (BioRad, Hercules, CA, USA) and a FluorChemE imaging system (Protein Simple, San Jose, CA, USA).

6.2.2 Cell culture and cell uptake assay

Human monocytic THP-1, Raji B cell lymphoma, and Jurkat T-acute lymphoblastic leukemia cells were obtained from the University of North Carolina at Chapel Hill Tissue Culture Facility and were maintained at 1 x 10^6 cells/mL in RPMI 1640 medium containing 10% fetal bovine serum and 1X penicillin-streptomycin, with incubation at 37°C and 5% CO_2. The anti-CD20 (αCD20) fusion proteins (1F5$(scFv)_4$SA [239, 342], B9E9$(scFv)_4$SA [343]) and anti-TAG72 (αTAG72) fusion proteins (CC49$(scFv)_4$SA[262]) were generously provided by the Oliver Press group (Fred Hutchinson Cancer Research Center). For the phagocytic uptake studies, THP-1 cells seeded into 24 well plates at 1.70 x 10^5 cells/mL were differentiated in culture medium containing 200 nM phorbol 12-myristate 13-acetate (PMA; Sigma-Aldrich, St. Louis, MO, USA) [341]. The PMA-containing medium was removed 3 days later and replaced with fresh culture medium, followed by incubation with various PS-PEG-biotin particles at a 1:10^4 cell:particle ratio for 12 h. For the lypmhoma cell uptake studies, 1 x 10^5 cells were seeded into 96-well plates and incubated with 500 nM fusion protein (FP) for 4 h. After washing to remove unbound FP, the cells were then incubated with various PS-PEG-biotin beads for 12 h at a 10^4:1 particle:cell ratio. Flow cytometry was performed using a FACSCanto instrument (BD, Franklin Lakes, NJ, USA). At least 10,000 events were recorded per sample, and the data were analyzed using BD FACSDiva software. The data represent n = 3 independent experiments performed in triplicate.

6.2.3 Pharmacokinetics and biodistribution of biotinylated nanoparticles

Female BALB/c mice (19−24 g body weight) were obtained from Charles River Laboratories (Wilmington, MA, USA), and all animal experiments carried out in accordance with an animal use protocol (#14-098) approved by the University of North Carolina Animal Care and Use Committee. The mice were injected with fully modified PS-PEG-biotin nanoparticles (15 mg/kg, i.v.) in a total of 100 μL of PBS via the tail vein, and the mice were sacrificed at various time points (0, 1, 2, and 6 h). Tissues (heart, liver, kidneys, spleen, lungs) and blood were collected, and the tissue biodistribution of the particles was determined using an IVIS Kinetic fluorescence imaging system with excitation at 465 nm. The fluorescence of particles in the blood was measured using a SpectraMax 2 microplate reader and compared to a standard curve generated using green fluorescent PS beads added to untreated blood. PK analysis of the blood concentration data was conducted with PKSolver using a one-compartment model fit to the data [49, 306].

6.2.4 Biodistribution of pre-targeted nanoparticles in mouse models containing single and dual tumors

Female athymic nude mice (20-24 g body weight) were obtained from the University of North Carolina at Chapel Hill Small Animal Core, and all animal experiments carried out in accordance with an animal use protocol (#14-054) approved by the University of North Carolina Animal Care and Use Committee. For single tumor-bearing mice, the animals were inoculated with Raji cells (2.5×10^7 cells each) on the right flank, and, for dual tumor-bearing mice, the animals were also inoculated with Jurkat cells (2.5×10^7 cells each) on the left flank. The mice were maintained on a biotin-free diet (Harlan Laboratories, Indianapolis, IN, USA) for at least 7 d prior to the start of the biodistribution studies. After the tumors reached ≥100 mm^3 in size, αCD20

and/or αTAG72 FP (250 μg each) were administered i.v., followed by P/S-PEG-biotin particles (15 mg/kg, i.v.) after 24 h. After another 24 h, the mice were sacrificed, and tissues (heart, liver, spleen, lungs, kidneys, tumors) were collected. The tissues from treated and untreated animals were imaged using an IVIS Kinetic fluorescence imaging system with excitation at 465 nm. The fluorescent signal present in the tissues was calculated as a percentage of the total recovered fluorescence for the collected tissue samples.

6.2.5 Statistical analysis

Group comparisons were performed using one-way ANOVA, followed by Dunnett's post hoc test, on SAS 9.3 software. A p-value <0.05 was considered to indicate statistical significance. All data are presented as mean ± SD.

6.3. Results

6.3.1 Synthesis and characterization of PS-PEG-biotin

Pretargeting molecules based on scFv chains linked to SA represent an appealing platform for proof-of-concept studies due to the exceptionally high affinity between biotin and streptavidin. To formulate biotinylated nanoparticles for use with the SA-based pretargeting molecules, we prepared a series of densely PEGylated polystyrene beads (~100 nm diameter) with different molar ratios of terminal biotin substitution, ranging from 0-100 mol% of all grafted PEG chains. All particles ranged between ~110-140 nm in average diameter (Fig. 6.2a), exhibited nearly neutrally charged surfaces (≥-10 mV) (Fig. 6.2a), and possessed very dense PEG coverage (≥ 2.0 PEG/nm^2) irrespective of the biotin density (Fig. 6.2b). The total number of biotin groups per nanoparticle was estimated based on the number of grafted PEG chains and the input molar ratio of biotin PEG

(Fig. 6.2c); increasing biotin substitution at higher biotin PEG ratios was validated by a dot blot assay (Fig. 6.3).

Presentation of surface ligands at high densities typically result in increased phagocytic clearance of nanoparticles [168, 170, 344]. Although biotin is exceedingly small (244 Da) and is a naturally occurring molecule in biological systems, we decided to quantify the uptake of PS-PEG-biotin beads by differentiated human macrophage-like THP-1 cells *in vitro*. Similar to beads modified with only methoxy PEG (0 mol% biotin), which are exceptionally resistant to uptake by phagocytic cells and exhibit prolonged circulation profiles *in vivo* [341], PS-PEG-biotin nanoparticles effectively evaded uptake by differentiated THP-1 cells across all biotin densities (Fig. 2d).

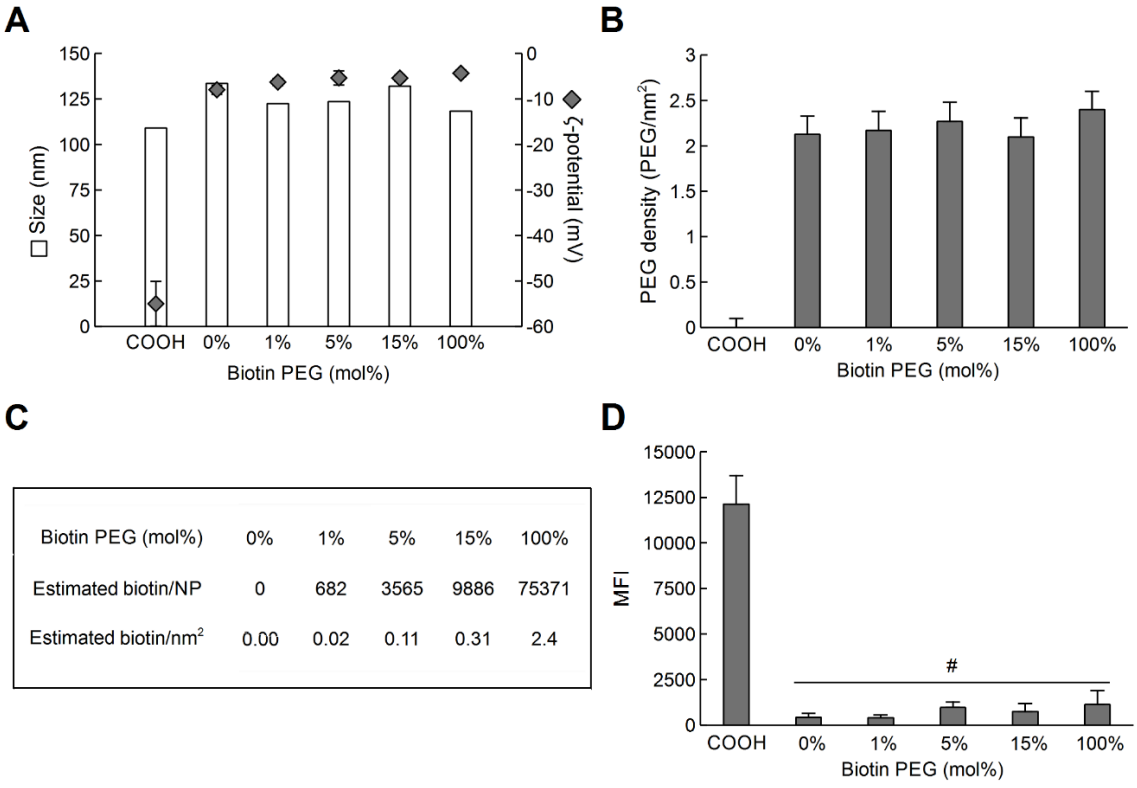

Figure 6.2. PS-PEG-biotin nanoparticle characterization. a) Hydrodynamic diameter (white bars) and surface charge (diamonds) of unmodified PS beads (COOH) and beads modified with varying mol% of

biotin PEG. **b)** Total PEG density of unmodified PS beads (COOH) and beads modified with varying mol% of biotin PEG. **c)** Estimated biotin PEG density and number for various PS-PEG-biotin beads. **d)** Mean cellular fluorescence intensity (MFI) of differentiated human THP-1 cells incubated with PS-COOH, PS-PEG and PS-PEG-biotin beads. # indicates $P < 0.01$ vs. PS-COOH beads. The data represent $n \geq 2$ independent experiments performed in at least triplicate.

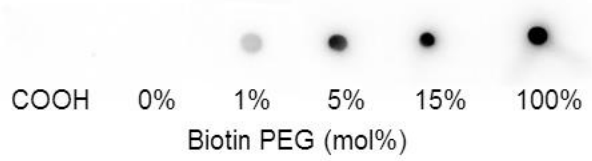

Figure 6.3. Dot blot confirming the relative biotin density on PS-COOH, PS-PEG and PS-PEG-biotin beads.

6.3.2 Pretargeted delivery of PS-PEG-biotin nanoparticles in vitro

To validate our hypothesis that pretargeting cells with different bispecific FPs can facilitate specific delivery of nanoparticles to distinct lymphoma cells, we measured the binding of various PS-PEG-biotin nanoparticles with different levels of biotin substitution to Raji (B lymphoma; $CD20^+/TAG72^-$) and Jurkat (T lymphoma; $CD20^-/TAG72^+$) cells pretargeted with bispecific streptavidin-based fusion proteins containing scFvs against CD20 or TAG72. In both cell lines, when pretargeted with the corresponding FP, increasing surface biotin density improved nanoparticle binding (Fig. 6.4). In contrast, no significant differences in nanoparticle binding were observed between particles of varying biotin density, even at the highest biotin densities, in the absence of FP and when pretargeted with control FP (i.e., αTAG72 FP for Raji cells and αCD20 FP for Jurkat cells). Pretargeting of Raji cells with αCD20 FP resulted in a ~15-fold greater uptake of fully biotinylated PS-PEG-biotin nanoparticles (100 mol% biotin) compared to methoxy PEG-coated nanoparticles without biotin functionalization (i.e., PS-PEG; $p < 0.01$), as well as ~9- and 6- fold greater nanoparticle uptake than with no FP or pretargeting using αTAG72 FP, respectively ($p < 0.01$). Similarly, in Jurkat cells, pretargeting with αTAG72

FP enhanced the binding of fully biotinylated PS-PEG-biotin nanoparticles by ~18-fold compared to PS-PEG nanoparticles without biotin ($p < 0.01$), as well as by ~8- and 6-fold relative to cells pretreated with no FP or αCD20 FP, respectively ($p < 0.01$). Compared to nanoparticles with lower biotin substitution, the fully biotinylated PS-PEG-biotin nanoparticles exhibited the greatest uptake with pretargeting yet were resistant to uptake by macrophage-like THP-1 cells *in vitro*; thus, we proceeded with subsequent *in vivo* studies using fully biotinylated PS-PEG-biotin nanoparticles.

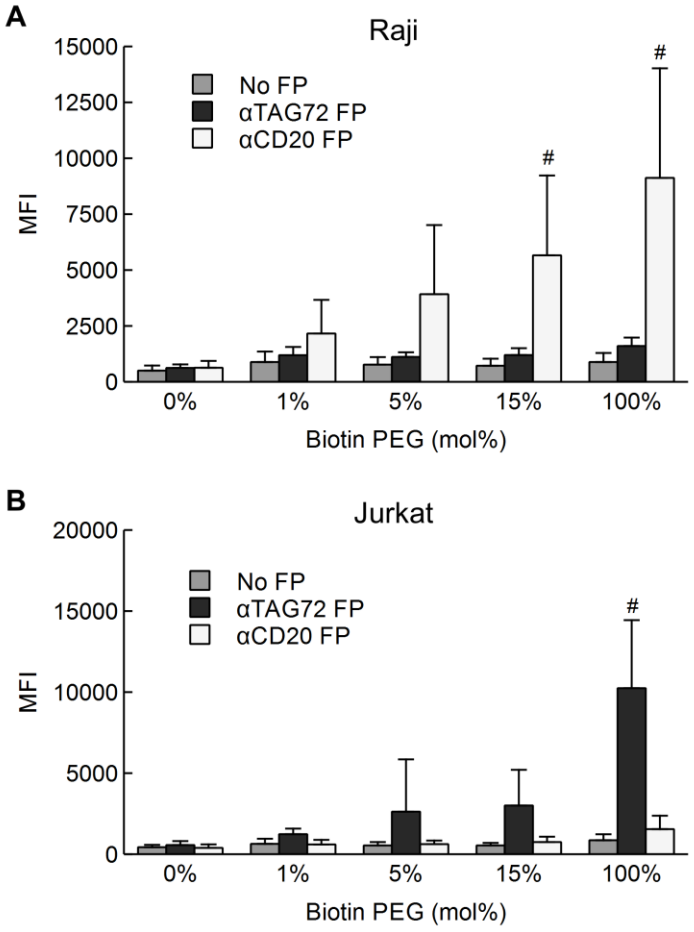

Figure 6.4. Pretargeted nanoparticle delivery to B- and T-cell lymphomas in vitro. a) Raji and **b)** Jurkat cells preincubated with or without CD20- or TAG72-specific pretargeting fusion proteins (FPs) for 4 h, followed by incubation with various PS-PEG-biotin beads for 12 h. The mean cellular fluorescence

intensity (MFI) was quantified using flow cytometry. All data represent at least n = 3 independent experiments performed in triplicate. # indicates $P < 0.01$ vs. no FP group and control FP group.

6.3.3 PS-PEG-biotin circulation kinetics and tissue biodistribution

Since effective accumulation of nanoparticles in tumor tissue is thought to be highly dependent on the extended circulation times in the blood, we evaluated the circulation kinetics and tissue biodistribution of fully biotinylated PS-PEG-biotin nanoparticles in normal BALB/c mice. Interestingly, despite the demonstrated resistance to macrophage uptake *in vitro* (Fig. 6.2d), we observed very rapid elimination of the PS-PEG-biotin nanoparticles from the blood (Fig. 6.5a), with a circulation half-life of only ~40 min. Similar to most nanoparticle systems, the liver, along with the spleen, represents the primary organ of nanoparticle disposition, both in relative (%ID/g) and absolute (%ID) quantities (Fig. 6.5b). Although the *in vivo* pharmacokinetic profile of the fully biotinylated PS-PEG-biotin particles did not reflect prolonged circulation that was expected based on the *in vitro* THP-1 uptake results or the extended circulation kinetics of similar nanoparticles modified with only methoxy-PEG (e.g., $t_{1/2}$ ~14 h) [341], we nevertheless proceeded to evaluate the tumor targeting potential of pretargeting *in vivo* using the fully biotinylated PS-PEG-biotin nanoparticles due to the high cell-specific uptake observed *in vitro*.

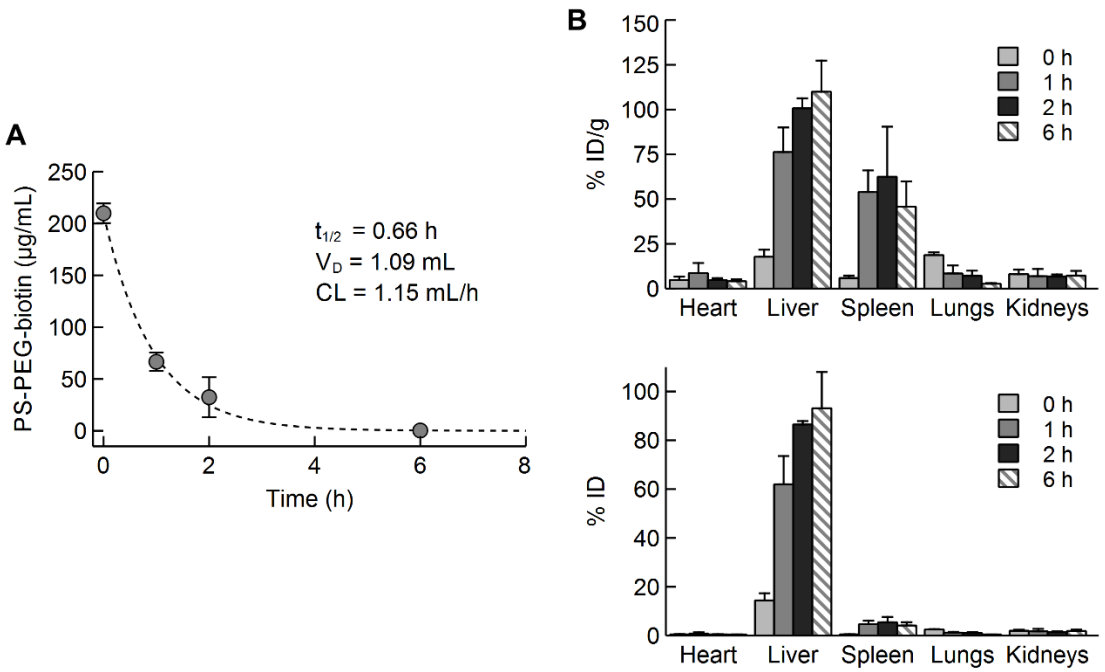

Figure 6.5. Circulation kinetics and tissue biodistribution of fully biotinylated nanoparticles. a) The blood circulation profile of PS-PEG-biotin (100 mol%) particles in normal BALB/c mice ($n \geq 3$). The dashed line represents the fit for a one-compartment model used to calculate the circulatory half-life ($t_{1/2}$), volume of distribution (V_D), and clearance (CL). **b)** Tissue biodistribution of fully biotinylated PS-PEG-biotin at various time points after i.v. injection. Injected dose/g (%ID/g; top) and injected dose (%ID; bottom) was quantified from the 2D fluorescent organ image signal intensities. All data represent the mean ± SD of at least n = 3 animals.

6.3.4 Biodistribution and tumor accumulation of pretargeted PS-PEG-biotin nanoparticles in single tumor mouse model

To determine whether pretargeting could enable specific delivery of biotinylated nanoparticles to tumors in spite of the poor circulation kinetics of the PS-PEG-biotin (100 mol%) beads, we dosed single Raji tumor-bearing mice with 250 µg of αCD20 or αTAG72 FP and then, 24 h later, administered 15 mg/kg of PS-PEG-biotin nanoparticles. Pretargeting with αCD20 FP significantly increased the amount of nanoparticles distributed in the Raji tumor ($p < 0.05$), with a ~4-fold increase in the tumor %ID/g compared to no FP and control αTAG72 FP (Fig. 6.6a). Prior administration of αCD20 or αTAG72 did not significantly affect the biodistribution of PS-

PEG-biotin beads to normal organs, and the nanoparticles were mainly distributed in the liver and spleen, as is common for the clearance of particles ~100 nm in size (Fig. 6.6b). In agreement with the short circulation half-life observed in BALB/c mice, no particles were detectable in circulation when the animals were sacrificed at 24 h post-injection (data not shown).

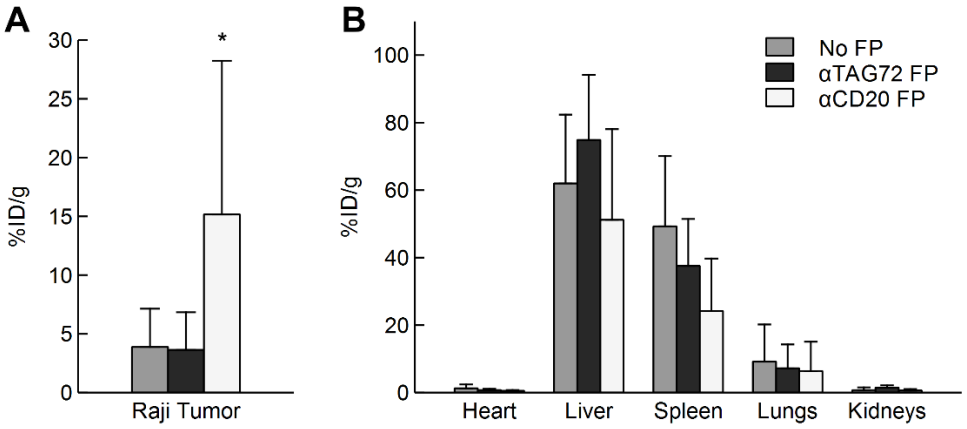

Figure 6.6. Organ biodistribution of pretargeted PS-PEG-biotin nanoparticles in single tumor-bearing mice. a) Raji tumor biodistribution and **b)** normal organ biodistribution of pretargeted PS-PEG-biotin at 24 h. Tumor cells were pretargeted with αCD20 or αTAG72 FPs (250 μg each), followed by nanoparticle injection after 24 h. All data represent the mean ± SD of at least n = 4 animals. Tissue injected dose/g (%ID/g; top) was quantified from the 2D fluorescent organ image signal intensities. * indicates $p < 0.05$ vs. no FP and αTAG72 groups.

6.3.5 Biodistribution and tumor accumulation of pretargeted PS-PEG-biotin nanoparticles in dual tumor mouse model

Despite the convenience and ease of xenograft models, a major shortcoming with tumor xenografts is that the animals are typically inoculated with a homogenous population of cancer cells with an identical genetic background, which naturally suppresses delivery challenges associated with tumor heterogeneity. To evaluate pretargeted nanoparticle delivery to distinct tumor cell populations *in vivo*, we decided to inoculate athymic nude mice with Raji and Jurkat cells on the right and left flanks of the same mice, respectively, to generate a dual tumor

xenograft model. The animals were then given 250 μg each of αCD20 and/or αTAG72 FP, followed by 15 mg/kg of PS-PEG-biotin nanoparticles after 24 h. The use of FP pretargeting increased the amount of particles found in both the Raji and Jurkat tumors (Fig. 6.7a), with the combination FP group exhibited ~4-fold higher tumor accumulation compared to the no FP group for Raji tumors ($p < 0.05$). While the combined use of αCD20 and αTAG72 FPs appeared to increase PS-PEG-biotin present in Jurkat tumors as well, no statistically differences were found between groups, likely due to high mouse-to-mouse tumor variability. The extent of nanoparticle accumulation, as measured by %ID/g, was substantially different between the Raji and Jurkat tumors, with markedly higher accumulation in Raji vs. Jurkat tumors (3.5%ID/g and 12.5%ID/g vs. 1.4%ID/g and 4.4%ID/g without FP and with combined FP, respectively), likely reflecting differences in tumor physiology and extravasation of the nanoparticles. Similar to the results above with single tumor-bearing mice, pretargeting did not significantly alter the biodistribution of the particles to normal organs compared to the no FP control (Fig. 6.7b); the vast majority of particles were found in the liver and spleen, and the nanoparticles were completely eliminated from systemic circulation by 24 h (data not shown).

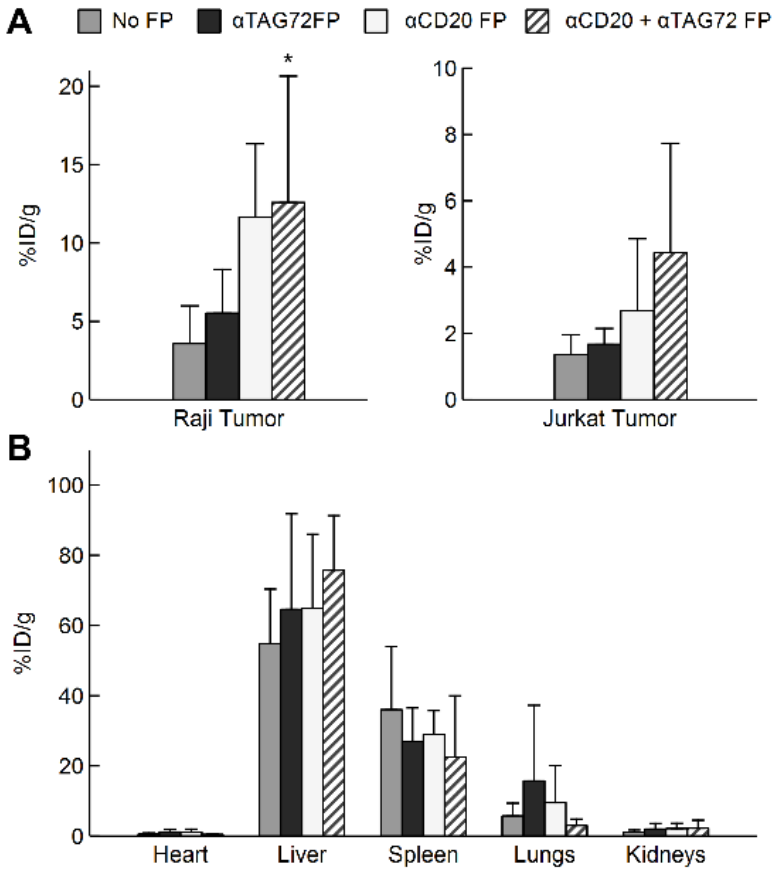

Figure 6.7. Organ biodistribution of pretargeted PS-PEG-biotin nanoparticles in dual tumor-bearing mice. a) Raji (left) and Jurkat (right) tumor biodistribution and **b)** normal organ biodistribution of pretargeted PS-PEG-biotin at 24 h. Tumor cells were pretargeted with αCD20 and/or αTAG72 FPs (250 μg each), followed by nanoparticle injection after 24 h. All data represent the mean ± SD of at least n = 4 animals. * indicates $p < 0.05$ vs. no FP and αTAG72 groups.

6.4. Discussion

The complexity of the tumor physiology and its microenvironment, including inter- and intra- tumoral heterogeneity, necessitates the exploration of alternative, multi-faceted strategies that can more effectively deliver therapeutics to the full spectrum of tumor cells than can be typically achieved with single ligand-conjugated nanoparticles. Notably, many of the shortcomings of common delivery systems for chemotherapy are the same deficiencies associated with conventional radioimmunotherapy. Nevertheless, despite the promise and early success of PRIT, the use of pretargeting molecules to enhance nanoparticle delivery has

remained largely underexplored to date. The few studies that have investigated pretargeting of nanoparticles to cancer cells [263, 264, 266, 267, 270, 339] all evaluated delivery to a homogeneous cell population *in vivo*, or relied on multiple unique pairs of pretargeting molecules and nanoparticles for detection of different cancer cells. This overlooks one of the primary advantages to pretargeting: by decoupling cellular targeting from nanoparticle design/formulation, the same nanoparticles can easily be targeted to multiple different cells by simply tuning the pretargeting molecule(s) used. Here, in good agreement with theory, we demonstrated that pretargeting can enhance cellular delivery of a single nanoparticle formulation to at least two molecularly distinct lymphoma cells *in vitro* and *in vivo*. Although many further improvements are needed, we believe the pretargeting approach, precipitated by the convergence of biotechnology, nanotechnology and drug delivery, represents a promising strategy that could more effectively deliver therapeutics to diverse cell populations. Improved therapeutics delivery to different cells simultaneously may in turn lead to more durable suppression or elimination of the tumor while minimizing eventual recurrence and/or the development of drug-resistant tumors.

The origins of the pretargeting concept is rooted in the pioneering work of Press and colleagues, who widely explored pretargeting as a strategy to overcome the shortcomings of conventional radioimmunotherapy, in particular the non-specific deposition of radiolabeled MAbs in normal organs that result in low tumor-specific delivery of radiation and significant toxicity [194]. By utilizing bispecific proteins that are non-radioactive, along with radiolabeled effector molecules that can be rapidly cleared, PRIT significantly improved the therapeutic index of radioisotope treatment compared to conventional radioimmunotherapy [194, 197, 198] and increased the maximum tolerated dose for radionuclides [196]. Pretargeting has been broadly

tested for a variety of blood malignancies *in vivo* including leukemia (CD45), B cells (CD20, HLA-DR and CD22) and multiple myeoloma (CD38), achieving tumor-to-blood ratios ranging from 2:1 to 638:1, and markedly improved survival rates [199-205]. These encouraging results in animal models have translated into clinical studies of PRIT, which to date have yielded promising results with reasonable tumor response rates and limited toxicity in phase I/II trials [345, 346].

The extent of nanoparticle targeting to the B- and T- lymphoma tumors in our mouse model remain limited relative to other organs, particularly the liver and spleen. One possible reason is inadequate accumulation of the pretargeting molecules within the tumor milieu [238, 347]. When coupled with the relatively weak affinity between scFvs and the tumor, this likely results in limited retention and binding of extravasated pretargeting molecules on cancer cells in the tumor and, consequently, limited capture of the nanoparticles by bound FP on cancer cells. For both single and dual tumor-bearing mice, we observed an increase in nanoparticle tumor accumulation with αCD20 FP, even in the case of $CD20^-$ Jurkat tumors, suggesting that more αCD20 FP may have extravasated into and remained at the tumor site compared to αTAG72 FP. This nonspecifically accumulation of pretargeting FP in the tumor tissue may have agglutinated subsequently dosed nanoparticles that extravasated into the tumor, thus improving nanoparticle retention rather than enabling specific homing and binding to target cancer cells, which may have required further penetration into the tumor tissue.

We had initially hypothesized that the presence of biotin on the surface of nanoparticles would not compromise the prolonged circulation of densely biotinylated PEGylated nanoparticles. The hypothesis was based in part on the low MW of biotin relative to the MW of PEG and the effective pretargeting observed with PRIT using biotinylated radiolabels, and was

supported by the limited uptake by macrophage-like cells *in vitro*. Nevertheless, fully biotinylated nanoparticles were quickly eliminated in mice; at 6 hours post-injection, and there was no detectable amount of PS-PEG-biotin nanoparticles in the blood compared to ~70% of the injected dose for previously evaluated PS-PEG-methoxy nanoparticles [341]. The poor circulation kinetics likely limited the fraction of the injected nanoparticle dose that could reach and extravasate at the tumor site. Since biotin is a naturally occurring vitamin, we speculate that the rapid accumulation of biotin-modified nanoparticles, particularly in the liver, can probably be attributed the presence of vitamin receptors in the liver and on MPS cells [348, 349] combined with the highly multivalent nature of biotin presentation on nanoparticles. Together, this likely led to more efficient capture of nanoparticles decorated with multiple biotin groups than radioisotopes functionalized with a single biotin group. The poor nanoparticle circulation kinetics might be partially resolved by lowering the biotin density on the nanoparticle surface, thus widening the time window during which the particles can circulate and permeate into tumors. Nevertheless, reduced surface biotin density would also decrease the binding rate of nanoparticles to the pretargeting FPs present on the cell surface and in the tumor site. Instead, we expect the use of alternative binding pairs (i.e., nanoparticle-pretargeting molecule linkages) would avoid the problematic use of biotinylation and improve nanoparticle circulation and extravasation, as well as overcome immunogenicity commonly observed with streptavidin. However, the likely reduction in nanoparticle-pretargeting FP affinity (relative to that of streptavidin-biotin bonds) would reduce the efficiency of pretargeting molecules crosslinking nanoparticles to target cells. In our opinion, the development of pretargeting molecules with high binding affinities to both cells and nanoparticles and bio-inert binding pairs represent the most critical challenge for future development of pretargeted delivery of nanoparticles.

The use of multiple pretargeting molecule combinations have been previously evaluated for PRIT of lymphoma with variable expression of CD20, CD22, and HLA-DR [202, 284]. Interestingly, the authors found that a single pretargeting molecule treatment provided superior tumor-to-normal organ ratios and survival rates, whereas a cocktail of three different pretargeting molecules (against CD20, CD22 and HLA-DR) resulted in increased liver biodistribution of the radioactive payload and increased toxicity. In contrast, pretargeting with αCD20 and/or αTAG72 FPs did not alter nanoparticle biodistribution to normal organs in single and dual tumor-bearing mice in our study (Fig. 6.6-6.7). This disparity in the effects of extraneous pretargeting molecules most likely resulted from differences in the features and properties of the therapeutic agents used. Unlike the small-molecule radionuclide carriers used in the PRIT studies, the majority of systemically dosed nanoparticles are eventually eliminated by MPS organs such as the liver and spleen, which may eclipse any changes in biodistribution caused by mismatched pretargeting FP administration. Nevertheless, the potential effects of pretargeting molecules cocktails on nanoparticle biodistribution and toxicity should be further evaluated in the future, particularly for different pretargeting molecule/nanoparticle combinations.

6.5 Conclusions

Tumor heterogeneity presents a complex delivery challenge, as nanoparticle drug carriers must accumulate in tumor tissue while also maximally targeting the diverse cell populations present within a given tumor and/or patient. Here, we explored the simultaneous use of multiple pretargeting bispecific fusion proteins to enhance nanoparticle delivery to heterogeneous target cell populations. We found that increasing amounts of surface biotin on the nanoparticles enabled highly specific cell uptake by tumor cells pretargeted by corresponding fusion proteins

in vitro, and, for single tumor-bearing mice, pretargeting with tumor-specific fusion protein also significantly improved nanoparticle tumor accumulation even in the face of the poor circulation kinetics of the biotinylated nanoparticles. Additionally, in dual tumor-bearing mice, the use of pretargeting with a fusion protein cocktail directly increased nanoparticle delivery to both tumor types. Our findings support further investigations into the use of pretargeting fusion protein cocktails as an alternative targeting strategy to enhance nanoparticle delivery to a diverse array of molecularly distinct target cells.

CHAPTER 7: CONCLUSIONS AND PERSPECTIVES

In this dissertation, I systematically investigated the interactions between PEGylated nanoparticles and both the innate and adaptive immune system, which play a crucial role in determining the biological fate of PEGylated nanoparticles but remain poorly understood in general. Additionally, to overcome limitations associated with active targeting of nanoparticles to tumors, I evaluated a pretargeting approach for homing of nanoparticles to tumors through the use of bispecific fusion proteins. The findings presented in this dissertation provide a basis for engineering the next generation of nanoparticle systems for targeted delivery of therapeutics.

PEGylation continues to be the most popular strategy for extending the systemic circulation of nanoparticle systems, but the critical characteristics of PEG that enable stealth properties for PEG coatings remain underexplored for most nanoparticle systems. I developed an indirect assay to measure the PEG density on PS nanoparticles, and used PS-PEG beads carefully engineered to encompass a range of PEG MW and densities to evaluate the impact of these PEG coating characteristics on uptake by MPS cells *in vitro* and *in vivo*. I found that exceptionally high PEG densities, whereby each chain assumes a dense brush conformation, were necessary for nanoparticles to evade immune cell clearance. Interestingly, the necessary PEG grafting density for prolonged systemic circulation *in vivo* was even more stringent than those deduced from the *in vitro* differentiated THP-1 studies. Indeed, no difference in THP-1 cell uptake was observed between PS-PEG beads with 0.6 and $\geq$1.5 PEG/nm^2 (both dense brush PEG) at 4 h, with only minor differences at 12 h and 24 h; however, the circulatory half-lives of these nanoparticles were 0.4 h vs. 13.5 h, respectively, a >30-fold difference. The major disparity

between the *in vitro* and *in vivo* results highlights the need for improved cell culture models that will better predict potential MPS cell clearance in animal models, and likely human patients as well. The use of primary human MPS cells, which appeared to take up even very densely modified PS-PEG nanoparticles more avidly than the differentiated THP-1 cells, along with much longer experimental time points (e.g., >48 h) may enable more rigorous screening for nanoparticle systems that can effectively evade sequestration by the immune system *in vivo*.

In contrast to the findings here, others have reported PEGylated nanoparticles with far lower PEG densities, resulting in brush or mushroom conformation PEG, that nevertheless exhibit prolonged systemic circulation [8, 48, 289]. These discrepancies likely result from the varying properties of the underlying nanoparticles. Indeed, nanoparticle features such as size, shape, and deformability are critical design parameters that also influence MPS uptake and elimination [6]. At extremes (e.g., particle diameters >200 nm [350] or soft nanoparticles with high deformability [351]), the influence of these parameters may exceed that of PEGylation. Thus, the PEG density and conformation requirements for evading immune cell uptake must be evaluated within the context of each individual nanoparticle class/type. For more rigid polymeric nanoparticles sized ~100 nm or below, the observed relationship between PEG density and conformation and *in vitro* and *in vivo* interactions with MPS cells likely holds, and similar PEG coating requirements have been reported for metallic nanoparticles [50]. To satisfy these requirements, a "grafting to" strategy involving conjugation of PEG chains to reactive groups on the nanoparticle surface was used to achieve high PEG surface densities; however, such "grafting to" approaches are rarely used to formulate polymeric drug carrier systems. Instead, PEGylation of most polymeric nanoparticle systems typically relies on PEG copolymers or coating with amphiphilic PEG-containing molecules, which may result in lower surface PEG densities due to

poor or variable partitioning of PEG to the nanoparticle surface. An interesting approach would be the synthesis of functional polymeric drug carriers with high surface densities of reactive groups such as COOH or NH_2 (e.g., using block copolymers with large hydrophobic blocks and short highly charged hydrophilic blocks) that would allow grafting of PEG chains at tunable densities and MWs.

Despite the popularity of nanoparticle PEGylation, as well as PEGylation of protein and other macromolecule drugs, recent studies have shown that antibodies that can bind PEG, typically referred to as anti-PEG Ab, can be induced in humans. In particular, several reports have described the existence of pre-existing anti-PEG Ab, which raises potential concerns about the widespread use of various PEG-containing drugs in humans. Unfortunately, our current understanding of the prevalence and concentration of anti-PEG Ab amongst the general population remains limited, due in part to the lack of appropriate reagents for evaluating such responses. Using competitive ELISAs with various chimeric anti-PEG Ab standards prepared for this purpose, I measured the level and prevalence of pre-existing anti-PEG Ab in contemporary plasma and historical serum samples from healthy donors. Surprisingly, I found that the majority of samples analyzed (>70% and >50% of contemporary and historical samples, respectively) contained detectable levels of anti-PEG Ab. These values were far higher than the incidence rates of pre-existing anti-PEG Ab observed from clinical trials of PEGylated drugs and other studies [17, 100, 104, 105, 124], likely because the quantitative ELISA method used here offers much greater detection sensitivity than the end-titer ELISA and/or hemagglutination assays employed in previous reports. Indeed, most of the samples positive for anti-PEG Ab contained only low levels of anti-PEG IgG and/or IgM, often <100 ng/mL.

Part of PEG's enduring appeal as a component of pharmaceutical formulations has been its long history of safe use in humans, and the clinical implications of anti-PEG Ab, particularly at low levels, remains unclear. The efficacy of certain PEGylated drugs (e.g., PEG-interferon-2α and β [102, 124] and PEG-phenylalanine ammonia lyase [103]) does not appear to be affected by anti-PEG Ab. In contrast, pre-existing and/or induced anti-PEG Ab has been associated with rapid clearance of PEG-uricase [98, 104] and PEG-asparaginase [106], as well as serious adverse reactions to both a PEGylated aptamer drug [17, 110] and contraceptive containing PEG as an excipient [103]. These effects were generally observed for individuals with high-titer anti-PEG Ab, suggesting the possibility of critical threshold(s) above which anti-PEG Ab can mediate clearance of and/or adverse immune responses to PEGylated drugs. Such thresholds will likely be dependent on the specific PEGylated drug being administered, as well as the immunological status and genetics of individual patients. While it may not directly result in altered pharmacokinetic profiles or toxicity upon initial dosing, the presence of low level anti-PEG Ab may reflect immunological memory against PEG that could be readily triggered upon exposure to PEGylated therapeutics, particularly those dosed through parental routes of administration, and ultimately result in a rapid increase in the levels of anti-PEG Ab after treatment.

Due to the immunogenicity of PEG, researchers have been exploring alternative polymers to PEG, such as zwitterioinic polymers, other hydrophilic polymers, "self" peptides, and autologous cell membrane coatings [6, 115, 147]. However, these approaches are far from clinical approval and/or may not be applicable to large classes of therapeutics, such as protein drugs. Given the long history of relatively safe use of PEG, it is unlikely that PEG will be abandoned in the near future, nor does it need to be. With numerous PEGylated therapeutics on the market and in clinical development, further research should be conducted to better

understand the potential clinical impact of anti-PEG Ab, as well as mechanisms and factors involved in anti-PEG Ab induction. Improved monitoring of patient anti-PEG Ab levels prior to and during treatment with certain PEGylated drugs, along with tracking of previous exposure to PEG and PEGylated drugs, will likely help to offer a more complete view of PEG-specific adaptive immunity in humans, and may provide crucial insights into dosing regimens that could enable effective and safe use of PEGylated systems even in individuals with anti-PEG immunity. Additionally, animal models that better recapitulate the features of potential anti-PEG Ab responses in humans (e.g., mixture of IgG and IgM isotypes, predominance of IgG2 subclass, PEG-specific immunological memory, induction through continuous low-dose PEG exposure) should be developed.

Researchers often rely on a combination of PEGylation and ligand-based active targeting to improve nanoparticle delivery to cancer cells. However, the use of PEG coatings can offset the beneficial effects of ligand modification and vice versa; PEGylation provides extended systemic circulation but can also hinder ligand-receptor binding, whereas surface ligand groups enable specific cell uptake but can also result in rapid nanoparticle clearance by MPS cells even with well PEGylated systems [125, 170]. In this dissertation, I investigated a pretargeting approach for nanoparticle delivery to tumor cells. Pretargeting with bispecific fusion proteins that bind to both tumor cell receptors and effector nanoparticles may enable both efficient cellular targeting and extended circulation of nanoparticles. Furthermore, the use of a cocktail of bispecific fusion proteins that all bind to the same nanoparticle but recognize different tumor cell receptors should theoretically enable targeting of the same nanoparticles to heterogeneous mixtures of tumor cells. Using streptavidin-based fusion proteins that recognize distinct lymphomas (i.e., αCD20 to Raji B-lymphoma and αTAG72 FP to Jurkat T-lymphoma), I found that pretargeting resulted in high

receptor-specific cell uptake of biotinylated nanoparticles *in vitro* and enhanced tumor biodistribution *in vivo*, compared to no FP controls.

While multistep drug delivery approaches such as pretargeting can offer important advantages, they also introduce additional complexity in terms of pretargeting molecule design and nanoparticle formulation. For example, the pharmacokinetics/pharmacodynamics of each component must be taken into account to enable optimal accumulation of the delivery payload at target tissue(s). An additional challenge in the use of pretargeting approaches is the selection of appropriate binding pairs for *in vivo* and clinical use. The streptavidin-biotin binding pair offers one of the highest non-covalent binding affinities (K_d ~10^{-14}-10^{-15} M), allowing more effective capture of nanoparticles by cell surface-bound FPs. Unfortunately, streptavidin-based fusion proteins are immunogenic and are thus a poor choice for drug delivery applications in humans [207, 209]. Additionally, biotin modification, at densities that enabled optimal specific cell targeting and minimal differentiated THP-1 cell uptake *in vitro*, surprisingly led to rapid nanoparticle clearance *in vivo*, with fully modified PS-PEG-biotin possessing a circulating half-life of only 40 min. Therefore, while the availability of previously developed streptavidin-based FPs targeting different tumor cell receptors allowed for convenient testing of pretargeted nanoparticle delivery to molecularly distinct tumors, the combination of streptavidin-based FPs and biotinylated NPs does not appear to represent an ideal platform for further development. One very promising direction is to harness the body's ability to generate PEG-specific humoral responses by replacing the streptavidin component of the pretargeting FPs with anti-PEG Ab sequences. The development of anti-PEG Ab-PEG binding pairs has the added advantage of being compatible with the multiple PEGylated nanoparticles and macromolecule drugs in development or already available the market. With additional modifications of the FP sequences

and structure to optimize tumor accumulation, binding to target receptors, and capture of PEG-coated nanoparticles, such an approach may help realize the full potential of pretargeting for drug delivery to heterogeneous tumors by combining efficient cell targeting and extended circulation kinetics provided by fully PEGylated drug carriers.

REFERENCES

[1] V. Weissig, T.K. Pettinger, N. Murdock, Nanopharmaceuticals (part 1): products on the market, Int J Nanomedicine, 9 (2014) 4357-4373.

[2] T.M. Allen, P.R. Cullis, Drug Delivery Systems: Entering the Mainstream, Science, 303 (2004) 1818-1822.

[3] T.L. Andresen, S.S. Jensen, K. Jørgensen, Advanced strategies in liposomal cancer therapy: Problems and prospects of active and tumor specific drug release, Progress in Lipid Research, 44 (2005) 68-97.

[4] D.E. Owens, 3rd, N.A. Peppas, Opsonization, biodistribution, and pharmacokinetics of polymeric nanoparticles, Int J Pharm, 307 (2006) 93-102.

[5] R. Gref, Y. Minamitake, M.T. Peracchia, V. Trubetskoy, V. Torchilin, R. Langer, Biodegradable Long-Circulating Polymeric Nanospheres, Science, 263 (1994) 1600-1603.

[6] E. Blanco, H. Shen, M. Ferrari, Principles of nanoparticle design for overcoming biological barriers to drug delivery, Nat Biotech, 33 (2015) 941-951.

[7] S.I. Jeon, L.H. Lee, J.D. Andrade, P.G. De Gennes, Protein-surface interactions in the presence of polyethylene oxide. I. Simplified theory., J Colloid Interf Scie, 142 (1991) 149-158.

[8] A. Hamilton, L. Biganzoli, R. Coleman, L. Mauriac, P. Hennebert, A. Awada, M. Nooij, L. Beex, M. Piccart, I. Van Hoorebeeck, P. Bruning, D. de Valeriola, EORTC 10968: a phase I clinical and pharmacokinetic study of polyethylene glycol liposomal doxorubicin (Caelyx®, Doxil®) at a 6-week interval in patients with metastatic breast cancer, Annals of Oncology, 13 (2002) 910-918.

[9] J.V. Jokerst, T. Lobovkina, R.N. Zare, S.S. Gambhir, Nanoparticle PEGylation for imaging and therapy, Nanomedicine (Lond), 6 (2011) 715-728.

[10] B. Alberts, A. Johnson, J. Lewis, M. Raff, K. Roberts, P. Walter, Molecular biology of the cell, in, Garland Science, New York, 2002.

[11] I.J. Amanna , N.E. Carlson , M.K. Slifka Duration of Humoral Immunity to Common Viral and Vaccine Antigens, New England Journal of Medicine, 357 (2007) 1903-1915.

[12] G. Vidarsson, G. Dekkers, T. Rispens, IgG subclasses and allotypes: from structure to effector functions, Front Immunol, 5 (2014) 520.

[13] W.Y.K. Hwang, J. Foote, Immunogenicity of engineered antibodies, Methods, 36 (2005) 3-10.

[14] E.A. Hammond, R.L. Yowell, J. Greenwood, L. Hartung, D. Renlund, C. Wittwer, Prevention of adverse clinical outcome by monitoring of cardiac transplant patients for murine monoclonal CD3 antibody (OKT3) sensitization, Transplantation, 55 (1993) 1061-1063.

[15] F.A. Harding, M.M. Stickler, J. Razo, R. DuBridge, The immunogenicity of humanized and fully human antibodies, mAbs, 2 (2010) 256-265.

[16] J. Link, M. Lundkvist Ryner, K. Fink, C. Hermanrud, I. Lima, B. Brynedal, I. Kockum, J. Hillert, A. Fogdell-Hahn, Human Leukocyte Antigen Genes and Interferon Beta Preparations Influence Risk of Developing Neutralizing Anti-Drug Antibodies in Multiple Sclerosis, PLoS One, 9 (2014) e90479.

[17] N.J. Ganson, T.J. Povsic, B.A. Sullenger, J.H. Alexander, S.L. Zelenkofske, J.M. Sailstad, C.P. Rusconi, M.S. Hershfield, Pre-existing anti–polyethylene glycol antibody linked to first-exposure allergic reactions to pegnivacogin, a PEGylated RNA aptamer, Journal of Allergy and Clinical Immunology, 137 (2016) 1610-1613.e1617.

[18] M. Krishna, S.G. Nadler, Immunogenicity to Biotherapeutics – The Role of Anti-drug Immune Complexes, Front Immunol, 7 (2016) 21.

[19] A.S. Abu Lila, H. Kiwada, T. Ishida, The accelerated blood clearance (ABC) phenomenon: clinical challenge and approaches to manage, J Control Release, 172 (2013) 38-47.

[20] Q. Yang, S.K. Lai, Anti-PEG immunity: emergence, characteristics, and unaddressed questions, Wiley Interdiscip Rev Nanomed Nanobiotechnol, 7 (2015) 655-677.

[21] J.K. Armstrong, The occurence, induction, specificity and potential effect of antibodies against poly(ethylene glycol), in: F.M. Veronese (Ed.) PEGylated Protein Drugs: Basic Science and Clinical Applications, 2009, pp. 147-168.

[22] P.E. Lipsky, L.H. Calabrese, A. Kavanaugh, J.S. Sundy, D. Wright, M. Wolfson, M.A. Becker, Pegloticase immunogenicity: the relationship between efficacy and antibody development in patients treated for refractory chronic gout, Arthritis Res Ther, 16 (2014) R60.

[23] P. Carter, Improving the efficacy of antibody-based cancer therapies, Nat Rev Cancer, 1 (2001) 118-129.

[24] J. Folkman, D.M. Long, Jr., F.F. Becker, Growth and metastasis of tumor in organ culture, Cancer, 16 (1963) 453-467.

[25] S. Taurin, H. Nehoff, T. van Aswegen, K. Greish, Tumor Vasculature, EPR Effect, and Anticancer Nanomedicine: Connecting the Dots, in: H.Y. Bae, J.R. Mrsny, K. Park (Eds.) Cancer Targeted Drug Delivery: An Elusive Dream, Springer New York, New York, NY, 2013, pp. 207-239.

[26] J.A. Nagy, S.H. Chang, A.M. Dvorak, H.F. Dvorak, Why are tumour blood vessels abnormal and why is it important to know?, Br J Cancer, 100 (2009) 865-869.

[27] Y. Matsumura, H. Maeda, A new concept for macromolecular therapeutics in cancer chemotherapy: mechanism of tumoritropic accumulation of proteins and the antitumor agent smancs, Cancer Res, 46 (1986) 6387-6392.

[28] Z. Amoozgar, Y. Yeo, Recent advances in stealth coating of nanoparticle drug delivery systems, Wiley Interdiscip Rev Nanomed Nanobiotechnol, 4 (2012) 219-233.

[29] F.M. Veronese, G. Pasut, PEGylation, successful approach to drug delivery, Drug Discov Today, 10 (2005) 1451-1458.

[30] J.M. Harris, R.B. Chess, Effect of pegylation on pharmaceuticals, Nat Rev Drug Discov, 2 (2003) 214-221.

[31] A.S. Zahr, C.A. Davis, M.V. Pishko, Macrophage uptake of core-shell nanoparticles surface modified with poly(ethylene glycol), Langmuir, 22 (2006) 8178-8185.

[32] A.L. Klibanov, K. Maruyama, V.P. Torchilin, L. Huang, Amphipathic polyethyleneglycols effectively prolong the circulation time of liposomes, FEBS Lett, 268 (1990) 235-237.

[33] E.T. Dams, P. Laverman, W.J. Oyen, G. Storm, G.L. Scherphof, J.W. van Der Meer, F.H. Corstens, O.C. Boerman, Accelerated blood clearance and altered biodistribution of repeated injections of sterically stabilized liposomes, J Pharmacol Exp Ther, 292 (2000) 1071-1079.

[34] X. Wang, T. Ishida, H. Kiwada, Anti-PEG IgM elicited by injection of liposomes is involved in the enhanced blood clearance of a subsequent dose of PEGylated liposomes, J Control Release, 119 (2007) 236-244.

[35] J.J. Verhoef, J.F. Carpenter, T.J. Anchordoquy, H. Schellekens, Potential induction of anti-PEG antibodies and complement activation toward PEGylated therapeutics, Drug Discov Today, (2014).

[36] R.P. Garay, R. El-Gewely, J.K. Armstrong, G. Garratty, P. Richette, Antibodies against polyethylene glycol in healthy subjects and in patients treated with PEG-conjugated agents, Expert Opin Drug Deliv, 9 (2012) 1319-1323

[37] R.P. Garay, R. El-Gewely, J.K. Armstrong, G. Garratty, P. Richette, Antibodies against polyethylene glycol in healthy subjects and in patients treated with PEG-conjugated agents, Expert Opin Drug Deliv, 9 (2012) 1319-1323.

[38] O. Tirosh, Y. Barenholz, J. Katzhendler, A. Priev, Hydration of polyethylene glycol-grafted liposomes, Biophys J, 74 (1998) 1371-1379.

[39] C. Branca, S. Magazù, G. Maisano, F. Migliardo, P. Migliardo, G. Romeo, Hydration Study of PEG/Water Mixtures by Quasi Elastic Light Scattering, Acoustic and Rheological Measurements, The Journal of Physical Chemistry B, 106 (2002) 10272-10276.

[40] D.D. Lasic, F.J. Martin, A. Gabizon, S.K. Huang, D. Papahadjopoulos, Sterically stabilized liposomes: a hypothesis on the molecular origin of the extended circulation times, Biochim Biophys Acta, 1070 (1991) 187-192.

[41] D. Needham, T.J. McIntosh, D.D. Lasic, Repulsive interactions and mechanical stability of polymer-grafted lipid membranes, Biochim Biophys Acta, 1108 (1992) 40-48.

[42] S. Sharma, R.W. Johnson, T.A. Desai, XPS and AFM analysis of antifouling PEG interfaces for microfabricated silicon biosensors, Biosens Bioelectron, 20 (2004) 227-239.

[43] V.B. Damodaran, C.J. Fee, T. Ruckh, K.C. Popat, Conformational studies of covalently grafted poly(ethylene glycol) on modified solid matrices using X-ray photoelectron spectroscopy, Langmuir, 26 (2010) 7299-7306.

[44] A. Vonarbourg, C. Passirani, P. Saulnier, J.P. Benoit, Parameters influencing the stealthiness of colloidal drug delivery systems, Biomaterials, 27 (2006) 4356-4373.

[45] S.K. Lai, Y.Y. Wang, J. Hanes, Mucus-penetrating nanoparticles for drug and gene delivery to mucosal tissues, Adv Drug Deliv Rev, 61 (2009) 158-171.

[46] E.A. Nance, G.F. Woodworth, K.A. Sailor, T.Y. Shih, Q. Xu, G. Swaminathan, D. Xiang, C. Eberhart, J. Hanes, A dense poly(ethylene glycol) coating improves penetration of large polymeric nanoparticles within brain tissue, Sci Transl Med, 4 (2012) 149ra119.

[47] P.G. de Gennes, Conformation of polymers attached to an interface, Macromolecules, 13 (1980) 1069-1075.

[48] J.L. Perry, K.G. Reuter, M.P. Kai, K.P. Herlihy, S.W. Jones, J.C. Luft, M. Napier, J.E. Bear, J.M. DeSimone, PEGylated PRINT nanoparticles: the impact of PEG density on protein binding, macrophage association, biodistribution, and pharmacokinetics, Nano Lett, 12 (2012) 5304-5310.

[49] Q. Yang, S.W. Jones, C.L. Parker, W.C. Zamboni, J.E. Bear, S.K. Lai, Evading Immune Cell Uptake and Clearance Requires PEG Grafting at Densities Substantially Exceeding the Minimum for Brush Conformation, Mol Pharm, (2014).

[50] C.D. Walkey, J.B. Olsen, H. Guo, A. Emili, W.C. Chan, Nanoparticle size and surface chemistry determine serum protein adsorption and macrophage uptake, J Am Chem Soc, 134 (2012) 2139-2147.

[51] A.W. Richter, E. Akerblom, Antibodies against polyethylene glycol produced in animals by immunization with monomethoxy polyethylene glycol modified proteins, Int Arch Allergy Appl Immunol, 70 (1983) 124-131.

[52] M.R. Sherman, L.D. Williams, M.A. Sobczyk, S.J. Michaels, M.G. Saifer, Role of the methoxy group in immune responses to mPEG-protein conjugates, Bioconjug Chem, 23 (2012) 485-499.

[53] D.A. Wunderlich, M. Macdougall, D.V. Mierz, J.G. Toth, T.M. Buckholz, K.J. Lumb, H. Vasavada, Generation and characterization of a monoclonal IgG antibody to polyethylene glycol, Hybridoma (Larchmt), 26 (2007) 168-172.

[54] T. Shimizu, M. Ichihara, Y. Yoshioka, T. Ishida, S. Nakagawa, H. Kiwada, Intravenous administration of polyethylene glycol-coated (PEGylated) proteins and PEGylated adenovirus elicits an anti-PEG immunoglobulin M Response, Biol Pharm Bull, 35 (2012) 1336-1342.

[55] T.L. Cheng, P.Y. Wu, M.F. Wu, J.W. Chern, S.R. Roffler, Accelerated clearance of polyethylene glycol-modified proteins by anti-polyethylene glycol IgM, Bioconjug Chem, 10 (1999) 520-528.

[56] S.M. Moghimi, T. Gray, A single dose of intravenously injected poloxamine-coated long-circulating particles triggers macrophage clearance of subsequent doses in rats, Clin Sci (Lond), 93 (1997) 371-379.

[57] T. Ishida, K. Masuda, T. Ichikawa, M. Ichihara, K. Irimura, H. Kiwada, Accelerated clearance of a second injection of PEGylated liposomes in mice, Int J Pharm, 255 (2003) 167-174.

[58] T. Ishida, R. Maeda, M. Ichihara, K. Irimura, H. Kiwada, Accelerated clearance of PEGylated liposomes in rats after repeated injections, J Control Release, 88 (2003) 35-42.

[59] G. Bendas, U. Rothe, G.L. Scherphof, J.A. Kamps, The influence of repeated injections on pharmacokinetics and biodistribution of different types of sterically stabilized immunoliposomes, Biochim Biophys Acta, 1609 (2003) 63-70.

[60] P. Laverman, M.G. Carstens, O.C. Boerman, E.T. Dams, W.J. Oyen, N. van Rooijen, F.H. Corstens, G. Storm, Factors affecting the accelerated blood clearance of polyethylene glycol-liposomes upon repeated injection, J Pharmacol Exp Ther, 298 (2001) 607-612.

[61] T. Ishida, M. Ichihara, X. Wang, H. Kiwada, Spleen plays an important role in the induction of accelerated blood clearance of PEGylated liposomes, J Control Release, 115 (2006) 243-250.

[62] T. Ishida, M. Harada, X.Y. Wang, M. Ichihara, K. Irimura, H. Kiwada, Accelerated blood clearance of PEGylated liposomes following preceding liposome injection: effects of lipid dose and PEG surface-density and chain length of the first-dose liposomes, J Control Release, 105 (2005) 305-317.

[63] T. Ishida, X. Wang, T. Shimizu, K. Nawata, H. Kiwada, PEGylated liposomes elicit an anti-PEG IgM response in a T cell-independent manner, J Control Release, 122 (2007) 349-355.

[64] T.L. Cheng, B.M. Chen, J.W. Chern, M.F. Wu, S.R. Roffler, Efficient clearance of poly(ethylene glycol)-modified immunoenzyme with anti-PEG monoclonal antibody for prodrug cancer therapy, Bioconjug Chem, 11 (2000) 258-266.

[65] A. Judge, K. McClintock, J.R. Phelps, I. Maclachlan, Hypersensitivity and loss of disease site targeting caused by antibody responses to PEGylated liposomes, Mol Ther, 13 (2006) 328-337.

[66] C. Li, J. Cao, Y. Wang, X. Zhao, C. Deng, N. Wei, J. Yang, J. Cui, Accelerated blood clearance of pegylated liposomal topotecan: influence of polyethylene glycol grafting density and animal species, J Pharm Sci, 101 (2012) 3864-3876.

[67] R. Saadati, S. Dadashzadeh, Z. Abbasian, H. Soleimanjahi, Accelerated Blood Clearance of PEGylated PLGA Nanoparticles Following Repeated Injections: Effects of Polymer Dose, PEG Coating, and Encapsulated Anticancer Drug, Pharm Res, 30 (2013) 985-995.

[68] L.M. Kaminskas, V.M. McLeod, C.J. Porter, B.J. Boyd, Differences in colloidal structure of PEGylated nanomaterials dictate the likelihood of accelerated blood clearance, J Pharm Sci, 100 (2011) 5069-5077.

[69] K. Shiraishi, M. Hamano, H. Ma, K. Kawano, Y. Maitani, T. Aoshi, K.J. Ishii, M. Yokoyama, Hydrophobic blocks of PEG-conjugates play a significant role in the accelerated blood clearance (ABC) phenomenon, J Control Release, 165 (2013) 183-190.

[70] Y. Zhao, L. Wang, M. Yan, Y. Ma, G. Zang, Z. She, Y. Deng, Repeated injection of PEGylated solid lipid nanoparticles induces accelerated blood clearance in mice and beagles, Int J Nanomedicine, 7 (2012) 2891-2900.

[71] T. Ishida, M. Ichihara, X. Wang, K. Yamamoto, J. Kimura, E. Majima, H. Kiwada, Injection of PEGylated liposomes in rats elicits PEG-specific IgM, which is responsible for rapid elimination of a second dose of PEGylated liposomes, Journal of Controlled Release, 112 (2006) 15-25.

[72] M. Ichihara, T. Shimizu, A. Imoto, Y. Hashiguchi, Y. Uehara, T. Ishida, H. Kiwada, Anti-PEG IgM response against PEGylated liposomes in mice and rats, Pharmaceutics, 3 (2011) 1-11.

[73] K. Sroda, J. Rydlewski, M. Langner, A. Kozubek, M. Grzybek, A.F. Sikorski, Repeated injections of PEG-PE liposomes generate anti-PEG antibodies, Cell Mol Biol Lett, 10 (2005) 37-47.

[74] T. Ishida, K. Atobe, X. Wang, H. Kiwada, Accelerated blood clearance of PEGylated liposomes upon repeated injections: effect of doxorubicin-encapsulation and high-dose first injection, J Control Release, 115 (2006) 251-258.

[75] T. Ishida, S. Kashima, H. Kiwada, The contribution of phagocytic activity of liver macrophages to the accelerated blood clearance (ABC) phenomenon of PEGylated liposomes in rats, J Control Release, 126 (2008) 162-165.

[76] M. Kawanishi, Comprehensive analysis of PEGylated liposome-asscociated proteins relating to the accelerated blood clearance phenomenon by combination with shotgun analysis and conventional methods, Biotechnol Appl Biochem, (2014) n-a-n/a.

[77] Q. Yang, Y. Ma, Y. Zhao, Z. She, L. Wang, J. Li, C. Wang, Y. Deng, Accelerated drug release and clearance of PEGylated epirubicin liposomes following repeated injections: a new challenge for sequential low-dose chemotherapy, Int J Nanomedicine, 8 (2013) 1257-1268.

[78] H. Xu, F. Ye, M. Hu, P. Yin, W. Zhang, Y. Li, X. Yu, Y. Deng, Influence of phospholipid types and animal models on the accelerated blood clearance phenomenon of PEGylated liposomes upon repeated injection, Drug Delivery, (2014) 1-10.

[79] T. Ishihara, M. Takeda, H. Sakamoto, A. Kimoto, C. Kobayashi, N. Takasaki, K. Yuki, K. Tanaka, M. Takenaga, R. Igarashi, T. Maeda, N. Yamakawa, Y. Okamoto, M. Otsuka, T. Ishida, H. Kiwada, Y. Mizushima, T. Mizushima, Accelerated blood clearance phenomenon upon repeated injection of PEG-modified PLA-nanoparticles, Pharm Res, 26 (2009) 2270-2279.

[80] Guidance for industry: immunogenicity assessment for therapeutic protein products, in, U.S. Department of Health and Human Services

Food and Drug Administration.

[81] S.C. Semple, T.O. Harasym, K.A. Clow, S.M. Ansell, S.K. Klimuk, M.J. Hope, Immunogenicity and rapid blood clearance of liposomes containing polyethylene glycol-lipid conjugates and nucleic Acid, J Pharmacol Exp Ther, 312 (2005) 1020-1026.

[82] H. Koide, T. Asai, K. Hatanaka, S. Akai, T. Ishii, E. Kenjo, T. Ishida, H. Kiwada, H. Tsukada, N. Oku, T cell-independent B cell response is responsible for ABC phenomenon induced by repeated injection of PEGylated liposomes, Int J Pharm, 392 (2010) 218-223.

[83] A. Cerutti, M. Cols, I. Puga, Marginal zone B cells: virtues of innate-like antibody-producing lymphocytes, Nat Rev Immunol, 13 (2013) 118-132.

[84] T. Shimizu, T. Ishida, H. Kiwada, Transport of PEGylated liposomes from the splenic marginal zone to the follicle in the induction phase of the accelerated blood clearance phenomenon, Immunobiology, 218 (2012) 725-732.

[85] Z. Sha, R.W. Compans, Induction of CD4(+) T-cell-independent immunoglobulin responses by inactivated influenza virus, J Virol, 74 (2000) 4999-5005.

[86] M.J. Colombo, G. Sun, K.R. Alugupalli, T-Cell-Independent Immune Responses Do Not Require Cxc Ligand 13-Mediated B1 Cell Migration, Infection and Immunity, 78 (2010) 3950-3956.

[87] M. Balázs, F. Martin, T. Zhou, J.F. Kearney, Blood Dendritic Cells Interact with Splenic Marginal Zone B Cells to Initiate T-Independent Immune Responses, Immunity, 17 (2002) 341-352.

[88] Y. Zhao, C. Wang, L. Wang, Q. Yang, W. Tang, Z. She, Y. Deng, A frustrating problem: Accelerated blood clearance of PEGylated solid lipid nanoparticles following subcutaneous injection in rats, European Journal of Pharmaceutics and Biopharmaceutics, 81 (2012) 506-513.

[89] M.G. Saifer, L.D. Williams, M.A. Sobczyk, S.J. Michaels, M.R. Sherman, Selectivity of binding of PEGs and PEG-like oligomers to anti-PEG antibodies induced by methoxyPEG-proteins, Mol Immunol, 57 (2014) 236-246.

[90] T. Tagami, K. Nakamura, T. Shimizu, T. Ishida, H. Kiwada, Effect of siRNA in PEG-coated siRNA-lipoplex on anti-PEG IgM production, Journal of Controlled Release, 137 (2009) 234-240.

[91] C. Wang, X. Cheng, Y. Sui, X. Luo, G. Jiang, Y. Wang, Z. Huang, Z. She, Y. Deng, A noticeable phenomenon: Thiol terminal PEG enhances the immunogenicity of PEGylated emulsions injected intravenously or subcutaneously into rats, European Journal of Pharmaceutics and Biopharmaceutics, 85 (2013) 744-751.

[92] C. Oussoren, G. Storm, Effect of repeated intravenous administration on the circulation kinetics of poly(ethyleneglycol)-liposomes in rats, J Liposome Res, 9 (1999) 349-355.

[93] B. Goins, W.T. Phillips, R. Klipper, Repeat injection studies of technetium-99m-labeled PEG-liposomes in the same animal, J Liposome Res, 8 (1998) 265-281.

[94] T. Tagami, K. Nakamura, T. Shimizu, N. Yamazaki, T. Ishida, H. Kiwada, CpG motifs in pDNA-sequences increase anti-PEG IgM production induced by PEG-coated pDNA-lipoplexes, Journal of Controlled Release, 142 (2010) 160-166.

[95] A. Nagao, A.S. Abu Lila, T. Ishida, H. Kiwada, Abrogation of the accelerated blood clearance phenomenon by SOXL regimen: promise for clinical application, Int J Pharm, 441 (2013) 395-401.

[96] J. Cui, C. Li, C. Wang, Y. Li, L. Zhang, L. Zhang, H. Yang, Repeated injection of pegylated liposomal antitumour drugs induces the disappearance of the rapid distribution phase, Journal of Pharmacy and Pharmacology, 60 (2008) 1651-1657.

[97] H. Koide, T. Asai, H. Kato, H. Ando, K. Shiraishi, M. Yokoyama, N. Oku, Size-dependent induction of accelerated blood clearance phenomenon by repeated injections of polymeric micelles, Int J Pharm, 432 (2012) 75-79.

[98] N.J. Ganson, S.J. Kelly, E. Scarlett, J.S. Sundy, M.S. Hershfield, Control of hyperuricemia in subjects with refractory gout, and induction of antibody against poly(ethylene glycol) (PEG), in a phase I trial of subcutaneous PEGylated urate oxidase, Arthritis Res Ther, 8 (2006) R12.

[99] A. Gabizon, H. Shmeeda, Y. Barenholz, Pharmacokinetics of PEGylated liposomal doxorubicin, Clin Pharmacokinet, 42 (2003) 419-436.

[100] J.K. Armstrong, R. Leger, R.B. Wenby, H.J. Meiselman, G. Garratty, T.C. Fisher, Occurrence of an antibody to poly(ethylene glycol) in normal donors, Blood, 102 (2003) 556.

[101] A.W. Richter, E. Akerblom, Polyethylene glycol reactive antibodies in man: titer distribution in allergic patients treated with monomethoxy polyethylene glycol modified allergens or placebo, and in healthy blood donors, Int Arch Allergy Appl Immunol, 74 (1984) 36-39.

[102] H. Tillmann, N.J. Ganson, K. Patel, A.J. Thompson, M. Abdelmalek, T. Moody, J.G. McHutchison, M.S. Hershfield, High prevalence of pre-existing antibodies against polyethylene glycol (PEG) in hepatitis C (HCV) patients which is not associated with impaired response to PEG-interferon, Journal of Hepatology, 52 (2010) S129.

[103] N. Longo, C.O. Harding, B.K. Burton, D.K. Grange, J. Vockley, M. Wasserstein, G.M. Rice, A. Dorenbaum, J.K. Neuenburg, D.G. Musson, Z. Gu, S. Sile, Single-dose, subcutaneous recombinant phenylalanine ammonia lyase conjugated with polyethylene glycol in adult patients with phenylketonuria: an open-label, multicentre, phase 1 dose-escalation trial, Lancet, 384 (2014) 37-44.

[104] M.S. Hershfield, N.J. Ganson, S.J. Kelly, E.L. Scarlett, D.A. Jaggers, J.S. Sundy, Induced and pre-existing anti-polyethylene glycol antibody in a trial of every 3-week dosing of pegloticase for refractory gout, including in organ transplant recipients, Arthritis Res Ther, 16 (2014) R63.

[105] C. Lubich, P. Allacher, M. de la Rosa, A. Bauer, T. Prenninger, F.M. Horling, J. Siekmann, J. Oldenburg, F. Scheiflinger, B.M. Reipert, The Mystery of Antibodies Against Polyethylene Glycol (PEG) - What do we Know?, Pharm Res, 33 (2016) 2239-2249.

[106] J.K. Armstrong, G. Hempel, S. Koling, L.S. Chan, T. Fisher, H.J. Meiselman, G. Garratty, Antibody against poly(ethylene glycol) adversely affects PEG-asparaginase therapy in acute lymphoblastic leukemia patients, Cancer, 110 (2007) 103-111.

[107] S. Chaffee, A. Mary, E.R. Stiehm, D. Girault, A. Fischer, M.S. Hershfield, IgG antibody response to polyethylene glycol-modified adenosine deaminase in patients with adenosine deaminase deficiency, J Clin Invest, 89 (1992) 1643-1651.

[108] J.S. Sundy, N.J. Ganson, S.J. Kelly, E.L. Scarlett, C.D. Rehrig, W. Huang, M.S. Hershfield, Pharmacokinetics and pharmacodynamics of intravenous PEGylated recombinant mammalian urate oxidase in patients with refractory gout, Arthritis Rheum, 56 (2007) 1021-1028.

[109] J.S. Sundy, H.S.B. Baraf, R.A. Yood, N.L. Edwards, S.R. Gutierrez-Urena, E.L. Treadwell, J. Vazquez-Mellado, W.B. White, P.E. Lipsky, Z. Horowitz, W. Huang, A.N. Maroli, R.W. Waltrip, S.A. Hamburger, M.A. Becker, Efficacy and tolerability of Pegloticase for the treatment of chronic gout in patients refractory to conventional treatment, JAMA, 306 (2011) 711-720.

[110] T.J. Povsic, M.G. Lawrence, A.M. Lincoff, R. Mehran, C.P. Rusconi, S.L. Zelenkofske, Z. Huang, J. Sailstad, P.W. Armstrong, P.G. Steg, C. Bode, R.C. Becker, J.H. Alexander, N.F. Adkinson, A.I. Levinson, Pre-existing anti-PEG antibodies are associated with severe immediate allergic reactions to pegnivacogin, a PEGylated aptamer, Journal of Allergy and Clinical Immunology, (2016).

[111] H. Schellekens, W.E. Hennink, V. Brinks, The immunogenicity of polyethylene glycol: facts and fiction, Pharm Res, 30 (2013) 1729-1734.

[112] D. Chen, W. Liu, Y. Shen, H. Mu, Y. Zhang, R. Liang, A. Wang, K. Sun, F. Fu, Effects of a novel pH-sensitive liposome with cleavable esterase-catalyzed and pH-responsive double smart mPEG lipid derivative on ABC phenomenon, Int J Nanomedicine, 6 (2011) 2053-2061.

[113] A.M. Abeles, PEG-ing down (and preventing?) the cause of pegloticase failure, Arthritis Res Ther, 16 (2014) 112.

[114] M. Cavadas, A. Gonzalez-Fernandez, R. Franco, Pathogen-mimetic stealth nanocarriers for drug delivery: a future possibility, Nanomedicine (Lond), 7 (2011) 730-743.

[115] K. Knop, R. Hoogenboom, D. Fischer, U.S. Schubert, Poly(ethylene glycol) in Drug Delivery: Pros and Cons as Well as Potential Alternatives, Angewandte Chemie International Edition, 49 (2010) 6288-6308.

[116] A.S. Abu Lila, K. Nawata, T. Shimizu, T. Ishida, H. Kiwada, Use of polyglycerol (PG), instead of polyethylene glycol (PEG), prevents induction of the accelerated blood clearance phenomenon against long-circulating liposomes upon repeated administration, Int J Pharm, 456 (2013) 235-242.

[117] T. Ishihara, T. Maeda, H. Sakamoto, N. Takasaki, M. Shigyo, T. Ishida, H. Kiwada, Y. Mizushima, T. Mizushima, Evasion of the Accelerated Blood Clearance Phenomenon by Coating of Nanoparticles with Various Hydrophilic Polymers, Biomacromolecules, 11 (2010) 2700-2706.

[118] A. Soshee, S. Zürcher, N.D. Spencer, A. Halperin, C. Nizak, General In Vitro Method to Analyze the Interactions of Synthetic Polymers with Human Antibody Repertoires, Biomacromolecules, 15 (2013) 113-121.

[119] C. Specht, B. Schlüter, M. Rolfing, K. Brüning, H.-G. Pauels, E. Kölsch, Idiotype-specific CD4+CD25+ T suppressor cells prevent, by limiting antibody diversity, the occurrence of anti-dextran antibodies crossreacting with histone H3, Eur J Immunol, 33 (2003) 1242-1249.

[120] T. Suzuki, M. Ichihara, K. Hyodo, E. Yamamoto, T. Ishida, H. Kiwada, H. Ishihara, H. Kikuchi, Accelerated blood clearance of PEGylated liposomes containing doxorubicin upon repeated administration to dogs, Int J Pharm, 436 (2012) 636-643.

[121] S.M. Moghimi, Re-establishing the long circulatory behaviour of poloxamine-coated particles after repeated intravenous administration: applications in cancer drug delivery and imaging, Biochimica et Biophysica Acta (BBA) - General Subjects, 1472 (1999) 399-403.

[122] K. Taguchi, Y. Urata, M. Anraku, H. Watanabe, D. Kadowaki, H. Sakai, H. Horinouchi, K. Kobayashi, E. Tsuchida, T. Maruyama, M. Otagiri, Hemoglobin vesicles, polyethylene glycol (PEG)ylated liposomes developed as a red blood cell substitute, do not induce the accelerated blood clearance phenomenon in mice, Drug Metab Dispos, 37 (2009) 2197-2203.

[123] C. Zhang, K. Fan, X. Ma, D. Wei, Impact of large aggregated uricases and PEG diol on accelerated blood clearance of PEGylated canine uricase, PLoS One, 7 (2012) e39659.

[124] J.T. White, S.D. Newsome, B.C. Kieseier, R.A. Bermel, Y. Cui, A. Seddighzadeh, S. Hung, M. Crossman, M. Subramanyam, Incidence, characterization, and clinical impact analysis of peginterferon beta1a immunogenicity in patients with multiple sclerosis in the ADVANCE trial, Ther Adv Neurol Disord, 9 (2016) 239-249.

[125] N. Bertrand, J. Wu, X. Xu, N. Kamaly, O.C. Farokhzad, Cancer nanotechnology: the impact of passive and active targeting in the era of modern cancer biology, Adv Drug Deliv Rev, 66 (2014) 2-25.

[126] Y.H. Bae, K. Park, Targeted drug delivery to tumors: Myths, reality and possibility, J Control Release, 153 (2011) 198-205.

[127] V.J. Venditto, F.C. Szoka Jr, Cancer nanomedicines: So many papers and so few drugs!, Advanced Drug Delivery Reviews, 65 (2013) 80-88.

[128] S. Stapleton, M. Milosevic, I.F. Tannock, C. Allen, D.A. Jaffray, The intra-tumoral relationship between microcirculation, interstitial fluid pressure and liposome accumulation, Journal of Controlled Release, 211 (2015) 163-170.

[129] F. Yuan, M. Leunig, S.K. Huang, D.A. Berk, D. Papahadjopoulos, R.K. Jain, Microvascular permeability and interstitial penetration of sterically stabilized (stealth) liposomes in a human tumor xenograft, Cancer Res, 54 (1994) 3352-3356.

[130] F. Janku, Tumor heterogeneity in the clinic: is it a real problem?, Therapeutic Advances in Medical Oncology, 6 (2014) 43-51.

[131] P.L. Bedard, A.R. Hansen, M.J. Ratain, L.L. Siu, Tumour heterogeneity in the clinic, Nature, 501 (2013) 355-364.

[132] L. Ding, T.J. Ley, D.E. Larson, C.A. Miller, D.C. Koboldt, J.S. Welch, J.K. Ritchey, M.A. Young, T. Lamprecht, M.D. McLellan, J.F. McMichael, J.W. Wallis, C. Lu, D. Shen, C.C. Harris, D.J. Dooling, R.S. Fulton, L.L. Fulton, K. Chen, H. Schmidt, J. Kalicki-Veizer, V.J. Magrini, L. Cook, S.D. McGrath, T.L. Vickery, M.C. Wendl, S. Heath, M.A. Watson, D.C. Link, M.H. Tomasson, W.D. Shannon, J.E. Payton, S. Kulkarni, P. Westervelt, M.J. Walter, T.A. Graubert, E.R. Mardis, R.K. Wilson, J.F. DiPersio, Clonal evolution in relapsed acute myeloid leukaemia revealed by whole-genome sequencing, Nature, 481 (2012) 506-510.

[133] S. Blatter, S. Rottenberg, Minimal residual disease in cancer therapy – Small things make all the difference, Drug Resistance Updates.

[134] F. Fu, M.A. Nowak, S. Bonhoeffer, Spatial Heterogeneity in Drug Concentrations Can Facilitate the Emergence of Resistance to Cancer Therapy, PLoS Comput Biol, 11 (2015) e1004142.

[135] J. Fang, H. Nakamura, H. Maeda, The EPR effect: Unique features of tumor blood vessels for drug delivery, factors involved, and limitations and augmentation of the effect, Adv Drug Deliv Rev, 63 (2011) 136-151.

[136] H. Kobayashi, R. Watanabe, P.L. Choyke, Improving conventional enhanced permeability and retention (EPR) effects; what is the appropriate target?, Theranostics, 4 (2013) 81-89.

[137] V. Torchilin, Tumor delivery of macromolecular drugs based on the EPR effect, Adv Drug Deliv Rev, 63 (2011) 131-135.

[138] R. Toy, P.M. Peiris, K.B. Ghaghada, E. Karathanasis, Shaping cancer nanomedicine: the effect of particle shape on the in vivo journey of nanoparticles, Nanomedicine (Lond), 9 (2014) 121-134.

[139] D. Banerjee, R. Harfouche, S. Sengupta, Nanotechnology-mediated targeting of tumor angiogenesis, Vasc Cell, 3 (2011) 3.

[140] M.A. Phillips, M.L. Gran, N.A. Peppas, Targeted Nanodelivery of Drugs and Diagnostics, Nano Today, 5 (2010) 143-159.

[141] V.P. Torchilin, Passive and active drug targeting: drug delivery to tumors as an example, Handb Exp Pharmacol, (2010) 3-53.

[142] Z. Amoozgar, J. Park, Q. Lin, Y. Yeo, Low Molecular-Weight Chitosan as a pH-Sensitive Stealth Coating for Tumor-Specific Drug Delivery, Molecular Pharmaceutics, 9 (2012) 1262-1270.

[143] C. Passirani, G. Barratt, J.P. Devissaguet, D. Labarre, Long-circulating nanoparticles bearing heparin or dextran covalently bound to poly(methyl methacrylate), Pharm Res, 15 (1998) 1046-1050.

[144] H. Takeuchi, H. Kojima, H. Yamamoto, Y. Kawashima, Evaluation of circulation profiles of liposomes coated with hydrophilic polymers having different molecular weights in rats, Journal of Controlled Release, 75 (2001) 83-91.

[145] V.P. Torchilin, V.S. Trubetskoy, K.R. Whiteman, P. Caliceti, P. Ferruti, F.M. Veronese, New synthetic amphiphilic polymers for steric protection of liposomes in vivo, J Pharm Sci, 84 (1995) 1049-1053.

[146] Z. Cao, L. Zhang, S. Jiang, Superhydrophilic zwitterionic polymers stabilize liposomes, Langmuir, 28 (2012) 11625-11632.

[147] S. Salmaso, P. Caliceti, Stealth properties to improve therapeutic efficacy of drug nanocarriers, J Drug Deliv, 2013 (2013) 374252.

[148] S. Zalipsky, C.B. Hansen, J.M. Oaks, T.M. Allen, Evaluation of blood clearance rates and biodistribution of poly(2-oxazoline)-grafted liposomes, J Pharm Sci, 85 (1996) 133-137.

[149] J. Kopecek, P. Kopeckova, HPMA copolymers: origins, early developments, present, and future, Adv Drug Deliv Rev, 62 (2010) 122-149.

[150] E. Jäger, A. Jäger, P. Chytil, T. Etrych, B. Říhová, F.C. Giacomelli, P. Štěpánek, K. Ulbrich, Combination chemotherapy using core-shell nanoparticles through the self-assembly of HPMA-based copolymers and degradable polyester, Journal of Controlled Release, 165 (2013) 153-161.

[151] K.Y. Choi, K.H. Min, J.H. Na, K. Choi, K. Kim, J.H. Park, I.C. Kwon, S.Y. Jeong, Self-assembled hyaluronic acid nanoparticles as a potential drug carrier for cancer therapy: synthesis, characterization, and in vivo biodistribution, Journal of Materials Chemistry, 19 (2009) 4102-4107.

[152] H. Maeda, Toward a full understanding of the EPR effect in primary and metastatic tumors as well as issues related to its heterogeneity, Adv Drug Deliv Rev, (2015).

[153] T.T. Konno, H. Maeda, K. Iwai, S. Maki, S. Tashiro, M. Uchida, Y. Miyachi, Selective targeting of anti-cancer drug and simultaneous image enhancement in solid tumors by arterially administered lipid contrast medium, Cancer, 54 (1984) 2367-2374.

[154] B.M. Fenton, S.F. Paoni, B.K. Beauchamp, I. Ding, Zonal image analysis of tumour vascular perfusion, hypoxia, and necrosis, Br J Cancer, 86 (2002) 1831-1836.

[155] L. Jiang, T.R. Greenwood, D. Artemov, V. Raman, P.T. Winnard, Jr., R.M. Heeren, Z.M. Bhujwalla, K. Glunde, Localized hypoxia results in spatially heterogeneous metabolic signatures in breast tumor models, Neoplasia, 14 (2012) 732-741.

[156] S.N. Ekdawi, J.M. Stewart, M. Dunne, S. Stapleton, N. Mitsakakis, Y.N. Dou, D.A. Jaffray, C. Allen, Spatial and temporal mapping of heterogeneity in liposome uptake and microvascular distribution in an orthotopic tumor xenograft model, J Control Release, 207 (2015) 101-111.

[157] S. Stapleton, C. Allen, M. Pintilie, D.A. Jaffray, Tumor perfusion imaging predicts the intra-tumoral accumulation of liposomes, J Control Release, 172 (2013) 351-357.

[158] E. Huynh, G. Zheng, Cancer nanomedicine: addressing the dark side of the enhanced permeability and retention effect, Nanomedicine (Lond), (2015) 1-3.

[159] U. Prabhakar, H. Maeda, R.K. Jain, E.M. Sevick-Muraca, W. Zamboni, O.C. Farokhzad, S.T. Barry, A. Gabizon, P. Grodzinski, D.C. Blakey, Challenges and key considerations of the enhanced permeability and retention effect for nanomedicine drug delivery in oncology, Cancer Res, 73 (2013) 2412-2417.

[160] R. Bazak, M. Houri, S. El Achy, S. Kamel, T. Refaat, Cancer active targeting by nanoparticles: a comprehensive review of literature, J Cancer Res Clin Oncol, 141 (2015) 769-784.

[161] L. Fiandra, S. Mazzucchelli, C. De Palma, M. Colombo, R. Allevi, S. Sommaruga, E. Clementi, M. Bellini, D. Prosperi, F. Corsi, Assessing the in vivo targeting efficiency of multifunctional nanoconstructs bearing antibody-derived ligands, ACS Nano, 7 (2013) 6092-6102.

[162] B. Hoang, S.N. Ekdawi, R.M. Reilly, C. Allen, Active targeting of block copolymer micelles with trastuzumab Fab fragments and nuclear localization signal leads to increased tumor uptake and nuclear localization in HER2-overexpressing xenografts, Mol Pharm, 10 (2013) 4229-4241.

[163] E. Sayari, M. Dinarvand, M. Amini, M. Azhdarzadeh, E. Mollarazi, Z. Ghasemi, F. Atyabi, MUC1 aptamer conjugated to chitosan nanoparticles, an efficient targeted carrier designed for anticancer SN38 delivery, Int J Pharm, 473 (2014) 304-315.

[164] Y.A. Shen, C.S. Liu, Y.H. Chang, P.H. Chen, C.L. He, H.C. Wu, C.M. Chuang, Subtype-specific binding peptides enhance the therapeutic efficacy of nanomedicine in the treatment of ovarian cancer, Cancer Lett, 360 (2015) 39-47.

[165] A. David, P. Kopeckova, J. Kopecek, A. Rubinstein, The role of galactose, lactose, and galactose valency in the biorecognition of N-(2-hydroxypropyl)methacrylamide copolymers by human colon adenocarcinoma cells, Pharm Res, 19 (2002) 1114-1122.

[166] G. Wu, Z. Wang, X. Bian, X. Du, C. Wei, Folate-modified doxorubicin-loaded nanoparticles for tumor-targeted therapy, Pharm Biol, 52 (2014) 978-982.

[167] T.M. Allen, Ligand-targeted therapeutics in anticancer therapy, Nat Rev Cancer, 2 (2002) 750-763.

[168] J.R. Beech, S.J. Shin, J.A. Smith, K.A. Kelly, Mechanisms for targeted delivery of nanoparticles in cancer, Curr Pharm Des, 19 (2013) 6560-6574.

[169] Z. Cheng, A. Al Zaki, J.Z. Hui, V.R. Muzykantov, A. Tsourkas, Multifunctional nanoparticles: cost versus benefit of adding targeting and imaging capabilities, Science, 338 (2012) 903-910.

[170] F. Gu, L. Zhang, B.A. Teply, N. Mann, A. Wang, A.F. Radovic-Moreno, R. Langer, O.C. Farokhzad, Precise engineering of targeted nanoparticles by using self-assembled biointegrated block copolymers, Proc Natl Acad Sci U S A, 105 (2008) 2586-2591.

[171] D.R. Elias, A. Poloukhtine, V. Popik, A. Tsourkas, Effect of ligand density, receptor density, and nanoparticle size on cell targeting, Nanomedicine (Lond), 9 (2013) 194-201.

[172] A. Fakhari, A. Baoum, T.J. Siahaan, K.B. Le, C. Berkland, Controlling ligand surface density optimizes nanoparticle binding to ICAM-1, J Pharm Sci, 100 (2011) 1045-1056.

[173] E. Moradi, Vllasaliu, D., Garnett, M., Falcone, F., & Stolnik, S, Ligand density and clustering effects on endocytosis of folate modified nanoparticles, RSC Advances, 2 (2012) 3025-3033.

[174] T.A. Denison, and You Han Bae. Cancer Targeted Drug Delivery., Heterogeneity of Cancers and Its Implication for Targeted Drug Delivery, Springer, (2013) 337-362.

[175] M.R. Junttila, F.J. de Sauvage, Influence of tumour micro-environment heterogeneity on therapeutic response, Nature, 501 (2013) 346-354.

[176] M.P. Smith, B. Sanchez-Laorden, K. O'Brien, H. Brunton, J. Ferguson, H. Young, N. Dhomen, K.T. Flaherty, D.T. Frederick, Z.A. Cooper, J.A. Wargo, R. Marais, C. Wellbrock, The immune microenvironment confers resistance to MAPK pathway inhibitors through macrophage-derived TNFalpha, Cancer Discov, 4 (2014) 1214-1229.

[177] Y. Jung, J.K. Kim, Y. Shiozawa, J. Wang, A. Mishra, J. Joseph, J.E. Berry, S. McGee, E. Lee, H. Sun, T. Jin, H. Zhang, J. Dai, P.H. Krebsbach, E.T. Keller, K.J. Pienta, R.S. Taichman, Recruitment of mesenchymal stem cells into prostate tumours promotes metastasis, Nat Commun, 4 (2013) 1795.

[178] M. Jamal-Hanjani, S.A. Quezada, J. Larkin, C. Swanton, Translational implications of tumor heterogeneity, Clin Cancer Res, 21 (2015) 1258-1266.

[179] H.J. Lee, A.N. Seo, E.J. Kim, M.H. Jang, K.J. Suh, H.S. Ryu, Y.J. Kim, J.H. Kim, S.A. Im, G. Gong, K.H. Jung, I.A. Park, S.Y. Park, HER2 heterogeneity affects trastuzumab responses and survival in patients with HER2-positive metastatic breast cancer, Am J Clin Pathol, 142 (2014) 755-766.

[180] L. Ding, M.J. Ellis, S. Li, D.E. Larson, K. Chen, J.W. Wallis, C.C. Harris, M.D. McLellan, R.S. Fulton, L.L. Fulton, R.M. Abbott, J. Hoog, D.J. Dooling, D.C. Koboldt, H. Schmidt, J. Kalicki, Q. Zhang, L. Chen, L. Lin, M.C. Wendl, J.F. McMichael, V.J. Magrini, L. Cook, S.D. McGrath, T.L. Vickery, E. Appelbaum, K. Deschryver, S. Davies, T. Guintoli, L. Lin, R. Crowder, Y. Tao, J.E. Snider, S.M. Smith, A.F. Dukes, G.E. Sanderson, C.S. Pohl, K.D. Delehaunty, C.C. Fronick, K.A. Pape, J.S. Reed, J.S. Robinson, J.S. Hodges, W. Schierding, N.D. Dees, D. Shen, D.P. Locke, M.E. Wiechert, J.M. Eldred, J.B. Peck, B.J. Oberkfell, J.T. Lolofie, F. Du, A.E. Hawkins, M.D. O'Laughlin, K.E. Bernard, M. Cunningham, G. Elliott, M.D. Mason, D.M. Thompson, Jr., J.L. Ivanovich, P.J. Goodfellow, C.M. Perou, G.M. Weinstock, R. Aft, M. Watson, T.J. Ley, R.K. Wilson, E.R. Mardis, Genome remodelling in a basal-like breast cancer metastasis and xenograft, Nature, 464 (2010) 999-1005.

[181] A.P. Albino, K.O. Lloyd, A.N. Houghton, H.F. Oettgen, L.J. Old, Heterogeneity in surface antigen and glycoprotein expression of cell lines derived from different melanoma metastases of the same patient. Implications for the study of tumor antigens, J Exp Med, 154 (1981) 1764-1778.

[182] M. Gerlinger, A.J. Rowan, S. Horswell, J. Larkin, D. Endesfelder, E. Gronroos, P. Martinez, N. Matthews, A. Stewart, P. Tarpey, I. Varela, B. Phillimore, S. Begum, N.Q. McDonald, A. Butler, D. Jones, K. Raine, C. Latimer, C.R. Santos, M. Nohadani, A.C. Eklund, B. Spencer-Dene, G. Clark, L. Pickering, G. Stamp, M. Gore, Z. Szallasi, J. Downward, P.A. Futreal, C. Swanton, Intratumor heterogeneity and branched evolution revealed by multiregion sequencing, N Engl J Med, 366 (2012) 883-892.

[183] C. Arslan, E. Sari, S. Aksoy, K. Altundag, Variation in hormone receptor and HER-2 status between primary and metastatic breast cancer: review of the literature, Expert Opin Ther Targets, 15 (2011) 21-30.

[184] C.E. Meacham, S.J. Morrison, Tumour heterogeneity and cancer cell plasticity, Nature, 501 (2013) 328-337.

[185] J.N. Jakobsen, J.B. Sorensen, Intratumor heterogeneity and chemotherapy-induced changes in EGFR status in non-small cell lung cancer, Cancer Chemother Pharmacol, 69 (2012) 289-299.

[186] K. Taniguchi, J. Okami, K. Kodama, M. Higashiyama, K. Kato, Intratumor heterogeneity of epidermal growth factor receptor mutations in lung cancer and its correlation to the response to gefitinib, Cancer Sci, 99 (2008) 929-935.

[187] Y.P. Choi, H.S. Shim, M.Q. Gao, S. Kang, N.H. Cho, Molecular portraits of intratumoral heterogeneity in human ovarian cancer, Cancer Lett, 307 (2011) 62-71.

[188] B. Vogelstein, N. Papadopoulos, V.E. Velculescu, S. Zhou, L.A. Diaz, Jr., K.W. Kinzler, Cancer genome landscapes, Science, 339 (2013) 1546-1558.

[189] R.F. Schwarz, C.K. Ng, S.L. Cooke, S. Newman, J. Temple, A.M. Piskorz, D. Gale, K. Sayal, M. Murtaza, P.J. Baldwin, N. Rosenfeld, H.M. Earl, E. Sala, M. Jimenez-Linan, C.A. Parkinson, F. Markowetz, J.D. Brenton, Spatial and temporal heterogeneity in high-grade serous ovarian cancer: a phylogenetic analysis, PLoS Med, 12 (2015) e1001789.

[190] J. Liu, S.K. Lau, V.A. Varma, R.A. Moffitt, M. Caldwell, T. Liu, A.N. Young, J.A. Petros, A.O. Osunkoya, T. Krogstad, B. Leyland-Jones, M.D. Wang, S. Nie, Molecular mapping of tumor

heterogeneity on clinical tissue specimens with multiplexed quantum dots, ACS Nano, 4 (2010) 2755-2765.

[191] Z.Z. Yang, D.M. Grote, S.C. Ziesmer, B. Xiu, A.J. Novak, S.M. Ansell, PD-1 expression defines two distinct T-cell sub-populations in follicular lymphoma that differentially impact patient survival, Blood Cancer J, 5 (2015) e281.

[192] T.A. Yap, M. Gerlinger, P.A. Futreal, L. Pusztai, C. Swanton, Intratumor heterogeneity: seeing the wood for the trees, Sci Transl Med, 4 (2012) 127ps110.

[193] F.C. van de Watering, M. Rijpkema, M. Robillard, W.J. Oyen, O.C. Boerman, Pretargeted imaging and radioimmunotherapy of cancer using antibodies and bioorthogonal chemistry, Front Med (Lausanne), 1 (2014) 44.

[194] R.B. Walter, O.W. Press, J.M. Pagel, Pretargeted radioimmunotherapy for hematologic and other malignancies, Cancer Biother Radiopharm, 25 (2010) 125-142.

[195] D.M. Goldenberg, C.H. Chang, E.A. Rossi, W. J, McBride, R.M. Sharkey, Pretargeted molecular imaging and radioimmunotherapy, Theranostics, 2 (2012) 523-540.

[196] D.J. Green, J.M. Pagel, A. Pantelias, N. Hedin, Y. Lin, D.S. Wilbur, A. Gopal, D.K. Hamlin, O.W. Press, Pretargeted radioimmunotherapy for B-cell lymphomas, Clin Cancer Res, 13 (2007) 5598s-5603s.

[197] J.M. Pagel, N. Hedin, K. Subbiah, D. Meyer, R. Mallet, D. Axworthy, L.J. Theodore, D.S. Wilbur, D.C. Matthews, O.W. Press, Comparison of anti-CD20 and anti-CD45 antibodies for conventional and pretargeted radioimmunotherapy of B-cell lymphomas, Blood, 101 (2003) 2340-2348.

[198] D.J. Green, J.M. Pagel, E.R. Nemecek, Y. Lin, A. Kenoyer, A. Pantelias, D.K. Hamlin, D.S. Wilbur, D.R. Fisher, J.G. Rajendran, A.K. Gopal, S.I. Park, O.W. Press, Pretargeting CD45 enhances the selective delivery of radiation to hematolymphoid tissues in nonhuman primates, Blood, 114 (2009) 1226-1235.

[199] J.M. Pagel, D.C. Matthews, A. Kenoyer, D.K. Hamlin, D.S. Wilbur, D.R. Fisher, A.K. Gopal, Y. Lin, L. Saganic, F.R. Appelbaum, O.W. Press, Pretargeted radioimmunotherapy using anti-CD45 monoclonal antibodies to deliver radiation to murine hematolymphoid tissues and human myeloid leukemia, Cancer Res, 69 (2009) 185-192.

[200] J.M. Pagel, A.L. Kenoyer, T. Back, D.K. Hamlin, D.S. Wilbur, D.R. Fisher, S.I. Park, S. Frayo, A. Axtman, N. Orgun, J. Orozco, J. Shenoi, Y. Lin, A.K. Gopal, D.J. Green, F.R. Appelbaum, O.W. Press, Anti-CD45 pretargeted radioimmunotherapy using bismuth-213: high rates of complete remission and long-term survival in a mouse myeloid leukemia xenograft model, Blood, 118 (2011) 703-711.

[201] J.M. Pagel, N. Orgun, D.K. Hamlin, D.S. Wilbur, T.A. Gooley, A.K. Gopal, S.I. Park, D.J. Green, Y. Lin, O.W. Press, A comparative analysis of conventional and pretargeted radioimmunotherapy of B-cell lymphomas by targeting CD20, CD22, and HLA-DR singly and in combinations, Blood, 113 (2009) 4903-4913.

[202] J.M. Pagel, A. Pantelias, N. Hedin, S. Wilbur, L. Saganic, Y. Lin, D. Axworthy, D.K. Hamlin, D.S. Wilbur, A.K. Gopal, O.W. Press, Evaluation of CD20, CD22, and HLA-DR targeting for radioimmunotherapy of B-cell lymphomas, Cancer Res, 67 (2007) 5921-5928.

[203] D.J. Green, N.N. Orgun, J.C. Jones, M.D. Hylarides, J.M. Pagel, D.K. Hamlin, D.S. Wilbur, Y. Lin, D.R. Fisher, A.L. Kenoyer, S.L. Frayo, A.K. Gopal, J.J. Orozco, T.A. Gooley, B.L. Wood, W.I. Bensinger, O.W. Press, A preclinical model of CD38-pretargeted radioimmunotherapy for plasma cell malignancies, Cancer Res, 74 (2014) 1179-1189.

[204] K. Subbiah, D.K. Hamlin, J.M. Pagel, D.S. Wilbur, D.L. Meyer, D.B. Axworthy, R.W. Mallett, L.J. Theodore, P.S. Stayton, O.W. Press, Comparison of immunoscintigraphy, efficacy, and toxicity of conventional and pretargeted radioimmunotherapy in CD20-expressing human lymphoma xenografts, J Nucl Med, 44 (2003) 437-445.

[205] M. Zhang, Z. Zhang, K. Garmestani, J. Schultz, D.B. Axworthy, C.K. Goldman, M.W. Brechbiel, J.A. Carrasquillo, T.A. Waldmann, Pretarget radiotherapy with an anti-CD25 antibody-streptavidin fusion protein was effective in therapy of leukemia/lymphoma xenografts, Proc Natl Acad Sci U S A, 100 (2003) 1891-1895.

[206] D.B. Axworthy, J.M. Reno, M.D. Hylarides, R.W. Mallett, L.J. Theodore, L.M. Gustavson, F. Su, L.J. Hobson, P.L. Beaumier, A.R. Fritzberg, Cure of human carcinoma xenografts by a single dose of pretargeted yttrium-90 with negligible toxicity, Proc Natl Acad Sci U S A, 97 (2000) 1802-1807.

[207] A. Forero, P.L. Weiden, J.M. Vose, S.J. Knox, A.F. LoBuglio, J. Hankins, M.L. Goris, V.J. Picozzi, D.B. Axworthy, H.B. Breitz, R.B. Sims, R.G. Ghalie, S. Shen, R.F. Meredith, Phase 1 trial of a novel anti-CD20 fusion protein in pretargeted radioimmunotherapy for B-cell non-Hodgkin lymphoma, Blood, 104 (2004) 227-236.

[208] P.L. Weiden, H.B. Breitz, O. Press, J.W. Appelbaum, J.K. Bryan, S. Gaffigan, D. Stone, D. Axworthy, D. Fisher, J. Reno, Pretargeted radioimmunotherapy (PRIT) for treatment of non-Hodgkin's lymphoma (NHL): initial phase I/II study results, Cancer Biother Radiopharm, 15 (2000) 15-29.

[209] P.L. Weiden, H.B. Breitz, Pretargeted radioimmunotherapy (PRIT) for treatment of non-Hodgkin's lymphoma (NHL), Crit Rev Oncol Hematol, 40 (2001) 37-51.

[210] F. Kraeber-Bodere, S. Bardet, C.A. Hoefnagel, M.R. Vieira, J.P. Vuillez, A. Murat, T.C. Ferreira, M. Bardies, L. Ferrer, I. Resche, E. Gautherot, E. Rouvier, J. Barbet, J.F. Chatal, Radioimmunotherapy in medullary thyroid cancer using bispecific antibody and iodine 131-labeled bivalent hapten: preliminary results of a phase I/II clinical trial, Clin Cancer Res, 5 (1999) 3190s-3198s.

[211] F. Kraeber-Bodere, A. Faivre-Chauvet, C. Sai-Maurel, L. Campion, M. Fiche, E. Gautherot, J. Le Boterff, J. Barbet, J.F. Chatal, P. Thedrez, Toxicity and efficacy of radioimmunotherapy in carcinoembryonic antigen-producing medullary thyroid cancer xenograft: comparison of iodine 131-labeled F(ab')2 and pretargeted bivalent hapten and evaluation of repeated injections, Clin Cancer Res, 5 (1999) 3183s-3189s.

[212] F. Kraeber-Bodere, C. Rousseau, C. Bodet-Milin, L. Ferrer, A. Faivre-Chauvet, L. Campion, J.P. Vuillez, A. Devillers, C.H. Chang, D.M. Goldenberg, J.F. Chatal, J. Barbet, Targeting, toxicity, and efficacy of 2-step, pretargeted radioimmunotherapy using a chimeric bispecific antibody and 131I-labeled bivalent hapten in a phase I optimization clinical trial, J Nucl Med, 47 (2006) 247-255.

[213] A.C. Society, Cancer Facts & Figures, in, American Cancer Society, Atlanta, 2015.

[214] S.M. Swain, S.B. Kim, J. Cortes, J. Ro, V. Semiglazov, M. Campone, E. Ciruelos, J.M. Ferrero, A. Schneeweiss, A. Knott, E. Clark, G. Ross, M.C. Benyunes, J. Baselga, Pertuzumab, trastuzumab, and docetaxel for HER2-positive metastatic breast cancer (CLEOPATRA study): overall survival results from a randomised, double-blind, placebo-controlled, phase 3 study, Lancet Oncol, 14 (2013) 461-471.

[215] Y. Koyama, T. Barrett, Y. Hama, G. Ravizzini, P.L. Choyke, H. Kobayashi, In vivo molecular imaging to diagnose and subtype tumors through receptor-targeted optically labeled monoclonal antibodies, Neoplasia, 9 (2007) 1021-1029.

[216] T. Barrett, Y. Koyama, Y. Hama, G. Ravizzini, I.S. Shin, B.-S. Jang, C.H. Paik, Y. Urano, P.L. Choyke, H. Kobayashi, In vivo Diagnosis of Epidermal Growth Factor Receptor Expression using Molecular Imaging with a Cocktail of Optically Labeled Monoclonal Antibodies, Clinical Cancer Research, 13 (2007) 6639-6648.

[217] J.B. Haun, N.K. Devaraj, S.A. Hilderbrand, H. Lee, R. Weissleder, Bioorthogonal chemistry amplifies nanoparticle binding and enhances the sensitivity of cell detection, Nat Nanotechnol, 5 (2010) 660-665.

[218] M.R. Karver, R. Weissleder, S.A. Hilderbrand, Bioorthogonal reaction pairs enable simultaneous, selective, multi-target imaging, Angew Chem Int Ed Engl, 51 (2012) 920-922.

[219] B.A. Khaw, K.S. Gada, V. Patil, R. Panwar, S. Mandapati, A. Hatefi, S. Majewski, A. Weisenberger, Bispecific antibody complex pre-targeting and targeted delivery of polymer drug conjugates for imaging and therapy in dual human mammary cancer xenografts: targeted polymer drug conjugates for cancer diagnosis and therapy, Eur J Nucl Med Mol Imaging, 41 (2014) 1603-1616.

[220] D.T. Reardan, C.F. Meares, D.A. Goodwin, M. McTigue, G.S. David, M.R. Stone, J.P. Leung, R.M. Bartholomew, J.M. Frincke, Antibodies against metal chelates, Nature, 316 (1985) 265-268.

[221] D.A. Goodwin, C.F. Meares, M.J. McCall, M. McTigue, W. Chaovapong, Pre-targeted immunoscintigraphy of murine tumors with indium-111-labeled bifunctional haptens, J Nucl Med, 29 (1988) 226-234.

[222] H. Karacay, R.M. Sharkey, W.J. McBride, G.L. Griffiths, Z. Qu, K. Chang, H.J. Hansen, D.M. Goldenberg, Pretargeting for Cancer Radioimmunotherapy with Bispecific Antibodies: Role of the Bispecific Antibody's Valency for the Tumor Target Antigen, Bioconjug Chem, 13 (2002) 1054-1070.

[223] F.G. van Schaijk, E. Oosterwijk, J.D. Molkenboer-Kuenen, A.C. Soede, B.J. McBride, D.M. Goldenberg, W.J.G. Oyen, F.H.M. Corstens, O.C. Boerman, Pretargeting with Bispecific Anti-Renal Cell Carcinoma x Anti-DTPA(In) Antibody in 3 RCC Models, J Nucl Med, 46 (2005) 495-501.

[224] J.F. Gestin, A. Loussouarn, M. Bardies, E. Gautherot, A. Gruaz-Guyon, C. Sai-Maurel, J. Barbet, C. Curtet, J.F. Chatal, A. Faivre-Chauvet, Two-step targeting of xenografted colon carcinoma using a bispecific antibody and 188Re-labeled bivalent hapten: biodistribution and dosimetry studies, J Nucl Med, 42 (2001) 146-153.

[225] M. Hillairet de Boisferon, O. Raguin, M. Dussaillant, W. Rostène, J. Barbet, A. Gruaz-Guyon, Enhanced Targeting Specificity to Tumor Cells by Simultaneous Recognition of Two Antigens, Bioconjug Chem, 11 (2000) 452-460.

[226] W.J. McBride, P. Zanzonico, R.M. Sharkey, C. Noren, H. Karacay, E.A. Rossi, M.J. Losman, P.Y. Brard, C.H. Chang, S.M. Larson, D.M. Goldenberg, Bispecific antibody pretargeting PET (immunoPET) with an 124I-labeled hapten-peptide, J Nucl Med, 47 (2006) 1678-1688.

[227] M.V. Pimm, R.A. Robins, M.J. Embleton, E. Jacobs, A.J. Markham, A. Charleston, R.W. Baldwin, A bispecific monoclonal antibody against methotrexate and a human tumour associated antigen augments cytotoxicity of methotrexate-carrier conjugate, Br J Cancer, 61 (1990) 508-513.

[228] S. Yoon, Y.H. Kim, S.H. Kang, S.K. Kim, H.K. Lee, H. Kim, J. Chung, I.H. Kim, Bispecific Her2 x cotinine antibody in combination with cotinine-(histidine)2-iodine for the pre-targeting of Her2-positive breast cancer xenografts, J Cancer Res Clin Oncol, 140 (2014) 227-233.

[229] K.S. Gada, V. Patil, R. Panwar, A. Hatefi, B.A. Khaw, Bispecific antibody complex pre-targeted delivery of polymer-drug conjugates for cancer therapy, Drug Deliv Transl Res, 2 (2012) 65-76.

[230] J.M. Le Doussal, M. Martin, E. Gautherot, M. Delaage, J. Barbet, In vitro and in vivo targeting of radiolabeled monovalent and divalent haptens with dual specificity monoclonal antibody conjugates: enhanced divalent hapten affinity for cell-bound antibody conjugate, J Nucl Med, 30 (1989) 1358-1366.

[231] E. Janevik-Ivanovska, E. Gautherot, M. Hillairet de Boisferon, M. Cohen, G. Milhaud, A. Tartar, W. Rostene, J. Barbet, A. Gruaz-Guyon, Bivalent hapten-bearing peptides designed for iodine-131 pretargeted radioimmunotherapy, Bioconjug Chem, 8 (1997) 526-533.

[232] O.C. Boerman, M.H. Kranenborg, E. Oosterwijk, G.L. Griffiths, W.J. McBride, W.J. Oyen, M. de Weijert, J. Oosterwijk-Wakka, H.J. Hansen, F.H. Corstens, Pretargeting of renal cell carcinoma: improved tumor targeting with a bivalent chelate, Cancer Res, 59 (1999) 4400-4405.

[233] H.P. Lesch, M.U. Kaikkonen, J.T. Pikkarainen, S. Yla-Herttuala, Avidin-biotin technology in targeted therapy, Expert Opin Drug Deliv, 7 (2010) 551-564.

[234] M.V. Pimm, H.F. Fells, A.C. Perkins, R.W. Baldwin, Iodine-131 and indium-111 labelled avidin and streptavidin for pre-targetted immunoscintigraphy with biotinylated anti-tumour monoclonal antibody, Nucl Med Commun, 9 (1988) 931-941.

[235] J.R. Newton-Northup, S.D. Figueroa, T.P. Quinn, S.L. Deutscher, Bifunctional phage-based pretargeted imaging of human prostate carcinoma, Nucl Med Biol, 36 (2009) 789-800.

[236] S.J. Knox, M.L. Goris, M. Tempero, P.L. Weiden, L. Gentner, H. Breitz, G.P. Adams, D. Axworthy, S. Gaffigan, K. Bryan, D.R. Fisher, D. Colcher, I.D. Horak, L.M. Weiner, Phase II trial of yttrium-90-DOTA-biotin pretargeted by NR-LU-10 antibody/streptavidin in patients with metastatic colon cancer, Clin Cancer Res, 6 (2000) 406-414.

[237] Y. Lin, J.M. Pagel, D. Axworthy, A. Pantelias, N. Hedin, O.W. Press, A genetically engineered anti-CD45 single-chain antibody-streptavidin fusion protein for pretargeted radioimmunotherapy of hematologic malignancies, Cancer Res, 66 (2006) 3884-3892.

[238] N.K. Cheung, S. Modak, Y. Lin, H. Guo, P. Zanzonico, J. Chung, Y. Zuo, J. Sanderson, S. Wilbert, L.J. Theodore, D.B. Axworthy, S.M. Larson, Single-chain Fv-streptavidin substantially improved therapeutic index in multistep targeting directed at disialoganglioside GD2, J Nucl Med, 45 (2004) 867-877.

[239] J.M. Pagel, Y. Lin, N. Hedin, A. Pantelias, D. Axworthy, D. Stone, D.K. Hamlin, D.S. Wilbur, O.W. Press, Comparison of a tetravalent single-chain antibody-streptavidin fusion protein and an antibody-streptavidin chemical conjugate for pretargeted anti-CD20 radioimmunotherapy of B-cell lymphomas, Blood, 108 (2006) 328-336.

[240] M.D. Stachler, I. Chen, A.Y. Ting, J.S. Bartlett, Site-specific modification of AAV vector particles with biophysical probes and targeting ligands using biotin ligase, Mol Ther, 16 (2008) 1467-1473.

[241] H.P. Kalofonos, M. Rusckowski, D.A. Siebecker, G.B. Sivolapenko, D. Snook, J.P. Lavender, A.A. Epenetos, D.J. Hnatowich, Imaging of tumor in patients with indium-111-labeled biotin and streptavidin-conjugated antibodies: preliminary communication, J Nucl Med, 31 (1990) 1791-1796.

[242] K. Yumura, M. Ui, H. Doi, T. Hamakubo, T. Kodama, K. Tsumoto, A. Sugiyama, Mutations for decreasing the immunogenicity and maintaining the function of core streptavidin, Protein Sci, 22 (2013) 213-221.

[243] D.L. Meyer, J. Schultz, Y. Lin, A. Henry, J. Sanderson, J.M. Jackson, S. Goshorn, A.R. Rees, S.S. Graves, Reduced antibody response to streptavidin through site-directed mutagenesis, Protein Sci, 10 (2001) 491-503.

[244] M. Rusckowski, M. Fogarasi, B. Fritz, D.J. Hnatowich, Effect of endogenous biotin on the applications of streptavidin and biotin in mice, Nucl Med Biol, 24 (1997) 263-268.

[245] K.J. Hamblett, O.W. Press, D.L. Meyer, D.K. Hamlin, D. Axworthy, D.S. Wilbur, P.S. Stayton, Role of biotin-binding affinity in streptavidin-based pretargeted radioimmunotherapy of lymphoma, Bioconjug Chem, 16 (2005) 131-138.

[246] D.S. Wilbur, S.I. Park, M.K. Chyan, F. Wan, D.K. Hamlin, J. Shenoi, Y. Lin, S.M. Wilbur, F. Buchegger, A. Pantelias, J.M. Pagel, O.W. Press, Design and synthesis of bis-biotin-containing reagents for applications utilizing monoclonal antibody-based pretargeting systems with streptavidin mutants, Bioconjug Chem, 21 (2010) 1225-1238.

[247] M. Steiner, K. Gutbrodt, N. Krall, D. Neri, Tumor-targeting antibody-anticalin fusion proteins for in vivo pretargeting applications, Bioconjug Chem, 24 (2013) 234-241.

[248] J.C. Knight, M. Mosley, M.R. Stratford, H.T. Uyeda, H.A. Benink, M. Cong, F. Fan, S. Faulkner, B. Cornelissen, Development of an enzymatic pretargeting strategy for dual-modality imaging, Chem Commun (Camb), 51 (2015) 4055-4058.

[249] G. Liu, S. Dou, Y. Liu, Y. Wang, M. Rusckowski, D.J. Hnatowich, 90Y labeled phosphorodiamidate morpholino oligomer for pretargeting radiotherapy, Bioconjug Chem, 22 (2011) 2539-2545.

[250] G. Liu, S. Dou, P.H. Pretorius, X. Liu, L. Chen, M. Rusckowski, D.J. Hnatowich, Tumor pretargeting in mice using MORF conjugated CC49 antibody and radiolabeled complimentary cMORF effector, Q J Nucl Med Mol Imaging, 54 (2010) 333-340.

[251] G. Liu, C. Liu, S. Zhang, J. He, N. Liu, S. Gupta, M. Rusckowski, D.J. Hnatowich, Investigations of 99mTc morpholino pretargeting in mice, Nucl Med Commun, 24 (2003) 697-705.

[252] G. Liu, J. He, S. Dou, S. Gupta, M. Rusckowski, D.J. Hnatowich, Further investigations of morpholino pretargeting in mice--establishing quantitative relations in tumor, Eur J Nucl Med Mol Imaging, 32 (2005) 1115-1123.

[253] J. He, G. Liu, S. Gupta, Y. Zhang, M. Rusckowski, D.J. Hnatowich, Amplification Targeting: A Modified Pretargeting Approach with Potential for Signal Amplification—Proof of a Concept, J Nucl Med, 45 (2004) 1087-1095.

[254] R.M. Sharkey, D.M. Goldenberg, Cancer radioimmunotherapy, Immunotherapy, 3 (2011) 349-370.

[255] J. He, Y. Wang, S. Dou, X. Liu, S. Zhang, G. Liu, D. Hnatowich, Affinity enhancement pretargeting: synthesis and testing of a 99mTc-labeled bivalent MORF, Mol Pharm, 7 (2010) 1118-1124.

[256] L. Carroll, H.L. Evans, E.O. Aboagye, A.C. Spivey, Bioorthogonal chemistry for pre-targeted molecular imaging--progress and prospects, Org Biomol Chem, 11 (2013) 5772-5781.

[257] J.C. Knight, B. Cornelissen, Bioorthogonal chemistry: implications for pretargeted nuclear (PET/SPECT) imaging and therapy, American Journal of Nuclear Medicine and Molecular Imaging, 4 (2014) 96-113.

[258] R. Rossin, P. Renart Verkerk, S.M. van den Bosch, R.C.M. Vulders, I. Verel, J. Lub, M.S. Robillard, In Vivo Chemistry for Pretargeted Tumor Imaging in Live Mice, Angewandte Chemie International Edition, 49 (2010) 3375-3378.

[259] R. Rossin, S.M. van Duijnhoven, T. Lappchen, S.M. van den Bosch, M.S. Robillard, Trans-cyclooctene tag with improved properties for tumor pretargeting with the diels-alder reaction, Mol Pharm, 11 (2014) 3090-3096.

[260] B.M. Zeglis, K.K. Sevak, T. Reiner, P. Mohindra, S.D. Carlin, P. Zanzonico, R. Weissleder, J.S. Lewis, A pretargeted PET imaging strategy based on bioorthogonal Diels-Alder click chemistry, J Nucl Med, 54 (2013) 1389-1396.

[261] S.B. Lee, H.L. Kim, H.-J. Jeong, S.T. Lim, M.-H. Sohn, D.W. Kim, Mesoporous Silica Nanoparticle Pretargeting for PET Imaging Based on a Rapid Bioorthogonal Reaction in a Living Body, Angewandte Chemie International Edition, 52 (2013) 10549-10552.

[262] J. Gunn, S.I. Park, O. Veiseh, O.W. Press, M. Zhang, A pretargeted nanoparticle system for tumor cell labeling, Mol Biosyst, 7 (2011) 742-748.

[263] T.W. Chu, J. Yang, R. Zhang, M. Sima, J. Kopecek, Cell surface self-assembly of hybrid nanoconjugates via oligonucleotide hybridization induces apoptosis, ACS Nano, 8 (2014) 719-730.

[264] L. Nobs, F. Buchegger, R. Gurny, E. Allemann, Biodegradable nanoparticles for direct or two-step tumor immunotargeting, Bioconjug Chem, 17 (2006) 139-145.

[265] J. Bushman, A. Vaughan, L. Sheihet, Z. Zhang, M. Costache, J. Kohn, Functionalized nanospheres for targeted delivery of paclitaxel, J Control Release, 171 (2013) 315-321.

[266] M. Pulkkinen, J. Pikkarainen, T. Wirth, T. Tarvainen, V. Haapa-aho, H. Korhonen, J. Seppälä, K. Järvinen, Three-step tumor targeting of paclitaxel using biotinylated PLA-PEG nanoparticles and avidin–

biotin technology: Formulation development and in vitro anticancer activity, European Journal of Pharmaceutics and Biopharmaceutics, 70 (2008) 66-74.

[267] S.A. Longman, P.R. Cullis, L. Choi, G. de Jong, M.B. Bally, A two-step targeting approach for delivery of doxorubicin-loaded liposomes to tumour cells in vivo, Cancer Chemother Pharmacol, 36 (1995) 91-101.

[268] S.H. Frost, H. Jensen, S. Lindegren, In vitro evaluation of avidin antibody pretargeting using 211At-labeled and biotinylated poly-L-lysine as effector molecule, Cancer, 116 (2010) 1101-1110.

[269] Y. Cao, M.R. Suresh, Bispecific MAb aided liposomal drug delivery, J Drug Target, 8 (2000) 257-266.

[270] J.J. Mulvey, C.H. Villa, M.R. McDevitt, F.E. Escorcia, E. Casey, D.A. Scheinberg, Self-assembly of carbon nanotubes and antibodies on tumours for targeted amplified delivery, Nat Nanotechnol, 8 (2013) 763-771.

[271] M.K. Rahim, R. Kota, J.B. Haun, Enhancing reactivity for bioorthogonal pretargeting by unmasking antibody-conjugated trans-cyclooctenes, Bioconjug Chem, 26 (2015) 352-360.

[272] I. Navarro-Teulon, C. Lozza, A. Pelegrin, E. Vives, J.P. Pouget, General overview of radioimmunotherapy of solid tumors, Immunotherapy, 5 (2013) 467-487.

[273] N. Sato, R. Hassan, D.B. Axworthy, K.J. Wong, S. Yu, L.J. Theodore, Y. Lin, L. Park, M.W. Brechbiel, I. Pastan, C.H. Paik, J.A. Carrasquillo, Pretargeted radioimmunotherapy of mesothelin-expressing cancer using a tetravalent single-chain Fv-streptavidin fusion protein, J Nucl Med, 46 (2005) 1201-1209.

[274] D.M. Goldenberg, E.A. Rossi, R.M. Sharkey, W.J. McBride, C.H. Chang, Multifunctional antibodies by the Dock-and-Lock method for improved cancer imaging and therapy by pretargeting, J Nucl Med, 49 (2008) 158-163.

[275] R.M. Sharkey, H. Karacay, S. Litwin, E.A. Rossi, W.J. McBride, C.H. Chang, D.M. Goldenberg, Improved therapeutic results by pretargeted radioimmunotherapy of non-Hodgkin's lymphoma with a new recombinant, trivalent, anti-CD20, bispecific antibody, Cancer Res, 68 (2008) 5282-5290.

[276] R.M. Sharkey, F.J. Primus, D.M. Goldenberg, Second antibody clearance of radiolabeled antibody in cancer radioimmunodetection, Proc Natl Acad Sci U S A, 81 (1984) 2843-2846.

[277] E. Mirallié, C. Saï-Maurel, A. Faivre-Chauvet, N. Regenet, C.-H. Chang, D. Goldenberg, J.-F. Chatal, J. Barbet, P. Thedrez, Improved pretargeted delivery of radiolabelled hapten to human tumour xenograft in mice by avidin chase of circulating bispecific antibody, Eur J Nucl Med Mol Imaging, 32 (2005) 901-909.

[278] H.B. Breitz, P.L. Weiden, P.L. Beaumier, D.B. Axworthy, C. Seiler, F.M. Su, S. Graves, K. Bryan, J.M. Reno, Clinical optimization of pretargeted radioimmunotherapy with antibody-streptavidin conjugate and 90Y-DOTA-biotin, J Nucl Med, 41 (2000) 131-140.

[279] G. Liu, S. Dou, X. Chen, L. Chen, X. Liu, M. Rusckowski, D.J. Hnatowich, Adding a clearing agent to pretargeting does not lower the tumor accumulation of the effector as predicted, Cancer Biother Radiopharm, 25 (2010) 757-762.

[280] G. Paganelli, C. Grana, M. Chinol, M. Cremonesi, C. De Cicco, F. De Braud, C. Robertson, S. Zurrida, C. Casadio, S. Zoboli, A.G. Siccardi, U. Veronesi, Antibody-guided three-step therapy for high grade glioma with yttrium-90 biotin, Eur J Nucl Med, 26 (1999) 348-357.

[281] C. Grana, M. Chinol, C. Robertson, C. Mazzetta, M. Bartolomei, C. De Cicco, M. Fiorenza, M. Gatti, P. Caliceti, G. Paganelli, Pretargeted adjuvant radioimmunotherapy with yttrium-90-biotin in malignant glioma patients: a pilot study, Br J Cancer, 86 (2002) 207-212.

[282] D.M. Goldenberg, J.F. Chatal, J. Barbet, O. Boerman, R.M. Sharkey, Cancer Imaging and Therapy with Bispecific Antibody Pretargeting, Update Cancer Ther, 2 (2007) 19-31.

[283] R. Sabatier, A. Goncalves, F. Bertucci, Personalized medicine: present and future of breast cancer management, Crit Rev Oncol Hematol, 91 (2014) 223-233.

[284] A. Pantelias, J.M. Pagel, N. Hedin, L. Saganic, S. Wilbur, D.K. Hamlin, D.S. Wilbur, Y. Lin, D. Stone, D. Axworthy, A.K. Gopal, O.W. Press, Comparative biodistributions of pretargeted radioimmunoconjugates targeting CD20, CD22, and DR molecules on human B-cell lymphomas, Blood, 109 (2007) 4980-4987.

[285] T.E. Witzig, L.I. Gordon, F. Cabanillas, M.S. Czuczman, C. Emmanouilides, R. Joyce, B.L. Pohlman, N.L. Bartlett, G.A. Wiseman, N. Padre, A.J. Grillo-Lopez, P. Multani, C.A. White, Randomized controlled trial of yttrium-90-labeled ibritumomab tiuxetan radioimmunotherapy versus rituximab immunotherapy for patients with relapsed or refractory low-grade, follicular, or transformed B-cell non-Hodgkin's lymphoma, J Clin Oncol, 20 (2002) 2453-2463.

[286] M. Jain, N. Kamal, S.K. Batra, Engineering antibodies for clinical applications, Trends Biotechnol, 25 (2007) 307-316.

[287] A.J. Pertsin, M. Grunze, Computer simulation of water near the surface of oligo(ethylene glycol)-terminated alkanethiol self-assembled monolayers, Langmuir, 16 (2000) 8829-8841.

[288] M.C. Woodle, D.D. Lasic, Sterically stabilized liposomes, Biochim Biophys Acta, 1113 (1992) 171-199.

[289] T.M. Allen, C. Hansen, F. Martin, C. Redemann, A. Yau-Young, Liposomes containing synthetic lipid derivatives of poly(ethylene glycol) show prolonged circulation half-lives in vivo, Biochim Biophys Acta, 1066 (1991) 29-36.

[290] J. Senior, C. Delgado, D. Fisher, C. Tilcock, G. Gregoriadis, Influence of surface hydrophilicity of liposomes on their interaction with plasma protein and clearance from the circulation: studies with poly(ethylene glycol)-coated vesicles, Biochim Biophys Acta, 1062 (1991) 77-82.

[291] S.M. Ryan, G. Mantovani, X. Wang, D.M. Haddleton, D.J. Brayden, Advances in PEGylation of important biotech molecules: delivery aspects, Expert Opin Drug Deliv, 5 (2008) 371-383.

[292] S.M. Moghimi, J. Szebeni, Stealth liposomes and long circulating nanoparticles: critical issues in pharmacokinetics, opsonization and protein-binding properties, Progress in Lipid Research, 42 (2003) 463-478.

[293] Y. Cu, W.M. Saltzman, Controlled surface modification with poly(ethylene)glycol enhances diffusion of PLGA nanoparticles in human cervical mucus, Mol Pharm, 6 (2009) 173-181.

[294] S. Lelu, S.P. Strand, J. Steine, L. Davies Cde, Effect of PEGylation on the diffusion and stability of chitosan-DNA polyplexes in collagen gels, Biomacromolecules, 12 (2011) 3656-3665.

[295] H. Du, P. Chandaroy, S.W. Hui, Grafted poly-(ethylene glycol) on lipid surfaces inhibits protein adsorption and cell adhesion, Biochim Biophys Acta, 1326 (1997) 236-248.

[296] S.D. Li, L. Huang, Nanoparticles evading the reticuloendothelial system: role of the supported bilayer, Biochim Biophys Acta, 1788 (2009) 2259-2266.

[297] M. Garcia-Fuentes, D. Torres, M. Martin-Pastor, M.J. Alonso, Application of NMR spectroscopy to the characterization of PEG-stabilized lipid nanoparticles, Langmuir, 20 (2004) 8839-8845.

[298] T. Riley, C.R. Heald, S. Stolnik, M.G. Garnett, L. Illum, S.S. Davis, Core-shell structure of PLA-PEG nanoparticles used for drug delivery, Langmuir, 19 (2003) 8428-8435.

[299] C.S. Levin, S.W. Bishnoi, N.K. Grady, N.J. Halas, Determining the conformation of thiolated poly(ethylene glycol) on Au nanoshells by surface-enhanced Raman scattering spectroscopic assay, Anal Chem, 78 (2006) 3277-3281.

[300] S.J. Budijono, B. Russ, W. Saad, D.H. Adamson, R.K. Prud'homme, Block copolymer surface coverage on nanoparticles, Colloids and Surfaces A: Physicochemical and Engineering Aspects, 360 (2010) 105-110.

[301] S.K. Lai, Y.Y. Wang, K. Hida, R. Cone, J. Hanes, Nanoparticles reveal that human cervicovaginal mucus is riddled with pores larger than viruses, Proc Natl Acad Sci U S A, 107 (2010) 598-603.

[302] S.K. Lai, D.E. O'Hanlon, S. Harrold, S.T. Man, Y.Y. Wang, R. Cone, J. Hanes, Rapid transport of large polymeric nanoparticles in fresh undiluted human mucus, Proc Natl Acad Sci U S A, 104 (2007) 1482-1487.

[303] Y. Li, R. Lander, W. Manger, A. Lee, Determination of lipid profile in meningococcal polysaccharide using reversed-phase liquid chromatography, J Chromatogr B Analyt Technol Biomed Life Sci, 804 (2004) 353-358.

[304] M. Daigneault, J.A. Preston, H.M. Marriott, M.K. Whyte, D.H. Dockrell, The identification of markers of macrophage differentiation in PMA-stimulated THP-1 cells and monocyte-derived macrophages, PLoS One, 5 (2010) e8668.

[305] T.J. Merkel, S.W. Jones, K.P. Herlihy, F.R. Kersey, A.R. Shields, M. Napier, J.C. Luft, H. Wu, W.C. Zamboni, A.Z. Wang, J.E. Bear, J.M. DeSimone, Using mechanobiological mimicry of red blood cells to extend circulation times of hydrogel microparticles, PNAS, 108 (2011) 586-591.

[306] Y. Zhang, M. Huo, J. Zhou, S. Xie, PKSolver: An add-in program for pharmacokinetic and pharmacodynamic data analysis in Microsoft Excel, Comput Methods Programs Biomed, 99 (2010) 306-314.

[307] M.C. Woodle, K.K. Matthay, M.S. Newman, J.E. Hidayat, L.R. Collins, C. Redemann, F.J. Martin, D. Papahadjopoulos, Versatility in lipid compositions showing prolonged circulation with sterically stabilized liposomes, Biochim Biophys Acta, 1105 (1992) 193-200.

[308] A. Mori, A.L. Klibanov, V.P. Torchilin, L. Huang, Influence of the steric barrier activity of amphipathic poly(ethyleneglycol) and ganglioside GM1 on the circulation time of liposomes and on the target binding of immunoliposomes in vivo, FEBS Lett, 284 (1991) 263-266.

[309] E. Fattal, H. Hillaireau, M. Simona, J. Nicolas, N. Tsapis, Targeted delivery using biodegradable polymeric nanoparticles, in: J. Siepmann, R.A. Siegel, M.J. Rathbone (Eds.) Fundamentals and Applications of Controlled Release Drug Delivery, Springer US, 2012, pp. 255-288.

[310] S.W. Jones, R.A. Roberts, G.R. Robbins, J.L. Perry, M.P. Kai, K. Chen, T. Bo, M.E. Napier, J.P. Ting, J.M. Desimone, J.E. Bear, Nanoparticle clearance is governed by Th1/Th2 immunity and strain background, J Clin Invest, 123 (2013) 3061-3073.

[311] S.D. Perrault, C.D. Walkey, T. Jennings, H.C. Fischer, W.C.W. Chan, Mediating tumor targeting efficiency of nanoparticles through design, Nano Lett, 9 (2009) 1909-1915.

[312] D.C. Litzinger, A.M.J. Buiting, N. van Rooijen, L. Huang, Effect of liposome size on the circulation time and intraorgan distribution of amphipathic poly(ethylene glycol)-containing liposomes, Biochim Biophys Acta, 1190 (1994) 99-107.

[313] J.S. Lee, M. Ankone, E. Pieters, R.M. Schiffelers, W.E. Hennink, J. Feijen, Circulation kinetics and biodistribution of dual-labeled polymersomes with modulated surface charge in tumor-bearing mice: comparison with stealth liposomes, J Control Release, 155 (2011) 282-288.

[314] Y. Geng, P. Dalhaimer, S. Cai, R. Tsai, M. Tewari, T. Minko, D.E. Discher, Shape effects of filaments versus spherical particles in flow and drug delivery, Nat Nanotechnol, 2 (2007) 249-255.

[315] C. Jeppesen, J.Y. Wong, T.L. Kuhl, J.N. Israelachvili, N. Mullah, S. Zalipsky, C.M. Marques, Impact of polymer tether length on multiple ligand-receptor bond formation, Science, 293 (2001) 465-468.

[316] C. Sacchetti, K. Motamedchaboki, A. Magrini, G. Palmieri, M. Mattei, G. Bernardini, N. Rosato, N. Bottini, M. Bottini, Surface PEG conformation influences the protein corona of polyethylene glycol-modified single-walled carbon nanotubes: potential implications on biological performance, ACS Nano, 7 (2013) 1974-1989.

[317] S. Tenzer, D. Docter, J. Kuharev, A. Musyanovych, V. Fetz, R. Hecht, F. Schlenk, D. Fischer, K. Kiouptsi, C. Reinhardt, K. Landfester, H. Schild, M. Maskos, S.K. Knauer, R.H. Stauber, Rapid formation of plasma protein corona critically affects nanoparticle pathophysiology, Nat Nanotechnol, 8 (2013) 772-781.

[318] C.J. Fristrup, K. Jankova, S. Hvilsted, Surface-initiated atom transfer radical polymerization-a technique to develop biofunctional coatings, Soft Matter, 5 (2009) 4623-4634.

[319] S.H. Lee, D.R. Dreyer, J.H. An, A. Velamakanni, R.D. Piner, S. Park, Y.W. Zhu, S.O. Kim, C.W. Bielawski, R.S. Ruoff, Polymer Brushes via Controlled, Surface-Initiated Atom Transfer Radical Polymerization (ATRP) from Graphene Oxide, Macromolecular Rapid Communications, 31 (2010) 281-288.

[320] K. Rahme, L. Chen, R.G. Hobbs, M.A. Morris, C. O'Driscoll, J.D. Holmes, PEGylated gold nanoparticles: polymer quantification as a function of PEG lengths and nanoparticle dimensions, RSC Advances, 3 (2013) 6085-6094.

[321] W.P. Caron, J.C. Lay, A.M. Fong, N.M. La-Beck, P. Kumar, S.E. Newman, H. Zhou, J.H. Monaco, D.L. Clarke-Pearson, W.R. Brewster, L. Van Le, V.L. Bae-Jump, P.A. Gehrig, W.C. Zamboni, Translational Studies of Phenotypic Probes for the Mononuclear Phagocyte System and Liposomal Pharmacology, J Pharmacol Exp Ther, (2013).

[322] R. Mazor, M. Onda, I. Pastan, Immunogenicity of therapeutic recombinant immunotoxins, Immunological Reviews, 270 (2016) 152-164.

[323] N. Chirmule, V. Jawa, B. Meibohm, Immunogenicity to Therapeutic Proteins: Impact on PK/PD and Efficacy, The AAPS Journal, 14 (2012) 296-302.

[324] C.H. Chung, B. Mirakhur, E. Chan, Q.T. Le, J. Berlin, M. Morse, B.A. Murphy, S.M. Satinover, J. Hosen, D. Mauro, R.J. Slebos, Q. Zhou, D. Gold, T. Hatley, D.J. Hicklin, T.A. Platts-Mills, Cetuximab-induced anaphylaxis and IgE specific for galactose-alpha-1,3-galactose, N Engl J Med, 358 (2008) 1109-1117.

[325] J. Descotes, A. Gouraud, Clinical immunotoxicity of therapeutic proteins, Expert Opin Drug Metab Toxicol, 4 (2008) 1537-1549.

[326] <Aptamer-functionalized ultrasmall silica nanoconj for target dual imaging of LN and met supp.Tang et al.Angew chem.2012.pdf>.

[327] P.L. Turecek, M.J. Bossard, F. Schoetens, I.A. Ivens, PEGylation of Biopharmaceuticals: A Review of Chemistry and Nonclinical Safety Information of Approved Drugs, J Pharm Sci, 105 (2016) 460-475.

[328] T.L. Cheng, S.R. Roffler, K.H. Chuang, S.J. Lu, Anti-polyethylene glycol antibody expressing cell quantify any free polyethylene glycol and polyethylene glycol-derivatized molecules, in, Kaohsiung Medical University, 2012.

[329] A. Frey, J. Di Canzio, D. Zurakowski, A statistically defined endpoint titer determination method for immunoassays, J Immunol Methods, 221 (1998) 35-41.

[330] J. Thompson, R. Islam, Evaluation and Validation of a Commercial ELISA Kit for the Detection of Antibodies to Pegylated Therapeutic Drug (Pegfilgrastim) in Human Serum for Use in Support of Clinical Studies, in, AAPS Annual Meeting and Exposition, 2015.

[331] D. Weiskopf, B. Weinberger, B. Grubeck-Loebenstein, The aging of the immune system, Transpl Int, 22 (2009) 1041-1050.

[332] A. Kolate, D. Baradia, S. Patil, I. Vhora, G. Kore, A. Misra, PEG - a versatile conjugating ligand for drugs and drug delivery systems, J Control Release, 192 (2014) 67-81.

[333] U.S.D.o.H.a.H. Services, F.a.D. Administration, C.f.D.E.a.R. (CDER), C.f.B.E.a.R. (CBER), C.f.D.a.R.H. (CDRH), Assay Development and Validation for Immunogenicity Testing of Therapeutic Protein Products: Guidance for Industry.

[334] L. Zhou, S.A. Hoofring, Y. Wu, T. Vu, P. Ma, S.J. Swanson, N. Chirmule, M. Starcevic, Stratification of Antibody-Positive Subjects by Antibody Level Reveals an Impact of Immunogenicity on Pharmacokinetics, The AAPS Journal, 15 (2013) 30-40.

[335] S.A. Plotkin, Correlates of Protection Induced by Vaccination, Clinical and Vaccine Immunology : CVI, 17 (2010) 1055-1065.

[336] T. Shimizu, Y. Mima, Y. Hashimoto, M. Ukawa, H. Ando, H. Kiwada, T. Ishida, Anti-PEG IgM and complement system are required for the association of second doses of PEGylated liposomes with splenic marginal zone B cells, Immunobiology, 220 (2015) 1151-1160.

[337] D.B. Kirpotin, D.C. Drummond, Y. Shao, M.R. Shalaby, K. Hong, U.B. Nielsen, J.D. Marks, C.C. Benz, J.W. Park, Antibody Targeting of Long-Circulating Lipidic Nanoparticles Does Not Increase Tumor Localization but Does Increase Internalization in Animal Models, Cancer Res, 66 (2006) 6732-6740.

[338] C.P. Leamon, S.R. Cooper, G.E. Hardee, Folate-Liposome-Mediated Antisense Oligodeoxynucleotide Targeting to Cancer Cells: Evaluation in Vitro and in Vivo, Bioconjug Chem, 14 (2003) 738-747.

[339] Q. Yang, C.L. Parker, J.D. McCallen, S.K. Lai, Addressing challenges of heterogeneous tumor treatment through bispecific protein-mediated pretargeted drug delivery, J Control Release, (2015).

[340] A. Forero-Torres, S. Shen, H. Breitz, R.B. Sims, D.B. Axworthy, M.B. Khazaeli, K.H. Chen, I. Percent, S. Besh, A.F. LoBuglio, R.F. Meredith, Pretargeted radioimmunotherapy (RIT) with a novel anti-TAG-72 fusion protein, Cancer Biother Radiopharm, 20 (2005) 379-390.

[341] Q. Yang, S.W. Jones, C.L. Parker, W.C. Zamboni, J.E. Bear, S.K. Lai, Evading immune cell uptake and clearance requires PEG grafting at densities substantially exceeding the minimum for brush conformation, Mol Pharm, 11 (2014) 1250-1258.

[342] S.I. Park, J. Shenoi, J.M. Pagel, D.K. Hamlin, D.S. Wilbur, N. Orgun, A.L. Kenoyer, S. Frayo, A. Axtman, T. Bäck, Y. Lin, D.R. Fisher, A.K. Gopal, D.J. Green, O.W. Press, Conventional and pretargeted radioimmunotherapy using bismuth-213 to target and treat non-Hodgkin lymphomas expressing CD20: a preclinical model toward optimal consolidation therapy to eradicate minimal residual disease, Blood, 116 (2010) 4231-4239.

[343] J. Schultz, Y. Lin, J. Sanderson, Y. Zuo, D. Stone, R. Mallett, S. Wilbert, D. Axworthy, A tetravalent single-chain antibody-streptavidin fusion protein for pretargeted lymphoma therapy, Cancer Res, 60 (2000) 6663-6669.

[344] Z. Cheng, A. Al Zaki, J.Z. Hui, V.R. Muzykantov, A. Tsourkas, Multifunctional Nanoparticles: Cost Versus Benefit of Adding Targeting and Imaging Capabilities, Science, 338 (2012) 903-910.

[345] C. Rousseau, F. Kraeber-Bodéré, J. Barbet, J.-F. Chatal, Pretargeted radioimmunotherapy: clinically more efficient than conventional radioimmunotherapy?, Eur J Nucl Med Mol Imaging, 40 (2013) 1373-1376.

[346] S.M. Larson, J.A. Carrasquillo, N.-K.V. Cheung, O.W. Press, Radioimmunotherapy of human tumours, Nat Rev Cancer, 15 (2015) 347-360.

[347] Y. Lin, J.M. Pagel, D. Axworthy, A. Pantelias, N. Hedin, O.W. Press, A Genetically Engineered Anti-CD45 Single-Chain Antibody-Streptavidin Fusion Protein for Pretargeted Radioimmunotherapy of Hematologic Malignancies, Cancer Res, 66 (2006) 3884-3892.

[348] J. Zempleni, D.M. Mock, Uptake and metabolism of biotin by human peripheral blood mononuclear cells, Am J Physiol, 275 (1998) C382-388.

[349] D.L. Vesely, S.F. Kemp, M.J. Elders, Isolation of a biotin receptor from hepatic plasma membranes, Biochem Biophys Res Commun, 143 (1987) 913-916.

[350] V.D. Awasthi, D. Garcia, B.A. Goins, W.T. Phillips, Circulation and biodistribution profiles of long-circulating PEG-liposomes of various sizes in rabbits, Int J Pharm, 253 (2003) 121-132.

[351] L. Zhang, Z. Cao, Y. Li, J.R. Ella-Menye, T. Bai, S. Jiang, Softer zwitterionic nanogels for longer circulation and lower splenic accumulation, ACS Nano, 6 (2012) 6681-6686.